6876

DECARBURIZATION OF IRON-CARBON ALLOYS WITH OXIDISING SLAGS.

by

Oscar Miguel Ojeda Luna

M.Met., M.I.M.

Thesis submitted to the Council for National Academic Awards in partial fulfilment of the requirements for the award of the Degree of Doctor of Philosophy. A research study sponsored by Sheffield City Polytechnic.

December 1977.

Preface

This dissertation is submitted for the degree of Doctor of Philosophy of the Council for National Academic Awards. The research described was carried out during the period of October 1974 to September 1977 in the Department of Metallurgy, Sheffield City Polytechnic. No part of this dissertation has been submitted for a degree at any other university or college.

During the period of this work, the author attended post-graduate lecture courses on the following topics:

1) Process Metallurgy.
2) Oxygen Steelmaking.
3) Continuous Casting.
4) Thermodynamics.

The author wishes to express his thanks to his supervisors Dr. M. Sunderland and Dr. R. Baker and for the many valuable discussions to Dr. G. Briggs, Dr. G.S.F. Hazeldean and Dr. R. Acheson.

The author would also like to extend his gratitude to all those members of the departmental staff and research colleagues who contributed in various ways during the course of this work.

The provision of a grant from CONACYT, MEXICO, and Sheffield City Polytechnic are gratefully acknowledged. The author wishes to thank Dr. A.W.D. Hills for the facilities provided to carry out the present research. The author is indebted to Mrs. J. Czerny for typing this thesis.

Synopsis

Reactions which are generated from slag-metal-gas systems, such as those found in Oxygen Steelmaking, have been studied in the present research. A system has been developed whereby one gram iron-carbon alloys have been decarburized by synthetic slags. Fayalite slags were initially used for decarburization after which lime bearing slags from the $CaO-FeO-SiO_2$ ternary followed. The slags, although highly reactive, were found to be contained adequately in iron crucibles. By protecting the iron crucibles with a zirconia film the iron crucibles can be safely used up to 1400°C. The experimental technique has been well established. The data obtained from the decarburization experiments indicated an increase in rate of decarburization with increasing lime content up to a certain composition. For slags containing about 26% CaO the rates for decarburization commence to decrease. The range of temperatures under which reactions were studied (1240°C to 1600°C) indicated that the decarburization takes place more rapidly by the presence of a more fluid and consequently more turbulent system.

Gas lancing was used to change the hydrodynamic state of the system. The increase in turbulence caused a more rapid decarburization of the iron-carbon alloys as compared to those when no gas lancing was used. Little effect was found on the rate of decarburization when the oxygen potentials of the gas were changed. There is clear evidence that the overall rates of the decarburization process are not controlled by the rate of chemical reaction itself. Experimental observation from

X-ray analysis and scanning electron microscopy, have established that internal heterogeneous nucleation takes place in the metal phase. The nucleation sites are extremely small particles of entrapped slag.

Mass Transfer Coefficients have been calculated for the various iron-carbon/slag reactions. For fayalite slag, values of the mass transfer coefficient were found to be from 3.20×10^{-4} cm/sec to 11.40×10^{-4} cm/sec for 1240 and 1400°C respectively. Maximum values for the mass transfer coefficient in lime bearing slags were found to be in the range of 12.75×10^{-4} cm/sec at 1300°C to 19.95×10^{-4} cm/sec at 1400°C.

It has not been possible to establish a precise correlation for the mass transfer coefficients with the simple models for mass transfer proposed by other authors. The generation of carbon monoxide gives rise to a situation which is very complex to describe in terms of mathematical models. Nevertheless the experimental kinetics have been discussed in relationship to the classical film theory for mass transfer across an interface between two phases. This has allowed conclusions to be drawn about the rate controlling step of the overall mechanism of transfer. Some agreement between experimental data and the model has allowed estimates to be made of relative velocity between slag and metal, Sh, Gr and Re numbers. In addition, the penetration theory has also been examined and analysis indicated that it has some potential applicability to this type of system. Finally, the discussion suggests that Danckwerst surface renewal adaptation of the penetration theory is worthy of future examination.

CONTENTS

NOMENCLATURE

Chapter II
Section 2.2

$\underline{X}$	element dissolved in liquid iron.
( )	element dissolved in slag.
a_x	Henrian activity of X.
e_x^y	interaction parameter of y on x (where Y and X are not Fe)
γ	Roultian activity coefficient.
h	Henrian activity coefficient.
x	mole fractions.

Section 2.3

CFS	lime-iron oxide-silica.
C_2S	dicalcium silicate.
F_2S	fayalite.
C_xF_y	calcium ferrites.

Section 2.3.5

O^-	oxygen singly bonded.
O^o	oxygen doubly bonded.
O^{2-}	oxygen as free ion.
P_{O_2}	partial pressure for oxygen.

Section 2.5

γ	surface tension.
μ	viscosity.

Chapter V.

P_{CO}	carbon monoxide pressure.
P_A	atmospheric pressure.
P_γ	pressure difference between concave and convex side of a curved interface.

ρ	density.
g	acceleration due to gravity.
γ	surface tension.
$\gamma_{MG,MS,SG}$	surface tension between two phases (e.g. MS = metal/slag).
θ	contact angle
r	radius.
C	concentrations.
C_x^b	concentration of X in the bulk.
C_x^i	concentration of X at the interface.
C_o	initial concentration.
C_s	concentration at surface.
C_f	final concentration.
k_d	mass transfer coefficient for discontinuous phase.
D	diffusivity.
J	flux.
δ	film thickness.
d	diameter.
v	velocity.
$\mu_{d,c}$	viscosity of discontinuous or continuous phase.
V_d	volume of drop.
A	area.
k_R	rate constant.
E	activation energy.
R	gas constant.
t	time.

Re	Reynolds number.	$\frac{d\,\bar{v}\,\rho}{\mu}$	$\left(\frac{\text{inertial forces}}{\text{viscous forces}}\right)$
Sc	Schmidt number.	$\frac{\mu}{\rho D}$	$\left(\frac{\text{momentum diffusivity}}{\text{molecular diffusivity}}\right)$
Sh	Sherwood number.	$\frac{kd}{D}$	$\left(\frac{\text{total mass transfer}}{\text{molecular diffusivity}}\right)$
Pe	Peclet number.	$\frac{dV}{D}$	$\left(\frac{\text{bulk mass transport}}{\text{mass transfer by diffusion}}\right)$
Gr	Grashof number.	$\frac{g\rho^2 d^3 \beta' \Delta X}{\mu^2}$ (Re)	$\left(\frac{\text{buoyancy force}}{\text{viscous force}}\right)$

β' = coefficient of density change with concentration.

ΔX = concentration of driving force.

CHAPTER ONE

INTRODUCTION

Since the initial trials in Austria during the late 1940's, oxygen steelmaking has been extensively adopted throughout the world. In most industrialised countries the adoption has been mainly at the expense of the open hearth process. Paramount development has taken place during the last decade mainly on the L.D. process as opposed to the Kaldo, Rotor, O.L.P., etc. Renewed interest in using tonnage oxygen in bottom blown converters has arisen fairly recently. The ability to operate at extremely high refining rates has been the primary reason for the enthusiastic adoption of L.D. converters.

During the refining of steel in a Basic Oxygen Furnace, the various dissolved elements transfer from the metal phase into the slag or the gas phase. There is evidence that much of this transfer takes place when drops of steel are thrown up from the bath and have motion through the slag phase, which is in high degree of turbulence and foaming. The mechanism of oxidation of the dispersed metal phase, and particularly carbon monoxide evolution, are not fully understood. It is only recently that interest has arisen to explore the decarburization mechanisms which take place in the foaming slag. Industrial experience of the role played by the presence of the foam in the L.D. process indicates that a large interfacial area is generated across which mass is transferred. The turbulence and the foam are promoted by the injection of a gas

stream of high momentum and by evolution of large quantities of CO gas. The transfer of the elements, Mn, Si, P and S is dependent upon foam formation, foam stability, fluid dynamics and metal/slag interfacial area. Consequently the total time of refining is dependent upon these phenomena. Control of the refining cycle and end point specification relies heavily on these characteristics of the gas-slag-metal emulsions. The precise mechanisms by which the jet transfers momentum and oxygen to the slag, and then to the metal, are not fully understood. The factors which control the nucleation of the carbon monoxide bubbles are not well established. The action of the evolving CO gas from the bath, and how this action gives rise to metal drop motion and turbulence in general, has not been fully investigated.

Studies within the LD process itself when operating commercially, are inhibited by the inherent practical difficulties associated with making measurements of the highly turbulent process which is occurring at high temperatures and in the highly reactive conditions of the converter. There are two approaches to facilitate research. The first is pursue room temperature models of the whole process and converter. The second is to experiment at high temperatures with real LD slags but with restrictions of scale whereby only a drop of metal is refined. The second approach has been adopted here.

A great number of experiments have been made on decarburization mechanisms but the majority has been confined to gas-metal systems. The results indicate that the kinetics of the

process are extremely rapid, and occur more quickly than in the L.D. vessel. The main advantage of these studies is the high temperatures which can be achieved without contamination problems, and more importantly, the well defined geometry and fluid mechanisms which permits thorough analytical description of the process. The main disadvantage is that of the absence of the slag. The oxidizing species may not be in the gaseous phase when a slag is present. The presence of a slag/metal interface must certainly give rise to different decarburization mechanisms, particularly with respect to CO bubble nucleation. Studies on actual slag-metal systems have been inhibited due mainly to reactivity of slags with crucibles used for containment. Very few studies have been undertaken, and of those carried out, only qualitative descriptions have been obtained or only a narrow range of variables has been studied. There are three possible paths which the experimental study may take. A full range of typical slag compositions and temperatures can be covered only if vast sums of money are available: the reactive slags can be contained in expensive metals (e.g. platinum) or expensive refractories (e.g. zirconia). In the absence of unlimited funds, recrystallised alumina crucibles may offer some possibility of success. However, the slags must be heavily doped with alumina in order to prevent crucible failure. The oxidising slags then become far removed from the $CaO-FeO-SiO_2$ system which is of interest. The third, and realistic approach, is to reduce the upper temperature limit and use iron crucibles which are known to sustain attack from these corrosive slags (now alumina free).

Although little is known of the possibility of holding a liquid iron-carbon drop within a slag matrix within a solid iron container, the technique offers scope for investigation.

This thesis will report on an investigation which follows the third approach. After reviewing the literature and scientific findings which are pertinent to the topic, a tentative experimental technique could be designed. This is described in Chapter 3 which also gives a description of the technique and of the large number of preliminary results required to prove the viability of the project. The limitations of the project become clear in this section. Chapter 4 will give the full results obtained which then permit an analysis in Chapter 5. This discussion, along with the conclusions and suggestion for future studies, emphasises the complexity of the mechanisms even in this simplified laboratory system.

CHAPTER TWO

LITERATURE SURVEY

2.1 Pneumatic Steelmaking

It has been over a century that pneumatic steelmaking processes have been in use. The advantage of using oxygen instead of air had long been appreciated but severe attack on tuyere refractories was experienced when oxygen was used. Before these refractory problems were overcome the top blown oxygen processes were introduced. The availability of pure, cheap tonnage oxygen enabled a variety of processes - such as Kaldo, Rotor, L.D. or Basic Oxygen Steelmaking (BOS), L.D.-A.C. to be developed. Only recently the tuyere refractory problems have been overcome and processes such as OBM and Q-BOP have been introduced at an industrial scale. The top blown process continues to account for the great majority of oxygen refined steel.

The main features of the above mentioned steelmaking processes are subsequently described.

2.1.1 The Kaldo Process.

The Kaldo process was developed specifically for the refining of pig iron (hot metal) with high phosphorus contents. The Kaldo converter is a cylindrical, pear-shaped vessel whose axis is inclined 17^{o} to 20^{o} from the horizontal and may be rotated up to 35 rpm. A single oxygen jet is blown onto the surface of the metal. The rotation of the vessel provides good mixing of slag and metal, this in turn provides for

good heat transfer from the hot lining to the charge. This practice avoids overheating of the lining when carbon monoxide (from the oxidation of carbon) is burnt to carbon dioxide by a secondary oxygen lance above the bath. The heat evolved from the combustion of carbon monoxide allows for up to 35% of the charge to be in the form of cold scrap (1). Operation on an industrial scale began with a 30 ton vessel in May 1956(2).

2.1.2 Rotor Process.

The Rotor process is based on a rotating cylinder converter with an opening at each end. Through one opening the vessel is charged and oxygen is blown through two lances. A primary oxygen lance is introduced beneath the metal surface for oxidation and gentle stirring of the bath. The secondary oxygen lance (or enriched air) is positioned above the metal surface where carbon monoxide is burnt to carbon dioxide. The opposite end of the vessel has a water-cooled offtake through which the hot gases are extracted. Originally the vessel was used for pretreating hot metal for final refining in the open hearth process. High and low phosphorus hot metal was subsequently found to be adequately refined in the vessel similar to the Kaldo process. Due to the low rotational speed achieved (1-5 rpm) there is no great influence in the refining process kinetics and the first 60 ton converter had a tap to tap time of 2 hours (3).

In the United Kingdom the Kaldo and Rotor processes never gained the popularity expressed by foreign authors; for both proved an expensive engineering innovation.

2.1.3 Bottom Oxygen Blowing.

The air blown Bessemer converter has continuously been handicapped by a low scrap charge, high phosphorus and nitrogen in the steel. The replacement of air by oxygen posed severe problems due to high temperatures and attack on tuyere refractories. Oxygen mixed with steam on a 1:1 ratio has been tried with some success (4) but scrap consumption was limited to 15% of the charge. The refractories problems were overcome when an injector was conceived by Eisenwerk Gesselshaft Maximillianshute mbh (5). The refractories could be protected by enveloping the oxygen in a gaseous or liquid shield. The injector consists of two concentric tubes; through the annulus a small amount of protective hydrocarbon fluid is introduced. The temperature around and near the injector is reduced by endothermic cracking of the hydrocarbon (light fuel oil, propane or natural gas) thereby reducing possible damage of adjacent refractory.

When using air or enriched air the campaign life for the bottom of the converter ranges from 50 to 75 heats, whereas with the injection technique (OBM), the refractory bottoms have typical lives of 300 heats (i.e. one bottom replacement for each lining replacement) (5,6). Very regular wear has also been found (6). The first commercial OBM converter was commissioned in 1968 (5). Another feature of the process is that powder lime may be blown together with oxygen, so phosphorus can be removed readily during decarburization of the bath. From the thermodynamic point of view in the bottom blown process even with a short time of refining

(30 min tap to tap time) the slag and bath were found to be close to equilibrium. If equilibrium with the slag is reached, the lowest possible phosphorus contents are obtained (6). The results obtained by Nilles et al. (6) indicate that a rapid determination of the oxygen activity of the bath metal, and of its temperature, offer excellent control possibilities for the process. Injection of the gaseous oxidant at the vessel bottom must lead to some refining across a gas-metal interface. The nature of the slag is quiescent.

2.1.4 L.D. Basic Oxygen Steelmaking.

Greatest contribution to the world steel production by usage of oxygen has been made by the BOS process. Initial plants using charges from 3 to 5 tons were operated in Linz and Donawitz, Austria, around 1949 and for a period of over four years (8). However, not until the 1960's has its industrial application become widely adopted. In these past seventeen years spectacular growth of the BOS process has taken place achieved only by steady development of plant and operating techniques. Larger vessels have been adopted with a general trend towards a decrease in height to diameter ratio. The quantity of oxygen required by the process in short cycle times has been made available by using convergent-divergent nozzles to produce supersonic jets which can provide flow rates of around 2000 Nm^3 per minute (9). In order to achieve better mixing in the vessel and to reduce the possibility of refractory damage due to the severe action of the jet; multihole nozzles have been universally adopted. Increasing

use of computers has also taken place for charge calculations and storage of operating data. Although these and many other changes have taken place and have made possible an increase in production rates of BOF's furnaces, it has not yet been fully explained how these high rates are obtained or by what mechanism they come about.

The usual operation of the process in the UK begins by charging the converter with scrap followed by liquid pig iron known as hot metal. Lime and flux additions may be made from overhead hoppers at this point of time to promote early slag formation, but usually additions are also made during the blowing period. The oxygen blow is commenced and a water-cooled copper-tipped lance is lowered to a predetermined distance from the metal bath. Variations of the lance height are dictated by the type of scrap used, available oxygen pressure, analysis of hot metal and also on plant practice. A calculated amount of oxygen is blown after which, a spot check of bath carbon is made to guide the later blowing stages to ensure coincidence of end point carbon and temperature level. Timing of this spot check for composition and temperature (unless a continuous temperature sensor has been used) is a compromise between being early enough to allow time for corrective action to take place and late enough for satisfactory accuracy (10). When bath carbon and temperature are found to be correct the furnace is tilted for tapping, alloy additions are made in the ladle. Slagging-off the vessel is performed by rotating the vessel through 180^{o} to an inverted position. In the case of temperature being above

that desired, coolant such as scrap, BOS slag, lime stone, or iron ore may be added. When temperature overshoot is not very large, the vessel is left to cool naturally to a satisfactory level. However, when bath temperature is too low at turndown, reblowing for a short period will be required. Higher carbon levels than that aimed for also require reblowing. Low bath carbon is adjusted by ladle recarburization.

At the end of the cycle it is common practice to carry out a rapid check on refractory wear, possible damage and deterioration of lance and to clean debris from the nose of the vessel. The next charge can then be made immediately.

2.1.5 LDAC Process.

During the introduction of the LD process possibilities were obtained for refining high phosphorus hot metal by introduction of lime powder in suspension in the oxygen stream. The LDAC (or oxygen-limepowder) process was developed mainly by IRSID (7) over several years of research in the field of blowing finely divided materials into liquid baths. In studies of the LDAC process on high phosphorus iron, it was recognised that foaming-slags were associated with a high degree of dephosphorization (7a). The general steps during LDAC operation consists of 1) blowing of powder lime with oxygen from the beginning to the end of the refining period, 2) adjustment of lime concentration to hot-metal composition, phase of refining and steel grade to be produced, 3) removal of one or two intermediate slags, rich in lime and poor in iron, which take away an important part of the phosphorus and sulphur from the hot metal (7).

2.2 Physical Chemistry.

Physico-chemical Theory aims to reduce complex phenomena to the fewest possible understandable single phenomena, which can be proved and examined according to idealized experimental models.

In essence, oxygen steelmaking involves the refining of a charge of hot metal and scrap with the aid of producing a steel of a special composition and temperature. Impurities must be removed to meet specification and sufficient heat must be generated by exothermic reactions to make the process autogenous. Considering tapping temperatures of 1600 to 1650^{o} C, heat will be required to raise the temperature of both hot metal and scrap and to compensate for thermal losses. Impurities leave the metal to either join the slag or to be swept away in the gas phase. Thus, silicon, manganese and phosphorus oxides enter the slag along with iron oxides formed. Carbon removal is mainly as carbon monoxide which is carried away by the outgoing gases.

It is generally recognised that the oxidation mechanisms are complex and that more than one mechanism exists. Representing the slag/metal/gas reactions in a meaningful way is difficult. Consistent with the visualization of the slag phase as a molten ionic mixture oxidation reactions may be represented in different ways:

$$\begin{aligned}
&\text{i.} - \quad Mn + O \rightarrow Mn^{++} + O^{=} \\
&\qquad \text{(creation of one cation and one anion)} \\
&\text{ii.} - \quad Mn + Fe^{++} \rightarrow Mn^{++} + Fe \\
&\qquad \text{(exchange of cation)} \qquad (2.2.1) \\
&\text{iii.} - \quad Mn + 2Fe^{3+} \rightarrow Mn^{++} + 2Fe^{++} \\
&\qquad \text{(Redox reaction)}
\end{aligned}$$

Chemical reactions will subsequently be represented by equations chosen more on the basis of clarity rather than from a knowledge of the exact mechanism involved.

Basic thermodynamic data for the oxidation reactions have been well documented (11,12,13) and the order of removal of the elements on theoretical basis has been calculated. The oxygen activity for which equilibrium is achieved with the elements decreased in the order P<Fe<Mn<C<Si. The reverse direction indicating the order of removal. The actual sequence is found however to be Si, Mn, C, P, Fe as shown in figure 1.

2.2.1 Carbon oxidation.

The removal of carbon is of great importance during oxygen steelmaking since it gives rise to a gaseous reaction which is vital for a dynamic metal-slag-gas foam to be maintained.

In order to consider the onset of carbon oxidation, from dissolved carbon in the metal bath, according to the reaction

$$\underline{C} + \underline{O} = CO_{gas} \qquad (2.2.1.1)$$

the activities of the three species must be known. The source for this oxygen is the gaseous phase delivered through the lance and iron oxide from the slag. For convenience the oxygen is represented as dissolved in the metal phase, although in reality the overall reaction sequence is more complex when considering the oxygen source.

From chemical analysis of the outgoing gases at approximately one atmosphere pressure, 90% correspond to CO. The activity of CO can therefore be taken to be unity from the

above consideration. During the initial stages of the blow the activity of carbon is calculated by considering the interaction which other elements have with carbon atoms in the melt. To this end a series of interaction parameters have been calculated (12) which are then related to the interaction activity coefficient by

$$\log f_c = \Sigma e_c^X \cdot \% X \qquad (2.2.1.2)$$

The interaction activity coefficient is further related to the Henrian activity as

$$f_c = a_c \div \% C \qquad (2.2.1.3)$$

With the above relations it is thus possible to calculate the activity of carbon from a given melt. In the case of iron carbon alloys the interaction parameter e_c^c is given (11) as 0.22 and f_c is then calculated as 7.59. When the carbon content is taken as 4% the activity of carbon is equal to 1.9.

At the start of the blow at a temperature of 1300° C, for reaction (2.2.1.1) the equilibrium constant K is 624 (12) and since

$$K = \frac{a_{co}}{a_{\underline{C}} \cdot a_{\underline{O}}} = 624 \qquad (2.2.1.4)$$

and

$$a_{\underline{O}} = 8.4 \times 10^{-4}$$

Therefore, from thermodynamic considerations, oxidation of carbon would not be expected to occur until the oxygen activity in the metal reaches the value of 8.4×10^{-4}.

As the end of the blow is approached the carbon content falls to 0.1 wt% and the activity coefficient is close to unity due to lower solute concentration. At 1600° C the

equilibrium constant is about 500 (11) and the oxygen activity from (2.2.1.4) is calculated as 0.02. The hyperbolic relationship between %C and % oxygen, which is used for calculating oxygen contents, was studied by Marshal and Chipman (14) at different pressures as shown in figure 2.

2.2.2 Iron Oxidation.

Although silicon is the most readily oxidized of the species present in metallic bath, the removal of manganese and iron would not be expected until carbon removal was well advanced. Iron oxidation is almost certainly promoted by its high concentration and the difficulty of transferring other solute elements to the reaction zone in sufficient quantities to fully utilize the oxygen supply.

Several mechanisms have been proposed by which oxygen is transferred to the reaction site (11,13). Under the lance, in the impingement zone, oxygen goes into solution with some oxidation of the bath surface:

$$\begin{aligned} &\tfrac{1}{2}\, O_2 = \underline{O} \text{ (\% in Fe)} \\ &Fe + \underline{O} = (FeO) \qquad (2.2.3) \\ &(2FeO) + \tfrac{1}{2}\, O_2 = (Fe_2O_3) \end{aligned}$$

From chemical analysis of BOS slags the presence of FeO and Fe_2O_3 in a ratio of 3:1 is typically found (see table I).

2.2.3 Silicon Oxidation.

Silicon is the first impurity to be oxidized. In the BOS process practically all the silicon is oxidized during the first third of the blow (16). The reactions considered are:

$$\underline{Si} + 2\,\underline{O} = (SiO_2)$$
$$\underline{Si} + 2(FeO) = (SiO_2) + 2Fe(liq) \qquad (2.2.4)$$

The product of silicon oxidation is not however pure silica but SiO_2 dissolved in a basic slag. The heat effects associated with solution of silica in the slag would be expected to be large and in the absence of reliable data the heat is assumed to be equal to the heat of formation of dicalcium silicate. This heat release contributes to the formation of an early fluid slag.

2.2.4 Manganese Oxidation.

Oxidation of manganese from metal to slag is represented by:

$$\underline{Mn} + \underline{O} = (MnO) \qquad (2.2.5)$$

and is governed by the equilibrium constant given by (12):

$$K_{Mn} = \frac{a_{MnO}}{a_{Mn} \cdot a_{\underline{O}}} = \frac{11900}{T} - 5.07 \qquad (2.2.6)$$

The reaction product can either be a liquid or a solid solution of MnO in FeO which changes with temperature and manganese content of the metal. Manganese and iron form approximately ideal solutions and so do their oxides in both liquid and solid state (17).

In steelmaking the manganese slag distribution is most easily described by:

$$\underline{Mn} + (FeO) = (MnO) + Fe \qquad (2.2.7)$$

for which

$$K = \frac{(a_{MnO})[a_{Fe}]}{(a_{FeO})[h_{Mn}]} = \frac{(\gamma_{MnO} \cdot X_{MnO})[\gamma_{Fe} \cdot X_{Fe}]}{(\gamma_{FeO} \cdot X_{FeO})[f_{Mn} \cdot Wt\%\ Mn]} \qquad (2.2.8)$$

$$K' = K \frac{\gamma_{FeO} \cdot f_{Mn}}{\gamma_{MnO} \cdot \gamma_{Fe}} = \frac{(X_{MnO})[X_{Fe}]}{(X_{FeO})[Wt\%\ Mn]} \qquad (2.2.9)$$

although K may be calculated from chemical analysis of slag and metal, K' is no longer a constant but dependent on slag composition, except in the case of ideal slag composition (11). The effect can be seen in figure 1 where a period of manganese reversion is observed during the reduction of the slag by decarburization. Towards the end of the end-blow, manganese is again transferred to the slag. The final distribution being dependent upon temperature and iron oxide content of the slag (18). An inverse relationship between combined oxygen with manganese and oxygen combined with iron as Fe^{++} and Fe^{3+} has also been pointed out (19).

2.2.4 Phosphorus Oxidation.

The feasibility of oxidizing phosphorus in dilute solution in iron to form pure P_2O_5 may be assessed by considering the reaction:

$$2\underline{P} + 5\underline{O} = P_2O_5 \qquad (2.2.10)$$

the oxygen activity for phosphorus oxidation is higher than Fe, Mn, C and Si such that no dephosphorization could be envisaged by such reaction in the presence of other solutes. It is therefore necessary that the slag which is present is one which lowers the activity of P_2O_5. It is generally

recognised that phosphorus dissolves in the slag as an oxianion, for example PO_4^{3-}, as follows:,

$$2P + 5\,\underline{O} + 3\,O^{=} = 2\,PO_4^{3-} \qquad (2.2.11)$$

From this reaction it is deduced that a high basic slag (high $O^{=}$) under oxidizing conditions (high $\underline{O}$) will favour dephosphorization. The strength of the attraction between the PO_4^{3-} ion and the cation in the basic slag is reflected in the high negative value for the heats of formation such that the activity coefficient of P_2O_5 can be as low as 10^{-18}(11).

2.2.5 Sulphur.

For the reactions corresponding to sulphur removal from the initial charge as SO_2:

$$\underline{S}_{(\% \text{ in Fe})} + 2\underline{O}_{(\% \text{ in Fe})} = SO_{2\,(g)} \qquad (2.2.12)$$

$$\log K = - \frac{364}{T} + 2.86 \qquad \ldots\ldots\ldots \qquad (2.2.13)$$

the oxygen activity obtained is much higher than that at which other solutes start to oxidise. In practice no more than 10% of the sulphur removed from the metal is carried away as SO_2 in the waste gases.

The removal of sulphur from the metal takes place mainly by transfer to the slag where it exists as $S^{=}$. The reaction is represented by:

$$\underline{S} + O^{=} = S^{=} + \underline{O} \qquad (2.2.14)$$

It may be appreciated that a highly basic slag and low bath oxygen content encourages desulphurization. An equation

has been quoted (159) in terms of a series of parameters by which the sulphur level in the refined steel may be predicted as follows:

$$\%\underline{S} = 0.11 + 23.6S_1 - 0.003V - 0.003Fe - 0.00005T$$

$\underline{S}$ = turndown sulphur,

S_1 = sulphur in metallic charge, (tons/ton of metallic charge)

V = basic (molar) ratio,

Fe = iron in slag,

T = turndown temperature.

Again, a highly basic slag is required. High slag iron and temperature also favour desulphurization. The last two requirements (high slag FeO and temperature) are achieved towards the end of the blow. Even with a highly basic fluid slag, sulphur elimination in the BOF vessel is relatively inefficient (20).

2.3 Slag Constitution and Phase Diagrams.

In the following section an outline is made of the most important features of phase equilibria between the different oxides present in the slags used in the present work.

Practical experience during steelmaking has shown that slag formation varies for each particular practice as well as for melts made under similar circumstances (as shown in figure 3) since it depends on factors such as oxygen flow rate, lance height, starting temperature, lime dissolution rate and flux additions.

In selecting a slag which may be said to be representative of steelmaking slags the most important components have to be

considered. It is well known that lime is the only oxide which is added to impart basic properties to the slag. The most important acid oxide is silica, and, due to the amount of iron present and oxygen blown into the system, iron oxide is a major component of the slag formed.

Although other oxides may be found in the slag as shown in table I, difficulty arises in representing in an adequate and simple way the phase diagrams with more than three components. It has become a common practice to group the oxide components mainly on the basis of their chemical behaviour (i.e. basic or acid components (21,22,23), although it may not be true in a strict sense. The period of the blow of a particular interest is the first seven minutes during which time an acid slag, Fayalite, is formed which contributes to their rapid fluxing of lime. Due to the acidic character of this initial slag it is thought that severe lining wear occurs during this period either by chemical reaction and/or due to the fluidity of the slag causing severe abrasion. As discussed later in section (2.6) the initial stages for oxygen steelmaking require close control of the developing slag.

Having therefore Lime, Silica and Iron Oxide as major constituents of Basic Oxygen Steelmaking, the system $FeO-SiO_2$ or, more specifically Fayalite ($2FeO.SiO_2$) was selected as most convenient to initiate the present work. Additions of lime would then follow in such a way as to move the chemical composition of the system close to the line joining ($2FeO.SiO_2$ - $2CaO.SiO_2$).

Initial description of single oxide systems of FeO, SiO_2 and CaO are briefly reviewed following with combined systems of FeO-SiO_2; Fe_2O_3-CaO and finally the ternary phase diagram of CaO-FeO-SiO_2.

2.3.1 The Fe-O System.

Oxides of iron have been widely studied due to their importance in ironmaking, steelmaking and refining of steel. Studies on the stability ranges of the condensed phase (liquid and solid) existing among metallic and liquid iron, and the corresponding oxides formed have been thoroughly made. The most valuable contribution in the study of this important system was made by Darken and Gurry (24,25).

These authors summarized results of earlier work in addition to providing a large amount of new data. Figure 4 gives the temperature-composition phase diagram together with equilibrium partial pressure of oxygen. The solubility of oxygen in liquid iron under slags containing essentially iron-oxide was determined by Chipman et al. (26,27) and the variation of solubility with temperature was found to be represented by: $\log(\%O) = (-6320/T) + 2.734$, at 1600° C, %O =.23% and %O = 0.052% at 1300° C.

There are three well known compounds in the system, (see Figure 4), Hematite-(Fe_2O_3), Magnetite (Fe_3O_4) and Wustite, whose composition is represented as FeO. From figure 4a it is seen that a maximum solubility of 0.16% Oxygen is reached at the eutectic 1524° C and above this concentration a liquid oxide is formed with 22.6% Oxygen. The stoichiometric ferrous oxide

does not exist and wustite, which has a variable composition, is not stable below 560° C but decomposes to form magnetite and metallic iron. Wustite in equilibrium with iron corresponds to a composition of $Fe_{0.95}O$ (28). The situation in the wustite field is one which involves changes in the oxidation state. The equilibrium is represented by:

$$MO_{x(\text{in soln.})} = MO_{y(\text{in soln.})} + \frac{X - Y}{2} \; O_{2(\text{gas})}$$

The metal M occurs in two different states of oxidation M^{2x} and M^{2y}. Any change occurring in the oxygen pressure will cause a change in the ratio M^{2x}/M^{2y} in the condensed phase and vice versa. The oxygen pressure up to liquidus temperature within the wustite region (fig.4) are very low and are a function of the Fe^{3+}/Fe^{2+} ratio, increasing rapidly as this ratio increases. In the equilibrium of wustite and magnetite the latter has a constant composition Fe_3O_4 but, in the presence of hematite (Fe_2O_3) the magnetite becomes depleted in oxygen with increasing temperature. The oxygen isobars are straight lines parallel to the composition axis where two condensed phases coexist in equilibrium. Where one condensed phase is present in addition to the gas phase, the oxygen isobars run diagonally, indicating that temperature and oxygen pressure can vary simultaneously. This is readily determined by applying the Phase rule (29) (F=C+2-P=2+2-2=2).

The phase diagram in figure 4 can thus be used to determine the equilibrium phases in the Fe-O system that would appear when for example a constant pressure is maintained in

the system or, when the chemical composition is constant and oxygen partial pressure is variable.

Oxygen pressures of the gas phase decreases continuously with decrease in temperature from 10^{-2} atm at 1700° C to about 10^{-26} atm at 560° C (30). At 1300 the oxygen potential, partial pressure, is seen to be of the order of 10^{-11} to 10^{-10} near the gamma-iron + wustite-wustite interphase. An increase in temperature to 1600° C increases the oxygen pressure to 10^{-8} to 10^{-7} at approximately the same composition.

The importance for iron oxidation during oxygen steel-making lies mainly in the fact that it results in a serious loss of iron units into the slag and fume. On the other hand, FeO in the slag is essential due to its influence on fluxing properties, liquidus temperature, viscosities of slags and sulphur removal capacity.

2.3.2 The Fe-O-Si System.

Initial studies carried out on the equilibrium between silicon and oxygen in liquid iron were concerned more with the role played by silicon as deoxidizer of steel. Gockcen and Chipman (32,31) studied the equilibrium reaction: $SiO_2 = \underline{Si} + 2O$ in H_2O/H_2 atmospheres at 1600° C in liquid iron. Comparing their results with previous work they established that the constant for the reaction depended on the activity of oxygen which was strongly diminished with small amounts of silicon additions. The so-called silicon deoxidation constant, the product $[\%Si] \times [\%O]^2$ indicated a constant product of 2.8×10^{-5} for a very wide range of compositions. The greatest

deviations were found at very low silicon contents, where the silicon analysis is inaccurate or at very high silicon, where the oxygen-concentration is low and rather uncertain (32). Figure 5 represents the isothermal section of the iron rich corner of the ternary system at 1600° C.

For the conditions found under steelmaking, the condensed phases which form diminish the range of interest of the ternary diagram to that bounded by the $FeO-Fe_2O_3-SiO_2$ phase field which is a section of the Fe-O-Si system as indicated in figure 6.

Different aspects of the system have been investigated and great amounts of data are now available. The data are amplified by the binary section representing the $FeO-SiO_2$ shown in figure 7, obtained by Bowen and Schairer (33). It is shown that there are two crystalline forms of silica; cristobalite above 1470° C and tridymite below this same temperature. The liquidus curve rises steeply from the eutectic at 1178° C with about 40% FeO up to 1698° C, indicating immiscibility between FeO and silica. An intermediate compound, Fayalite, is formed at 1205° C which in turn forms a eutectic with wustite at 1177° C and with tridymite at 1178° C. Bowen and Schairer pointed out initially (33) that ferric oxide was present in all the equilibrium melts studied by them. Thus, their data are for limiting mixtures with minimum contents of ferric iron.

Darken (34) investigated the fusion temperature of iron oxide in contact with silica under CO_2/CO ratio of 20.8 to pure oxygen, the temperature changed from 1131° C to 1447° C

for the equilibrium of silica, magnetite, melt, gas. The univariant equilibrium point silica, fayalite, melt, gas was found to have melting points of 1120° C and 1130° C for CO_2/CO ratios of 14.1 and 4.02 respectively.

The inconvenience of the system represented on a pressure-temperature coordinate, is that no detail is given for the chemical composition of the condensed phases.

Liquidus surfaces in the $FeO-Fe_2O_3-SiO_2$ system from 1250° C to 1400° C and 1 atm pressure have been determined by equilibrating, quenching and microscopic examination of the phases present (35). The results obtained showed that ferric oxide in amounts of 10 to 12% has little effect on the freezing point of fayalite; but progressively increases as the Fe_2O_3 content increases. For slag saturated with silica, the SiO_2/FeO ratio is nearly independent of the Fe_2O_3 content of the slag. A. Muan (35) obtained liquidus data at oxygen pressures ranging from $10^{-10.9}$ to 1 atm. Within the ranges studied by Muan two invariant points were defined at 1140° C and at 1150° C with oxygen partial pressures of 10^{-9} and $10^{-9.9}$ atm.

Thermodynamic studies on the activity of the different components of the iron oxide-silica system have been carried out in contact with solid iron (36,37) and silica (38) under CO_2-CO and H_2-H_2O atmospheres. By determining the ratios of CO_2/CO and H_2/H_2O in equilibrium with the iron oxide silica system a measurement of the oxidation state of the slag is obtained (38).

For the chemical analysis in the present work with Fayalite the oxygen pressures vary from 10^{-10} to 10^{-12} as seen in figure 8. The free energy of formation for $2FeO.SiO_2$ (F_2S) is given by Bodsworth (12) as:

$$2Fe + O_2 + SiO_2 = 2FeO.SiO_2$$

$$\Delta G^o = -85 \text{ Kcal} = RT\ln P_{O_2}$$

and the partial pressure is calculated as 1.54×10^{-12} atm.

By comparing the latter oxygen pressure with those in the FeO system at 1300° C it is seen that their orders of magnitude are about the same.

With respect to activities of FeO, in the Fe - O system a_{FeO} may be regarded as 1 but it is markedly decreased by additions of silica (36,37) in the temperature range 1250-1560° C. The relation of a_{FeO} versus wt% SiO_2 is shown in figure 9. For the compositions of fayalite used in this work the activities of iron oxide ranges from about 0.42 to 0.52. Schuhmann has related the activity of iron oxide to oxygen pressure for the closed melt area at 1300° C in figure 8. For the melt-wustite equilibrium and partial pressure of 10^{-11} atm a_{FeO} varies from .39 to .69 (39).

2.3.3 The Lime-Silica System.

The phase diagram shown in figure 10 has been widely investigated. The most important observation is the steep rise of the liquidus curve from the eutectic (1436° C) with about 36% CaO to a plateau in which two liquids are found in equilibrium with cristobalite (1707° C). In this region a

big increase in temperature (1436 to 1706° C) will cause an increase of only 3% liquid (69). Four polymorphic forms of Ca_2SiO_4 are well known to form, known as α,- α', γ and β. Except for β-C_2S all other three forms are considered to exist as stable forms. Dicalcium silicate (C_2S) is formed as the initial product in solid state reactions between lime and silica over a wide range of compositions and reacts relatively slowly with excess of either of one components to form CS, C_3S_2 or C_3S (42). In the phase diagram of figure 10 the straight lines between two adjacent areas are a result from different Ca_2SiO_4 modifications being present in the two areas. Horizontal lines denote modifications changes in SiO_2 and in $CaSiO_3$ (43).

The free energy of formation of C_2S is obtained from Ellingham diagrams (12) for the reaction $2Ca + O_2 + SiO_2 = 2CaO.SiO_2$ (2.3.3.1) ΔG^o = -260 Kcal. The oxygen partial pressure is calculated at 1300° C to be 5.24×10^{-37} atm. This indicates the great stability of dicalciumsilicate. At 1400° C and 1600° C the oxygen partial pressures correspond to 1.07×10^{-34} and 4.54×10^{-31} atm respectively.

2.3.4 The Lime-Iron Oxide System.

The equilibrium relations have been studied at different oxygen pressures in great detail (43,44,45). Two diagrams are shown in figure 11. in contact with metallic iron and air. The CaO-FeO is not a true binary above 10% FeO due to the presence of Fe_2O_3. In both systems the liquidus and solidus lines in the central part of the systems are well below the

1300° C isotherm, which give an indication of the fluxing power of iron oxides for lime. It can also be seen that by increasing oxygen pressure a number of intermediate phases are formed known as calcium ferrites (C_2F,CF,CF_2).

At temperatures above 1200° C under slightly oxidizing conditions, a liquid oxide is formed but if the solubility of iron oxide is exceeded under reducing conditions, metallic iron is formed. At all oxygen pressures, lime increases the stability of the ferric state. It has been found that FeO has a stabilizing effect on lime with respect to hydration by moisture in air (46).

The agglomeration of L.D. dust with limestone into briquettes and pellets prior to calcination has been tried in Germany (47). Compared with heats using only lime, the charging of the special lime pellets resulted in a considerable acceleration of dephosphorisation. Millscale is another oxide flux used in steelmaking (48). Swedish ore (86.3% Fe_2O_3-9.8%FeO) has been proved to be a good lime flux (49). Ilmenite (52%FeO_x,33%TiO_2) has shown good fluxing properties (48a) although it is suggested not to be as good as fluorspar even with a 2:1 replacment ratio (50).

2.3.5 The Lime-Iron Oxide-Silica System.

From the previous description of binary diagrams it was mentioned that neither the FeO-SiO_2 nor the CaO-FeO systems form true binaries. Consequently the ternary phase diagram CaO-FeO-SiO_2, which is shown in figure 12, cannot be considered a true ternary diagram but should be regarded as a curved plane in the quaternary CaO-FeO-Fe_2O_3-SiO_2 system. Most investigators

carried out their experiments in iron crucibles (33,44,36,37) and therefore the quaternary plane and associated ferric iron concentrations correspond to equilibrium with pure iron. The system $CaO-FeO-Fe_2O_3-SiO_2$ is not well enough known to permit portrayal of a tetrahedral form of phase relations (43) and is further complicated by the fact that the method by which FeO and Fe_2O_3 have been made to represent total FeO(Fe_TO) have been different between different workers. The difference in plotting compositions are negligible (44,36) when the Fe_2O_3 contents are of the order of 3% but greatly differ for contents near 20%Fe_2O_3. The variations of Fe_2O_3 content within the $CaO-'FeO'-SiO_2$ systems are shown in figure 13. The ferric oxide contents range from 0.5% at about 10% FeO to 17.5% adjacent to the FeO-CaO binary. When studying crystallization paths it has been pointed out (44) that anomalies found near the FeO corner are probably due to the presence of high Fe_2O_3 as opposed to the SiO_2 corner.

The ternary diagram portrays a large number of crystalline phases as compared to other systems (e.g. MgO and Al_2O_3 with $FeO-SiO_2$) due to the relatively limited extent of solid solution among these phases, however, relatively low temperatures prevail over a large area of the diagram.

It can be seen from figure 12 that as the FeO content decreases and CaO content increases the liquidus temperature slightly increases up to 1400° C. Once the 1400° C isotherm has been reached the temperature increases rapidly and enters into the dicalcium silicate-(Ca_2SiO_4) region. Along the $2FeO.SiO_2-2CaO.SiO_2$ join the temperature decreases from fayalite

(1205° C melting temperature) to 1150° C at about 8% CaO. As the lime content increases to 18%CaO a plateau is crossed in which the liquidus temperature remains at 1150° C. On further increasing the lime content the liquidus temperature increases slowly crossing the CaO-FeO-SiO_2 at 1211° C (44) and ultimately joining the 1300° C isotherm at about 35% CaO. Beyond this latter lime content a steep increase in temperature takes place with small CaO increases entering into the dicalcium silicate region.

The effect of the oxygen potentials has been shown by Phillips and Muan (45) to have a marked effect upon the ternary diagram from studies carried out in equilibrium with air (0.21 atm.). Due to the increase in oxygen potential two new phases appear in the diagram (hematite and magnetite). This is expected when the iron oxide phases in air (Fig.11) and the oxygen isobars in the FeO-Fe_2O_3-SiO_2 system are considered (Fig.6). The CaO-Fe_2O_3-SiO_2 ternary is shown in figure 14.

Studies on the activity of iron oxide were first carried out by Taylor and Chipman (22) using a rotating magnesia crucible at 1600° C. The activities were determined from measurements of the oxygen content of liquid iron in equilibrium with basic or acid slags, relative to the iron in equilibrium with pure iron oxide at the same temperature. Small amounts of impurities MnO, MgO, Al_2O_3 were present in the slag creating difficulties in distinguishing between the effect of these impurities and that due to lime. A later study by Chipman et al. (51) established that in basic slags CaO and

MgO are not equivalent and that substitution of MgO for CaO on a molar basis increases the iron-oxide activity.

Iso-activities have been replotted or recalculated for FeO, CaO and SiO_2 by various authors (52, 53, 38). The results of Elliot (52) showed a very marked positive deviation from ideality along the FeO-$2CaO.SiO_2$ join for a slag system of FeO-(CaO + MgO)-SiO_2. Turkdogan and Pearson (53) determined the activity surface for ferrous oxide in the system FeO-(CaO+MgO+MnO)-(SiO_2+P_2O_5) in the 1550 to 1650° C temperature range and no temperature dependence could be detected as had been concluded by Taylor and Chipman (22).

Equilibrium measurements between hydrogen-steam mixtures and molten slags in solid iron crucibles have been used to determine the activity of ferrous oxide in CaO-FeO-SiO_2 type slags with temperature ranging from 1265° C to 1365° C (36). No temperature dependence was found in the presence of silica alone but the iron oxide activity was very temperature dependent in the presence of lime and silica. At constant lime content the activity coefficient is raised with increasing temperature in melts with high silica content, but is lowered at low silica concentrations. With low silica content CaO tends to increase the content and stability of the ferric state and may therefore combine to form $Ca_2Fe_2O_5$(C_2F), $CaFe_2O_4$(CF) $CaFe_4O_7$(CF_2) as previously discussed (see 2.3.4). Johnson and Muan (54) studied the activity-composition relations of CaO-FeO-SiO_2 system in contact with metallic iron at 1080° C. The same authors found that the orthosilicate solid solution

$2CaO.SiO_2$-$2FeO.SiO_2$ showed a strong positive deviation from ideality at both ends of the system, reflecting the difficulty of permutating large Ca^{2+} ions (0.99Å) with small Fe^{2+}(0.76Å) ions.

In the central part of the system a pronounced negative deviation from ideality was found for the activity-composition curve, reflecting a strong tendency towards formation of a compound in the vicinity of the $CaFeSiO_4$($CaO.FeO,SiO_2$) composition. A mixture of this composition was considered as but one member of a solid-solution series rather than a distinct compound (54). From silicate phase diagrams and thermal data, Richardson (55) concluded that mixtures of two molten metasilicates behave 'near to ideal' mixing (relative to separate silicates) even when large differences exist between the cations. In orthosilicates mixing is nearly ideal when the cations sizes are much the same ($FeSiO_4$-Mg_2SiO_4) but far from ideal when they are significantly different, such as Fe_2SiO_4-Ca_2SiO_4,Mn_2SiO_4-Ca_2SiO_4.

A concept which has been introduced through studies of polymerization of liquid silicates is that of a dimerization coefficient k_{1n} introduced by Toop and Samis (56,57). Three forms of oxygen are considered to exist in silicate melts: singly bounded (O^-), doubly bonded (O^o) and free ion (O^{2-}). Equilibrium between the three bonds is represented as

$$2O^- = O^o + O^{2-}$$

at equilibrium $$k = \frac{(O^o)\ (O^{2-})}{(O^-)^2}$$

k is not really an equilibrium constant and depends on composition (58). Masson has derived an expression for the activity of MO as a function of composition in binary in $MO-SiO_2$ melts when linear silicate chains exist and when other silicate configurations exist. The value for k_{11} has been calculated for various MO oxides (60) (e.g. CaO: k_{11} = 0.0016, 2.6 at 1600° C and 1450° C.; FeO: k_{11} = 1.0, 0.7 at 1600° C and 1300° C respectively).

The polymerization constant may be used to assess mixing behaviours of different meta- and orthosilicates. In the case of $CaO-SiO_2$ with either $MnO-SiO_2$ or $FeO-SiO_2$, ideal mixing cannot be expected because large differences in ionic constitution and in k_{11} values exist. Partial replacement of M'O in a binary melt $M'O-SiO_2$ by an oxide M''O of lower k_{11} value causes a decrease in the degree of polymerization, and hence in the value k_{11} for the ternary; replacement of M''O in the binary $M''O-SiO_2$ to the same extent by M'O does not yield a correspondingly large increase in k_{11} for the ternary. When two melts of equal silica content are mixed the activity coefficient is raised for the oxide of higher k_{11}, and vice versa (59). For example γFeO activity is raised by the addition of CaO to $FeO-SiO_2$ melts and is a maximum along the iron oxide-dicalcium silicate join in the ternary. γ_{MnO} in $CaO-MnO-SiO_2$ is consistently lower than the corresponding γ_{FeO} at similar compositions (k_{11} for FeO is greater than for MnO).

Among the many applications for calculating activities (61,62), one of the most important is to enable iron oxide

activity to be calculated with a high degree of accuracy. By convention the oxidizing power of a slag is reported in terms of its iron oxide activity, a_{FeO}, and not by its equilibrium oxygen partial pressure, p_{O_2}, which might be expected as more suitable (11). However, the two parameters are directly proportional to one another, as iron oxide has a far higher oxygen pressure than any other constituent in the slag. Therefore, the other constituents in the slag make a negligible contribution to the slag's oxygen partial pressure (11,12,63), i.e.

$p_{O_2} = a_{FeO} \cdot p^o_{O_2}$ where $p^o_{O_2}$ is the oxygen pressure of saturated iron, or of iron oxide in equilibrium with iron at the temperature considered (11).

2.4 The Oxygen Jet.

Extensive use of cold models has been made to study the jet-liquid interaction due to inherent practical difficulties of making precise measurements on systems at high temperatures. Although conditions differ between industrial converters and those used in the laboratory, and results obtained from models cannot necessarily be directly applied, it is probable that broad analogies can be drawn.

Several modes of jet/liquid interaction have been distinguished (64,65). With a low jet momentum and/or a large nozzle height a slight depression is formed having a cylindrical symmetry about the jet axis. By increasing jet momentum and decreasing lance height the depression deepens and its surface becomes increasingly unstable and oscillates both laterally and

vertically. The depression is frequently surrounded by a raised lip or rim. A further increase in momentum causes liquid metal droplets to be torn off from the rim of the depression and become dispersed into the gas phase; this is referred to as "splashing". With further increase of momentum and/or reduced nozzle height, there is a deeper penetration of the jet into the bath and the total amount of splashing rises to a maximum and more vertical trajectories are observed. The impact crater becomes unstable at this time, oscillating asymetrically about the vertical axis of the nozzle and possibly dispersing gas bubbles into the liquid phase. This is known as the penetration mode. Great numbers of investigations have been carried out in jet-liquid interaction on which jet momentum, lance height, nozzle diameter and properties of liquid and gas phase have been correlated to the depression produced. A review of this topic has been made by A. Chatterjee and Bradshaw (66).

The shape and dimensions of this depression have also an important effect on slag formation (67). A concept which has developed from plant practice associated with jet-liquid interaction is that of jet hardness.

Although it is a mathematical inexact parameter, hardness describes the apparent momentum with which the oxygen stream strikes the surface of the bath. The "hard" jet produces a relatively deep penetration into the metal bath, whereas the "soft" jet is more widespread over the surface of the bath (67). In relation to refining reaction, hardness can be regarded

as the ratio: [The tendency of oxygen to combine with carbon to form CO]/[the tendency of oxygen to combine with other element to form slag].

There is not a generally accepted method for the calculation of depth of jet penetration into the bath.

Experimental observations of chemical and thermal gradients in an experimental LD have been made [68]. These authors found that variations, both thermal and chemical were less the deeper the lance was introduced. A metal circulation pattern was determined as being upwards from the jet cavity and radially outward to the surface. By introducing a spray collector above the bath, it was found that hard blowing causes the ejections of droplets which, after five minutes of blowing, weighed about the same as the weight remaining in the bath.

2.5 Foams and Emulsions in steelmaking.

Systems consisting of small liquid droplets (liquid II) or gas bubbles embedded in a liquid medium (liquid I), may be called emulsions when the distances separating neighbouring droplets or bubbles are large enough to allow the independent movement of the said drops or bubbles. When the volume of the liquid medium in a gas-liquid emulsion is small compared with the total volume of the gas bubbles, the medium will be present only as thin films separating the adjacent bubbles. These cannot move freely and the system is then called a foam [70].

For many years foaming of slag was known to take place in Open Hearth Steelmaking (71,72), but the causes of slag foaming in general were not known. Foamy slags were considered a serious problem since a barrier is created and the distance which oxygen has to travel to reach the slag metal interface is increased. The foam also acts as a heat reflecting surface causing overheating of the furnace roof and outgoing end zones. A reduction in heat input is therefore necessary causing a change of burner operation.

Existence of foams in the Open Hearth according to Davis (73), is marked by three developments. 1) evolution of bubbles; 2) stabilization of the bubble structure, and 3) instability and collapse of the foam. Considering only processes 1 and 2, a 'static' foam is obtained which will last without any further gas supply. The third process is characteristic of a 'dynamic' foam, i.e., a foam which soon collapses if the gas supply is stopped.

The foam will collapse more readily if the bubbles can rise and escape quickly out of the upper surface of the slag. Such breaking through the liquid surface will be more readily facilitated by low surface tension. In addition, the rate of collapse of the foam will depend upon liquid viscosity. If the honeycombe structure of bubbles is well established, the liquid phase will drain downwards out of the foam. A viscous liquid will drain to the mother pool more slowly than a fluid medium.

The occurrence and classification of foaming slags was presented by Kitchner and Cooper in 1959 (74). A scheme was

developed on the basis of the order of "stability". Unstable foams are constantly breaking down as the liquid drains from between the bubbles. In metastable foams the process of drainage of liquid from between the bubbles eventually stops and the foam would persist indefinitely if absolute protection from disturbing influences (vibrations, draught, evaporation, radiant heat, temperature differences, dust, impurities) is given.

It is generally known that pure liquids do not foam but, can be caused to form a metastable foam with solutes which lower the surface tension (γ) strongly in dilute solutions, i.e. the highly surface active substances (75). Surfactants lower the surface tension of a liquid solvent by being adsorbed at the surface and favour the formation and durability of emulsions and foams even in a very fluid medium.

Measurements of surface tension for various binary and ternary oxide systems have been carried out (75,76,77). A review on interfacial phenomena in metal and metal oxide systems has also been published. (78). A noticeable feature is that the surface tension of slag foams are large compared to water and other common room temperature liquids. These high surface energies indicate that slag foams are energetically very unstable. Therefore, by considering surface tension alone, slags are difficult to foam compared to other liquids. However, the degree of foaming is influenced by other factors and properties.

In oxygen steelmaking, foaming of slag is initiated by a rapid supply of reactive gas from direct blowing and from

decarburization between the oxidizing slag and metal. The multiphase bubble dispersions encountered in oxygen steelmaking consists of gas bubbles, droplets of metal, minute solid oxide particles (dicalcium silicate) and large lumps (lime) suspended in the liquid slag. The foam is termed to be dynamic, in that its stability depends upon the continued evolution of CO from dispersed droplets (i.e. generation of gas) and to a lesser extent from the bulk bath. If gas evolution ceases or is reduced significantly, then the foam collapses (70).

There is not much work published on physical properties of slags typical of oxygen steelmaking. Evidence that most of the refining was taking place in a slag-metal emulsion, and not in the jet impinging zone was obtained from actual LD-AC and LD plant operation by various authors as is discussed in section 2.6.

2.6 Course of Refining.

The progress of a BOS blow is conventionally divided into three periods based on carbon removal rate. This somewhat idealized representation of the three periods is shown in figure 3a. Similar courses are shown from various plant operations. The three stages correspond to increasing, constant, and then decreasing carbon removal rates and represent approximately 40%, 40% and 20% of the total blowing period (79). The three periods have been found suitable for actual operation control even though the paths followed differ from blow to blow. Li et al. have shown that different decarburization paths can

exist even when blowing Fe-C melts (80). Formation of the emulsion begins almost as soon as refining itself. The oxygen jet on striking the metal bath surface causes a depression and eventually the momentum is sufficiently increased for splashing to occur with metal droplets being thrown up in the gas or slag. In these early stages the bath temperature is low and reaches 1400° C after 40% (82) or 60% (85) of the blowing time.

The early refining path has been shown to be influenced by the oxygen flux across the gas metal interface. Although silicon is the most readily oxidized of the species present the removal of iron is almost certainly promoted by its high concentration. The difficulty of transferring other solute elements to the reaction zone does not allow full utilization of the oxygen supply. Therefore, small amounts of CO are formed, and after combustion in the vessel mouth, analysis of the waste gas has shown the presence of small quantities of CO_2 (81).

Bardenheur et al. (82) have shown that the temperature of the slag reaches a level of up to 300° C above the metal bath temperature after the initial quarter of the blowing time. Much of the heat released by silicon oxidation is produced in the slag itself by oxidation of suspended droplets in the slag. From plant practice operation Meyer (86,87) has determined the amount of metal droplets by weight in the slag to be from 45-80% after 6-7 min of blowing. As is generally known the iron oxide increases with the lance distance from the bath during the first minutes of the blow. The first

slags formed are rich in FeO, MnO and SiO_2 and low in CaO. They correspond to the Olivine and Wustite range where the liquidus temperatures are of the order of 1250° C as shown in the FeO-CaO-SiO_2 phase diagram (see figure 12).

As the blow progresses through the first stage the rate of decarburization steadily increases. If the decarburization reaction is slow (i.e. soft blow) large amounts of iron will be oxidized. In later stages the oxygen from the slag reacts with carbon supplementing the oxygen-carbon reaction with the lance and sudden evolution of large quantites of gas causes the slag foam to overflow (i.e. slopping takes place). Trentini (83) has pointed out that metallic droplets from overflown slags are found to be more decarburized than the metallic bath. In addition, the smaller the droplet, the lower the carbon contents (84).

When a hard blow is initially used a faster rate of decarburization will be obtained and since less oxygen is used for iron oxidation this will cause the slag to rapidly approach the orthosilicate region before the slag is above 1400° C and a suspension in the slag of solid orthosilicate particles can occur (83). The presence of these dispersed particles gives rise to an effective increase in the viscosity of the emulsion and will make overflowing more likely. The slags are deficient in iron oxide content, are viscous, and are generally referred to as 'dry' slags.

As the temperature (82) volume and fluidity of liquid slags increases the decarburization curve builds up as decarburization within the slag becomes more important. It

is only at the end of this first stage when silicon oxidation is almost complete that the rate of decarburization reaches its greatest value and the emulsion is fully developed. This event outlines the importance of the operation and clearly shows that unless correct distribution of oxygen is achieved to ensure sufficient but not excessive formation of slag oxides, either satisfactory slag formation may be retarded or unstable refining may result. Figures 15a and 15b show the paths followed by the slags during actual oxygen steelmaking.

The most important reaction during the second stage is decarburization the rate of which is so high that virtually all of the oxygen supplied is consumed by such reaction. Ichione et al. [88] have found the decarburization efficiency of oxygen in this period to be from 80 to 100%. How such high refining rates could be achieved has been the subject of some speculation. At one point it was believed that excessively high temperatures in the jet impingement zone accounted for the rapid mass transfer [89]. More recently attention has been focused on the role of the emulsion and despite obvious practical difficulties, knowledge of the nature of emulsions has been extended. Meyer et al. [86] found by chemical analysis of ejected metal droplets from 230 t vessel, that the metal droplets are always lower in carbon than the bulk metal bath, sometimes by as much as 1.5%C. The oxygen contents were always higher than that required for equilibrium with CO. At the height of refining up to 30% of the metallic charge was dispersed in the emulsion as droplets of sizes between 14 and 100 mesh. This led to the theory that the

majority of refining was carried out in a slag-metal emulsion where the surface area of metal droplets in the slag could be as high as 600 m^2/ton of charged metal.

Meyer's concept of decarburization was that oxygen was pumped into the metal droplets from the oxidizing slag so that carbon monoxide equilibrium pressure of up to 100 atmospheres or more can build up. The droplet comes into contact with a CO bubble into which its own carbon monoxide is unloaded by explosive nucleation of CO within the droplet or possibly by nucleation at a metal/solid (lime particles) interface.

In view of the enormous slag-metal interfacial area and a plausible mechanism for carbon removal in the emulsion, it does not seem unreasonable that decarburization should proceed at the high rates observed and account for an estimated two thirds of the carbon removal (87).

Kootz and Altgeld (90) have proposed an alternative and conflicting mechanism. Under the oxygen jet the CO generated at the surface or adjacent to the hot spot circulates radially outwards, taking with it the bath particles of the surface. This effect will cause bath circulation and the creation of new reaction surfaces. Bubbles of CO are heterogeneously nucleated at the metal-slag interface, the reaction continuing as the metal bath circulates outwards towards the vessel wall. The same authors (90) found that in BOF and basic Bessemer steelmaking, decarburization occurred even when the slag became so viscous that reactions in the slag-metal emulsions could no

longer proceed. Price [79] has concluded that the calculations of Meyer as to the amount of refining in the slag were an overestimation. Price's estimate places more emphasis on bath decarburization with about 35% of refining taking place via the emulsion.

As decarburization is proceeding at its fastest rates, other changes in metal composition are occurring in a less dramatic way as indicated in figure 1. Early in the second period silicon and manganese contents have essentially obtained their lowest level. Further into stage II, however, manganese reversion from slag to metal occurs probably due to the effect of changes in temperature and composition of the slag upon the activity of manganese oxide. Turkdogan has suggested that reversion is directly associated with the cessation of silicon oxidation which in stage I prevents manganese from coming into equilibrium with the bulk slag due to the formation of $FeO.MnO.SiO_2$ particles via a vapour phase reaction. [20]

The third stage of the blow commences when the carbon content is about 0.3%, although this value can vary according to temperature and blowing practice. The rate determining step for decarburization is then beginning to change from oxygen supply to the metal to carbon diffusion in the metal [86]. Carbon supply for reaction becomes predominant at about 0.1%C, and the rate of decarburization is no longer dependent on the rate of oxygen supply through the lance, except insofar as the action of the jet supplies momentum to maintain turbulence

and foam in the bath. As the evolution of carbon monoxide decreases. the emulsion collapses and the interaction between droplets and slag is reduced.

The failure of the decarburization reaction to fully utilize the oxygen supply at the end of the blow results in oxidation of iron and the FeO content of the slag rises. Also, under these conditions of increasing slag bulk and FeO content manganese may again be oxidized into the slag.

Although sulphur removal is relatively steady throughout the blow as shown in figure 1, it is observed that basicity greatly increases towards the end part of the blow, slag bulk increases and therefore sulphur removal rate is increased (85).

2.7 Decarburization.

The importance of the decarburization reaction taking place in steelmaking lies in the fact that control of the process is mainly through this reaction. Of the various reactions which take place during refining it is the oxidation of carbon which, through generation of carbon monoxide gas influences to a greater extent the foaming of the slag creating a slag-metal-gas emulsion. If the mechanism of decarburization were made clear, the refining process could be effectively controlled. In view of its practical importance, the kinetics of decarburization has been widely studied.

From previous investigation of the kinetics of decarburization of iron-carbon melts the main experimental methods which outstand may be broadly divided into three sections.

The first experiments were carried out by reacting melts contained in static crucibles and a stream of gas or gases of known chemical composition which were blown on to the melt at a known rate and temperature. The drawback of this type of arrangement has been the degree contamination attainable by the melt from the recipient crucible used. A second and fairly recent technique has been the use of electro-magnetic levitation. This consists in the melting of a metallic alloy which is free from support under inert atmosphere and once a predetermined temperature is attained, a reactive gas is allowed to flow past the sample at a known rate. After the sample has been allowed to react the experiment is terminated by cutting off the power and the sample is cooled in less than one sec.

A third method consists of melting a metallic sample either from a wire of known composition or by electromagnetic means under inert atmosphere, and allowing the melted sample to fall freely into and through a reaction chamber.

Some of the most important results obtained by the above mentioned systems are outlined in subsequent sections.

2.7.1 Decarburization of Contained Melts.

Swisher and Turkdogan (91) carried out decarburization studies of Fe-C melts in CO_2-CO atmospheres. An Fe-1%C master alloy was contained in a 32 mm diameter recrystallized alumina crucible at one atm pressure and a temperature of 1580° C. Mixtures of CO_2-CO with a 0.02 ratio were used as reacting atmosphere and flowing at 1000 cc per minute. From their

observations these authors concluded that the rate of decarburization of the metal was controlled primarily by the transfer of oxygen or oxygen bearing species from the gas phase to the metal surface. Fruehan and Martonik (92) concluded that the rate controlling mechanism for high carbon contents was mass transfer in the gas film boundary layer near the liquid surface. These authors (92) carried out their experiments at 1527°C in recrystallized alumina boats, 40mmx10mm (in a horizontal furnace) and alumina or zirconia crucibles 20 mm diameter (in a horizontal furnace) with CO_2 and H_2 atmospheres. The rates of decarburization were measured by continuously measuring the weight change experienced by the metallic sample (Fe-4%C). The rates of decarburization at carbon levels lower than 0.5%C were found to be affected by carbon diffusion in the metal and at levels below 0.1%C diffusion control was the predominant mechanism. The rates of decarburization on molten Fe-C and Fe-C-X alloys with H_2O-Ar and CO_2-Ar gas mixtures have been studied by Ito and Sano (93). These authors concluded that the rates of decarburization were proportional to the partial pressure of the oxidant gas component prior to the formation of an oxide film on the melts surface. When the oxide film was present, the rate of decarburization varied with different oxides formed (MnO, Cr_2O_3, Al_2O_3 or SiO_2) and the amount of element (Mn, Cr, Al or Si) added to the melt. Recrystallized magnesia crucibles, 40mm internal diameter and 50mm high, or electro-fused zirconia crucibles were used by the above

authors. The effect of sulphur on the rate of decarburization of molten iron with 1-3%C and up to 3%S has been studied by Hayer and Whiteway (94) using Ar-O_2 at 1450° C. Their experimental results indicated a retarding effect on decarburization rate at sulphur levels of 0.3% but became less affected at higher sulphur levels. These authors concluded that the main rate-determining step was mass transport of oxidant (mainly CO_2 near the gas-metal interface) in the gas phase.

Blowing of CO_2 through a silica inlet with a 4.9 mm bore onto a carbon saturated or 3%C-iron between 1160° C and 1600° C was the system used by Sain and Belton (95). The gas inlet was maintained between 2 and 3 mm above the melt which was contained in an alumina crucible (16.3 mm internal diameter). A cemented graphite disc at the bottom of the crucible was used to maintain carbon saturation of the melt. The authors (95) found the slow step at high carbon contents to be independent of carbon concentration and first order with respect to carbon monoxide pressure. Their data were consistent with chemisorption process as the rate limiting step. Nomura and Mori (96) determined that in the concentration range above 0.05%C the rate of decarburization was influenced by mass transport in the gas phase and controlled by gaseous diffusion for carbon contents higher than 0.1 to 0.15% C.

For carbon contents below 0.05%C, the same authors (96) concluded that for CO_2/CO ratios below 0.25 the decarburization rate was controlled by chemical reaction ($CO_2 + \underline{C} = 2\ CO$ and

$\underline{C} + \underline{O} = CO$) and by mass transfer of carbon. The rates of absorption of CO onto and desorption from, liquid iron have been studied using a modified sieverts apparatus (97)(98). Parlee et al. (97) used liquid iron alloys containing from 0.15 to 4.4%C while King et al. (98) used carbon contents below 0.15%C. Parlee et al. postulated that the rate of the C-O reaction is controlled by oxygen diffusion across the relatively stagnant boundary layers at the gas-metal and crucible-metal interfaces. King et al. have shown that the rate of absorption for all carbon contents, and the rate of desorption from all alloys of medium carbon content, are compatible with rate control by transport of oxygen in the liquid. The rate of desorption from low carbon contents was found to be controlled by a slow surface reaction.

As can be seen from the above, most work on decarburization of contained melts are concerned with a reactive gas. Hazeldean et al. (99) on the other hand followed decarburization by passing an X-ray beam through the area containing the reacting system onto a screen and recording by video tape. A closed-ended alumina tube was used into which a slag of known composition was melted. Into this contained slag, droplets of Fe-C alloy were dispensed in the range from 1 to 3 g weight. A base slag of 47 wt% CaO, 38 wt% SiO_2 and 15 wt% Al_2O_3 was used and additions of 10, 20 or 30 wt% FeO, Fe_3O_4 or Fe_2O_3 were made prior to an experimental run. The use of Al_2O_3 in the slag was necessary to prevent corrosion of the tall crucibles. The same authors noted that an iron-carbon drop on entering the slag phase began

to react with it giving off carbon monoxide bubbles. Droplets of 3 g wt almost invariably remained at the bottom of the crucible although they appeared to rest on a cushion of gas. Smaller droplets however were floated up into the slag and foam phases where they tended to stay for considerable time bouncing up and down and from side to side. A gas halo was detected by the same authors who suggest that gas phase mass transfer is an essential step in the decarburization process although its contribution to the overall process is not known. Hazeldean et al. assumed that at high carbon concentrations, with the gas halo present, chemical reaction at the slag-gas interface with CO would lead to desorption of CO_2 into the gas phase. CO and CO_2 interdiffusion across the halo to the gas-metal interface would lead to desorption of CO_2 with accompanied dissolution of oxygen in the metal. At lower carbon contents internal nucleation took place giving rise to hollow droplets and they confirmed that nucleation of CO occurs not only on cooling but is an essential step which occurs during the decarburization reaction. For drops containing sulphur or phosphorus a retarding effect on gas evolution was found and thought to be caused by their surface active nature. Phosphorus additions to the slag aided the stabilization of the foam, possibly due to reduction of surface tension (see 2.5). When silicon and manganese were present an induction period was observed during which gas evolution was slow or did not occur at all.

The work by Hazeldean and coworkers is, to the best of the the author's knowledge, the only published study of decarburization

of iron alloys by oxidizing slags. Other equilibrium kinetic studies in this area have involved 1) decarburization of alloys without a slag present; 2) transfer of an element (e.g. sulphur, phosphorus) to an oxidizing complex slag where the element is not carbon, or 3) reduction of iron oxides by graphite.

2.7.2 Reduction of Iron Oxide by Graphite Crucibles

Few experimental results are found in the literature for molten iron oxide reduction. Some results have been obtained for the reduction of pure molten iron oxide by graphite (101) while others have been obtained from slags containing various amounts of iron oxide (100).

Dancy (101) measured rates of reaction of the pure liquid oxides FeO and Fe_3O_4, with 4.3% C alloy in a rotating MgO crucible. Dancy's results indicated that the reduction of FeO was of first order up to 80% reduction. Over the 30% initial reduction, the magnetite (Fe_3O_4) reaction was also interpreted as a first order process in the temperature range 1600 to 1840°C. The rates of reaction were extremely rapid indicated by 30% reduction for liquid Fe_3O_4 within 1 to 2 minutes. Due to the experimental procedure Dancy describes the reaction as of an ill-defined heterogeneous nature. An apparent activation energy was calculated from the maximum rates of reduction obtained and Dancy gives the values of -43.1 Kcal/mole for ferrous oxide and -37.3 Kcal/mol for magnetite.

Philbrook and Kirkbride (100) and Tarby and Philbrook (102) carried out experiments in slag-graphite and slag-metal-graphite

systems. The aim of the above authors was to determine the oxide reduction processes and to use the results of the slag-graphite reactions to adjust the results of the combined slag-metal graphite system.

Philbrook and Kirkbride (100) studied the reduction from blast furnace-type slags containing less than 5% ferrous oxide Their slags were melted in a high frequency induction furnace over carbon-saturated iron in stationary graphite crucibles (14 cm deep, 4.8 cm ID and 0.75 cm wall). The graphite crucibles were charged with 300 g of carbon saturated iron and either 65 or 100 g of slag (38% SiO_2, 15.4% Al_2O_3 and 47.1% CaO). Ferrous oxide was added as a prefused slag consisting of 73.6% FeO, 7.7% Al_2O_3 and 19% SiO_2, after reaching the required temperature of reaction. These latter slag additions were reported to have melted in less than one min. but a vigorous reaction proceeded for 1 to 2 min. after their introduction. The range of temperatures at which Philbrook and Kirkbride carried out their experiments was from 1430°C (8 experiments) to 1570°C (2 experiments); in two other experiments the temperature was uncertain. The time span for their experiments was up to 100 min. (1430°C) and up to 30 min (1570°C), depending on the initial ferrous oxide content of the slag used. Three of their experiments which were carried out at 1430°C did not contain any carbon-saturated iron. These experiments were therefore only for slag-graphite reaction. These authors (100) found that in slag-graphite reactions, the rate of FeO reduction was less than for slag-metal-graphite reactions. For a temperature increase of 140°C, from 1430 to 1570° C the rate of FeO reduction was found to increase only slightly.

From the above two effects these authors concluded that gas bubble nucleation was not a rate controlling step. If gas bubble nucleation was to be rate controlling, then the rate of reduction in slag-graphite reaction should have been faster than in slag-metal-graphite reactions. At the end of each run, metallic iron globules were observed by Philbrook and Kirkbride to be adhered to the crucible wall. In slag-metal experiments, the globules collected primarily at the gas-slag-graphite joint and in sufficient amount to form an almost continuous ring around the crucible wall. In runs with slag only, the beads were smaller and more evenly distributed throughout the slag-graphite interface. Metal drops were observed to be mainly next to the graphite wall and not in the body of the slag.

Although Philbrook and Kirkbride (100) carried out only a very small number of experiments they have, nevertheless, produced a lengthy discussion from their results. By using conventional methods of chemical kinetics, analyses were made to determine the apparent order of reaction. The reaction considered was:

$$FeO_{(slag)} + \underline{C} = Fe(liq) + CO_{(gas)}.$$

The order of reaction was found to vary from 1.6 to 2.3 with an average value of 2. The order of reaction was therefore inconsistent with the above equation. These authors (100) postulated the possibility for the true reaction to be that of a dissociation product as; $FeO \rightleftarrows Fe^* + O^*$. The asterisks indicating atoms or ions in the slag available

for reaction. Although this dissociation hypothesis is compatible with the ionic theory, the data of Philbrook and Kirkbride were insufficient to prove an ionic mechanism.

Tarby and Philbrook (102) carried out experiments similar to those of Philbrook and Kirkbride (100) at temperatures mainly from 1500 to 1575^{o} C, but also making additions of MnO-bearing slags. From their experiments with MnO slag-graphite reactions virtually no MnO was reduced after 160 min of reaction at 1500 or 1575^{o}C. In MnO slag-metal reactions the MnO was reduced from about 4% down to 1.5% in 40 min. Data for wt % FeO against time were omitted in their published work (102).

Tarby and Philbrook (102) pointed out that from the dependence of both the reaction rate and the apparent order of reaction on bubble stirring, as noted in their experiments, the rate controlling step was not primarily determined by an interfacial reaction. Therefore, mass transport models were considered. These authors suggested that the penetration theory may apply for their experiments. The penetration theory, proposed by Higbie (162) is treated in more detail in section 5.7. The reaction of iron oxide reduction was postulated to occur by the following sequence with oppositely charged ions;

$$Fe^{2+}(slag) + O^{2-}(slag) \xrightarrow{\text{transport}} (FeO) \rightleftarrows Fe(liq) + \underline{C}$$

$$\underline{C} + \underline{O} \xrightarrow{\text{transport}} (CO) \rightleftarrows CO(gas)$$

Where (FeO) and (CO) imply that transport of species must arrive in stoichiometric proportion to the reaction interface. The above model accounts for all possible reactants participating at a reaction site and conserves the electrical balance charges. From the mass transfer coefficients derived from the penetration theory these authors concluded the rate controlling step to be transport of reactants in the slag phase.

From the rate of decrease in MnO or FeO concentration in the slag the overall order of reaction was found to be zero for MnO but variable with temperature and slag composition for FeO. The nature of the values obtained for the order of reaction, i.e. variable and other than unity, was not consistent with a pseudo-first-order rate expression. This latter inconsistency led Tarby and Philbrook (102) to analyse their results by a differential method. From graphical investigation of the results of the differential method, these authors (102) indicated that the reduction processes could be described by two separate stages. The first stage of reaction had an apparent order of reaction with respect to concentrations of FeO and MnO which was greater than unity, while the second stage of reduction behaved as a pseudo first-order reaction with respect to concentrations.

Due to the dependence on flow conditions of the system during the first stage of reduction the authors were only able to propose a qualitative mass-transport-control mechanism consistent with kinetic behaviour. For the second stage of

reduction calculations were made for activation energies which were found to be from 12 to 46 kcal per mole for slag-metal reactions. With respect to mass transport, natural convection was adopted as the mechanism of mixing in the slag phase during the second stage of reaction.

Davies et al. (103) studied the reduction of ferrous oxide from $FeO-SiO_2$ and $FeO-CaO-SiO_2$ slags contained in crucibles made from either graphite or devolatilized coal over the temperature range 1400 to 1500° C. Iron oxide was added as Fe_2O_3, the analytical determinations were for total slag iron and the results expressed as %FeO. The kinetics measured were merely the rate of production of metallic iron from the slag. The results obtained were interpreted as zero- and first-order kinetics with respect to iron oxide concentration, but it was not possible for Davies et al. to distinguish between these two orders at high FeO concentrations. However, definite trends were detected towards first- and higher orders at low FeO concentrations. Appearance of slag surfaces from graphite crucibles reactions indicated that large CO bubbles were formed which caused visible disturbances on breaking through the surface. In coal crucibles little visible surface movement was detected. Lime additions were found to markedly reduce the reaction rate for the reduction of iron oxide.

Grievson and Turkdogan (104) studied the rate of oxidation of ferrous iron to ferric iron in pure molten iron oxide

by CO and CO_2 mixtures at 1550° C. The rate-controlling process was found to be the interdiffusion of iron and oxygen atoms within the melt. Fay Fun (105) studied the rate of ferrous oxide reduction with a graphite rod partially immersed in lime-silica slags contained in stationary magnesia crucibles. Although contamination from the MgO crucibles was present, Fay Fun compared his own results with previous workers and concluded that neither chemical rate of carbon gasification nor gas phase mass transfer could account for the rates observed, and, therefore pointed to an alternative method of convective transport of reactants and products and energy to explain the rate of reaction.

2.7.3 Decarburization of Levitated Drops

The development of the spray refining process by BISRA (106,18, 108) created means by which hot metal from the blast furnace could be rapidly refined. The process consists in the breaking up of the metal stream by high-velocity oxygen jets into a dispersion of metal droplets. The mechanism increases in this way the surface area through which reactions may take place. The spray of small droplets produced is refined in the turbulent spray, during free fall, on passing through the slag and finally in a receiving ladle (108).

The process prompted a series of investigations of metal droplet-gas reactions which have been carried out by levitation, by levitation and free fall and by melting a wire of known composition allowing the droplets formed to freely fall through a reacting gas. Levitation has been used by a number

of workers to study iron-carbon droplets reacting with a stream of oxidizing gas (109,110).

Baker et al. (109) studied decarburization of liquid iron carbon droplets levitated in CO_2 and O_2 (110) atmospheres using helium as diluent. Reaction times varied from 2 sec for runs using high flow rates of pure carbon dioxide to 20 min for those involving low flow rates or dilute carbon dioxide systems (109). In reactions with pure oxygen flow a flame front shrouded the specimen and, when the carbon concentration in the metal was low, ejections, swelling and temperature increase took place. The presence of oxide formation was observed just prior to a decreasing rate period. Their results have shown that the rate of decarburization at high carbon levels is independent of carbon concentration in the droplet. The results were shown to be consistent with control by gaseous diffusion except at low carbon concentrations (1%) where carbon diffusion within the droplet becomes the predominant rate controlling factor. From these findings (109,110) the carbon-oxygen reaction was shown to take place via two possible mechanisms. One mechanism was operative at high carbon concentrations involving surface reaction which caused no disruption of the droplet and the second mechanism involving a subsurface reaction, where carbon monoxide bubbles nucleated within the droplet leading to ejections of smaller droplets. Subsurface reaction was proposed to take place because the rate of carbon diffusion to the surface cannot keep pace with the rate of oxygen supply and some of the excess oxygen diffuses

into the specimen allowing the surface to become rich in oxygen. Thus carbon diffusion becomes significant and the rate of decarburization decreases from there on. This point corresponded to mixed control. The oxygen which does not dissolve in the melt or react with carbon at the surface forms iron oxide on the surface. These findings are in agreement with those of Distin et al. (111) who found that the transition from surface to subsurface reaction could occur at various compositions, down to 0.3%C, depending on the characteristic rate of decarburization while the first mechanism was operative. The iron carbon droplets began to boil as soon as a separate phase of iron oxide appeared on the surface but never at an earlier stage. On these bases carbon monoxide nucleation was proposed to be far less probable before the formation of a free oxide phase, than afterwards. The amounts of carbon and oxygen present in drops when they began to boil were such as would be in equilibrium with 10 - 40 atm pressure of carbon monoxide. Specimens containing 3.1%C and zero oxygen were spherical and showed no porosity Specimens taken just before the boil began contained 0.3%C, 0.07% O_2 and gave hollowed spheres. Distin (111) observed that once the boil commenced the rate of decarburization continued to be independent of carbon concentration until some lower carbon content was obtained. The cause was believed to be the increased surface area for reaction and the increased turbulence, associated with internal nucleation of carbon monoxide. Richardson (112) suggested a higher rate of carbon transport than Distin initially thought when the drop

starts to boil. It was suggested that slow chemical reaction at the interface (when carbon falls to low concentrations) prevented the oxygen being converted to carbon monoxide immediately on arrival. At this point the oxygen concentration is allowed to build up in the drop and free oxide appears on the drop surface. Richardson pointed out that when the oxygen in the drop reaches 0.5% the surface will be 97% covered with oxygen and thus carbon will virtually be squeezed out of the interface. As a result from the supersaturation of carbon monoxide in the metal, gas nucleates and new surface is created whereby the reaction can proceed. Thus oxygen will be converted to carbon monoxide almost as soon as it arrives but only after passing inside the drop.

Robertson (113,114) carried out studies on levitation of pure iron, iron-carbon and iron-carbon-silicon in pure oxygen. When pure iron was reacted with pure oxygen at 1600° C an oxide phase spread rapidly as a thin veil across the surface. This occurred in the first two or three milliseconds of reaction. After quenching of the specimens, the slag was determined as ferrous oxide. The oxide formation did not occur when using iron-carbon alloys. During total time of reaction of 4.5 sec. the following was observed: At about 2 sec. a flame front surrounded the specimen, the first signs of carbon boil appeared. The event was manifested by bursting of small bubbles close to the surface. At about 3.5 sec, the flame front was fully developed around the specimen. At about 4 sec. and about 1%C the main specimen

bulk was clearly distorted due to the onset of subsurface formation of carbon monoxide, although particle ejections, flame front and hence surface decarburization were still occurring. At 4.3 sec, the flame front persisted but the metal was distorted by a deep seated boil which swelled the specimen; at 4.5 sec the reaction ceased as the liquid bulk hit the tube walls. At no point was there indication of liquid iron oxide formation. Below 1%C there were less ejections and large bubbles grew within the liquid and deformed the drop as they broke through the surface.

Kaplan and Philbrook (118) studied the kinetics of gaseous oxidation of binary and ternary alloys of liquid iron at several temperatures in the range 1850° to 2050° C. These authors concluded that mass transport in the gas phase was the rate controlling step. Carbon contents of the alloys used ranged from 4.12% to 5.00%. Fume formation was observed during all their experiments. A model for mass transport was proposed but, as the same authors point out, involvement of mass heat and momentum transfer were too complicated to solve their model.

2.7.4 Decarburization of Free falling drops.

Studies of the reaction of iron alloy drops during free fall through oxidizing gases have been made by several authors (84 and 115 to 117). R. Baker (84) used single droplets melted from the end of a wire of known chemical composition. The drops fell from the melting zone under argon atmosphere to the reaction zone where oxygen was continuously flowing.

When using iron-carbon alloys with 3.3 to 4.9%C the samples quickly became enveloped in flames during fall through the oxygen column. Nucleation and coalescence of carbon monoxide bubbles well within the drops containing initially 0.86%C caused explosions similar to that described for levitated drops. Baker (84) determined that carbon removal was very dependent on drop size, the highest average rate being for drops of 1.5 to 2 mm diameter. Baker and Ward (115) used a combination of levitation and free fall of iron droplets through an oxygen chamber followed by quenching in a nitrogen gas flow. Drops of about 4 mm diameter with initial carbon content between 0.8% and 4.5%C were allowed to fall through 3 ft of oxygen and photographed at 4,000 frames/sec. During fall the specimens were associated with a tail of burning carbon dioxide produced by the primary reaction of oxygen with carbon in the specimen. Carbon boil and metal particle ejections occurred at all carbon concentrations. As the carbon concentration decreased the intensity of the boil increased causing the droplet to be destroyed by explosion at about 0.5%C. Calculated rates were in reasonable agreement with gaseous diffusion control. Subsurface nucleation was found to take place at much higher carbon concentration than for levitated drops. Although carbon diffusion becomes important in the control of decarburization, gaseous diffusion still predominates the rate control. Subsurface nucleation was proposed to take place homogeneously causing violent boil with mass losses of about 25%.

See and Warner (116) also used the levitation- free fall technique. Liquid iron-carbon and iron-carbon-silicon drops of 0.2 to 1.5 g weight were levitated in an inert atmosphere and allowed to fall through a reaction column counter to oxygen, carbon dioxide or air followed by water quenching. Reactions on the drop surfaces were observed using high speed photography. Carbon and/or silicon removals from the drops were also measured. When using iron-4%C carbon alloys the authors detected a tail of burning gas which indicated formation of carbon monoxide taking place at the gas metal interface. The samples were comparatively undisturbed by the carbon boil. There was also indication of subsurface nucleation at high carbon contents (about 1%C) with mass losses by bubble bursting. When using iron-4% carbon - 1% silicon alloy or blast furnace metal, there was no effect on the reactions previously mentioned. During the first four milliseconds of reaction a high emissivity oxide layer nucleated on the lower part of the specimen and spread over the entire surface. 0.002 sec after this event carbon monoxide bubbles burst through the surface; the material ejected formed fume and, as the reaction proceeded the specimen increased in size with ejections taking place in an irregular manner. After 0.26 s the specimen had a very irregular shape and was considered to be a foam. Mass losses varied from 17 to 30% for 1 g specimens reacted in oxygen. Alloys with 1%C 1%Si exploded after very short time. See and Warner concluded, as Distin (111), that it was essential to have oxide formation on the specimen surface before carbon

boil began. Explosions, which were all over the surface of the latter specimens were caused by subsurface nucleation of carbon monoxide.

Roddis (117) also used levitation and free fall technique to study decarburization of iron-carbon alloys of approximately 1g and ½g weight with carbon content between 5.0% and 0.4%. Experimental temperatures were in the range of 1300° to 1600°. The same author concluded that gaseous diffusion control was found to occur only at carbon contents greater than 4% and sample temperatures near 1600° C with pure oxygen. Surface reaction occurred until the carbon level had fallen to 3%, when subsurface reaction occurred. When using oxygen-nitrogen mixtures the change in reaction mechanism was found to decrease with oxygen content in the gas phase. For 70% oxygen-nitrogen mixtures surface to subsurface reaction change occurred at 2% C and for 50% oxygen-nitrogen the change in reaction mechanism occurred at 1%C.

2.8 Summary

It has been found from literature survey that pneumatic steelmaking processes involve the existence of a metal-slag-gas system. From purely physico-chemical considerations a given order for the elimination of impurities from the burden may be calculated. From practical operation a different order of removal is obtained and the carbon-oxygen reaction seems to have the greatest influence in determining overall refining times.

Phase diagram studies clearly indicate the complexity of the slags involved in basic oxygen steelmaking. The presence of gas bubbles, metal droplets and solid oxides within an oxygen converter in the form of a heterogeneous foam, further increases the complexity of the system.

Studies on decarburization reactions have been carried out mainly in the field of metal-gas systems. With respect to metal-slag-gas systems the qualitative studies by Hazeldean and coworkers are the only studies to have been made.

Very few experiments have been carried out to determine slag properties, foaming nature of slags, transfer mechanisms and nucleation mechanisms of CO which are important in oxygen steelmaking.

Many experimental difficulties obviously exist concerning the containment of reactive slags in crucibles which will adequately withstand reactions in the 1300° C to 1600° C temperature range.

CHAPTER THREE

EXPERIMENTAL TECHNIQUES AND PRELIMINARY STUDIES

Introduction

It was recognized that by studying or moving into a new area of research many difficulties would be encountered. Therefore, continuous development of experimental technique became necessary as the difficulties encountered were overcome. This type of approach to experimental investigation is not uncommon in pyrometallurgical studies, particularly where slags are involved.

This type of approach required early results to be obtained to act as a foundation on which to build and develop an improved technique.

The experiments were commenced knowing that certain constraints could not be crossed within the research project (e.g. availability of expensive materials for containment of slags). Constraints in upper and lower temperatures were uncompromisingly fixed.

A description is made in this chapter of apparatus, technique, materials which were ultimately used, and of the developing steps leading to the final results. The results which were necessarily obtained along these steps are also described.

3.1 Preliminary Work.

It has been generally recognised that high temperature experiments involve a great deal of problems particularly

those related to contamination by extraneous material other than that upon which research is to be carried out. When considering the study of steelmaking reactions, constraints are set by the size of amount of materials that can be used as compared with actual plant practice operations. The interaction and chemical composition of the different components either in the charge (iron ore, scrap, hot metal, lime, fluxes) or the refractory linings portray a complex system. On a laboratory scale a restriction is set initially by the reactivity of the slags found in plant practice to the possible choice of crucible suitable for use. By selecting the most important oxides which form the bulk of the slags in basic oxygen steelmaking (i.e. calcium, iron and silicon oxides) the selection is further reduced. The possible materials can be a refractory material with high melting point, platinum crucibles or iron crucibles. From the economic point of view crucibles of magnesia, zirconia or platinum are highly expensive as compared with iron crucibles. From equilibrium phase diagrams it has been established that iron crucibles may adequately contain synthetic slags of the type described above and for a wide range of chemical compositions. The limits which are set by the use of iron crucibles are the low temperatures at which reactions may be studied and also the low oxygen potentials which may be used.

During plant practice operation a typical melt of 300 tonnes of steel contains of the order of 30-36 tonnes of slag at turn-down (i.e. 10-12%). Consideration of the state of the system during actual blow should also be taken into account. After

one third of the blow the emulsion can contain from 45 to 80% by weight of metal droplets, the size of which range from 0.15 mm to 2 mm and the surface area for reaction has been calculated [86] of the order of 10^6 cm^2 per tonne.

The selection of iron-X alloy(s) to be used as metallic phase may be chosen by the type of synthetic slag to be used, the relative importance during basic oxygen steelmaking and the feasibility of being able to follow chemical reaction(s) at various temperatures and at reasonable rates.

From the preceeding considerations the system to be studied was limited to iron carbon alloys with approximately 4%C. Synthetic slags were selected from the lime-iron oxide-silica system, temperatures being dictated by the lowest melting point of slag (1204^o C) in the region of interest and, maximum possible temperature of 1400^o C limited by the use of iron crucibles.

3.2 Furnace for iron-carbon-slag reactions.

All the experiments for the reaction of iron-carbon alloys and synthetic slags used were carried out in a vertical tube furnace which is shown in plate I. The main working tube was of recrystallised alumina of 50 mm internal diameter by 1350 mm length. Heating was carried out by means of four silicon carbide rods adjacent to the working tube. To determine the length and position of the hot zone the furnace was initially heated to 1000^o C and allowed to stabilize for 12 hours. Readings for temperature were made with a Pt/Pt-13%Rh thermocouple and a Cambridge potentiometer. A temperature gradient was obtained along the length of the furnace from

which the hot zone was determined to be of the order of 7.5 cm length with temperature fluctuations of $\pm$ 5° C. By following the same procedure temperature measurements were made at 1150 and 1300° C. It was found that as the temperature of the furnace was increased the fluctuations within the hot zone were decreased from $\pm$ 3.5° C at 1150° C to $\pm$ 2.5° C at 1300° C. It was also found that the variations present at 1000° C could have been caused by the short time given for the furnace to attain equilibrium.

The head of the furnace, after alterations made during the course of this investigation, is shown diagrammatically in figure 16 and plate II. The lid was of stainless steel containing five orifices of varying diameter, of which two allowed for stainless steel wires to be moved in a vertical manner. One other orifice was used to mount a 90° angle prism which permitted very clear observation of the crucible contents from above. The other two orifices served as guides for introducing a stainless steel lance and a thermocouple. Two calibrated aluminium rods were set alongside the head which served as guides for two sliding mild steel platforms which in turn served for lowering crucibles and/or lance when required. Calibration of the two aluminium rods was made in a way such that a given height corresponded with a predetermined temperature within the working tube. Water cooling for the head and gas outlet were also provided.

The lower end of the furnace contained a retractable plate to allow for any sample to fall directly into a quenching

medium. A schematic diagram of this portion of the furnace is shown in figure 17 and also in plate III.

During all the experiments carried out with this furnace a controlled atmosphere was maintained by flushing high purity argon (99.999%). Flow rate was controlled by one or two flowmeters and a water bubbler was set on the outlet to ensure an air tight chamber (see plate IV).

3.3 Metallic Samples.

Iron-carbon alloys were prepared by melting, in a 15 KW UHF induction furnace, one kilogram of Armco iron (0.012%C, 0.04%Mn, 0.01%Si, 0.14%Cu, 0.008%P, 0.065%Ni, 0.015%Cr, 0.0014%Al, and 0.013%S) and a calculated amount of graphite powder to yield carbon contents from 4% to 4.3% C in the alloy. Graphite crucibles were used as susceptors for heat transfer and an inert atmosphere of argon was maintained throughout the entire operation.

Sampling of the melt was initially attempted using evacuated, sealed tubes. These laboratory-made tubes were dipped into the melt which melted the glassand flowed into the bore of the tube. Great difficulty was experienced in obtaining adequate vacuum and none of the tubes gave samples of a satisfactory length (3 to 5 cm). This method was abandoned. A second approach for sampling was made by connecting a vacuum pump to a series of plastic and glass tubing through a metallic safety reservoir. The suction power and speed of the vacuum pump were too high to allow time for withdrawal of the sampling tube and the high temperature

melted the tubing connections. This method was abandoned. A third approach was to use vacuum sealed silica glass tubing (supplied by Beecroft,Sheff.) with 6 mm internal diameter and with a small area which was thin walled to give a point of weakness. Although only 50 to 60% of the sampling tubes were effective, this system was finally adopted. The pin samples obtained weighed about 20 grams and were about 20 cm long. They were cleaned with a shot blast machine (using fine grit) and visually examined. Those pin samples with surface defects (pin holes, blow holes, discontinuities or with hollowed sections) were discarded. The selected pin samples were kept in a dessicator prior to cutting of the final samples to be used. A servomet spark-machine was used for cutting samples of 1 ± 0.2 grams weight. The aim of the sectioning was to obtain samples with height to diameter ratio of approximately 1:1. All the samples were cut with the same control settings on the spark machine. The ends obtained from the pin samples were always used as a reference together with an intermediate sample, for homogeneity of chemical composition. When the percentage of carbon content was not consistent along the length of the pin sample, the whole of the pin sample was discarded. Carbon analysis was performed by the non-aqueous titration method.

The method of analysis was briefly as follows. The sample weight was adjusted according to the carbon content. The sample is combusted in a stream of O_2 at 1350^{o} C in an open-ended tube. The resulting gases are aspirated through the apparatus by means of a suction pump. The products of

combustion (i.e. $CO_2 + SO_2 + O_2$) are passed through a drying tube containing anhydrone and MnO_2 (MnO_2 "fixes" SO_2) and are subsequently passed into a glass absorption cell. The cell contains a quantity of formdimethylamide to which is added ethanolamine and thymolphtalein the latter being the indicator for titration. When CO_2 passes into the above solution it liberates a proton and turns the indicator blue. This is then titrated using a solution of tetra-butyle-ammonium hydroxide in toluene to disappearance of the blue. An equivalence is obtained for the titrant and sample weight by standardization using either a standard steel or weighted quantities of benzoic acid. When carbon contents fell to within $\pm$ 0.05%C variation in each analysis from a given specimen only two analyses were carried out, but for wider variations a third analysis was made.

If the results from the three specimens (two ends and centre) from the pin sample were within $\pm$ 0.05%C variation the mean of the three was taken as representative of the whole of the pin sample, otherwise the whole pin sample was discarded. In this way chemical composition variations were kept to a minimum.

On occasions where an experiment required visual observation rather than a chemical variation or was merely a trial experiment, some of the physically "good" samples from the discards were used.

3.4 Slag Preparation.

Fayalite slags were prepared by mixing and melting corresponding amounts of calcined G.P.R. ferric oxide, coarse

filings of electrolytic iron and precipitated silica. A mixture calculated to yield a melt corresponding to fayalite ($2FeO.SiO_2$) was obtained from a mass balance from:

$$2/3\ Fe_2O_3 + 2/3\ Fe + SiO_2 \rightarrow 2\ FeO.SiO_2$$

Lime containing slags were prepared in the same way and adding calcium carbonate to yield:

$$CaCO_3 \rightarrow CaO + CO_2$$

Lime carbonate was selected in order to provide nascent CaO and avoid the possibility of hydroxide formation if pure CaO were to be used.

All the components were weighed in a four decimal balance to obtain the least variation on any aimed composition. Melting was carried out in a high-frequency induction furnace (plate V) and the amount of slag that could be melted at any one time was of the order of 100 grams. An inert atmosphere was maintained throughout the heating-melting-cooling operations to avoid oxidation of iron into one of its higher oxides (Fe_2O_3) as shown in fig.14. As discussed earlier (2.3.5) a higher state of oxidation would have created the conditions typical of quaternary phase equilibrium diagram to be present. Graphite crucibles were used as susceptors for heat transfer and also because the slags do not wet the crucible. Argon gas was delivered by an alumina sheath introduced through a porous refractory which served as a lid. Total heating and melting time varied from 40 to 50 minutes after which the furnace was switched off and the slag allowed to cool in the crucible down to room temperature.

Difficulty was experienced when removing the slag due to contamination from loose graphite. To avoid this problem it became necessary to clean the graphite crucible in an upside down position. The slag was then chipped out and immediately sieved (-60 mesh) after removal from the crucible. The following step was to crush and grind the slag in a Glen Creston ball mill down to -150 mesh. Magnetic separation was carried out on all slags before chemical analysis was performed. In this way the chemical analysis represented only the iron in the slag as ferrous or ferric oxide. Chemical determinations were made for ferrous and ferric oxides and silica. Lime was determined by difference.

Demagnetizing of the slag caused a lowering of the FeO and SiO_2 content which was later found to give a proportionate increase in lime content. This effect could have been due to the removal of Fayalite in the interstices of the magnetic material. There were no problems in preparing slags which followed the $2FeO.SiO_2$-$2CaO.SiO_2$ join line. In slags with silica and lime contents of 20% respectively there was always a great amount of magnetic material (mainly free iron) which was not possible to grind or dissolve back into the slag. Attempts were made to prevent iron precipitation by fast cooling and air quenching. This was made by pouring the slag in the liquid state into iron moulds, but still slow cooling was obtained. Open-channel iron moulds were then used, and, although free iron precipitation was prevented to a great extent, there was a high content of Fe_2O_3 present due to air oxidation (0.21 atm oxygen potential) (see figure 14).

Microstructure examination and viscosity measurements were made in collaboration with Edwards (119) and Pratt (120). The microstructures, which have been reported elsewhere (119,120) served to confirm that a full homogeneous liquid phase was obtained with the present slags used. Viscosity measurements were unsuccessful as has been reported by the above authors.

During the present investigation a slag obtained after tapping from an LD furnace used on a pilot basis was provided. The lumps of slag were crushed and ground to -150 mesh using a percusion mortar. Chemical analysis for the slag gave the following oxide contents on a wt% basis; after thorough demagnetizing:

20.48 SiO_2, 5.06MnO, 0.95Al_2O_3, 53.20 CaO,
5.82 Fe_2O_3, 6.25FeO, 2.8 P_2O_5, 4.8 MgO, 0.7 SO_2.

From the high lime content it was realised that a high melting temperature would be required and this was found to be so from cone fusion test carried out. The furnace available at the time for the cone fusion tests had a maximum operating temperature of 1500° C. After the cones were left for 30 min at 1500° C no melting was observed. The slag had therefore to be discarded as a possible alternative to the slags previously mentioned.

3.5 Decarburization Experiments at 1240° C and 1300° C

3.5.1 Iron Crucibles

Initial experiments consisted in reacting iron-carbon alloys with Fayalite slag. Iron crucibles with 0.023/0.027 %C

and 40 mm height x 40 mm internal diameter were used. A slag to metal ratio of 20 to 1 was chosen. It was suspected that the iron-carbon samples would possibly become welded to the crucible but several runs were carried out. Initially five grams of slag were set inside the crucible followed by the sample and covered with the appropriate amount of slag required. The then charged crucible was suspended from a protruding pin underneath the furnace's lid and introduced into the hot zone at 1240° C. The time for reaction was increased from experiment to experiment. After up to three minutes of reaction the samples were found undisturbed and visually showed only slight superficial reaction but no signs of melting were observed. The appearance of the slag was as if only melting had taken place on the periphery with sintering towards the centre. In experiments past the seven to ten minutes the samples were all found welded on the bottom of the crucible even when fifteen grams of slag were set under the iron-carbon sample. To avoid the welding of the samples, the iron crucibles required to be coated with a refractory material. A slurry of zircon ($ZrO_2.SiO_2$) "standard" (melting point 2420° C) grade was made with water. About five grams of slurry were poured into each crucible and by manually rotating them the walls and bottom were coated by a thin layer of zircon. The crucibles were then set to dry for six hours at about 100° C. In early attempts, oxidation of the iron crucibles took place, in most of the cases, between the wall and the actual coating, subsequently iso-propyl alcohol or acetone were used for making the slurry.

In experiments of up to ten minutes the samples were found welded onto the crucible. Other crucibles were coated using "zircon X" and dried in the same manner as the latter crucibles, but the results were the same. Then following trials were carried out but the coated crucibles were sintered at 1100° C for four hours and furnace-cooled under argon atmosphere. Compact coatings were obtained but crucibles coated with zircon standard grade showed signs of containing great amounts of impurities. For the trials carried out with fayalite at 1240° C both types of zircon were found to withstand the temperature and the reaction taking place. The inconvenience of using zircon standard besides the impurities it contains (Fe_2O_3 and Al_2O_3) is the high percentage of silica (near 33%), which could react with the slag when making lime additions. From these results a coating of stabilized zirconia was selected to be used for coating of crucibles. Because zirconia is greatly affected by thermal shock, it was necessary to slowly heat and cool each crucible during sintering. The heat treatment was achieved by drilling two holes in the lid of the furnace and gradually lowering the crucible (over a period of about one hour) into the hot zone by means of two stainless steel wires. By using this technique compact coatings were obtained on the crucibles but the drawback was the cycle time which was of the order of four hours. Shorter times for sintering were attempted so that the crucibles would be exposed for the least time at high temperatures but, in most cases the refractory coatings shattered into small pieces. Experiments were carried out

using synthetic Fayalite slag after which all the coatings were inspected after sectioning the crucibles longitudinally, and no visual damage could be detected. This practice for coating of the iron crucibles was adopted for subsequent experiments with iron crucibles. Although extremely time consuming, this method of preparation was the only way by which iron crucibles could be used satisfactorily.

3.5.2 Decarburization with Fayalite at 1240° C.

Trials were performed using Fe-4.17%C and Fe-3.6%C samples and fayalite slags. The crucible with a sample was introduced in the furnace from room temperature to 1240° C. The aim of this temperature (35° C above the fayalite melting point) was to determine if decarburization reaction could be followed with the proposed system while subjecting the system to the least thermal strain. The results obtained have been plotted in fig.18. From the plotted data it can be seen that, although a relatively low temperature is used, decarburization was taking place in such a way that the reaction could be well followed. The inconvenience of the results is the difficulty that arises in establishing the zero time for reaction, i.e. commencing of reaction. Several preheating sequences were followed and the drop in carbon content recorded as shown in figure 18. Following this method an approximation to the zero time of reaction was made. From the wide variations of carbon content in the alloys it was difficult to determine the appropriate preheating sequence. It was vital that the precise time at which the iron carbon drop became molten should be established.

3.5.3 Differential Thermal Analysis.

A differential thermal analysis between the iron-carbon sample in the slag and the crucible used was carried out. A first thermocouple (Pt/Pt13%Rh) was adjusted in the wall of the crucible just above top level of slag. A second thermocouple (Pt/Pt13%Rh) was used on to the end of which an Fe-C sample was attached. The arrangement is shown in fig.19. The difference in temperature recorded between the two thermocouples was continuously monitored by a recorder and for convenience some points were taken to redraw the results obtained which indicate replicability of the system and are shown in figure 19 and figure 20. It may be seen from the graphs obtained that, by holding the crucible at 800°C, the Fe-C sample required approximatel 10 mins. to equalize the temperature of the crucible. A further increase in temperature to 1000°C required 5 mins. by the sample to reach the same temperature and by increasing, after the two previous steps, the temperature to 1240° C, the sample needed not more than 30 sec to equalize the crucible temperature. The reason for the temperature difference going below 0° C is due to the distance of the two thermocouples from the hot zone (i.e., droplet practically at higher temperature).

Once the preheating sequence was established, the reaction of an Fe-4.13%C drop with fayalite slags at different times was carried out. The results are shown in fig.21. Although it may not be conclusively stated that the intersection between the %C axis and the curve drawn is the zero time for reaction, it was thought to be the best approximation. By carrying out a series of preheat-only experiments a mean value for

decarburization of 0.04% was obtained; this value was deducted from all the runs carried out in this manner.

By carrying out reactions between Fe-C and slags for different times it was possible for one point to be determined on a plot of%C vs time for each successful run. Although this is a lengthy process it facilitates the checking of the reproducibility of the system.

The results for decarburization with fayalite slag at 1240° C are shown in fig.21.from where it is seen that decarburization is taking place very slowly. The reason could be due to the low temperature used. From the iron-carbon phase diagram it was determined that the liquidus line at 1240° C is reached when the carbon content is about 3.5%C, or after about 7.5 minutes of reaction with fayalite slag. As decarburization proceeds below the 3.5%C content, the liquid iron-carbon sample will move towards a mushy region of liquid plus solid and ultimately reach complete solidification at 0.95%C content. Although the latter may be taking place it is shown from these results (figure 21) that decarburization could be monitored for up to 60 min with a carbon content of 1.66%. Decarburization can be seen to be still taking place up to 60 minutes. Another reason for the slow reaction could be that the slag is becoming depleted in oxygen (O^{2-}) content which in turn could slow down the decarburization rate. By considering the following reaction:

$$2\,FeO + \underline{C} = 2Fe + CO_2$$

and carrying out a mass balance it has been calculated that the

amount of FeO consumed by a 2.5%C decrease from a one gram droplet would be 0.3g FeO which on 20g of Fayalite slag represents 1.5%FeO (or 0.33% oxygen). Although the amount of oxygen consumed is small it was decided to increase the slag to metal ratio so that oxygen supply should not be restricted. This was done by effectively increasing the slag weight as opposed to decreasing the sample weight. The main parameter, temperature, was increased to 1300° C to allow for longer periods of existence of a liquid Fe-C phase and indirectly for a less viscous slag phase.

The droplets obtained after decarburization at 1240° C showed a definite increase in diameter in most cases and several of such samples were X-rayed prior to chemical analysis. The droplets shown in fig. 22 clearly show signs of porosity which was caused by the presence of gas bubbles which were trapped on quenching. The amount of gas contained inside the droplets seems definitely to increase with time as shown in fig.22. By analysing the set of X-rays obtained a time of forty minutes was chosen for carrying out a similar run. However, this time the sample was mounted, sectioned and polished for microscopic examination. The photomicrograph shown in fig.23 indicates the result obtained and shows that besides the two great central cavities formed there are signs of gas pockets entrapped in the walls of the droplet. This effect tends to increase the surface area available for reaction in the system. The possibilities for bubble nucleation and reaction mechanisms are dealt with in a subsequent section (5.3).

Observations of the crucible contents at 1240° C had indicated slight increase in slag volumes.

In order to increase the slag to metal ratio to 30 to 1 it was found from the first trials at 1300°C that the crucibles originally used were not tall enough. In some instances the slag showed signs of reaching the top of the crucible at 1300°C. It therefore became necessary to increase the height of the crucibles. This was done by welding together the rims of two crucibles, and then cutting off the circular base at one end. The new crucible was 80 mm in height. All the subsequent runs were carried out in this type of crucible with zirconia coating as previously described.

The usual procedure on preparing each run consisted in weighing an iron crucible and adding 15 g of slag. Before the Fe-C sample was set in the crucible it was cleaned in a normal solution of hydrochloric acid, rinsed in water and finally immersed in acetone. The sample was then set in the crucible resting on the powder surface. The total slag required was then calculated by knowing the Fe-C sample weight and an aim slag to metal ratio of 30:1. This second amount of slag was added on top of the sample.

The iron-carbon samples used in all the experiments were maintained at a weight of one gram $\pm$ 0.2 grams. The nature of the decarburization reaction was known to be potentially violent and drop disintegration could be expected. A check was therefore carried out to ensure that the whole drop retained its integrity throughout the reaction. By weighing before and after reaction with the slag, any small particle loss of iron from the mother drop should be observed. Table II shows typical checks chosen at random. They show that weight decreases and also increases occurred. The decrease in weight could have been caused by carbon loss, and iron particle ejection; however, there was no visual evidence of the latter. The weight increase could have been caused by slag entrapment within the drop and by slag adhesion on the surface of the drop. The correlations between the weights, although difficult to explain and although following no pattern, in no way affect the accuracy of the chemical analysis.

Before any run was carried out, temperature measurements were made at the centre of the working tube at three different heights (e.g. 800, 1000 and 1300°C) in order to be able to adjust the heights at which the crucibles were to be set. Argon

before the crucibles were introduced. The crucible was suspended with two stainless steel wires passing through the lid of the furnace and supported by a platform. The platform was subsequently fixed for a period of 10 min in a way that the bottom of the crucible was at 800° C. The platform was then lowered and the crucible reached the 1000° zone and was left for five minutes, after which the platform was further lowered until the 1300° C zone was reached by the crucible where it was left for a predetermined time followed by quenching in water at room temperature. The time required for opening the bottom of the furnace and dropping the crucible never exceeded five seconds. To increase the cooling rate the crucible was agitated inside the water reservoir. The slag was then crushed or hammered out of the crucible and the sample taken for carbon analysis.

All of the runs were observed during the whole period of reaction but no detectable difference was seen to take place when different slags were used. The time required for the surface of the slag to become melted varied from 20 to 30 seconds. During the first three minutes a considerable degree of turbulence took place which could be due to escaping of entrapped gases (air). After these three minutes the amount of turbulence gradually decreased and sporadically minute bubbles were seen to escape through the surface. The latter effect took place mainly after three to five minutes of reaction and became less frequent at longer times. Plate VI shows four stages of the slag surface as seen during the reaction and illustrates the general visual appearance for most of the reaction observed. The first figure of plate VIa shows the slag after

30 seconds of being at 1300° C. At this point in time most of the surface is liquid and the remaining portions quickly become liquid. The second figure shows the sample floating on the surface of the slag. The emergence of the liquid drop on the surface occurred randomly and intermittently and usually lasted for 5 to 7 seconds before submerging. The last two photographs (plate VIc,d) give the appearance of the slag surface as the turbulence commences to subside. They clearly show the eruption of bubbles, both large and small, out of the slag. The bubbles can only be CO and they burst through the entire area of the surface. The slag was always seen to be highly agitated at the surface with a random motion. Various attempts were made to obtain sharp still photographs, this was not possible due to the foaming effect of the slag (height fluctuations), the narrow area of view (i.e. prism vs camera lens) and, focusing within the range required.

The results obtained from reaction of Fayalite slag with iron 4.2% carbon at 1300° C are shown in figure 24. The results follow a general path and a smooth curve was drawn through the points in the same way as for the 1240° C experiments. By comparing the data obtained for decarburization with fayalite slag at 1240° C and 1300° C (60° C increase in temperature) a small increase in rate is observed.

From the latter results it was concluded that before investigating the effects due to temperature on decarburization rate the effects due to lime additions were necessary. Other temperatures would be investigated in a later stage of research.

The preliminary slags used contained 11.06, 12.66% and 14.32% CaO. Decarburization curves were plotted for these three slags as shown in figures 25, 26 and 27. Comparing the four curves a cursory observation shows that the rates of decarburization are similar and this will be discussed in more detail later in the next chapter. Decarburization with slags containing 14.32% CaO (figure 27) shows slightly more scatter of results but still a general smooth trend is observed. There is not a great variation in the chemical composition between the lime-containing slags, but, the initial carbon content in the samples used is 0.3% higher for the latter slag.

Visual observations of the crucible contents, and the height reached by the foamed slag, were about the same for all four different slag compositions. The success of these trials indicated that results at higher lime contents and higher temperature should be possible with the present technique.

From the above trials, one variable (%C) was maintained constant and an iron-3.9%C alloy was reacted with a slag containing 25.83% lime. The decarburization rate was found to be greatly increased but, although only four experiments were made practically no scatter of the results was found as can be seen in figure 28. There was,on the other hand,a new change which was mainly the physical aspect of the reacted droplets.

The reacted droplets indicated that from ten minutes of reaction onwards the droplets had their surface covered with craters of varying sizes. The final diameter of the droplets was greater than that of the original sample used, as in the previous experiments. Photographs were taken of the reacted

droplets which are shown in plates VIII and IX. The sample reacted for fifteen minutes clearly shows that gas bubble growth is taking place inside the droplet. A large bubble was obviously erupting through the drop surface as quenching occurred. Internal gas bubbles were also detected by taking X-ray photographs, which were reproduced by the 'contact' method and shown in plate IX. Unfortunately the prints from the X-ray negatives do not give the same sharpness as the negatives themselves. The negatives themselves quite clearly indicate the porosity which must have developed in the liquid drop.

3.5.5 Slag Path Analysis.

The importance of the paths which are followed by slag during oxygen steelmaking has been outlined in section 2.6. The slags obtained from decarburization of 3.9%C alloys were chemically analysed in an attempt to relate, the path followed by the slags and the surface effects on the reacted drops. Three slags were similarly analysed after reaction with iron carbon droplets. The changes in chemical composition with time, are given by the curves plotted in figure 29 to 32. The decarburization curves obtained from the decarburized droplets are given in figures 28, 33 and 34.

Chemical analysis of the slag created several problems. The first is that the slags were water-quenched and therefore the Fe^{3+} content would tend to be higher than that found at the reaction temperature. A second problem is caused by the zirconia coating which was entrapped when crushing the slag

out from the iron crucible. It was therefore necessary to subtract the percentage of zirconia and recalculate the remaining components back to 100%. After the removal of the slag from the quenched crucible,the presence of magnetic material was detected. The slag path presented in figure 30 was calculated from the chemical analysis without removal of magnetic material from the reacted slags. The presence of magnetic material tended to give an erroneous percentage of the iron present as Fe^{2+} and Fe^{3+} which in turn altered the final slag composition. The slag paths given in figures 29,31 and Figure 32 were thoroughly demagnetised and the remainder of the slag was analysed for Fe^{2+}, Fe^{3+} and silica with lime being determined by difference.

In all the slags which were analysed the FeO and Fe_2O_3 contents do show decreases with time. This is consistent with the iron oxides being the source of oxygen for the carbon reaction. However, the magnitudes of decrease are not self consistent and it is impossible to relate them to the analysis of the metal phase. The changes in lime and silica contents with time are more likely to be due to sampling errors caused by heterogeneity of the slag after quenching rather than by decarburization of the drop. Due to the number of difficulties presented in following the slag paths the study was not pursued any further in this direction. The only possible conclusions that can be drawn from the slag path analysis is that there is a definite decrease in FeO and Fe_2O_3.

3.6 Decarburization at 1400° C.

The slags used for decarburization of Fe-C alloys at 1300° C were further used to study the effect of temperature

on the rate of decarburization. The zirconia coated iron crucibles and the sequence followed for preheating were maintained throughout as previously described (3.5.1).

From visual observations during the reaction at 1400° C it was noted that the slag began to melt at about 15 sec after it had been taken from the 1000° C to 1400° C hot zone. The following 30 sec showed signs of vigorous agitation taking place mainly in the radial direction. The latter pattern changed after about one minute to a random pattern, i.e. boiling effect at different places on the surface. The agitation or boiling effect prevailed for a mean of three and a half minutes and subsequently subsided.

Difficulties were encountered in experiments performed at 1400° C and were due either to crucible failure (dripping of slag through the bottom side) or to the droplets welding on to the crucible. The zirconia coating, which was of similar thickness to that used at 1300° C, was most probably too thin and the increase in turbulence of the slag, the high temperature used and the sudden increase of 400° C could have accounted for the problems presented. In an attempt to overcome the latter problems, zirconia coatings of nearly 2 mm thickness were applied to the iron crucibles. Sintering of these thick zirconia-coated crucibles was carried out at 1300° C for 3 hours after which the temperature was slowly raised to 1400° C and maintained for 30 min followed by furnace cooling down to 1200° C or 1100° C. The crucibles were then slowly removed from the furnace to avoid subsequent thermal shock of the coating.

Experiments were then carried out at 1400° C with different slags but successful runs were obtained only for periods of up to 7.5 minutes, after which most samples welded to the crucibles.

A different form of coating was made using facilities provided by BISRA at Hoyle St. Sheffield. The technique consisted of using an oxygen acetylene torch and introducing zirconia powder into the gaseous streams which was then delivered on to the interior of the crucible. Before the actual sintering was made the crucibles were cleaned by blasting with fine grit. Immediately the crucibles were heated with the torch to 'red hot' and then the zirconia powder allowed to flow. In many cases a great amount of oxidation took place which prevented the zirconia from adhering to the crucible. Various flow rates were used but almost all of the powder was swept out. This was due to the blasting into the internal geometry of the crucible. A thick coating of about 2 to 3 mm was eventually achieved by progressive forming of thin coatings allowing for cooling of the crucible in between each coating.

By this method five crucibles were produced and kept in a desiccator prior to use. Reactions carried out at 1400° C were successful only for a period of 8 minutes (two experiments), at ten minutes one crucible failed, and in the remaining two crucibles the droplets welded on to the crucible. The conclusion was drawn that flame spraying of zirconia gave no better protective films than the established sintering technique.

Due to the many difficulties found and the need for maintaining a systematic method (i.e. use of zirconia-coated iron

crucibles, preheating sequence previously used) it became necessary to carry out a great number of experiments. A large number of runs were unsuccessful due to failure of the zirconia film to protect the iron crucible. Eventually sufficient successful runs were performed to enable a decarburization curve to be plotted.

3.7 Conclusions.

The preliminary experiments show that decarburization of Fe-C alloys by synthetic slags of $FeO-SiO_2$ and $CaO-FeO-SiO_2$ can be studied by the system adopted.

The zirconia-coated iron-crucibles were found adequate to withstand temperatures of up to 1300^{o} C but began to fail intermittently at 1400^{o} C after 8 minutes of reaction.

The size of Fe-C samples and slag to metal ratios used allows the establishment of a continuous slag phase with sufficient supply of reactant (oxygen) and a discontinuous phase (Fe-C) with varying reactant concentration (carbon).

Differential Thermal Analysis has been used to determine a preheating sequence in order to approach the zero-time for reaction. The data obtained from preliminary experiments have been presented in the form of %C vs time graphs for the different slags, temperatures and Fe-%C alloys used.

The results show that reactions carried out with fayalite at 1240^{o} C have relatively slow decarburization rates which implies the need for reaction times of up to 60 minutes, fig.21. From the point of view of the Fe-C alloys used, the 1240^{o} C temperature would cause a change from liquid to solid

phases. An intermediate condition known as mushy region being present from about 3.4%C to just under 2%C. Reaction temperatures of 1300° C show a faster rate for decarburization with fayalite as compared to 1240° C and tend to increase when lime additions are made. The scatter in results obtained when using fayalite slags at both 1240 and 1300° C suggest it is preferable to use synthetic slags with lime additions. With high lime contents reaction of droplets from about 4%C to carbon contents of less than 2.1%C have shown a characteristic surface effect which may be related to the actual mechanisms of reaction. The X-ray photographs from various samples may also be used to substantiate the kinetics of the process. There is clear evidence of gas bubbles existing in the drop.

Reactions carried out at 1400° C have shown that there are limitations on the times allowable for actual experimentation, i.e., there are indications that 1400° C is on the upper temperature limits for this experimental system with iron crucibles, and other materials must therefore be explored if higher temperatures are to be achieved.

CHAPTER FOUR

EXPERIMENTAL RESULTS AND OBSERVATIONS

4.1 Introduction.

Having established the viability of a system to study decarburization of Fe-C alloys by synthetic slags it became necessary to substantiate the preliminary results by obtaining a greater number of experimental results.

In the following chapter a description is made of the decarburization studies at 1300° C and 1400° C. Studies were then pursued at higher temperatures. Using the experience gained in overcoming the problems at 1400° C, a method was found which allowed studies to be made at 1500° C and 1600° C. No definite conclusions were obtained which allowed comparison with studies at lower temperatures but the results do give rise for discussion to be made.

The hydrodynamic state of the system was found to be altered, as could be expected, by both increasing the reaction temperature and by gas lancing. The injection of gas allowed the effects of increasing slag momentum to be studied. The injection of reactive gases into the slag allowed various oxygen potentials to be studied and their effect on the rates of decarburization obtained. With the aim of having an insight into the kinetics of the process, reacted droplets, as well as slags and unreacted droplets, were examined by use of a Scanning Electron Microscope in addition to X-ray photography.

4.2 Reactions at 1300° C.

From the results obtained for the preliminary experiments the decarburization curves show a well defined (i.e. smooth) trend with increases in reaction time. However, the amount of preliminary data was small, therefore, it became necessary, for confirmation, to either duplicate results, (i.e., same slag, Fe-C alloy, time and temperature) or to follow a decarburization path with a greater number of experiments. As explained earlier difficulties were encountered in obtaining a slag with an exact predetermined chemical composition. Therefore shorter intervals of time were chosen and a greater number of experiments were made. Reaction times from 4 to 20 minutes were used with 2 min interval for each experiment. The slag used was of 38.34%FeO, 2.43%Fe_2O_3, 27.01%CaO and 32.22%SiO_2. Fe-C samples chosen contained 4.25%C. The data obtained are shown in figure 35. Before the samples were analysed photographs and X-ray photographs were taken in order to obtain external as well as internal variations during reaction. Plates X, XI and XII show the surface appearance while Plate XIII shows the internal appearance of the reacted droplets. The numbers found in plate XIII were used only as reference to the experimental sequence followed in the present study. Plate X clearly shows that up to four minutes of reaction, the sample (No.9) remains virtually unchanged, surface reaction has taken place to a small extent and this is supported by the X-ray photograph where the sample shows no sign of internal cavities being formed. The following three sampl Nos. 0 and 1 in plate X and 2 of plate XI show a sequence of transition through an oblate shape followed by a spherical

shape. The effect is outlined by the surface appearance which becomes gradually covered with a layer like (c.f. kneading dough in bread making) overlapping in the oblated droplets. From the X-ray photographs the internal cavities formed appear mainly near the surface of the droplet. The fifth droplet (No. 3 in plate XI) showed a distinct eruption on the surface, while an internal cavity was revealed by the X-ray (see plate XIII). The surface began to show the same layer-like structure with minute crater-like cavities. The spherical shape of the droplet is maintained from this moment onwards. The following sample (No. 4 of plate XI) clearly shows the entire surface covered with the crater-like structures of various sizes while the internal cavities as shown in plate XIII are more randomly distributed. The last three samples (No. 5, 6 and 7 of plate XII) have equally as before the surface covered with crater-like cavities with greater depth throughout although the actual diameters of the crater present are smaller than those for sample No. 4 of plate XI. The internal cavities shown in plate XIII seem to concentrate towards the centre ultimately changing the droplet shape into spherical shell.

Experiments were carried out using a slag with 39.9%FeO 3.33%Fe_2O_3, 25.85%SiO_2 and 30.92%CaO and an Fe4.02%C alloy. The physical appearance of the drops was similar to that from the latter decarburization runs. The results obtained are given in figure 36 which equally shows the same smooth trend found in previous runs.

From the previous experiments the results obtained have been plotted on a %C vs time coordinate system. Differential

Thermal Analysis was made at the beginning of this research attempting to establish a zero time for reaction. If the curves drawn are continued to the initial carbon content of the Fe-C alloys a very slow decarburization rate is obtained during the first two and a half minutes of reaction. It was thought that the melting time of the slag and drop had increased when changing to a thirty to one slag-metal ratio from a twenty to one ratio. The incubation period for reaction was rechecked. A new Differential Thermal Analysis was therefore needed for the system and was carried out as previously discussed (3.5.3). The results, which were obtained on a continuous graph, have been replotted in figure 37. As shown in this latter figure the increase in slag content had in fact increased the time required for the sample to attain the 1000^{o} C temperature of the slag. The preheating sequence was changed accordingly and decarburization of Fe-C alloys due to the now determined preheating sequence was determined. An average carbon drop of 0.07% was obtained which was later deducted from the total carbon analysed in pin samples.

The results obtained from these latter decarburization studies defines, although each point is a separate experiment, the continuous path followed during reaction. The photographs and X-ray analysis have in turn defined a situation where internal nucleation takes place. The internally nucleated gas bubbles and the union of the cavities present tend to increase the size of the droplets, causing an effective swelling of the droplets. Surface nucleation could be detected at carbon levels

below 2.25%C but this does not imply that this was the only point at which it was taking place. This assumption is made by considering the time taken for bubble nucleation and growth to enable the establishment of the well defined crater-like structure.

4.3 Decarburization at 1400° C.

From the preliminary experiments which were carried out at 1400° C the data obtained were insufficient to enable a decarburization trend to be established. A series of experiments was therefore followed with the aim of obtaining, and if possible, establishing such a trend. Shorter intervals of time were predetermined for the required experiments based on previous results. The aim again being to follow changes in decarburization to within closer variations with time. As expected from previous experiments a great number of experiments was needed in order to define a trend during decarburization but successful droplets were obtained up to 11 and 12 minutes of reaction time. Four slags were chosen for this set of experiments, Fayalite and 14%, 25.85% and 31% CaO contents. Fayalite and 14% CaO slags showed greater scatter of results as compared with high (25 and 31%) CaO contents. Scattered results were expected and therefore duplicate or triplicate experiments were carried out so as to define the path followed by decarburization. The data obtained from decarburization of an FeO-4.26%C alloy with fayalite slag are shown in fig.38 and those for decarburization with 14%CaO in fig.39. From visual observations fayalite slag showed greater signs of turbulence but in no case was slag over-flow detected from the

quenched crucibles. The reacted droplets were of spherical shape but there were no signs that bubble nucleation (i.e. cratered surface) had taken place on the surface. Overall diameters were greater for reacted droplets as compared with initial sample. Signs of internal nucleation were found when crushing the droplets for chemical analysis. Due to the scattered results obtained no further experiments were made at 1400° C with these two slags.

The results from decarburization of an Fe-4.35%C alloy with 31.94%CaO slag are shown in fig.40 and those for an Fe-4.02%C alloy decarburized in 25.85%CaO slag are shown in fig.41. The same smooth trend was found for these two slags at 1400° C as in the 1300° C decarburization reactions. By continuing the trend followed by the data obtained (i.e. assuming the decarburization rate to continue in the same fashion) it may be seen from the graphs that in order to obtain low carbon levels, reaction times of about 15 min would be required for high lime contents.

The reacted droplets with final carbon levels under 2.2%C were completely covered with craters. The internal surfaces (when exposed by subsequent fracture) clearly showed craters where bubble nucleation must have taken place.

4.4 Experiments at 1500° C.

The experimental arrangement used at 1240° C, 1300° C and 1400° C was found adequate for the study of decarburization with various CaO-FeO-SiO_2 slags, although at 1400° C many difficulties were found. By scrutiny of the rates of decarburization for the above mentioned experiments it is seen that

an increase in temperature causes an increase in the rate of decarburization for corresponding slags. Also due to the short time required for the carbon content to attain levels below 1%, a series of experiments was envisaged to carry out decarburization reactions at temperatures of 1500° C which could perhaps require only a small number of experiments to establish the trend followed.

4.4.1 Crucibles for decarburization at 1500° C.

Due to the highly reactive slags under which decarburization reactions were being studied it became necessary to adopt crucibles which could withstand the 1500° C temperature proposed.

Two options were open, the use of either zirconia crucibles or, as in the case of iron crucibles, the use of a zirconia coating on a refractory crucible. The two options could be followed with stabilized zirconia crucibles, and, depending on the results obtained, (i.e. reaction times, foaming of slag, scatter in results) the same type of experiments with a zirconia-coated refractory crucible could be continued. Stabilized zirconia crucibles of 40mm ID x 40 mm high were initially used. Because the crucibles are prone to thermal shock it became necessary to support them inside graphite crucibles to prevent any run-out or slag from attacking the working tube. Graphite rods were machined to give a crucible 100 mm high 42 mm internal diameter and 1.5mm wall thickness. The graphite crucibles were held with Pt-Pt/10% Rh wire with a lead of about 16cm above the crucible and subsequently suspended with stainless steel wire.

4.4.2 Decarburization at 1500° C.

Due to the small volume provided by the zirconia crucibles the slag to metal ratio was set at 20:1. The size of the metallic sample was maintained at one gram. Slags used in the present experiments varied from fayalite to 20.68% and 28.2%CaO. Preheating of the zirconia crucibles was carried out in increments of approximately 150° C every 5 min. The system (crucible + sample + slag) was held at a final preheating temperature of 1000° C for 10 min giving a total preheating time of 50 min. The system was then taken to the reaction temperature of 1500° C where the melting time for the slags was always of the order of 30 to 45 sec. A considerable degree of turbulence took place during the first three minutes but generally subsided after 3.5 min. The foamed slag in most cases reached the top of the zirconia crucible, the latter usually remained visible for most of the reaction time indicating this, that the slag did not rise above 40mm height.

The data obtained are plotted in figures 42 to 44 for the three slags used. Decarburization rates obtained from fayalite reactions were found to be far slower than expected for a reaction at a temperature of 1500° C.

In the following trials a 20.68%CaO slag was used to decarburize Fe-4.12%C alloys. The results obtained indicated a fast decarburization rate down to carbon levels of about 2% after which the reaction seems to drastically slow down. After 10 min of reaction the results become scattered and tend to oscillate at about 1.5%C up to 15 min of reaction time. The effect could be due to a rapid depletion of carbon content

on the droplets and causing partial solidification of the outer surface. The rate for decarburization thus decreases and proceeds slowly (dependent on carbon diffusivity) until a homogeneous and higher carbon content on the surface is achieved which in turn will lower the melting temperature and a new cycle repeated.

Experiments with 28.05%CaO-slag were conducted to decarburize Fe-4.26%C droplets under the same conditions.

The decarburization trends obtained from these experiments were found to be similar to using a 20.68%CaO-slag. A high rate of decarburization is obtained down to carbon levels of about 1% with 7 minutes of reaction. Immediately follows a sudden decrease in rate which continues to 12 minutes which was the maximum time for reaction obtained. The lower carbon levels reached (i.e. 1%) during the period of rapid decarburization were expected. The previous experiments had indicated that higher lime contents of the slag yielded steeper rate curves.

The physical appearance of the reacted droplets was similar to that found at 1300 and 1400° C with carbon contents under 2.2%. Some of these reacted droplets are shown from plate XIV to plate XVI. These findings confirm that the evolution of carbon monoxide from the drop is vigorous which results in motion of the drop within the bulk slag phase. In plate XIV the tearing effect of violent gas evolution is shown by the various entrapped bubbles explosively escaping (or attempting to escape) from the bulk of the drop. A similar effect has been shown earlier in plate IX, for drops which had reacted at 1300° C.

Results obtained from 1500° C experiments using zirconia crucibles indicated that faster decarburization rates were reached. An attempt was then made to continue along the same lines using recrystallized alumina crucibles with zirconia coating. It was first necessary to determine any alumina pick-up by the slags from the coated crucibles and the significance of this alumina loss from the crucible wall. The chemical composition of the slag was 27.30%FeO. 1.14%Fe_2O_3.38.76%CaO and 32.80%SiO_2 with a corresponding melting point of about 1400° C from fig.12. The recrystallized alumina crucible 2.54mm ID x 3.76mm height was covered with zirconia slurry leaving a small uncovered area on the base of about half sq.cm. The aim was to determine if any severe attack would occur and lead to crucible failure during any one experiment. The sintered crucible was packed with slag. Only 17.2g could be charged when 80% of the crucible was filled. The alumina crucible was held in a graphite crucible of 100mm height in the same way as the zirconia crucibles. The crucibles and slag were then held at 1500° C for 26 minutes. During melting the slag had an initial turbulent ebullition period of nearly one minute but remained quiescent for the rest of the time. The crucibles were allowed to freely fall into water for quenching. A section of the crucible was inspected metallographically and no severe attack was observed. The areas from the recrystallized alumina which was in direct contact with the slag showed very slight superficial attack even though a slag layer had adhered to it.

The slag analysis indicated an alumina pick-up of 0.06% but zirconia content was 10.38%. This indicated that most probably zirconia had spalled in other areas of the crucible. The latter results indicated that the zirconia coated alumina crucibles could be used at 1500°C or 1600° C. To ensure an adequate zirconia coating, the coating technique was similar to that previously described. However, the sintering had to be carried out with more care and more time than with the iron crucibles. The sintering involved heating up the crucible to 1500° C over a 4 hour period. After a further 4 hours at this temperature, the furnace and crucible were cooled slowly.

Due to the small amount of slag that could be used in these experiments and the turbulence created during decarburization, it became necessary to increase the height of the crucibles. This was done by cutting the bottom of some recrystallized alumina crucibles and, after sintering as before, the sleeves were set on top of one full crucible. This arrangement was then inserted into an outer graphite crucible for support.

By using this method it was found that one 'sleeve' alone could not withstand the thrust from the violent foaming of the slag and it was raised by nearly two centimeters above its original position. Up to three 'sleeves' were used but without preventing the same effect taking place.

This latter procedure was abandoned because there was no way in preventing the slag from reacting with the graphite crucible. In most cases a great number of small (0.5mm)

metallic drops were found within the slag, which indicated that the FeO from the slag was being reduced by the graphite. The decarburization of the Fe-C alloy was therefore taking place under a different situation, and could not have been correlated to the previous results.

The solution to the problem of slag-graphite reaction would be to have crucibles which were sufficiently tall to contain the foaming slag without having to resort to sleeves. Unfortunately, there are no recrystallised alumina crucibles on the market with such a large height-diameter ratio. The crucibles which are sufficiently tall to contain the foam have diameters in excess of the diameter of the working tube of the resistance furnace. The use of such crucibles therefore necessitated an alternative heating system.

4.5 Decarburization at 1600° C.

An attempt was made to determine decarburization of metallic samples by slags at 1500° C. The approach consisted in using alumina crucibles of 70 mm ID and 150 mm height. In this way, problems of overflowing could be avoided, and the slag to metal ratio of 30:1 could be maintained. Zirconia coating and sintering was as for recrystallized alumina crucibles.

For these experiments, it was necessary to use an induction furnace which could reach the required temperature and at the same time allow close control of temperature during a time span of about 5 to 10 minutes minimum. Graphite crucibles were used as susceptors and a graphite sleeve enclosed the upper half of

the crucible up to the rim. Trials to obtain 1500° C were made originally with a small induction furnace (15 KW-UHF) used for melting of slags but a temperature of only 1470° C maximum could be reached. A larger induction furnace (50 KW unit MF) was used which could reach up to 1600° C with the arrangement of graphite susceptors indicated in figure 45. Temperatures near 1600° C ± 5° C were obtained after an hour and thirty minutes to two hours of the power turned on. Power input at 1600° C varied for each run between 130/140A, 105/115V and 16/19KW. The time at which the temperature could be maintained to within ± 5° C was of the order of 15 to 25 minutes, which was adequate for the present study.

The experiments were carried out by first allowing the graphite susceptors to reach the temperature required. The slag was added at this point and melting time varied from 30 to 40 sec. After four minutes of the slag being at 1600° C the power was turned off and the Fe-C sample was introduced through the top side by a pair of tongs. For all the experiments, as the droplet was introduced the slag temporarily collapsed while the droplet remained on the surface. The next 20 sec consisted of the slag covering the droplet followed by violent ebullition. The droplet appeared on the surface on several occasions and was seen as a complete sphere which was pulsating. At about forty seconds after the sample was introduced the droplet was seen to swell to about 1.5 times its original size. Reaction times ranged from 1 min 24 sec to 5 min after which the alumina-zirconia coated crucible was withdrawn and quenched in water.

From these experiments only three runs were successful in the sense that a complete droplet could be recovered. There were many problems beyond five minutes of reaction. The most important of which was attack of the slag to the crucible. Because the crucibles used were not recrystallized alumina,a great amount of porosity was present. Even when many of the pores could have been filled with the zirconia slurry it did not prevent the slag from infiltrating once a crevice had been initiated. In many cases the alumina crucible was so contaminated with slag that virtually all the slag had been "absorbed" into the crucible. After three successful runs were made the samples were visually examined before analysing for carbon content. One of such samples is shown in Plate XVII where it is seen that after one minute of reaction the sample has internally nucleated a considerable amount of gases. This porosity was further seen when crushing the sample which was more of a shell than a droplet. The variation of chemical analysis from the droplets with time have been plotted in figure 46.

Although no definite conclusion can be made from these findings it has, nevertheless, indicated that swelling of the droplet can be considered to take place as soon as a liquid phase is formed (allowing for the droplet to reach melting point) when in contact with the slag phase. This indicates that oxygen from the slag or slag itself is very rapidly delivered into the Fe-C droplet and, chemical reaction as could be expected, cannot be a controlling factor. The effect of increase in temperature is seen to have greatly

increased the decarburization rate. From previous experiments (see fig.41) a maximum decarburization rate of 0.3%C/min was obtained which is less than the minimum obtained under the latter set of experiments (i.e. 0.5%C/min) which is obtained by considering the point at 2m 14s in isolation. The maximum decarburization rate obtained at 1600° C was of 1.16%C/min which is obtained by considering the point at 1m 24s in isolation. The mean of maximum and minimum rate is 0.83%C/min which is similar to that obtained after three minutes of reaction (0.9%C/min).

The 1600° C experiments have shown that in the presence of slag the metallic drops swell rapidly, as in the case of levitated and free fall experiments (113), even when the carbon contents are high. It also confirms findings that high FeO in the slag serves as an oxygen reservoir which, on coming in contact with a droplet of high carbon content causes violent reaction which may lead to overflowing of slag in LD furnace operation (see section 2.6) or even explosion as suggested by Meyer (86). It may be argued that the induction current could have aided the droplet in achieving a higher degree of turbulence leading perhaps to slag being dragged into the droplet itself. When considering the impact which the oxygen jet exerts when lancing onto the metal and slag-metal-gas emulsion, it is not unreasonable to assume that a similar effect may be achieved. Both effects may be similar. It has been stated that induction stirring does not affect the decarburization rate (123).

4.6 Gas Injection.

Decarburization reactions of metallic samples with synthetic slag have been studied at various temperatures. The results obtained have shown that by increasing lime content and/or temperature an increase in decarburization rate is obtained. In order to further increase such decarburization rates, various alternatives could be followed. An increase in temperature and/or lime content in the $CaO-FeO-SiO_2$ slags would impose the necessity of adopting a different procedure to that previously used. In order to maintain consistency and at the same time allow comparison of results to be made the same procedure should be continued.

From the literature review no publications were found on decarburization reactions involving bubbling gases through the slag reacting with Fe-C alloys on a laboratory scale. Systems which could be said to be similar to the present study are mainly those carried out in plant operations as also are the works of Riboud (121-122) and Meyer (86-87). By blowing a gas either inert or with a predetermined oxygen potential a situation is created where by a greater turbulence could be achieved generating foams and emulsions typical of the condition found in industrial BOS furnace. The kinetics of metal-slag-gas reactions could be influenced by the foaming state of the crucible charge and the reactive oxidizing gases. The rate of decarburization when using gas injection could therefore be expected to be greater than when the system is in a semiquiescent state (i.e. turbulence due only to escaping of carbon monoxide bubbles).

A lance was designed for bubbling purposes from a stainless steel tube (4mm ID) and an Armco-iron nozzle (or tip) which are shown in plate VII. The tip was machined to 13mm outside diameter and 100 mm length with a gas delivery outlet of 1mm diameter made with a spark machine. Although several alterations were made to the joining of the tip with the stainless steel tube, the final arrangement consisted of welding a stainless steel segment of larger diameter than the lance and tip used. The latter arrangement allowed the tip to be cut-off when required and a new tip to be welded in place. In order for the lance to be centrally positioned a collar-guide was welded to the lance which at the same time served for guiding of the stainless steel wires by which the crucibles were suspended.

The gases used for bubbling into the slag at 1300° C were high purity argon, argon-5%CO_2, 100%CO_2 argon-1%O_2 and argon-10%O_2. All gas injection results were obtained at 1300° C and with zirconia coated iron crucibles.

4.6.1 Argon injection.

Before any decarburization experiment using gas bubbles was carried out, it was necessary to establish an approximate flowing rate to be used throughout the series. This was made by using fayalite slag and high purity argon. The working tube was always kept under inert atmosphere for all experiments made. The argon delivered into the slag was first allowed to bubble through dibutylphthalate and controlled by a needle valve to give initially one bubble every seven seconds. The gas was then delivered through the lance into the slag. Under these conditions (one bubble was allowed to burst every 7 sec)

by observing the surface of the slag only a sudden burst, or periodical movement, was seen to take place although the actual size of the bubble could not be detected. The flow was further increased to one bubble per second but again only general movement throughout the slag was detected. There was in general no appearance of foaming taking place, only the sudden rise of the surface while the bubble escaped. When the lance was withdrawn the slag returned to its quiescent state. The lance and crucible were then withdrawn from the hot-zone very slowly to a cool-zone and ultimately taken out for inspection. The lance tip was covered with slag to just over (25.4mm) 1" height, the slag was taken off very easily and there was no attack on the lance itself. The crucible, which was used for a total time of 3 hours at 1300° C showed no sign of defects.

By carrying out similar trials it was ultimately established that a flow rate of 300 cc/min would create greater turbulence within the slag without causing any overflowing. Decarburization of Fe-C alloys was carried out initially using 300 cc/min flow rate and with the preheating sequence previously established (i.e. 800° C for 10 min, 1000° C for 7.5 min) and a final reaction temperature of 1300° C.

Because of the time required for the slag to be fully molten the lance was introduced after the crucible had been at 1300° C for approximately one minute. Argon bubbling was carried out for five minutes after which the crucible was released and quenched in water. After the slag was removed at least fourteen droplets of metal with diameters varying from 0.5 mm,

1 mm (4 samples) and 2 mm (1 sample) were recovered. As expected, the marking of the slag on the crucible was found to be higher (about 80% of the crucible height) than when using fayalite slag alone. The lance tip had more slag adhered to it and to a height of approximately 1½" (37mm) but again easily detached. The section of the lance tip which was not covered with slag was slightly oxidized due most probably to vapours from the quenching operation while the furnace bottom was opened.

The following trials consisted in reducing the gas flow rate used in injection, from 300 to 200, to 150 and ultimately to 75 cc/min. The latter flow rate (75 cc/min) produced turbulence which covered 60% to 80% of the crucible (about 48mm to 64mm height) and over 25mm of the lance tip. The drops did not shatter at this flow rate as they had done at 150, 200 and 300 cc/min. Below 75 cc/min (at about 50 cc/min) the bubbles just detached from the lance tip without creating noticeable turbulence in the bath. On this basis, the gas injection rate was chosen to be 75 cc/min which was the compromise between a guarantee of no drop dissemination and yet a reasonable transfer of momentum to the slag. The slags used during bubbling appeared to be highly foamed. They were easily removed from the crucibles. These conditions prevailed throughout the following gas injection experiments.

Once the minimum flow rate was established the most common problems encountered during the present experiments consisted mainly of the droplets welding on to the lance tip and a few welding on to the crucible. The lance tip after each

experiment was surface ground in order to remove surface scale or, in cases when a drop had welded, heavy grinding was needed. The lance tips were generally used for not more than ten experiments after which replacement with a new lance tip was made. Although some lance tips were not greatly reduced by grinding (i.e. when most experiments had been carried out successfully) it was nevertheless removed in order to maintain consistent conditions for depth of tip in the slag.

Having established the flow rate for gas injection at 75 cc/min and the procedure by which the experiments were to be made, fayalite was used to decarburize an Fe-4.16%C alloy at 1300^{o} C. The decarburization curve obtained is shown in fig.47. By comparing the latter results with those carried out without gas injection (see fig.24) it was found that the decarburization rate had increased to some extent but less than had been expected.

Further experiments were made using argon injection, a 25.85% CaO-slag and an Fe-4.16%C alloy. The decarburization rates obtained with this set of conditions shown in figure 48 were greater than those without gas injection but less than for the 1400^{o} C experiments. It was therefore apparent that the turbulence created by lancing does tend to increase the decarburization rate although perhaps not as much as might be expected. It must be kept in mind that the gas flow rate was small (75 cc/min) and an inert gas was being used.

4.6.2 Argon-Carbon dioxide.

The experiments on decarburization of Fe-C alloys by fayalite and 28.85%CaO slags with argon injection have shown, as expected, an increase in the rate of decarburization. It was suspected that in order to obtain a significant increase in decarburization rate the oxygen potential within the system needed to be increased.

By injecting an Argon-5%CO_2 gas mixture an oxygen potential of 1.034×10^{-9} atm is obtained as calculated in Appendix I. Oxygen potentials of the various slags are also given in Appendix I for comparison. From the literature survey (see 2.3.2) it was found that the highest oxygen potential of any of the slags used in the present work is that of fayalite (1.55×10^{-12} atm); consequently the gas gives an oxygen potential increase of 10^3. A slag with 28.05%CaO content was used to study the effect of varying oxygen potential on the decarburization rate. The results obtained are given graphically in fig.49. The appearance of the reacted droplets was similar to the previous cases; after 7 minutes of reaction and carbon contents of 2.65% and 2.82%C the surfaces appeared "smooth" whereas the surfaces of the drops with 1.80%C and less were covered in craters.

The decarburization data were compared with those obtained when argon injection was used and the results were found to follow an identical path (i.e. the same decarburization rate was found). Calculations were needed to determine the theoretical effect on decarburization rate by using an argon-5%CO_2

gas mixture. From previous decarburization experiments without gas injection a range of decarburization rates from 0.1% to 0.3% C/m was observed. From a mass balance (see AppendixII) a maximum decarburization rate of 0.2%C/min could be expected from the use of argon-5%CO_2 mixture at 75 cc/min if all reactive content of the gas were consumed. The results indicated that a change in the oxygen potential of the gas injected had very little effect under the present experimental conditions, except the effect due to turbulence alone on the decarburization rate. This can be said from the findings after argon and argon-5%CO_2 gas mixture had been injected through the slag at 1300^{o} C.

Further experiments were required to substantiate the latter findings. By using 100%CO_2 an oxygen potential of 2.16×10^{-8} atm would be delivered via the gas phase without the inert gas being present (i.e. the gas injected would be totally reactive). The slag used was of the same chemical composition as that previously used. Carbon dioxide was delivered from a cylinder into a heating unit prior to passing a flow meter. A safety trap was found necessary when using carbon dioxide due to gas contraction when gas flow was stopped. The trap was installed prior to the dibutylphthalate bubbler which delivered the gas through plastic tubing to the lance and into the slag.

No change was detected in the pattern while gas injection was being carried out into the slag. From visual observations during the reaction time, the reacted samples were similar to

previous samples. In some cases the lance tip showed signs of greater turbulence as indicated by slag-spots found above the slag level markings. The results for 100% CO_2 gas injection are given in figure 50. It may be observed that the overall decarburization rate has decreased (compared to Argon-5% CO_2 gas injection) although the gas injected was, in this case, of higher oxygen potential. Because the experimental technique was carried out following the same steps during all of the gas injection experiments, it may be concluded that, under the present conditions, the oxygen potential of the gas injected does not alter to a great extent the rate of decarburization. In fact by comparing the latter results with experiments with no gas injection at all (see figures 28 and 26) the rates for decarburization obtained may be said to be equal.

4.6.3 Argon-Oxygen Injection.

Decarburization rates obtained by bubbling 5% CO_2 and pure CO_2 indicate very little influence with regards to oxygen potential. Under the present experimental condition difficulties might be expected with the iron lance tip and also with the iron crucibles used if going to higher oxygen potentials. From calculations (Appendix I) it has been determined that by blowing an Argon-1%Oxygen mixture the available decarburization rate would be less than if using an argon-5% CO_2 gas mixture, although the actual oxygen potential of the gas is higher. This is mainly due to the amount of oxygen made available for reaction (i.e. $75 \times .01 \times 10^{-3}/22.4 = 3.348 \times 10^{-5}$ g-mol of oxygen per min).

Considering the reaction

$$O_2 + 2C = 2CO$$

$$\tfrac{1}{2}n_{O_2} = n_C = n_{CO}, \text{ and,}$$

$$3.348\times10^{-5}\times12 \times 2 = 0.08\%C \text{ per min,}$$

which is less than half the value obtained with Argon-5%CO_2 (0.2%C/min). Gas injection to slags was carried out using an Argon-1% oxygen mixture, 28.05%CaO slag, and, an Fe-4%C alloy.

The experimental procedure did not present any problems except that the lance tip orifice did increase by about 0.5mm to 1mm. Consequently the lance tip required changing three times for the whole of this series.

The decarburization curve obtained is shown in figure 51, which, compared to the results obtained when blowing an argon-5%CO_2, has a lower decarburization rate, but at the same time, is higher than for a pure CO_2 bubbling.

Further experiments were made by using an Argon-10% oxygen gas mixture. Only three experiments were made since the lance tip rapidly deteriorated and heavy oxidation was taking place. After each run the slag and oxide were removed from the tip and in each case the gas outlet had greatly increased in diameter, up to 2 mm and more. No further trials were made because the times involved for each experiment would be very short and a great deal of error would be anticipated.

The results obtained from the bubbling of gases into slags have shown that the oxygen potential of the gases themselves has no great direct influence on the decarburization rate.

The gases seem to aid decarburization mainly by the turbulence generated within the system and to a lesser extent by the supply to the slag with oxygen for reaction.

4.7 Scanning Electron Microscope.

Several slags, reacted and unreacted droplets were examined using a Phillips Scanning Electron Microscope PSEM 500 at an accelerating voltage of 25 KV.

One of the advantages of the use of a scanning electron microscope is that it enables fractured unpolished surfaces to be examined. With iron-carbon droplets which have been decarburized in slags the fractured surface can thus be examined avoiding possible contamination or removal of entrapped impurities in polishing. Various fragments, obtained from reacted droplets were mounted on aluminium stubs using colloidal silver and dried in vacuum. The surfaces observed were chosen from either the fractured interface or from internal cavities formed.

Qualitative Energy Disperse Analysis System (EDAX) was used to detect elemental components as Si, Ca and Fe.Slags and drops were analysed and the peaks, showing the existence of Si, Ca and Fe regularly observed were as shown in figure 53. Fe-C unreacted samples were then analysed in a similar manner and as expected only Fe was detected as shown in figure 52. which indicates that the samples were free from impurities.

Several fragments from reacted droplets were analysed using the EDAX method which showed small quantities of Ca and Si. A selection of energy levels was then made for each element and

fed to the display monitor unit. In this way, by X-ray mapping, a picture of the distribution for each element was obtained.

The results obtained initially indicated great variation of concentration for different areas inspected and it was therefore decided to inspect a wider area which could give an overall view of a Ca and Si distribution. The area shown in figure 54 corresponds to the interface of a cross section from the droplet near the centre. X-ray mapping was made to detect Ca and Si from which photographs were taken with a polaroid camera.

The results are given in figures 55 and 56 which clearly show that calcium and silicon had been entrapped well within the droplet and this effect was found in most of the samples examined. The patterns or contours for the location of both silicon and calcium were found to follow each other for different samples observed.

The evidence of the presence of calcium and silicon in the metal phase was assumed to be indicative of the presence of silica and lime which could have come only from the slag. This evidence has vital ramifications for the discussion later (section 5.3.2) and therefore was explored further.

X-ray mapping was made of other areas and showed similar patterns for calcium and silicon. Mapping was done at other higher magnifications and again showed similar patterns. Even at the highest magnifications the presence of these elements continued to show but they were always as small discrete points,

scattered in large numbers throughout the surface. Attempts were made to identify these sources of calcium and silicon as a separate phase (slag inclusions) but even at a magnification of 25000 the particles were still too small to be detected as individual grains. It can be concluded from this that the particles of slag are extremely small: although it is difficult to estimate the minimum size of particle which can be seen on the screen, it seems likely that no slag particle is greater than 500 Å.

CHAPTER FIVE

DISCUSSION

5.1 Introduction.

It has now been well established that during oxygen steelmaking a great portion of the metallic charge is found dispersed in the slag forming a metal-slag-gas emulsion (70,83,86,87). In order to attain an insight into the reactions which take place within this emulsion the present investigation was carried out. A slag typical of those used in actual plant practice operation could not be used as previously discussed (see preliminary work). An approximation was therefore made by using synthetic slags of the lime-iron oxide-silica system. As carbon oxidation is one of the most important reactions in operation control and in the establishment of the emulsion itself by CO evolution, Fe-C alloys have been used to represent the metal phase. The results obtained from the decarburization studies have been reported graphically on a %C content vs time of reaction. Other phenomena observed have been reported appropriately in previous chapters. The discussion of the findings has been divided into several sections for convenience of presentation in this chapter which follows.

5.2 Slag Paths.

Slags with carbon in one form or another is undoubtedly one of the most important reactions. In open hearth steelmaking the interaction is apparent from the slag layer covering the

molten metallic bath. The oxygen steelmaking processes with a metal-slag-gas emulsion depend, to some extent, upon the decarburization of iron by reacting with the slag.

During the preliminary work attempts were made to determine the paths followed by the synthetic slags used during decarburization of Fe-C alloys. Although the quantity of carbon removed by the slag was small (2 to 3% from a one gram drop), a change in the chemical composition would indicate the most likely reaction taking place.

The slag path studies carried out under the present experimental conditions show that a reduction of iron oxide from the slag by carbon tends to move the composition towards the lime-silica join. In practical oxygen steelmaking the same tendency is found but, due to lime additions which are made during a given cycle, the compositions tend to move towards the CaO corner. This effect is shown in figures 15a and 15b which were determined from plant operations (10,107).

The changes in chemical composition with time for CaO-FeO-SiO_2 decarburization reactions are given graphically in figures 29 to 32. All the results clearly show a reduction of FeO and Fe_2O_3 content and therefore the silica and lime contents tend to increase. Since the actual amount of silica and lime remain constant throughout the experiments their actual percentages in the slag increases. The appearance of free iron in most of the experiments also confirms the reduction of iron oxide from the slags. The reactions taking place may thus be represented in the most simple way by:

$$\underline{C} + (FeO) \longrightarrow CO_{gas} + Fe(liq) \quad .... \quad 5.2.1$$

or $$\underline{C} + 2(FeO) \longrightarrow CO_{2gas} + Fe(liq) \quad .... \quad 5.2.2$$

The FeO may well participate in prior reactions as it acts as the oxygen donor, according to:

$$(FeO) = Fe(liq) + \underline{O} \quad ..... \quad 5.2.3$$

followed by $$\underline{C} + \underline{O} = CO_{gas} \quad ..... \quad 5.2.4$$

The first three reactions taking place at the metal/slag interface while the fourth takes place at the metal/gas interface.

The free iron was found to increase with time for all slags but was greater when high lime contents were involved. This can be expected as it has been shown (54) that with high silica contents and no lime (i.e. Fayalite) some FeO remains combined as silicate. On adding small quantities of lime, displacement of FeO from the silicate network takes place and some FeO is set free (i.e. effectively increasing γFeO) (43,36,52,54).

From the ternary diagram in figure 12 the liquidus isotherm is seen to decrease and consequently a less viscous slag is present which in turn favours a higher degree of turbulence to be generated within the slag bringing "fresh" FeO in contact with the Fe-C droplet. On further increasing the lime content (e.g. to 26%CaO) a small increase in the amount of free iron was obtained as compared to previous slags. These results may be accounted for when considering that the $CaFeSiO_4$ composition (29.78, 38.3 and 31.92 wt% respectively) is closely approached. As found by Johnson and Muan (54) a pronounced negative deviation from ideality is found within the vicinity

of this composition, indicating a strong tendency for the $CaFeSiO_4$ formation. At the highest lime contents used in the present investigation (32%CaO) a rapid increase in free iron was found. The free iron was again mainly from FeO although Fe_2O_3 was greatly reduced. The rates obtained for decarburization with slags containing 32% CaO were in fact lower than those found for slags with 26% CaO. The effect may be due to appearance of dicalcium silicate precipitates. Such precipitation has been found by Trentini (83) in oxygen steelmaking and by Kootz (90) in open hearth steelmaking. The latter states that the slag penetrates very soon into the heterogeneous zone. This leads to a reduction in the rate of decarburization. The penetration into the zone is shown in figure 15c.

With regards to surface nucleation effects on the reacted droplets, it was apparent that high lime contents may have had an effect simultaneously with carbon content. Evidence was found that only in high lime slags and at about 2.2%C contents did surface nucleation take place. The faster decarburization rates obtained with these slags may have caused depletion of carbon in the outer region, and therefore CO evolution was subsequently retarded. A lesser degree of turbulence can be expected due to this effect and detachment of CO bubbles is facilitated with less ease. The possibilities of bubble nucleation must therefore be considered as discussed in the following section.

Attempts were made to quantify the results of the slag path analyses obtained by reactions such as

$$FeO + C \longrightarrow Fe + CO \qquad 5.2.5$$

and $$Fe_2O_3 + Fe \longrightarrow 3\ FeO \qquad 5.2.6$$

The slag path followed by one of the slags studied, that which is shown in figure 29, will be discussed in detail having in mind that the slag paths given in figures 31 and 32 were similarly examined for mass balances.

The decrease of FeO and Fe_2O_3 contents from the initial slag were found to be 2.64% and 2.1% respectively after five minutes of reaction. The weight of slag used was 30 grams and therefore the Fe generated from 2.64 %FeO reduction is calculated as:

$$\frac{\text{wt. of slag x wt \% FeO x Fe (molecular wt)}}{100 \text{ x FeO (molecular wt)}} = \frac{30x2.64x56}{7200}$$

$$= 0.616\text{g Fe}$$

Assuming that 0.616 g of Fe react with Fe_2O_3 by reaction 5.2.6, the decrease of Fe_2O_3 is calculated as:

$$\frac{0.616x160}{56} = 1.76\text{g of } Fe_2O_3$$

The weight of Fe_2O_3 which the slag actually lost by reaction was $\frac{2.1x30}{100} = 0.63\text{g of } Fe_2O_3$. These last two values

differ by a factor of 2.8 and therefore it must be assumed that not all the free iron reacted with ferric oxide. Since, from chemical analysis, only 0.63g of ferric oxide were reduced, the quantity of free iron required is calculated as wt%Fe = 0.63x56/160 = 0.22g of Fe. The free iron generated by ferrous oxide would then be decreased by the above quantity (0.616 - 0.22) leaving 0.396g of Fe free from the slag. The weight of analysed free iron is less than 0.15g (i.e. 0.5%), which in turn differs from the calculated value of 0.396g by a factor of more than 2.6.

Slag paths given in figure 29, 31 and 32 were all analysed in a similar manner at the times corresponding to 5, 10 and 15 minutes. To facilitate comparison between the calculated values and those given in the corresponding figures in wt %, the calculated results have all been converted to wt%. Figure 30 was not used in the present calculations because the free iron present was not analysed as described in section 3.5.5. The results are given in table III-A together with the ratio of Fe analysed/ Fe calculated which is a measure of the disagreement. It can be seen from table III-A that only in two cases does the Fe analysed/Fe calculated approach unity. The results indicate a wide disagreement and therefore a low probability for a correlation would be obtained. The method described above clearly shows that the slag path analysis

data are not sensitive as means of quantifying, through mass balances, the reaction (or extent of reactions) which are taking place in the metal phase.

One other approach to quantify slag path analysis is to use the known carbon loss, from the iron carbon sample during reaction, and calculate the extent to which ferrous and ferric oxides in the slag would be reduced by this known carbon drop.

The mass of slag is 30 grams and the mass of iron-carbon is one gram. The carbon lost after 5 minutes of reaction (figure 32) with the slag given in figure 29 is 0.81%C. The reaction considered is 5.2.5:

$$FeO + C \longrightarrow Fe + CO \quad ,$$

The mass of ferrous oxide reduced by 0.0081g of carbon is thus 0.0081x72/12 = 0.0486 g of ferrous oxide. The value obtained from chemical analysis is 0.792g of ferrous oxide (or 2.64% FeO in figure 29).

The slag paths given in figure 29 and 32 (figure 31 was not used - no comparable decarburization curve) were analysed in the above manner and the results are given in table III-B. The calculated values in table III-B are clearly much smaller than the analysed values. This pronounced disagreement substantiates the previous disagreement between FeO, Fe_2O_3 and free Fe contents from the slag path analysis and mass balances. It is quite obvious that decarburization rates within the metal drop cannot be followed by sampling and measurements of the slag phase. As explained in section 3.5.5 the errors resulting from the chemical analysis of slags, the sampling of slags, the slag mass/metal mass ratio and the

interference of zirconia as a coating, all contribute to the wide range of scatter obtained.

5.3 Nucleation.

The nucleation of bubbles has been widely studied for many years (124). Two possibilities exist by which bubble nucleation may take place; they are either homogeneous or heterogeneous nucleation.

5.3.1 Homogeneous Nucleation.

The homogeneous nucleation of a bubble in a liquid medium requires that the pressure within the bubble must be greater than the sum of the pressures acting on the bubble. Considering the nucleation of carbon monoxide bubbles within a metallic bath the acting pressures (i.e. the pressure required to be overcome by the bubble for growth) are the sum of:

$$P_{CO} > P_A + P_f + P_\gamma \qquad (5.3.1)$$

where P_A denotes the pressure exerted by the atmosphere, P_f is the hydrostatic pressure above the bubble ($h\rho g$), and P_γ is the pressure which results from the curvature of the surface at the interface. The pressure P_γ is determined by considering the energy required for the surface area and volume of the bubble to experience an increase in size. The carbon monoxide is thus required to overcome the pressure (in atmospheres) given by:

$$P_{CO} > P_A + 9.7\times10^{-4}\ h\rho + 9.9\times10^{-7}\ 2\ \gamma/r \qquad (5.3.2)$$

From studies on surface tension of silicates (126) and lime-iron oxide-silica slags (127), corresponding with the synthetic slags used in the present work, values of 400 to 530 dynes/cm are found. The range of variation for the surface

tension of iron carbon melts (128) and for different elements dissolved in iron (77) is found from 1200 to 1800 dynes/cm.

From the droplets reacted in synthetic slags clear evidence was found, from X-ray analysis, that internal nucleation had taken place. The pressure required by a carbon monoxide bubble to homogeneously nucleate is calculated as follows: The atmospheric pressure is considered to be one atmosphere; slag height above the droplet of about 3.5 cm; slag density was taken from Gaskell (129) as 3.2 g/cm^3 and, for the iron carbon droplet, a surface tension of 1200 dynes/cm was selcted from Kitchner (128). The pressure to be overcome by a carbon monoxide bubble with a radius of 6Å(11) is calculated to be 2.96 x 10^{+4} atm. The figure of 6Å is chosen as a typical value for the radius of one CO molecule.

The calculated value, which is similar to those proposed for carbon monoxide nucleation in a steel bath, is extremely high. Under the present experimental system it is unlikely that such high pressures consistently developed, since many droplets which exhibited internal nucleation remained stable. When considering the internal pressure which would be required for homogeneous nucleation, the tearing effect would have shattered a great many of the droplets found. Under the present circumstances homogeneous nucleation is not considered to take place.

The pressure of 10^{+4} atm. required for homogeneous nucleation has not been observed experimentally (130). Von Bogdandy (131) calculated the probability of homogeneous

nucleation of carbon monoxide bubbles as a function of the oxygen content for a one percent carbon-iron melt. The results indicated that homogeneous nucleation is virtually impossible within the melt. Bradshaw (132) from a graphical representation of excess pressure vs bubble size has shown that for nucleation to take place either the critical nucleous must be of an appreciable size or there must be an appreciable supersaturation. Distin (111) on levitating Fe-C alloys in oxygen atmosphere at 1200 cc/min, calculated at 1790° C carbon monoxide supersaturation pressures approximately of 25 atm. The above mentioned observations confirm that under the iron-carbon/slag reactions studied homogeneous nucleation could not have taken place.

5.3.2 Heterogeneous Nucleation.

Having discarded homogeneous nucleation as a possible mechanism for CO formation, the possibility for heterogeneous nucleation will now be sought. In homogeneous nucleation it was found that high values of work for the formation of one nucleus are required. These values for work are drastically reduced by the type and nature of interfaces at which nucleation is taking place (i.e. nucleation sites). The intervention of an interface such as a slag/metal, gas/metal or the presence of impurities, give rise to heterogeneous nucleation.

It is well known that crevices within the refractory lining of a steelmaking furnace are potential nucleation sites for bubbles. Evidence of this effect was detected by Korber and Oeslen (124) and similarly by Turkdogan et al. (125). These authors found that a smooth or glazed surface retarded carbon

monoxide evolution whereas with a rough or scratched surface a vigorous boil was produced. Similar effects have been found by Larsen (133) and by Delve (134). Alexander et al. (135) have studied the effects of refractory surfaces on the growth of CO bubbles during vacuum degassing of iron melts.

Several factors have been found to affect bubble nucleation. The contact angle θ between two different surfaces (e.g. liquid iron on refractories, slag on graphite) has been found to determine a minimum radius for which bubble growth can be sustained (132). The contact angle is a measure of the relative surface tension developed at the interface concerned. At the junction of three phases (M metal, S slag and G, gas) the balance of interfacial tension can be solved so that on equilibrium:

$$\gamma_{MG} = \gamma_{MS}\cos\theta_{MS} + \gamma_{SG}\cos\theta_{SG} \qquad (5.3.2.1)$$

If the metallic phase is solid and the slag spreads over the surface (i.e. wetting takes place) then θ_{MS} is zero and

$$\gamma_{MG} = \gamma_{MS} + \gamma_{SG}\cos\theta_{SG} \qquad (5.3.2.2)$$

When the contact angle θ_{SG} is greater than 90^{o}, as could be expected from the surface appearance of the reacted droplets (see Plates X to XIII), then the slag cannot displace the gas and a stable bubble is obtained. Detachment of the bubble can take place either after the said bubble has grown to a given size, or by external effects due to buoyancy or stirring. Hazeldean et al. (99,103) noted from X-ray experiments, that particularly at low carbon concentrations, the carbon monoxide

bubbles could remain attached to the drops thereby inhibiting descent through the slag and in some cases causing them to be buoyed up. Similar effects have been noted by Acheson (136) when studying the reaction of sodium amalgams in aqueous solutions contained in an LD model. Discussions on size, shape and contact angles for various materials have been widely covered by many authors (11,12,132,135).

The above mentioned studies indicate that the system under study, whereby an Fe-C droplet is engulfed by a slag phase, is clearly one in which heterogeneous nucleation is greatly enhanced. This has been confirmed by visual observations during decarburization, where a high degree of turbulence was observed to take place during all the decarburization experiments carried out.

Considering heterogeneous nucleation as the possible mechanism by which carbon monoxide is nucleated, then the minimum radius at which nucleation may take place at the metal/slag interface can be calculated from (5.3.2) as follows:

$$r = \frac{9.9 \times 10^{-7} \times 2 \times \gamma}{P_{CO} - P_A - P_f} \qquad (5.3.2.3)$$

The following data are considered in the calculation:

γ = 450 dynes/cm

h_{slag} = 3 cm

ρ = 3.2 g/cm^3

P_A = 1 atm.

P_{CO} = 10, 5 and 1.5 atm.

The calculations yield values of radii of 0.0001, 0.0002 and 0.0018 centimeters for the nucleation site, if the CO bubble which so nucleates is then to grow from the slag/metal interface.

For heterogeneous nucleation the surface tension between an Fe-C alloy and a gas is 1200 dynes/cm (128). Similar calculations at CO overpressures of 10, 5 and 1.5 atm. yield values of radii of 0.00026, 0.00053 and 0.0048 centimeters. A cursory observation of this phenomenon may indicate that internal nucleation of CO bubbles requires that there be quite large nuclei present for heterogeneous nucleation to take place. However, a detailed examination of the formation of a bubble from one CO molecule which forms at an interface (such as a slag/metal interface which may well be highly irregular in shape and surface texture) leads to the conclusion that the size of the nucleation site is unimportant. All that is required for heterogeneous nucleation and following growth is the presence of an appropriate interface, i.e. nucleation and growth should be envisaged as occurring on or at the interface rather than around the nucleus body.

Consideration of the state of the droplet and the reaction taking place have also to be taken into account, and this will be discussed in the following section (5.4).

Another possibility for nucleation which is neither homogeneous nor heterogeneous in the accepted sense is that referred to as vortex nucleation. (137,113). This hypothesis postulates that the turbulence created may be of such

intensity that if eddy centres were assumed to constitute free vortices, then negative pressures of the order of 30,000 atmospheres could exist at four microns from their centres (137). As explained by Robertson (113) the life time that the free vortices may have would be extremely short, perhaps of one millisecond or less, prior to degeneration. The vortices could also serve as funnels through which the slag or gas could be entrained in the metal.

5.4 Drop Behaviour.

It is well known that a drop of one liquid falling into another behaves as a rigid sphere and obeys Stoke's law only when the Reynolds number is less than one. For a drop of steel or copper in slag this corresponds to a diameter of less than 0.5mm (138). A drop velocity is different from that of a rigid sphere because internal fluid circulation can take place and the drop can be deformed from spherical shape. The shape of a drop moving in a liquid is known to depart markedly from spherical, especially at high Reynolds numbers (141). Hu and Kitner (140) classified shapes of drops according to viscosity of the continuous phase in which the drops are moving. At high Reynolds numbers droplets falling in a low viscosity (one centipoise) continuous phase were distorted to the extent that an oblate shape is obtained. The eccentricity increasing with increasing size. When a critical size is reached, usually corresponding to a critical velocity, the surface tension cannot maintain the spherical shape and the drop begins to oscillate. Some of the causes are thought to include drop

formation, wake turbulence, vortex shedding and mass transfer. The transition from oblate to spherical shape was observed in the present decarburization experiments as shown in plates X and XI. Although the drops are not strictly falling as in many of the above studies, their changing shape does indicate that a high degree of turbulence was taking place, particularly in the first minutes of reaction as observed during the runs (see 3.5.4). The distortion from a spherical shape also indicates a high relative velocity between drop and slag.

The original sample as set in the slag is of cylindrical shape (height/diameter = 1). As melting commences, the drop is entrapped in a highly turbulent surrounding of low viscosity. The oblate shape is very soon attained by the sample and may be maintained at least up to eight minutes of reaction as shown in Plate X. The subsequent shape of the samples remain near spherical for all times, as seen in plates X and XII. This indicates that a critical size (volume) must have been reached which in most cases was near eight mm diameter. There was never any sample which exceeded 8.5 mm. From the X-ray photographs in plate XIII it is seen that for six and eight minutes of reaction a considerable amount of gas has been entrapped. Gas entrapment will have effects on the geometry (shape), size (volume) and on maintaining one complete sample (coherence of the drop). By increasing the volume of gases within the drop the external viscous forces will, more readily, distort the shape. The change in size (volume) of the drop serves to estimate the volume of gas entrapment which has taken place within the drop.

By considering the initial drop as a sphere with six mm diameter and comparing with a diameter of a reacted sample (see plates X to XII) an increase of two mm is found. The increase in volume is difficult to visualize from a two mm increase in diameter in the photograph. By comparing the initial (V_1=0.1131 cm^3) and the final volumes (V_2=0.268 cm^3) of a drop, an increase of 237% in volume is found. The volume of gas within an eight mm diameter drop after reaction gives rise to a porosity of $(V_2-V_1)/V_2)$ = 57.8% within the drop. The initial iron-carbon sample of 7.2 g/cm^3 density now becomes an emulsified drop with a bulk density of 3.02g/cm^3.

Because the relatively low temperatures at which the present reactions were carried, the samples were . of, and had time for, retaining and distributing the gas bubbles generated. Further increase in volume causes the sample to yield at a weak spot and allow the gas to escape. This latter mechanism is proposed from the evidence found from many reacted drops of which the few shown in plates VIII, IX and XI, are typical.

During experiments carried out at 1500°C and 1600°C the droplets were clearly seen to be pulsating (i.e. shape change on an oscillating basis) while reacting with the slag. Because of the relatively higher temperatures the droplet is more fluid, and the decarburization rate (i.e. CO evolution) is faster, than at 1300°C and 1400°C. The gas evolution at 1600°C cannot be counter-balanced or supported by the thin walls of the drop and thus ultimately shattering of the drop occurs (see section 4.5). The latter effect is clearly seen in plate XVII where two small drops are seen to be detaching from the mother drop.

With respect to the hydrodynamic behaviour within droplets a great number of studies have been made (139,141). Evidence

that internal circulation is taking place inside drops has been based on photographic patterns. For drops with internal noticeable circulation Handlos and Baron (142) have proposed a model where streamlines are circular and concentric (known as tori) as shown in figure 57. Mass transport across the streamlines occurs by diffusion. Experimental verification of Handlos and Baron's model has been made by Skelland and Welleck (144,145) and by Johnson and Hamielec (146).

In previous section 4.7, the presence of silicon and calcium inside reacted droplets was detected by means of a scanning electron microscope. The mechanism by which a carbon monoxide bubble was initiated inside the droplet could have been most certainly by slag entrapment through internal circulation of the drop. The surface appearance of the droplets (see plate X and XI) clearly show signs that a kneading-like effect is taking place. The above effect will most certainly entrap minute particles of liquid slag which will serve as potential subsurface nucleation sites. The volume increase experienced by the drop, due to CO nucleation, will tend to increase internal circulation within the drop. The dragging of CO bubbles to the centre then becomes more effective. When bubbles of carbon monoxide come together, either near the centre or the surface, a weak surface layer will be formed in the drop (see fig. 23). By the above mechanism the carbon and oxygen paths are decreased and the decarburization reaction rate will be increased. As the droplet increases further in volume the surface tension

of the droplet cannot counterbalance the carbon monoxide pressure and rupture of the surface layer takes place through a violent motion (see plate IX). When detachment of the internally nucleated bubbles takes place, slag and/or metal, collapses in and fills the cavity left and therefore the droplet becomes "emulsified" (see drop 3 in plate XII).

The surface nucleation of carbon monoxide bubbles could have been on account of various factors. It will be recalled that surface nucleation was detected only when decarburizing with high lime slags. The decarburization rates were of the highest values obtained when decarburizing with high lime slags. A rapid decrease in surface carbon content would have increased the solidification temperature of the Fe-C drop. With partial solidification of the drop surface, circulation within the drop decreases and the carbon monoxide bubbles adhere more closely to the drop. The carbon monoxide bubbles will continue to grow from carbon monoxide generated by adjacent reactions taking place between slag and melt. As the bubbles detach, entrainment of slag and metal can take place causing a further increase in the number of bubbles appearing per unit area (and time) due to the greater number of nuclei available for nucleation. As the number of bubbles generated increases, and the carbon content in the surface layer decreases, the actual size of the bubbles decreases; clear evidence is shown by comparing drop number four of plate XI with drop number seven of plate XII.

When gas lancing was carried out to increase the degree of turbulence within the system the frequency of detachment of

carbon monoxide bubbles and circulation of the drop were increased causing an increase in decarburization rate. Although the momentum of the jet could have caused the disruption of drops (e.g. shattering of drops when lancing at 300 cc/min), the effect was minimized by decreasing the flow rate down to 75 cc/min. The probability of direct impingement is further reduced when considering that the drops were constantly moving within the slag. The slag acted as a shield and the drops were rarely directly under the jet discharge tip.

When temperature was increased for the decarburization reaction, the violent agitation within the drop greatly increased and distortion of the drops becomes more pronounced. The latter effect is shown by drops reacted at 1500° (plate XIV). The effect was found to be even more pronounced at 1600° C as is shown by the drop in plate XVII which was reacted for less than two minutes. The photograph in the above plate shows two small droplets at the very instant of detachment from the mother drop. The effect of a vigorous agitation is also reflected by the higher decarburization rates obtained.

5.5 Simple models for Mass Transfer.

During mass transfer operations it is customary to draw a distinction between two types of reaction. Those in which the whole of the process is controlled by a slow chemical reaction at the phase boundary, and those reactions which are controlled by material transfer to or from the phase boundary.

This type of mass transfer is classically referred to as the film theory.

The decarburization reaction between Fe-C drops and synthetic slags

$$\underline{C} + (FeO) \longrightarrow Fe(liq) + CO_{gas} \qquad (5.5.1)$$

involves a number of steps including the following:

i) transport of FeO to the metal/slag interface.

ii) transport of C to the metal/slag interface.

iii) chemical reaction at the interface.

iv) transport of CO away from the interface

On further considering internal nucleation the following should also be taken into account:

$$(FeO) \longrightarrow Fe(liq) + \underline{O} \qquad (5.5.2)$$

$$\underline{O} + \underline{C} \longrightarrow CO_{gas} \qquad (5.5.3)$$

i) transport of oxygen through the metal phase.

ii) reaction between carbon and oxygen to nucleate CO

iii) transport of carbon and oxygen to allow growth of nucleated carbon monoxide.

Before establishing the possible rate controlling step, a general approach will be made by considering simple models for transport to establish whether continuous or discontinuous phase control are operative. In mass transfer studies between a continuous phase and a discontinuous phase, four categories are established depending on where the resistance to transfer occurs and whether or not internal circulation occurs in the dispersed or continuous phase.

5.5.1 Resistance in stagnant dispersed phase.

The first case considers resistance in a stagnant dispersed phase. The problem becomes one of diffusion inside the stagnant drop (or bubble). In the continuous phase the reactive species is readily transferred and available in abundance at the interface. In these circumstances application of Fick's second law for unsteady state diffusion in a spherical body may be written as:

$$\frac{\partial C}{\partial t} = D\left[\frac{\partial^2 C}{\partial r^2} + \frac{2}{r}\frac{\partial C}{\partial r}\right] \qquad 5.5.1.1$$

Only transfer in the radial direction is considered and the diffusivity is constant. The concentration gradient is as shown in figure 58.

If the whole sphere is initially at a uniform concentration C_o and the surface concentration is maintained constant at C_s at all subsequent times (where C_s is now the concentration in equilibrium with the reactive species in the continuous phase), the solution given by Crank (147) is:

$$\frac{C-C_o}{C_s-C_o} = 1 + \frac{2a}{\pi r}\sum_{n=1}^{\infty}\frac{(-1)^n}{n}\sin\frac{n\pi r}{a}\exp\left(-\frac{Dn^2\pi^2 t}{a^2}\right) \qquad 5.5.1.2$$

where (a) is the radius of the sphere, r is the distance from the centre of the sphere at which concentration C at any instant of time is evaluated, t is the time of diffusion and D is the diffusivity. Difficulties arise in finding a mean value of C for the whole sphere (i.e. the mean carbon content of the drop).

Carbon content varies for each r/a ratio at which each calculation must be made in equation 5.5.1.2. Equation 5.5.1.2 which is the integration of equation 5.5.1.1 for certain boundary conditions does not apply for short (low values of) time. Evaluations were made of equation 5.5.1.2 at D_c (diffusivity of carbon) = 4.5×10^{-5} cm^2/sec, a = 0.4 cm, C_o = 4.25 %C, C_s = 0, t = 0 to 1200 sec and ratios of r/a = 0.2, 0.4 and 0.8. The results have been graphically represented in figures 59a and 59b for values of n=1, n=2, and n=3. From 59 b it can be seen that solution for n=3 gives more than sufficient accuracy. It can also be seen from figure 59b that all solutions, regardless of the value of n present a problem of obtaining a mean value of C due to the need for a selection of an r/a ratio. Also figures 59a and 59b clearly show that this equation is inapplicable at short times. Calculations for diffusion using equation 5.5.1.2 would be useful only if the carbon gradient within the drop is required. Under the present experimental conditions the measured carbon content of the reacted droplets is a mean value for all radial positions of the whole of the drop and therefore comparisons would not be meaningful. A specific solution to equation 5.5.1.2 exists for the special limiting case of $r \to 0$ i.e. the concentration at the centre of the stagnant drop with diffusion control in the drop is given by:

$$\frac{C-C_o}{C_s-C_o} = 1 + 2 \sum_{n=1}^{\infty} (-1)^n \exp\left(- \frac{Dn^2\pi^2 t}{a^2} \right) \qquad 5.5.1.3$$

By using the following data of a = 0.4 cm, Dc = 4.5×10^{-5} cm^2/sec, C_o = 4.25 %C, C_s=0, n=1, n=2, n=3 and t=0 to 1200 sec, a graphical representation was obtained and is shown in figure 60. Again the inapplicability of equation 5.5.1.3 is clearly obvious at the small times, as would be expected since equation 5.5.1.3 is obtained by integration of 5.5.1.1 on such a basis.

Carbon concentration gradients may be visually presented by using the results from equation 5.5.1.1 for r/a = 0.2, 0.4, 0.8 and 1.0 and plotting a graph of %C against distance from the centre of the sphere. Equation 5.5.1.3 is also solved for r = 0, and then incorporated with the graphical presentation of equation 5.5.1.2. The graph which results is figure 61, which shows the carbon concentration gradients at 300, 600 and 1200 sec. for values when n = 1, n=2 and n=3. From figure 61 it may be noticed that the carbon gradient of a stagnant drop, for a carbon content at the surface of zero, gives carbon contents of 0.94% and 0.38% at 300 and 600 sec respectively after commencement of reaction at a distance of only 0.8 mm below the surface. Figure 61 again clearly shows that n=3 is a sufficiently high value of n to give an accurate solution.

An integration can be performed of equation 5.5.1.1 (147) which enables calculations to be made for relatively low times. The present experimental work is over such time periods that times of less than 200 sec (3.3 min) are not so important. Also the main interest is in a mean carbon concentration.

The following equation is another form of solution of equation 5.5.1.1 which allows the diffused material in time t to be calculated and expressed as a ratio of the diffused material when t = ∞ as:

$$\frac{M_t}{M_\infty} = 1 - \frac{6}{\pi^2} \sum_{n=1}^{\infty} \frac{1}{n^2} \exp - \frac{Dn^2\pi^2 t}{a^2} \qquad 5.5.1.4$$

Graphical solutions are available (147) to calculate the ratio M_t/M_∞ as a function of Dt/a^2. By using $D_c = 4.5 \times 10^{-5}$ cm^2/sec, a = 0.4 cm and n=3, calculations were made using equation 5.5.1.4 and the results have been plotted in figure 62. In order to compare the solution obtained from equation 5.5.1.4 with the present experimental results, data from a typical decarburization curve (figure 35) have also been plotted in figure 62. It can be seen that disagreement exists between the theoretical and experimental values. It may be noted from figure 62 that by extrapolating the experimental curve to coincide with the time axis it does not pass through the origin. This anomally arises due to the difficulties of establishing a zero time for reaction during the experimental work (i.e. what value should be taken for M_∞ - see section 3.5.3).

In order to facilitate comparison between theoretical and experimental results, conversion of M_t/M_∞ to wt%C has been made and the results have been plotted on a %C vs time curve and shown in figure 63. All the points from the experimental results were replotted and normalized for the zero time

(i.e. when C = the initial carbon content); the time deduced was determined from the intersection of the experimental curve with the time axis in figure 62.

The results from figure 63 indicate that for a stagnant drop the rate of decarburisation by diffusion processes alone is much faster than those indicated by the decarburization data given in figure 35. Further comparisons between the diffusion model and other experimental curves confirm this difference. Further discussion to explain the source of the discrepancy will be given in section 5.6.

5.5.2 Resistance in internally circulating Dispersed Phase.

The second case considers resistance in an internally circulating dispersed phase. The diagrammatic representation for discontinuous mass transfer control would be as shown in figure 64. Kronig and Brink (148) studied this case assuming the Hadamard-Rybczinski pattern for laminar circulation as shown in figure 65. The streamlines were derived for Reynolds number less than one which corresponds to Stoke's law. Solute diffusion was assumed to take place only in the direction perpendicular to the internal streamlines

while the continuous phase resistance was negligible. The relative velocity of the dispersed phase with respect to the continuous phase is zero and there is no slip at the interface. The same authors (148) compared the time of contact tc for a particle to pass once around a streamline with the time required for the concentration of a substance in the drop to fall 1/e of its original value due to the process of diffusion. The circulation time was found to decrease as the droplet diameter increased as 1/r. The diffusion time was found to decrease as the square of the droplet radius, ($t_d \propto r^2$). Handlos and Baron (142) have put forward a model to describe the dispersed phase mass transfer coefficient. By combining tangential motion caused by circulation with assumed random radial vibrations an eddy diffusivity was evaluated. Assuming no transfer in the continuous phase the dispersed phase mass transfer coefficient was correlated as:

$$k_d = \frac{\lambda V}{768\left(1 + \frac{\mu d}{\mu c}\right)} = \frac{3.75 \times 10^{-3} V}{\left(1 + \frac{\mu d}{\mu c}\right)} \qquad 5.5.2.1$$

where $\lambda = 2.88$

Wellek and Skelland (145) for the case of falling drops, when relative velocity between drop and continuous phase can be related to time, express the mass transfer coefficient as:

$$k_d = -\frac{d}{6t} \ln \left[\frac{3}{8} \sum_{n=1}^{\infty} A_n^2 \exp\left(-64\lambda n \frac{Dt_c}{d^2}\right) \right] \qquad 5.5.2.2$$

The above equations apply for the case of vigorously circulating drops (142) and for laminar circulations (148). Both equations also assume that the drop velocity, the continuous and dispersed phase viscosities and the contact times are known. The dimensionless group from the product of (Re) (Sc), which is often encountered in the literature on mass transfer, is called the Peclet number.

$$Pe = (Re)\ (Sc) = \left(\frac{dv\rho}{\mu}\right)\left(\frac{\nu}{D}\right) = \frac{dv}{D} \qquad 5.5.2.3$$

Manipulation of equation 5.5.2.1 and 5.5.2.3 then yields:

$$Sh = \frac{k_d\ d}{D} = \frac{3.75 \times 10^{-3}}{\left(1 + \frac{\mu d}{\mu c}\right)} \times \frac{dv}{D} \qquad 5.5.2.4$$

$$Sh = 3.75 \times 10^{-3}\ Pe/\left(1 + \frac{\mu d}{\mu c}\right) \qquad 5.5.2.5$$

The above model cannot be taken any further since it requires calculations of dimensionless numbers which are impossible to calculate from the present experiments. The inability to characterise the nature of the turbulent dynamics of slag and metal continues to be a stumbling block.

For the Fe-C reaction with slags the rate of carbon depletion (decarburization) for the drop is given by:

$$V_d\ \frac{dC}{dt} = k_c.A\ .\ (C_c^{\,b} - C_c^{\,i}) \qquad 5.5.2.6$$

Even if the above model were possible to apply and therefore give values of k_c, there is still the difficulty to account for carbon monoxide evolution (i.e. gas) which is taking place during decarburization. The growth within the drop, and the ejection through the interface, of CO gas

generates surface area which is large and varied compared to the area of the initial iron-carbon sample. Norwithstanding these difficulties of applying this model, what can be stated without contradiction is that the rate of decarburization for the internally stirred drop would be greater than the stagnant drop with mass transfer by diffusion alone. Referring to figure 63 the model predictions would give a curve below that for equation 5.5.1.4 i.e. even further removed from the experimental data.

Consideration must now be given to the possibility that conditions in the slag phase may be controlling the overall rate of mass transfer.

5.5.3 Resistance in continuous phase, dispersed phase stagnant.

Case three considers the resistance in the continuous phase, and no resistance in the stagnant dispersed phase. The diagrammatic representation for the concentration of reactants at the slag-metal interface is shown in figure 66. Experimental data for a variety of systems have been interpreted with the aim of finding suitable correlations between the mass transfer coefficients and fluid flow. Griffith (149) and Aeron (150) have reviewed most of the expressions obtained by other workers. Two of the most quoted correlations are those proposed by Steinberg and Treybal (151) in the form of:

$$Sh = A + B(Re)^n \qquad 5.5.3.1$$

The above correlation predicts a value of Sh = A for Re = 0; i.e. the limiting case when mass transport occurs by diffusion

and natural convection. A, is represented as a function of the Grashof and Schmidt numbers as:

$$A = 2.0 + 0.569\ (Gr\ Sc)^{0.25} \qquad 5.5.3.2$$

for $Gr\ Sc < 10^8$ and,

$$A = 2.0 + 0.0254\ (Gr\ Sc)^{0.33}(Sc)^{0.244} \qquad 5.5.3.3$$

in the case where $Gr\ Sc > 10^8$.

When the continuous fluid phase transport is the rate controlling process for reactions between a stagnant fluid and a spherical droplet (i.e. pure diffusion only) then:

$$Sh = 2.0 = k_{fluid}\ d_{drop}/D_{(reactant\ in\ fluid)} \qquad 5.5.3.4$$

where k is the mass transfer coefficient for the fluid, d_{drop} is the drop diameter and D is the diffusivity of reactant in the fluid.

The value for B and n in equation 5.5.3.1 has been determined as $B = 0.347\ Sc^{0.312}$ and $n = 0.62$ thus, equation 5.5.3.1 becomes:

$$Sh = 2.0 + 0.569\ (GrSc)^{0.25} + 0.347\ Re^{0.62}Sc^{0.31} \qquad 5.5.3.5$$

The coefficient 0.347 is dependent on the geometry of the system and Richardson (152) shows how the values can be determined by evaporation experiments.

The studies have been carried out for mass transfer control in the continuous phase by chemical engineers, but their application has always been to systems which are simpler and more easily quantified than the system in the present study.

Attempts were made to solve 5.5.3.5 by assuming that the controlling step is transfer of FeO from the bulk of the slag

to the drop surface. The FeO concentration in the slag bulk is an infinite source and therefore conditions for steady state apply. Equation 5.5.3.5 may be progressively solved by assuming three different mechanisms. The first and most simple mechanism to consider is when diffusion alone takes place in the slag i.e. the sole mechanism by which FeO is transferred from the bulk to the reaction interface at which carbon is always available. The Sherwood number for the above condition becomes:

$$Sh = k_{slag} \times d_{drop}/D_{FeO} = 2 \qquad 5.5.3.6$$

where k_{slag} is the mass transfer coefficient in the slag, D_{FeO} is the diffusivity of FeO in the slag and d_{drop} is the diameter of the reacting iron-carbon sample. From the work of Taylor (153) the diffusivities of calcium and silicon in lime-silica and lime-alumina-silica slags have been found to be $D_{ca} = 5.7 \times 10^{-6}$ cm^2/sec and $D_{si} = 2.2 \times 10^{-6}$ cm^2/sec at 1450^{o}C. Agarwal and Gaskell (154) measured the self diffusivities of Fe (D_{Fe}) in $2FeO.SiO_2$ (F_2S) and $CaO.FeO.SiO_2$ (CFS) in the temperature range of 1250^o C to 1540^o C. At 1307^{o}C D_{Fe} was found as 4.82×10^{-6} for CFS and 7.72×10^{-6} cm^2/sec for F_2S at 1346^o C. If equation 5.5.3.5 is to be solved, a numerical value must be produced for D_{FeO}. There are no values by measurement in the literature for the diffusivity of oxides including FeO; in addition, calculation of values of diffusivity in these slags is almost impossible. The difficulty is compounded by the argument that the appropriate diffusion coefficient should be that of the oxygen ion.

Obviously an accurate value for the diffusion coefficient cannot be obtained, however, the few values available are all in the same range i.e. 10^{-6} cm^2/sec. From the above considerations a value of 5.7×10^{-6} cm^2/sec has been selected and will subsequently be used in the following calculations. By considering a value of 0.8 cm for the diameter of the drop, the mass transfer coefficient for the slag is calculated as 1.43×10^{-5} cm/sec. Comparison of mass transfer coefficients will be made in more detail in section 5.6.

Having the value of 1.43×10^{-5} cm/sec for the mass transfer coefficient, the rates of decarburization may be calculated by use of the following equation:

$$\text{molar rate of mass transfer of FeO} = k_{slag} \times \text{Area} \times (C^{b}_{FeO} - C^{i}_{FeO})$$

Because the iron oxide is being consumed immediately on arrival at the interface, then $C^{i}_{FeO} = 0$ and the molar rate of mass transfer for FeO in the slag bulk is calculated from:

$$1.43 \times 10^{-5} \times \text{area} \times C^{b}_{FeO}$$

The concentration of FeO in the slag bulk is calculated as 0.017 (wt% FeO x density of slag in $g/cm^3/7200$) moles of FeO/cm^3. The molar rate of mass transfer of FeO is calculated as 4.8×10^{-7} moles/sec. The number of moles reacted during the decarburization reaction are equal for carbon and iron oxide as seen from reaction 5.5.1. Therefore it is possible to calculate the quantity of carbon consumed in a given time and construct a graph of %C against time.

Figure 67 shows the calculated values for decarburization when the mass transfer coefficient is 1.43×10^{-5} cm/sec (Sh = 2). In the same figure 67 a typical decarburization curve obtained from experiment (taken from figure 35) is shown for comparison. The lines for Sh = 5 to Sh = 12 will be introduced later.

To calculate the second term on the right hand side of equation 5.5.3.5 consideration must be given to the possibilities of setting up a density gradient. The density gradient may have two origins; a temperature gradient and a composition gradient. First a temperature gradient will be considered. Any temperature gradient which may arise during reaction between the iron-carbon drop and slag will be due to the chemical reaction alone, since all experiments were performed isothermally. The equation to consider for reaction is:

$$FeO(l) + \underline{C} \longrightarrow Fe(l) + CO(g) \qquad 5.5.3.7$$

for which $\Delta H = 90942$ J/mole.

The iron-carbon drop weighs one gram and the carbon loss will be taken as an extreme case of 2% (i.e. 0.02g). The enthalpy of reaction is then calculated as 151.57 J. The temperature gradient may then be calculated from: (enthalpy of reaction)/(molar mass(of the material which absorbs the heat) x (heat capacity). The heat capacity for the drop was taken as that of Fe, 0.753 J/mole deg. (165) and for $CaO.FeO.SiO_2$ (molecular wt of 188) slag as 1.09 J/mole.deg.(63).

Considering the case where the slag (30g) absorbs all of the heat evolved, the temperature difference created by reaction is calculated to be 4.6%C which is unlikely to cause a significant density gradient.

Assuming the extreme case, where the heat generated by the reaction of equation 5.5.3.7 is absorbed by the reacting drop alone, the temperature increase would be 201°C. In these conditions, a temperature gradient is set up between the slag bulk, which is at the furnace temperature of 1300° C and the drop which is now increased to 1501°C. The above temperature increase would take place for a 0.02 g loss in carbon and, as found from experimental work, the time required is of the order of about 10 min. The temperature increase per second, over the whole of the drops surface is then 0.34°C. From visual observations made when carrying out experiments, the slag was seen to be in a turbulent state and therefore heat generated would be quickly dissipated throughout the crucible contents. However even considering the extreme case of a temperature gradient existing at the metal slag interface of 201°C the density of the slag would not be altered significantly. This fact is based upon the data of Gaskell and Lee (129) who found that there is virtually no temperature dependence of density within the range studied.

The above results clearly indicate that no density gradient could exist due to temperature changes and therefore the Grashof number given by:

$$Gr = \frac{g \cdot d^3 \cdot \rho_{slag}^2}{\mu^2} \left[(\rho_{slag} - \rho_i)/\rho_i \right] \qquad 5.5.3.8$$

is zero. Having the natural convection term as negligible, the mass transfer will take place only by pure diffusion within the slag.

Considering the possibility of natural convection due to changes in density from variations in chemical composition the following approach is made. During the decarburization reaction the slag at the interface has been depleted in FeO and, in the extreme case, only lime and silica oxides (or compounds formed from them) will be encountered at the slag-metal interface. The density value at the interface will be that of dicalcium silicate, assuming no interference from free iron and gas evolution. For solid dicalcium silicate the densities of the different crystallographic forms are: Γ = 2.97, β = 3.28 and α = 3.27 g/cm^3. The high temperature crystallographic form is that of α and therefore this will be chosen to give a density at the interface, i.e. 3.27 g/cm^3. The values for the density of the bulk slag as measured by Gaskel and Lee (129) within the temperature and compositions studied in the present work are in the range of 3.1 to 3.22 g/cm^3. These values are not sufficiently accurate to allow a density difference to be predicted. Therefore, from the density value for the slags little change in the density is to be expected. The unreliability of the density differences values make the calculations of the Gr number per se unrealistic. The Grashof number is therefore negligible and again, as was the case when no temperature gradients were considered, there is no contribution to mass transfer due to natural convection.

Even though the above estimates for natural convection give a negligible Grashof number for both temperature and composition gradients, it was considered worthwhile to explore the values of Grashof number which would be required to increase mass transfer rates significantly. Greater values of Grashof number generate greater values of Sherwood number. The values of Sherwood number which would compel the solution of 5.5.3.5 to match the experimental data can be estimated. The magnitude of these values is significant when compared with the value of Sh = 2. This was done as described below.

It is first assumed that natural convection does occur and contribution to some extent is made to mass transfer. Different values for the Sherwood number are used in order to approach similar rates of decarburization as obtained by experiments. Once a value, or a range of values, is obtained, the corresponding Grashof number is calculated. In order to facilitate and allow calculations to be readily made, a graph has been plotted for the mass transfer coefficient against Sherwood number for the case when $D_{FeO} = 5.7 \times 10^{-6}$ cm^2/sec and a diameter of 0.8 cm for the iron carbon sample, and is shown in figure 68.

In the same manner as when Sh = 2 other values of Sherwood number were used to calculate decarburization curves as shown in figure 67 where the results from pure diffusion alone (Sh = 2) have been given.

From the results obtained in figure 67 it is seen that relatively low values for Sh numbers are needed to obtain similar decarburization curves to those obtained during experiment. A range of values for the Sh number has been plotted

in figure 68 in order to directly obtain values of the mass transfer coefficient for the slag phase. The range (i.e. Sh = 2, Sh = 22) was chosen on the basis which is discussed below.

To calculate the Grashof number from the Sherwood number by equation 5.5.3.5, it is necessary first to calculate the Schmidt numbers. The Schmidt number (Sc) contains viscosity as a parameter and viscosity values are not known with confidence for these slags. Therefore, a specific value cannot be quoted for viscosity and a best estimate must be made which will cover a range of values. The viscosities for $CaO.FeO.SiO_2$ system were measured by Kozakevitch (155) and Rontgen (156) both authors having found similar values. The viscosity values along the Fayalite-dicalcium silicate join vary from 0.5 poise at $10\%CaO.60\%FeO.30\%SiO_2$ to nearly 1 poise at $40\%CaO.30\%FeO.30\%SiO_2$ at $1400^{o}C$ (155), and from 0.5 to 2 poise at $1300^{o}C$ (156). For purposes of presentation and clarity for the reader at this stage in the thesis, viscosity extremes of 0.25 to 2 poise, with intermediate values, have been chosen. Calculations have been repeated using this range of values which then facilitate clear graphical presentation of the effects of viscosity on the ultimate values calculated, such as Gr number, Sc number and decarburization rate. Figure 69 gives the variation of Sc number over a range of viscosities.

For comparison, values for the Gr number have been calculated for viscosity values of 0.25 to 2 poise. The range

of Sherwood numbers were according to values found in figure 67. The variation of Gr number for the above conditions is shown in figure 70. The initial slopes are relatively steep and the slopes at high Gr numbers are tending to horizontal lines. It shows that for very low values of Gr number there is a relatively large increase in the Sherwood number, i.e. a large increase in the decarburization rate is to be expected when the ratio of the bouyancy forces to the viscous forces is slightly increased.

The conclusions from this discussion on natural convection are twofold. Firstly, estimates of Gr number from sparse knowledge of physical properties temperature gradient and composition gradient, indicate that Gr number if negligible. Secondly, values of Gr number need to be only relatively small in order to give Sh numbers which cause the theoretical curve to match the experimental data. The small values of Gr number may actually exist but from the present experimental system it is not possible to confirm or deny their existence.

To calculate the third term on the right hand side of equation 5.5.3.5 estimates for the Reynolds number are needed. This cannot be done based upon velocity as the relative velocity between slag and drop cannot be ascertained or measured. Following the sequence previously used in calculating Grashof numbers, it is possible to use the range of Sherwood numbers and Schmidt numbers to calculate corresponding values of Reynolds numbers. Once the Reynolds numbers have been obtained the velocity term in the Reynolds number can be calculated.

The values of Sh and Sc numbers used in the calculation for the Reynolds number are the same as those used previously. Values of the Re number obtained from:

$$Sh = 2 + 0.347\ Sc^{0.31} Re^{0.62} \qquad 5.5.3.9$$

have been plotted against Sh numbers and are given in figure 71. Values of the velocity have also been calculated and these have been plotted against Sh number as shown in figure 72. The results indicate that low relative velocities must exist during the decarburization reaction.

Further discussion on this matter will be continued in section 5.6. However,it is pertinent to conclude at this stage that the mass transfer model incorporating forced convection can give decarburization rates very similar to experimental data (see figure 67). The values of such characteristics as the Re number, the Sh number, relative velocity (and for that matter the Gr number) are not unrealistic. However, it must be remembered that these values have been obtained only through the known experimental data; in other words the models themselves cannot be used in isolation to predict decarburization rates.

5.5.4 Resistance in continuous phase, dispersed phase circulating.

The fourth case to be considered is that where the resistance is found in the continuous phase with an internally circulating dispersed phase. The mass transfer coefficient is again described through the Sherwood number and a number of correlations have appeared (157,158). Heertjes (157) has reviewed most of the proposed models and notes that the main difficulty encountered under these conditions is to estimate the contribution of the wake of the drop to mass transfer.

Most of the above models for either continuous or discontinuous phase control, requires the knowledge of specific data in order to enable mass transfer coefficients or dimensionless groups to be calculated. In the system under study most of the data cannot be as yet definitely established although attempts have been made on the preceding pages. The drop velocity, variations of contact area, changing contact times, and the fact that the so-called continuous phase is in reality a foam which contains a high proportion of a dynamic gas phase, allow only approximations to be made as shown in the previous calculations. The results of the experiments carried out here indicate that these chemical engineering type models based upon the existence of a well defined interface, are difficult to apply to the complex interactions observed between metal alloys and slags.

Another situation which may arise for transport control is that known as mixed control. The situation arises when resistances to transport in both the continuous (slag) and discontinuous (metal) phase are significant. The rates of transport to the interface are equivalent. It is usually assumed that equilibrium is established, so that in terms of slag metal phases:

$$\frac{dn_A}{dt} = k_m.A(C^{b,m} - C^{i,m}) = k_{SLG}.A.(C^{i,slg} - C^{b,slg}) \qquad 5.5.4.1$$

In the present metal/slag reactions the concentrations at the interface for both metal and slag are not known and therefore the equation cannot be solved.

5.5.5 Chemical Reaction.

The majority of processes by which steel is currently produced have received considerable attention in terms of thermodynamic analysis. The criteria are based upon the concept that every process corresponds to an equilibrium state in which, phenomenologically, the process does not proceed any further. The criteria for phase equilibria in systems of steelmaking interest are well documented and it is possible to predict with confidence the theoretical limits of refining or recovery attainable in any given situation. However, from the practical point of view, it is the rate at which reactions take place that is of greater importance. The rate at which a chemical reaction occurs may be a function of several factors including concentration of reactants and products, pressure and temperature. The observed behaviour of many reactions has been explained by two main theories known as the simple collision and the absolute reaction rate theory. In the Simple Collision Theory it is assumed that molecules behave as non-attracting hard spheres. By combining the forward and reverse velocities of reaction an equilibrium constant is determined which is expressed by an Arrhenius type equation:

$$k_R = A_f \exp(-E/RT) \qquad 5.5.5.1$$

Two factors are involved - a frequency factor, A_f, and an exponential factor which includes the activation energy, E. The latter factor is assumed to represent an energy barrier which has to be overcome if the reactions are to proceed.

The frequency factor represents the number of collisions between potentially reactive molecules, and therefore the exponential term becomes the fraction of collisions possessing the ability to undergo reaction.

The Absolute Reaction Theory considers the formation of an intermediate compound known as activated complex. At equilibrium, the flows through the configuration of the activated complex in the forward and backward direction are equal. It is generally assumed that the activated complex is in equilibrium with the species of origin although reactants and products may not be in equilibrium with one another. The mathematical expression, in the Arrhenius form, yields a relation of:

$$k_R = aT^b \exp\left(-\frac{E^o}{RT}\right) \qquad 5.5.5.2$$

and compared with k_R for simple collision theory indicates that $E = E^o + bRT$ and only when $b\,RT >> E^o$ may any difference be detected.

According to Darken (160) the above theories, applied to classical molecular reactions, differ from liquid metal systems because the molecular state as such does not exist and the electron bond is very much higher in liquid metals.

It has been generally accepted that most chemical reactions taking place at steelmaking temperatures occur at such high rates that local equilibrium generally exists and it is improbable for chemical kinetics to be the rate controlling step. Figure 73 shows a diagram representing chemical reaction control. The basis for this concept has been

established from calculated activation energies for typical chemical reactions which rarely exceed 60 k cal, and are generally in the region of 20 to 30 kcal (161). Only if the activation energy is much in excess of 250 kcal is chemistry likely to be rate controlling (161).

The influence of temperature on the rate of reaction is expressed by the Arrhenius equation:

$$\frac{d \ln k}{dT} = \frac{E}{RT^2} \qquad 5.5.5.3$$

This equation is applicable to either homogeneous or heterogeneous type reactions. On integrating equation (5.5.5.3) the rate constant is expressed as

$$k = \text{const. } \exp\left(-\frac{E}{RT}\right) \qquad 5.5.5.4$$

By plotting ln k vs 1/T a linear relation should be obtained (with a gradient equal to - E/R) provided the factors which control the rate of reaction remain the same throughout the temperature range under study. The order of a reaction is the measure by which the rate of reaction is proportional to the number of atoms or molecular groups taking part in the reaction. Considering the decarburization data as plotted on a %C vs time basis, a zero-order reaction would be expressed as

$$\frac{d C}{d t} = -k \qquad 5.5.5.5$$

and the carbon drop should be linear with time, i.e. $(C_o - C_f) = -kt$ which was not found in the present study.

For a first-order reaction

$$\frac{dC}{dt} = - kc \qquad 5.5.5.6$$

by integrating:

$$\int_{C_o}^{C_f} \frac{dC}{C} = -\int_{t=o}^{t=t} k \, dt$$

and

$$\ln \frac{C_f}{C_o} = - k t \qquad 5.5.5.7$$

From the plotted data of %C vs time, the values for k were found from the slopes of the curve which were obtained. A constant time of 360 seconds evaluated by the following technique, was taken for each calculation from graphs as typified in figure 74.

The fall in carbon content was read between the time interval considered. Because the graphs do not join the %C axis, the iterations were initiated after either one minute (e.g. at 1400° C) or three minutes, depending on the particular situation of each graph. Values of k were calculated along the curve from equation (5.5.5.7)

$$\frac{1}{t} \ln \frac{C_f}{C_o} = - k \qquad 5.5.5.7$$

The average value of all the k calculations was then taken to represent the overall rate of reaction. This procedure was repeated for all the decarburization graphs. The values calculated for all the decarburization experiments are given in table V.

Due to the limitations under the present experimental conditions, the temperatures at which reactions were made are of a restricted range. It was nevertheless attempted to determine an approximation for the activation energy values from the calculated values. The logarithm of k was plotted against the reciprocal of temperature in figure 75.

Fayalite decarburization was performed at 1240°C, 1300 and 1400°C, and the slope of the plot gave an activation energy of 29.436 Kcal. This figure is in close agreement with activation energies found from literature (100, 101, 102) for graphite-iron oxide reactions which are in the range of 32 to 40 Kcal. The slight discrepancy between the figures may stem from the fact that the presence of silica may have an effect on the bonding of FeO to form fayalite. Therefore, a decrease in the activation energy from the pure iron oxide case may be expected. Three other slags containing lime additions of about 26% to 32% were similarly analysed. The slopes of the straight lines allowed values of activation energies to be found and are given with the figure. The lowest value found was 13.8 Kcal. The results, although limited, indicate that as a second (SiO_2) or third (CaO) component is added to FeO, the characteristics for reaction become more towards transport control. The experiments carried out by Tarby and Philbrook (102) on slag-metal-graphite reactions contained alumina from 8.9 to 50.6%. For alumina contents of 8.9% in the slag, the apparent activation energy for slag-metal reaction was found by these authors to be 12 Kcal/mole.

It may therefore be concluded that the values obtained in the present experiments are in agreement with those observed with other workers, who in turn, concluded that chemical reaction control was not applicable. For such systems to have chemical reaction as the rate controlling mechanism, values of activation energies in excess of 250 Kcal are necessary (161) (see section 2.7.2).

From the preceding calculations it is concluded that chemical reaction within the present experiments is not rate controlling. Chemical reaction will not be further discussed. Therefore, mass transfer control of both continuous and dispersed phase will be discussed in more detail in the following section.

5.6 Mass transfer models and experimental results.

It has been established that the decarburization reaction between iron-carbon drops and synthetic slags is heterogeneous and not controlled by the chemistry of the process.

When considering simple mass transfer models (section 5.5), mechanisms for continuous and dispersed mass transfer control were discussed. When the conditions for the dispersed phase control were studied, two possibilities were considered. The first possibility was that of a well defined geometry of a stagnant drop. Unsteady state conditions apply and various solutions to Ficks second law were analysed. The results on a % C against time curve shown in figure 63 clearly indicate that mass transport in the drop is not rate controlling. Considering that the area available for reaction is greater under the present experimental conditions than that of a well defined sphere and that the drop is found in turbulent surroundings, the decarburization rate may be expected to be

even greater than that found from equation 5.5.1.4. The experimental decarburization curves obtained have been found to be slower than those predicted by equation 5.5.1.4. In addition there is clear evidence that gas bubble entrapment takes place well within the reacted droplet which is a clear indication that oxygen has diffused into the main body of the drop. Considering these three factors: greater surface area, turbulence within the system, and gas entrapment, high decarburization rates should be anticipated. This was not observed. The conclusion must be drawn that carbon diffusion is not rate controlling and therefore some other mechanism must be the rate controlling step. A fourth factor which must be considered when discussing the applicability of the unsteady state diffusion within the drop model is CO nucleation. From examination of fractured surfaces from reacted drops clear evidence was found that slag entrapment within the drop had taken place (see section 4.7). Minute particles of slag serve as potential nucleation sites for CO generation and the slag-metal interface is therefore altered. The above model does not take into account these latter events. However if the nucleation were significant and added to the model, then the theoretical predictions would be of a lower decarburization rate.

The second possibility considered was that of a well defined circulating sphere. When considering mass transport control from an internally circulating dispersed phase, the model predictions would give a curve depicting an even faster

decarburization rate than that found for a stagnant dispersed phase. Consequently the discrepancy between the experimental data and the model predictions would be enlarged further than the discrepancy for the first possibility and the experimental data considered above. The second possibility would only confirm again that mass transfer control within the drop is not operative. Further discussion about dispersed phase control is therefore unprofitable. From the preceding findings, attempts were then directed towards the study of possibilities for mass transport control in the continuous phase (slag).

A model which takes into account mass transfer due to diffusion, natural convection and forced convection in the continuous phase is that given by equation 5.5.3.5. Physical properties for the present system have been selected and used in the evaluation of equation 5.5.3.5. When considering mass transport due to diffusion alone (Sh = 2) the mass transfer coefficient for the slag was calculated as 1.43×10^{-5} cm/sec, and it became possible for a decarburization curve to be constructed. By comparison of the theoretical with the experimental decarburization curve, a slower theoretical decarburization rate was seen. The results, which are plotted in figure 67, indicate that diffusion of FeO in the slag as the only mechanism for mass transport could most certainly be a controlling step.

Subsequent calculations have been made to determine, separately, the contribution to mass transfer from natural convection and forced convection. In the case of natural convection the possibilities for density variations in the slag

close to the slag-metal interface were investigated for both a temperature gradient and a chemical composition gradient. The contribution from natural convection to mass transfer was probably negligible. Further calculations, by using different numberical values for the Sh number, also confirm that the contribution from natural convection is negligible, but it has not been possible to confirm or deny the small values obtained for the Gr number.

By following the same method to calculate Gr numbers, a range of values for the Re number has been calculated. The range of Re number was then used to evaluate relative velocities between slag and metal. The results indicate that relatively low velocities are required to obtain decarburization rates similar to those found from experiment.

Typical experimental data from decarburization experiments at 1300°C were used in discussing the mass transfer models in section 5.5. In the following discussion similar calculations will be made in more detail covering the full range of experimental parameters but the results will be discussed mainly from the point of view of mass transfer coefficients.

For decarburization reactions at 1240° C, data were taken from figure 21, and Sh numbers which gave similar rates of decarburization were calculated. The results are shown in figure 76. The results indicate that decarburization is taking place in a situation very close to that predicted by mass transport control by diffusion alone in the slag phase. The mass transfer coefficient from figure 68, is seen to be

of the order of 0.8×10^{-5} cm/sec to 2.2×10^{-5} cm/sec (i.e. Sh = 2.5, 3). For the case where Sh = 2, then the mass transfer coefficient is 1.43×10^{-5} cm/sec i.e. pure diffusion. The relative velocity between slag and metal, considering the highest value of Sh number for the above case of Sh = 3, is less than 0.03 cm/sec. The viscosity for the calculations of the relative velocity is taken as 0.7 poise. This viscosity value will be used in further calculations unless otherwise stated.

The calculated values from the mass transfer model for decarburization at 1240°C suggest that the slag is nearly stagnant. This is quite plausible for a slag at this low temperature of 1240°C. Due to the low temperature and for comparison, it was considered necessary to assess the effect of diffusivity in the slag phase. By taking an extreme case from the data given (5.5.3) when considering a possible value for the diffusivity of FeO, as 2.2×10^{-6} cm^2/sec, decarburization rates for Sh number of 2 were calculated. The results are shown in figure 76 as indicated by line A. The mass transfer coefficient for the above case is found to be 0.55×10^{-5} cm/sec. The Sh number required to obtain similar decarburization rates to the experimental results at 1240°C has now a new value of 10 and the mass transfer coefficient is 2.75×10^{-5} cm/sec.

By comparing values of the mass transfer coefficient at 1240°C for the case of $D_{FeO} = 2.2 \times 10^{-5}$ cm^2/sec and $D_{FeO} = 5.7 \times 10^{-6}$ cm^2/sec, a range of 0.55×10^{-5} to 2.75×10^{-5} cm/sec is found. The whole range of these results gives relative velocity values no greater than 0.03 cm/sec. The

values calculated for the mass transfer coefficient and relative velocity still continue to indicate that the slag is semi-quiescent, (i.e. nearly stagnant). From the above results it is seen that although other physical properties of the system, such as viscosity, may have or may begin to have influence in the mass transfer phenomena, the mass transfer model does predict rates of decarburization similar to those obtained during experiment.

Decarburization reactions when no gas lancing and when gas lancing was carried out are discussed below by applying the mass transport model as for the above cases. The calculated Sh numbers to obtain similar decarburization rates, as for the two above cases, are shown in figure 77. In the case where no gas lancing was performed, the mass transfer coefficient was found to vary from 6.4×10^{-5} cm/sec to 8.5×10^{-5} cm/sec (i.e. Sh = 9 to 12). The relative velocity from figure 72 is seen to range from 0.18 to 0.30 cm/sec in this case. When gas lancing was carried out, the Sh number range was changed to 11 to 13 (see figure 77) and the corresponding mass transfer coefficient was changed to 8×10^{-5} to 9.5×10^{-5} cm/sec. The relative velocity between slag and drop was similarly changed to a range from 0.26 to 0.36 cm/sec. Therefore the effect due to gas lancing, as predicted from the mass transfer model, is to cause an increase in the relative velocity between the slag and metal of 20% max (from Sh = 12 to Sh = 13).

A comparison can now be made between the experimental results and mass transport model. It will be recalled that one of the aims of gas lancing was to increase the turbulence

within the slag (see section 4.6). Due to problems of shattering of the iron-carbon samples a compromise was reached where ultimately a gas flow of 75 cc/min was selected. During the experimental trials with the above gas flow rate the slag was generally seen to be in a turbulent state. In experiments with argon injection (section 4.6.1) it was found that the turbulence created by gas injection increased the decarburization rate but not as much as expected (see page 110) The mass transfer model calculations indicated that the relative velocity for experiments with gas lancing is not significantly increased as compared with experiments where no gas lancing was carried out. The calculated values therefore serve to indicate the magnitude of the relative velocity which is operative for the present experiments between the slag and metal. The magnitude of the relative velocity was not possible to be calculated or approximated from experimental observations alone. It is also important to point out that irrespective of the turbulence (i.e. visual observations) which may prevail in a given system, it is the relative velocity between the different phases involved which is important. Also, the calculations from the model are in good agreement with those found from experiment. The model therefore applies and may serve to determine the trend and magnitude of mass transport taking place between the continuous and dispersed phase in the present experiments.

Sherwood numbers for decarburization experiments at 1400°C have been calculated and compared to experimental results taken

from figure 40. The results are shown in figure 78. By increasing the reaction temperature from 1300°C to 1400°C the Sh number increases by about 40% to a range from 17 to 20. The mass transfer coefficient lies in the range from 12.1 x 10^{-5} cm/sec to 14.25 x 10^{-5} cm/sec. By comparing the relative velocity from experiments at 1300 with the relative velocity at 1400°C the magnitude is seen to have more than doubled. Therefore it may be said that the effect of temperature is more significant than the effect due to gas lancing which increased the relative velocity by only 20%, under the present experimental conditions.

The effect of temperature may be greater than the effect of lancing due to the influence of temperature on the physical properties of the slag and the drop. As the temperature is increased, the viscosity of the slag and the drop are decreased, the slag is more fluid and therefore, greater turbulence is to be expected. Having a more fluid system the escape of the gas generated by the reaction at the slag metal interface is facilitated. The gas which is being removed from the interface will in turn create conditions which help to generate greater turbulence and greater relative velocities between the slag and metal. The increase in temperature is therefore of great importance, since the physical conditions of the system in general are beneficial to the present mass transport experiments.

Mass transfer coefficients and relative velocity values will be further investigated for the case of reaction at 1500°C. Data from figure 43 have been used and the Sh numbers calculated for 1500°C reactions are shown in figure 79.

It is clear that the number of experiments at 1500°C are only a few but nevertheless serve for comparison with previous results. The Sh number is seen from figure 79 to lie in the range from 14 to 25. The decarburization results clearly show that under 1% C a decrease in the decarburization rate suddenly occurs. This slow decarburization rate is seen to be maintained from 7 min up to 12 min. of reaction. The decarburization rates considered to be typical for 1500°C reactions are those limited by Sh numbers from 14 to 25. The mass transfer coefficients have been calculated as 9.97×10^{-5} cm/sec and 17.8×10^{-5} cm/sec respectively. The relative velocity is found to be from 0.42 to 1.2 cm/sec. At this point in the calculations due to the higher temperatures considered, it becomes necessary to assess the effect due to changes in viscosity. During the previous calculations the viscosity has been involved only when relative velocities were calculated. From the plotted data in figure 72 it is seen that by decreasing the viscosity from 0.7 poise to 0.25 poise for a constant Sh number the relative velocity value is reduced by about 50%. The increase in temperature for reaction therefore commences to influence to a significant extent the physical properties of the slag, and therefore mass transport. Figure 72 also indicates that by decreasing the viscosity of the system due to temperature effects (i.e. for a change in Sh number due to viscosity, the relative velocity remaining constant), the relative velocity will not increase while the decarburization rate is increased.

The effect of temperature on the diffusivity of FeO must also be taken into account. Up to now a typical value

of 5.7×10^{-6} cm/sec has been used. The significance of the diffusivity value can be shown by taking an extreme value. Taking the data of Agarwal and Gaskel (154) for the value of D_{FeO} as that of D_{Fe} at 1500° C, then, $D_{FeO} = 9.9 \times 10^{-6}$ cm^2/sec. By using the above value of the diffusivity of FeO, the Sh numbers required to obtain similar decarburization rates as those from experiment at 1500°C are calculated to be from 8 to 14. For a viscosity value of 0.7 poise, the relative velocity is found to be from 0.14 to 0.42 cm/sec and, for a viscosity value of 0.25 poise, the relative velocity between slag and drop are found to be from 0.08 to 0.25 cm/sec for Sh = 8 and Sh = 14 respectively.

Following the above method for determining Sh numbers, mass transfer coefficients and relative velocities, data from 1600° C experiments will now be calculated. The only experiments which were carried out at 1600°C are those shown in figure 46. The calculated Sh numbers to obtain similar decarburization rates are shown in figure 80. The value used in the above calculations for the diffusivity of FeO was taken as 5.7×10^{-6} cm/sec. The mass transfer coefficients for Sh = 20 and Sh = 50 are calculated to be 14.25×10^{-5} cm/sec and 35.6×10^{-5} cm/sec. To calculate the relative velocities for the above Sh values, two viscosity values will be considered as in the previous case for 1500°C. For a viscosity value of 0.7 poise, the relative velocities are calculated to be 0.8 and 3.96 cm/sec. For a viscosity value of 0.25 poise, the relative velocities were calculated to be from 0.48 to 2.35 cm/sec for Sh = 20 and Sh = 50 respectively.

In order to facilitate an overall comparison of the data calculated in the present section, the Sh number, mass transfer coefficients and relative velocity from 1240°C to 1600°C experiments have been included in table IV. Also included in table IV are results from experiments which were carried out with gas injection.

Tarby and Philbrook (102) (extensively discussed in section 2.7.2) calculated mass transfer during the reduction of FeO with blast furnace slags (i.e. less than 5% FeO). The calculated range from their experiments was from 5×10^{-5} to 56×10^{-5} cm/sec for slag metal reaction. These results are in good agreement with the values obtained for the present experiments (see table IV). It must be noted that the slags used by Tarby and Philbrook contained 8.9% alumina (see sections 2.7.2 and 5.5.5) which must have some effect on the overall reaction. Also, the experimental system itself was different from that used in the present study. Notwithstanding these slight differences, the mass transfer coefficients are extremely close over the range of conditions. The present work confirms the study of Tarby and Philbrook (102), and for that matter, the earlier work of Philbrook and Kirkbride (100).

In applying the mass transfer model given by equation 5.5.3.5 it has been possible to estimate values of dimensionless numbers (e.g.Sh, Sc, Gr and Re) and parameters such as the mass transfer coefficient and relative velocity. From the values calculated for the reaction between the continuous slag phase and a dispersed iron-carbon phase it is possible

to conclude that, although the mass transfer model provides solutions on a linear basis, certainly the trend predicted on a decarburization basis is in agreement with the present experimental work. By applying the mass transfer model, through approximated values and experimental results, estimates for the mass transfer coefficient and for the magnitude of the relative velocity have been possible. From visual observations, and due to the nature of the experimental method itself, estimates of relative velocity would not have been possible from experiment alone.

Calculations have been made considering mass transport control in the dispersed phase (i.e. carbon control). The results clearly indicate that mass transport within the dispersed phase is not a controlling step.

From considerations of the mass transport model for the continuous phase, it has been found that a transport model of FeO to the interface by diffusion and/or natural convection and/or forced convection can be in close agreement with the experimental data. The model is plausible and consistent with the decarburization results of the present experiments. The relative velocities predicted are not unrealistic. The model may apply.

5.7 Penetration Theory.

During experimental observations the iron-carbon drop during reaction with the slag was seen to be in a highly turbulent motion. Evidence from X-ray analysis and scanning microscopy indicate that the drop is most likely to be in a state of internal circulation which is not streamline or laminar.

The nucleation, growth, evolution and detachment of CO bubbles all give rise to an irregular liquid motion and even irregular shape. The liquid must certainly have local eddies and vortices generated within itself. The vortices created may be high in momentum and travel throughout the body of the drop and spend time at the surface. In addition the vortices may act as carriers of dissolved oxygen which has transferred from the slag. The eddies created through turbulence may be responsible for sweeping slag particles into the drop.

These latter observations indicate that a well defined interface between metal and slag may not exist and therefore the conditions are not compatible with the mass transfer model for laminar flow previously discussed in section 5.5.3.

Therefore, the possibility exists for other model or models to be more appropriate to the present experimental phenomena. One such model for which the above observations are more likely to be compatible is the penetration theory. The theory was originally proposed by Higbie (162). The model for the penetration theory requires only that laminar flow conditions exist at the reaction interface, though turbulent flow conditions prevail in the bulk phase. This theory is classically represented by a bubble of gas rising through a liquid which reacts with the gas bubble. A particle of liquid at the front of the rising bubble is in contact with the gas for time tc, which the bubble requires to rise a distance equal to its diameter while the liquid particles slip along the surface of the bubble. By knowing the velocity of rise and

the diameter of the bubble, the time may then be calculated from:

$$tc = d\ (cm) / v\ (cm/sec), \text{has the units of second} \quad 5.7..$$

and tc is assumed constant for all such particles of liquid. During the contact time tc, unsteady-state diffusion of the solute of the particle takes place and Ficks second law applies. With this concept, the flux of material at the interface between the liquid and the gas can be expressed as:

$$N = (D/\pi\ tc)^{\frac{1}{2}}\ (C^i - C^b) \qquad 5.7.2$$

if the concentration is expressed in moles/cm^3, the flux is given in moles/cm^2 sec.

The mass flux can be also represented as:

$$\text{Flux} = \text{coefficient (concentration difference)} \qquad 5.7.3$$

and therefore, k (mass transfer coefficient) $\equiv (D/\pi\ tc)^{\frac{1}{2}}$ 5.7.4

and from 5.7.1 $k = (D.v/\pi\ d)^{\frac{1}{2}}$ 5.7.5

The average flux over the time of contact tc is then:

$$\int_{t=0}^{t=tc} N\ dt = (C^i - C^b)\ (D/\pi)^{\frac{1}{2}} \int_{t=0}^{t=tc} t^{-\frac{1}{2}}\ dt \qquad 5.7.6$$

which on integration gives:

$$N_{av} = 2\ (C^i - C^b)\ (D/\pi\ tc)^{\frac{1}{2}} \qquad 5.7.7$$

therefore

$$k_{av} = 2\ (D/\pi\ tc)^{\frac{1}{2}} \qquad 5.7.8$$

and from 5.7.5

$$k_{av} = 2\,(D.v/\pi\, d)^{\frac{1}{2}} \qquad 5.7.9$$

Danckwerts (163) applied the unsteady-state concept to the absorption of a component from a drop or bubble in a turbulent liquid stream. His model assumes that the motion of the liquid is bringing fresh liquid eddies (or pockets) to displace elements previously on the surface which are exposed for varying lengths of time. The rate of solute penetration now depends on t_c. The average rate for unit surface area is the sum of all the individual values. A surface age distribution function $\phi(t)dt$ is defined as the fractional area dA covered by elements whose life is between t and dt, and is given by

$$\phi(t)dt = \frac{dA}{\text{total area}} \qquad 5.7.10$$

Danckwerts does not assume a correlation between the age of an element and the likelihood of it being replaced. He proposed a surface age distribution such that $t = S\, e^{-st}$ where s is the fractional rate of surface renewal. With the above assumptions the average flux is given as:

$$N_{av} = (C^i - C^b)\sqrt{D\,S} \qquad 5.7.11$$

therefore

$$k_d = (D\,S)^{\frac{1}{2}} \qquad 5.7.12$$

When this is compared to (5.5.3) above both state that:

$$k_d \propto D^{\frac{1}{2}} \qquad 5.7.13$$

Combining film and surface-renewal theory it has been shown (151) that as s approaches zero or with large diffusivities, the mass transfer coefficient takes on the character of the film theory, whereas, for small D or large s it follows equation 5.7.2.

The penetration theory may be applied to both, continuous and dispersed phases. Assuming equal contact times for both phases, equations 5.7.8 and 5.7.9 predict that mass transfer coefficients are at least an order of magnitude larger for the metal phase than those for the slag. This latter statement originates by considering the magnitude of diffusivities for the slag phase (10^{-6} cm^2/sec) and those for the metal phase (10^{-5} cm^2/sec). Therefore, since the mass transfer coefficients for the slag phase are small compared with those of the metal phase and, with the reduction reaction going to completion, the rate of FeO reduction process is determined by the transport of reactants in the slag. These findings are compatible with the results previously obtained in discussing simple mass transport models.

Due to the unsteady-state condition (equation 5.7.2) it is not possible to assign values for the constantly changing concentration of carbon in the drop and at the reaction interface. Therefore, calculations must be limited to the slag phase for which case the concentration of FeO at the interface may be taken as zero.

In order to adopt the penetration theory it is necessary either to measure contact times or, assume approximate values for the contact times. Experimental measurements of contact

time (i.e. relative velocity) are impossible. From calculations of relative velocity values between slag and metal in section 5.5.3, it is possible to calculate approximate contact times which can then be used in the model of penetration theory. The local relative velocity term can be considered as a measure of the stirring rate caused by CO evolution which, in turn, is dependent on the rate of the reduction reaction.

Since calculations have also been made in section 5.5.2 for the mass transfer coefficient it is now possible to compare with those values from equation 5.7.8. The comparison is made in table VI. Included in table VI is the ratio obtained from the mass transfer coefficient of both models. The ratio has been calculated for each corresponding value. The ratio indicates that the penetration theory predicts values for the mass transfer coefficient greater than the film theory model of equation 5.5.3.5, by a factor of about 19.

The results obtained indicate that, by calculating the molar flux of FeO from the slag as in section 5.5.3 and, ultimately decarburization rates, the penetration theory would give faster decarburization rates than those of the film theory by a factor of 19. For comparison, by taking values of the mass transfer coefficient at 1300^{o} C from table VI, a decrease in carbon content from 4.25% C to 1.18% C would require about 60 sec as calculated by the penetration theory. The film theory predictions for the time required for the same amount of decarburization to take place is about 1200 sec.

From the above comparison it is seen that the film theory seems to be more appropriate and compatible with the experimental results obtained in this work than the penetration theory.

The preceding examination of the applicability of the penetration theory has been made, by necessity (need for a relative velocity number), via the film theory model. The indications are that the penetration theory model based on the slag phase is not compatible with the present experimental work. In order to confirm these indications a more direct comparison with the experimental results themselves should be made. This is done below.

Typical rates of decarburization for all experimental condition can be approximated for the purpose of this comparison to 0.2%C/min. For a one gram drop this gives a consumption of carbon of 2.76×10^{-6} moles/sec. The equivalent flux of FeO is 1.37×10^{-6} moles of FeO/cm^2 sec. Solving equation 5.7.7 the contact time tc is calculated as 1118 sec which in turn through equation 5.7.1, gives a relative velocity value of 7.16×10^{-4} cm/sec. This relative velocity value is extremely low and would be that of an almost stationary drop. This is quite inconsistent with the experimental observations of highly turbulent crucible contents and the rapid motion of the drop (observed here and also by Hazeldean (99)).

It can be concluded from the above that the mechanism based upon Higbie's penetration theory cannot explain the experimental results obtained in the present work.

A possible cause of the above conclusion is that the surface area for the liquid eddies or pockets to contact is extremely large due to the irregular shape of the liquid metal perimeter and the porosity. The surface area is no longer proportional to the square of the diameter. In such cases Danckwerts' modification of the surface renewal theory may be more pertinent.

However, solution of equation 5.7.11 depends upon a knowledge of the surface age distribution; this is impossible to measure or estimate. Consequently the discussion can only suggest this model and cannot be pursued further.

Tarby and Philbrook (102) came to the same conclusion about the penetration theory and had to be content with the suggestion stage. The present work has pursued this suggestion further but predicts unrealistic relative velocities. Advancing a step further Danckwerts surface-renewal theory is suggested in the same manner as Tarby and Philbrook suggested the penetration theory.

5.9 General observations on slag-metal-gas phenomena.

In the previous sections of the discussion chapter attempts have been made to analyse different aspects related to the experimental work. It has been established that the decarburization reaction between Fe-C drops and synthetic slags is heterogeneous and not controlled by the chemistry of the process. Therefore, detailed considerations were then made to compare film and penetration theories with experimental results. Further observations can be made with respect to decarburization rates on a qualitative basis from slag-metal-gas phenomena.

The system under study is complex in the sense that gas evolution is constantly changing the available area of reaction. If this effect takes place within the metal drop, a gas-metal interface is generated while, if it takes place on the surface of the drop then a slag-metal-gas interface is generated. Although it is not possible to isolate these latter two effects in the present experiments, it is possible nevertheless, to

discuss the overall phenomena taking place. The following discussion will be based on the calculated rates of reaction (k) which take into account the amount of carbon loss in a given time. Szekely (164) notes that for homogeneous first-order reactions, the units of k are simply sec^{-1}, whereas for a first order heterogeneous reaction, k has units of length $time^{-1}$. The values calculated in table V can therefore be taken to represent mass transfer coefficients for the present experimental reactions.

From table V it is seen that by increasing the temperature of reaction for a given slag from 1300 to 1400° C an increase in the mass transfer coefficient is obtained. The magnitude of the increase in the mass transfer coefficient is in addition related to chemical composition, since, for fayalite slag an increase by a factor of about 2.5 takes place while for lime bearing slags the same factor is about 1.9. The effect was confirmed by plotting the calculated values in table V against lime contents of the various slags used. The results are shown in figure 81. The lines drawn through the points do not intend to depict the specific correlation between k and slag-lime content; the line is drawn simply to suggest the possibility of such a trend. It is recognised that a great many more experiments would be required to establish a definite relationship. In all probability, several factors may contribute to the trend shown in figure 81 as discussed below.

Except for those experiments where gas injection was carried out, all experiments had no external mechanical stirring whatsoever. Therefore the turbulence created during reaction was due to carbon monoxide evolution. Visual evidence of the turbulence

generated has been obtained by photographing the slag surface during reaction (see plates VIa - VId). Hazeldean et al. (99) have also found clear evidence of the turbulence created, from their X-ray observations on slag-metal reactions.

Considering the temperature effects, the rate of reaction would be expected to increase with temperature increases. Over the temperature range considered, the change in activities of the reactants is relatively small. The greater fluidity of the slag implies a more rapid transfer to, and products from, the reacting interface. The increase in the rate of reaction means more CO gas generated which in turn generates greater turbulence and again facilitates transport of reactants and products. Rapid evolution of CO bubbles in turn, gives more relative motion between the drop and slag due to greater buoyancy and explosive escape of the said bubbles. In turn a greater foam is generated. The viscosity of the metal is likely to be decreased with an increase in temperature. Although little is known about values of surface tension, it is quite likely that a decrease occurs as temperature is increased. The transfer of slag into the metal drop may thus be more readily facilitated. The increased entrapment of slag particles will enhance decarburization as the number of possible nucleation sites is increased (see sections 4.7 and 5.4). By further increasing the temperature for reaction, the above effects would take place more readily. Visual observations at 1600° C and the effects of violent foaming found at 1500° C (see sections 4.5 and 4.4.2), clearly indicate greater turbulence was taking place as compared with experiments at 1300° C.

From the chemical composition point of view figure 81 clearly indicates that lime content has also an effect on the rate of decarburization i.e. the mass transfer coefficient is altered. The effect of lime, within the range studied in this work, was found to give highest mass transfer coefficients for lime contents about 26% CaO. For the range of lime contents from 0 to 26% CaO an increase in the mass transfer coefficient is to be expected due to a decrease in the melting point of the slags (see figure 12) and also, because the introduction of lime to the slags will tend to break the silica network and therefore decrease the viscosity of the slag. Further increase in lime content above 26% CaO decreases the mass transfer coefficient as shown in figure 81. The lime content increase may cause precipitation of solid particles of dicalcium silicate and therefore increase the bulk viscosity of the slag. As pointed out by Kootz (90) for open hearth furnaces, the slag penetrates very soon into the heterogeneous region. The increase in viscosity and the presence of second phase particles must suppress the motion of the metal drop within the slag phase despite the violent nature of CO evolution. The decarburization rate consequently starts to fall.

When gas lancing was carried out an increase in the mass transfer coefficients was expected. The values obtained in Table V show that decarburization rates were increased but to a lesser extent than expected. When reactive gases of different oxygen potential were lanced it was found that there was not any marked effect on mass transfer coefficients. The main effect of gas injection appears to be solely physical in nature, in that

the dynamics of the system are changed. The effect of "oxygen" in the gas as either a source of raw material for decarburization or as a cause of increase in oxygen potential of the system, is undetectable. The increase in mass transfer coefficient due to the introduction of gas injection, although clearly detectable, is quite small. The magnitude of the increase is clearly related to the low flow rate of gas used for lancing (75 cc/min). There exists a transfer of momentum from jet to slag which results in increased turbulence. However, the blanketing effect on part of the slag prevents a large transfer of momentum, and therefore turbulence, to the drop. The hydrodynamic nature i.e. (Re) of the drop, is not directly altered by the introduction of low flow rate gas injection. The calculated values for relative velocity in section 5.5.2 also confirm a relatively small increment. The change over from inert gas to reactive gas did not initiate gas-metal reaction at a detectable level. The reactivity of the slag with the oxidizing gas may have "passivated" the oxygen available for reaction. In levitation studies of Fe-C-Si drops a similar effect has been proposed (113).

In terms of the value of the mass transfer coefficient it can be said that gas lancing at 75 cc/min corresponds to an increase in the dynamics of the system which is equivalent to an increase of 100^{o} C in temperature from 1300 to 1400^{o} C.

The importance of slag fluidity and temperature has been pointed out by Meyer et al. (86,87) Bardenheur et al. (82) and Trentini (83). When proposing the emulsion theory, Meyer et al. (86.87) suggest that the existence of a hot, fluid slag was essential for efficient carbon removal and illustrates this point

by comparing decarburization curves from normal LD refining with the case of a two-slag LD refining. This comparison showed that the increase in the rate of decarburization was much more rapid for the two-slag process. Unfortunately the results from this thesis cannot support or deny the latter comments, what can be said is that for a slag following the fayalite-dicalcium silicate join, decarburization rates by the slag will be slower for lime contents beyond 26% CaO. The path for the above case would be classified as a dry-slag path as shown in figure 15a. Dry-slag refining has been found to give high rates of decarburization (167). In LD steelmaking the presence of a dry viscous slag will only favour decarburization rates in the sense that the possibility for a gas-metal reaction may be established. This fact is also outlined by bottom blowing steelmaking process (Q-BOP) where direct gas-metal interface is generated. Lime powder which is also injected with the oxygen stream, in Q-BOP operation, will further provide a large number of nucleation sites for CO nucleation. During Q-BOP operation the decarburization reaction is more dependent on the rate of gas injection than the LD process. Great care is required during the initial stages of LD refining in order to have adequate control on slag formation (see section 2.6). Greatest disadvantages found during LD steelmaking can be said to be those due to slag control. Any deviation incurred during operation will ultimately lead to a loss in yield due to the amount of droplets which may be entrapped when slag overflow (slopping) or sparking takes place. The advantages of having a slag present is its capability to cater for other impurities such as sulphur and phosphorus which cannot

be removed by gas lancing alone. From the experiments carried out in this work during gas injection it was found that for a rate greater than 75 cc/min the majority of the drops shattered. Although the size and geometry of the crucibles used in the present work are not comparable to actual LD vessels, it does indicate the facility with which the drops may be generated and scattered throughout the slag phase in industrial vessels. With respect to bottom blowing the possibility of drops scattered throughout the slag is avoided and therefore this may be an advantage to this process with respect to iron yield. It is possible for many more comments to be made with respect to industrial operation but other factors must be taken into account which are beyond the scope of this thesis.

CHAPTER SIX

CONCLUSIONS

A system has been developed which simulates certain aspects of the slag-metal-gas reactions which generate a dynamic foam of the type found in Basic Oxygen Steelmaking. The system incorporated one gram iron-carbon samples and synthetic slags (in a ratio of 1:30) of the ternary lime-iron oxide-silica system. Decarburization rates were determined from reacting iron-carbon samples with slags for predetermined times so as to give one point on a plot of %C vs time. The plotted graphs indicated that a first-order reaction was taking place.

Slags of this nature, although highly reactive, can be contained in iron crucibles. With protection of a zirconia film, the iron crucibles can be safely used up to 1400^{o} C. At higher temperatures it has been shown that alumina crucibles can give adequate periods of service while containing these slags if zirconia is used to prevent alumina dissolution. Dispersed liquid iron alloys can be held in iron crucibles and alumina crucibles.

Rates of decarburization increase with increasing lime content of the slag up to a certain composition. The maximum rate commences to decrease with lime contents above 26%. The rates of decarburization increase with increasing temperature. The range of temperatures within which reactions were studied corresponds to the initial stages of oxygen steelmaking where it is well known that the complexly alloyed metal

is being oxidized. Results from the reactions in the range of 1300 to 1600° C indicated that the decarburization takes place more rapidly in the presence of a more fluid, and consequently more turbulent, system. The hydrodynamic characteristics of the system were changed by introduction of gas lancing. The increased turbulence caused more rapid decarburization. The changes of oxygen potential of the gas used as injectants had little effect upon the rate of decarburization.

There is clear evidence that the overall rates of the decarburization process are not controlled by the rate of the chemical reaction itself. Although a small number of results were used to compute activation energies, the results obtained agree favourably with those found in the literature. Experimental observation, X-ray analysis and scanning electron microscopy have established that internal heterogeneous nucleation takes place through entrapment of particles of slag. Surface nucleation was evident on samples reacted with high lime slags and when carbon levels of near 2.2% had been reached. The entrapped particles of slag which are in suspension in the drop are extremely small (below the limit of normal scanning electron microscopes).

Mass transfer coefficients have been measured. It has been possible to correlate mass transfer coefficients to simple models which have been proposed by other authors. Although the generation of carbon monoxide gives rise to a situation which is very complex to describe in terms of mathematical

models, assumptions have been made to allow calculations of relative velocity between slag and metal, Sh, Sc, Gr and Re numbers.

From application of film and penetration theories mass transport control in the metal phase was found to be not operative. It must be concluded that for the present experiments mass transfer is likely to be of a slag- or mixed-control.

The film theory has been found to be in better agreement than the penetration theory with the experimental results obtained on a decarburization rate basis.

The possible applicability of Danckwerts surface renewal model has been suggested as a potential model which may merit consideration.

Suggestions for Future Work

The decarburization studies in the present work have enabled the establishment of a method which may be more widely and further exploited. As a sequence to the present study involvement of other elements seems necessary. With respect to iron-carbon alloys additions of elements such as Si, Mn, P, S, or a combination of these elements should be studied. Slag components should be based around the $CaO-FeO-SiO_2$ ternary; additions of MnO, P_2O_5 or MgO may be made.

Physical properties of slags, such as viscosity, surface tension and densities are needed to establish (if any) correlation with rate of decarburization. The effect of various oxides on the foaming characteristics of slags may prove useful in controlling the course of refining.

Pursuing further the mechanisms of decarburization a study of slag entrapment by iron-carbon alloys may allow for a possible model to be proposed. Further electron microscopy will most certainly yield more information about the nucleation sites.

Future studies at higher temperatures would be useful if the extremely expensive materials which would be necessary were available. A wider range of temperatures would allow more detail of the decarburization mechanisms to be explored, in addition, permit the study of a wider range of slag compositions.

With respect to further studies the possibility exists to carry out similar experiments by exchanging the iron-carbon sample by a graphite sphere. This would provide a solid spherical geometry for the system. Mass transport models as discussed in this thesis could then be more readily applied to determine the rate controlling step for decarburization with slags.

REFERENCES

1. Pearson, T.F., Venkatadri, A.S. and O'hanlon, J., JISI, pp.997-1006, Oct. 1966.

2. Allen, J.A. Studies in Innovation in the Steel and Chem. Industries, Man.U.Press, 1967.

3. Graef, R., J. of Metals, Vol.9, pp.1435-1439, 1957.

4. Anonymous, Journal of Metals, pp.31-57, March, 1972.

5. Savard, G. and Lee, R., SEAISI Quarterly, p.8-12,April,1974.

6. Nilles, P., and Boudin, M., Iron and Steelmaking (Quarterly) No. 1, pp.22-27, 1974.

7. Trentini, B., Vaissiere, P. and Allard, M., JISI, June, 1959, pp.143-147.

7a. Jones, D.J., Parsons, A.E. and Morris, N. Journal of Metals, Aug. 1963, pp.577-580.

8. Cuscoleca O. and Rosner, K., JISI, June, 1959, Vol.192, pp.147-153.

9. Operations of Large BOF's. ISI SR.139.

10. Baker, R., BSC Open Report, CAPL/SM/A/31/74.

11. R.G. Ward, Physical Chemistry of Iron and Steelmaking, Edward Arnold (Publishers) Ltd., 1962.

12. C. Bodsworth and H.B. Bell, Physical Chemistry of Iron and Steel Manufacture, Longman Group Ltd., 1963.

13. A.K. Biswas and G.R. Bashforth. The Physical Chemistry of Metallurgical Processes, London, Chapman & Hall, 1962.

14. Marshall, S., and Chipman, J. Trans. ASM. 1942, 30, pp.195.

15. Phillbrook, W.O., Open Hearth Proc. 1961, 44, p.391.

16. Meyer, H.W. et al. Heat and Mass Transfer in Process Metallurgy, IMM, London, 1967, p.173.

17. Chipman, J., Gero, G.B. and Winkler, T.B. Trans.AIME, Feb.1950, Vol.188, J. of Metals, p.341-345.

18. Rhydderech, M.J., JISI, 1967, 205, p.814.

19. McBride, D.L., Journal of Metals, July, 1960, pp.531-537.

20. Turkdogan, E.T., Trans.IMM Section C, 1974,Vol.83, C.67-C81.

21. Grant, N.J. & Chipman, J., Trans.AIME, Feb.1946, pp.134-154, 167.

22. Taylor, C.R. and Chipman, J. Trans. AIME, 1943, Vol.154, pp.228-245.

23. Turkdogan, E.T., and Pearson, J., JISI, March, 1953, part I, p.217-223.

24. Darken, L.S. and Gurry, R.W., J.Am.Chem.Soc., 1945, Vol.67, pp.1398-1412.

25. Darken, L.S. and Gurry, R.W. J.Am.Chem.Soc. 1946, Vol.68, pp.798-816.

26. Chipman, J. and Fetters, K.L. Trans.ASM.Vol.29, pp.953-968.

27. Bishop, H.L., Grant, N.J. and Chipman, J. Trans.Met.Soc. AIME, Vol.212, p.185,1958.

28. The making shaping and treating of steel. U.S. Steel, 9th Edition, 1971.

29. Denbigh, K., The Principles of Chemical Equilibrium, Cambridge at the University Press, 1971.

30. Muan, A., Am.Journal of Science, March, 1958, Vol.256, pp.171-207.

31. Gockcen, N.A., and Chipman, J. J. of Metals, Feb.1952, pp.171-181.

32. Chipman, J., and Gockcen, N.A. J. of Metals, Aug.1953, pp.1017-1018.

33. Bowen, N.L. and Schairer, J.F. Am.J. of Science, 1932, Ser. 5, Vol.24, p.177.

34. Darken, L.S., Am.Chem.Soc. June, 1948, Vol.70, pp.2046-2053.

35. Muan, A., Trans. AIME, 1955, Vol.203, pp.965-976

36. Bodsworth, C., Ph.D. Thesis, University of Sheffield, 1957.

37. Schuhmann, R. and Ensio, P.J., Trans. AIME, J. of Metals, May, 1951, pp.401-411.

38. Michal, E.J., and Schuhmann, R., Trans. AIME, 1952, 194, pp.723-728.

39. Schuhmann, R., Jr., Trans. AIME, J. of M., June, 1950, Vol.188, pp.873-884.

40. Schuhmann, R. et al. Trans. AIME J. of M., Sept.1955, pp. 1097-1104.

41. Bodsworth, C., JISI, Sept. 1959, pp.13-24.

42. Taylor, C.R. & Chipman, J. Trans.AIME 1943, Vol.154, pp.228-245.

43. Muan, A., and Osborn, E.R., Phase Equilibria among Oxides in Steelmaking, Addison-Wesley Publishing Co., USA, 1965.

44. Allen, W.C. and Snow, R.B., J. of the Am.Soc., Vol.38, No. 8, Aug. 1955, pp.264-280.

45. Phillips, B., and Muan, A. Trans. AIME, Vol.218, Dec. 1960, pp.1112-1118.

46. Timucin, M. and Morris, A.E., Met.Trans. Nov.1970, Vol.1, pp.3193-3201.

47. Obst, K.H., Stradtmann, J., and Tromel, G., JISI, May, 1970, pp.450-455.

48. Rogotev, N.I., Steel in the USSR, 1972, 2, pp.518-520.

48a. Anonymous, 33 Mag., 11, 42, 1973.

49. Welbourn and Kulig, BSC. CAPL/SM/A/53/73.

50. Sharman, Open Hearth Proc. 1974, 57 pp.178-188.

51. Chipman, J., Bishop, H.L., Grant, N.J. Trans. Met. Soc. AIME, April, 1958, pp.185-192.

52. Elliot, J.F., Trans. AIME, J. of Metals, March, 1955, p.485.

53. Turkdogan, E.T., and Pearson, J. (see ref. 23), JISI, Vol. 175, Dec. 1953, pp.393-401.

54. Johnson, R.E., Muan, A., Trans. AIME, Dec. 1967, Vol.239, pp.1931-1939.

55. Richardson, D., The Physical Chemistry of Steelmaking, p.68, The MIT Press, Ed. J.F. Elliot, 1956.

56. Toop, G.W., and Samis, C.S. Trans. of Met. Soc. AIME, Vol.224, p.878 (October, 1962).

57. Toop, G.W., and Samis, C.S., Can. Met. Q., 1962, 1, No. 2, p.129.

58. Masson, C.R., JISI, Feb.1972, Vol.210, pp.89-96.

59. Chemical Metallurgy of Iron and Steel.
BSC Corporate Labs. University of Sheffield, Symposium 1971, ISI.

60. Masson, C.R., and Smith, J.G., Canadian J. of Chemistry, 1971, Vol.49, pp.683-690.

61. Metallurgical Society Conference, Vol.7, part 1, 1959.

62. Metallurgical Society Conference, Vol.8, part 2, 1959.

63. Elliot, J.F., Gleiser, M., Ramakishna, V., Thermochemistry for Steelmaking, American Iron and Steel Institute, Addison-Wesley Publishing Co., 1963.

64. Davenport, W.G., Wakelin, D.H., Bradshaw, A.V., Heat and Mass Transfer in Process Metallurgy, I.M.M. Ed. A.W.D. Hills, pp.207-245, London, 1967.

65. Molly, N.A., JISI, October, 1970, p.943.

66. Chaterjee, A., Bradshaw, A.V., 1972, JISI, Vol.210, pp. 179-187.

67. Mathieson, G.C.R., JISI, 1968, Vol.206, p.337.

68. Rote, F.E., Flinn, R.A., Met. Trans. June, 1972, 3, pp.1373-1384.

69. Chesters, J.H., Refractories, Production and Properties. The Iron and Steel Institute, 1973.

70. Kozakevitch, P., J. of Metals, pp.57-68, July, 1969. Open Hearth Proceedings, pp.64-75, 1969.

71. Larsen, B.M., Proc. Open Hearth, 1949, Vol.32, pp.231-233.

72. Basic Open Hearth Steelmaking, 1951, N.Y., AIME.

73. Davis, H.M., Proc. Open Hearth, 1949, Vol.32, p.238.

74. Kitchner, J.A., Cooper, C.F., Quarterly Reviews of the Chem.Soc., 1959, 13, pp. 71-97.

75. Richardson, F.D., Trans. ISIJ, 1974, Vol.14, pp.1-8, Special Lecture.

76. Kozakevitch, P., Rev. Met., 1949, Vol.46, p.505.

77. Kozakevitch, P., Surface Activity in Liquid Metal Solutions, p.223, S.C.I., Monograph No. 28,

78. Kitchner, J.A., Cooper, C.F. JISI, Sept. 1959, pp. 48-55.

79. Price, D.J., Process Eng. of Pyrometallurgy, I.M.M. 1974.

80. Li, K., Dukelov, D.A., Smith, G.C. Trans. AIME, Feb. 1964, Vol.230, pp.71-76.

81. O'Shaughnessy, E.J., Bickness, E.H. Open Hearth Proc. 1973, 56, p.369-376.

82. Bardenheuer, F., Vom Ende, H., Speith, K.G., Blast Furnace and Steel Plant, June, 1970, pp.401-407.

83. Trentini, B., Trans. Met. Soc. of AIME, Vol.242, pp.2377-2388, Dec. 1968.

84. Baker, R., JISI, June, 1967, Vol.205, pp.637-641.

85. Fuji, T., Arskai, T., Marukawa, K., Trans. ISIJ, 1969, Vol.9, pp.437-447.

86. Meyer, H.N., Porter, W.F., Smith, G.C., and Szekely, J., J. of Metals, July, 1968, pp.35-42.

87. Meyer, H.W., J. of Metals, June, 1969, pp.781-789.

88. Ichinoe, Yamamoto, Nagono, Miyamoro, Yamagushi and Tezuka, Proc. ICSTIS, 1971, Trans. ISIJ, p.232.

89. Kawakami, K., J. of Metals, July, 1966, pp.836-845.

90. Kootz, T., Altgeld, A., Trans. ISIJ, part I, ICSTIS, 1971, pp.527-531.

91. Swisher, J.H., Turkdogan, E.T., Trans. AIME, May, 1967, Vol. 239, pp.602-610.

92. Fruehan, R.J., and Martonik, L.J. Met. Trans., May, 1974, Vol.5, pp.1027-1032.

93. Ito, K., and Sano, K., Trans. ISIJ, 1968, Vol.8, pp. 165-171.

94. Hayer, M., and Whiteway, S.G., Canadian Met., 1973, Vol.12, No. 1, pp.35-44.

95. Sain, D.R., and Belton, G.R., Met. Transactions, June, 1976, Vol.7B, pp.235-244.

96. Nomura, H., and Mori, K., Trans. ISIJ, 1973, 13, pp.265-273, and pp.325-332.

97. Parlee, N.A., et al. Trans. Met. Soc. AIME, Feb., 1958, pp.132-138.

98. King, T.B., et al. Heterogeneous Kinetics at Elevated Temps. p.409, Plenum Press, 1970.

99. Hazeldean, G.S.F., Mulholland, E.W. and Davies, M.W., JISI, Sept. 1973, pp.632-639.

100. Philbrook, W.O., and Kirkbride, L.D., Trans. AIME, March, 1956, pp.351-355.

101. Dancy, T.E., JISI, Sept. 1951, pp.17-24.

102. Tarby, S.K., and Philbrook, W.O., Trans. Met. Soc. AIME, July, 1967, Vol.239, pp.1005-1017.

103. Davies, M.W., Hazeldean, G.S.F. and Smith, P.N. BSC Report CAPL/SM/H/36/73.

104. Grievson, P., and Turkdogan, E.T., Trans. Met. Soc. AIME, Dec. 1964, Vol.230, pp.1609-1614.

105. Fay Fun, Met. Trans. Sept. 1970, Vol.1, pp.2537-2541.

106. Davies et al. JISI, Aug. 1967, Vol.205, pp.810-813.

107. Bardenheur Oberhauser, BISI Translation No. 7919.

108. Anonymous. Metalurgia, Nov. 1966, pp.197-200.

109. Baker, L.A., Warner, N.A. and Jenkins, A.E., Trans.Met. Soc., AIME, Oct.1964, Vol.230, pp.1228-1235.

110. Baker, L.A., Warner, N.A. and Jenkins, A.E. Trans.Met. Soc. AIME, 1967, Vol.239, pp.857-864.

111. Distin, P.A., Hallet G., and Richardson, F.D. JISI, Aug.1968, Vol.206, pp.821-833.

112. Richardson, F.D., Proc.Int.Conf.Met.Chem., University of Sheffield, p.82, 1972.

113. Robertson, D.G.C., and Jenkins, A.E., Heterogeneous Kinetics at Elevated Temperatures. Belton & Worrel (Eds.), Plenum Press, N.Y., p.393, 1970.

114. Roberts, C.C., et al., Trans. of Met. Soc., Nov.1969, Vol.245, pp.2413-2420.

115. Baker, L.A., and Ward, R.G., JISI, July, 1967, pp.714-717.

116. See, J.B. and Warner, N.A., Jan. 1973, JISI, pp.44-52.

117. Roddis, P.G., JISI, Jan. 1973, pp.53-58.

118. Kaplan, R.S., and Philbrook, W.O., Trans.Met.Soc., AIME, 1969, Vol.245, pp.2195-2204.

119. Edwards, J., B.Sc., Sheffield City Polytechnic, 1976.

120. Pratt, R., B.Sc., Sheffield City Polytechnic, 1977.

121. Riboud, P.V., et al., BISI, 8990 (1970).

122. Riboud, P.V. et al., BISI, 7588, Ch.4., 1969.

123. Gosh, D.N., Iron Making and Steelmaking (quarterly), 1975, No. 1, pp.36-44.

124. Korber, F., and Oeslen, W., Mitt. Kaiser-Wilhelm-Inst. Eisenforsch, 17 (1935), 39.

125. Turkdogan, E.T., Davies, L.S., Leake, L.E., and Stevens,G.C. JISI, Oct. 1955, pp.123-128.

126. Boni, R.E., and Derge, G., Trans. AIME, 1956, Vol.206, p.53, Henderson, Hudson, Ward and Derge, Trans. AIME, J. of M. 1956, p.53.

127. Kozakevitch, P., Rev.Met., 1949, Vol.46, No. 9, pp.572-582.

128. Kitchener, J.A., and Barfield, R.N., JISI, Aug.1955, pp.324-329.

129. Gaskell, D.R., and Lee, Y.E., Met. Trans. 1974, Vol.5, pp.853-860.

130. Proceedings of the International Conference, Oct.1970, Kinetics of Metallurgical Processes in Steelmaking. Verlag Stahleisen, M.B.H., Dusseldorf, 1975.

131. von Bogdandy, L., Steelmaking: The Chipman Conference, The M.I.T. Press, June, 1962.

132. Bradshaw, A.V., Le Vide, Nov.-Dec. 1968, No. 138, pp.376-415.

133. B.M. Larsen, Basic Open Hearth Steelmaking, 1951, N.Y. AIME.

134. Delve, F.D., Duderstadt, G.C. and Kowal, R.F., JISI, 1968, 206, p.1218.

135. Alexander, J., Hazeldean, G.S.F. and Davies, M.W. Proc.Int.Conf.Met.Chem., University of Sheffield, p.107, 1972.

136. Acheson, R., Ph.D. Thesis, Sheffield Polytechnic, 1976.

137. Dean, R.B., J. of Applied Physics, May, 1944, pp.446-451.

138. Richardson, F.D., see ref.112.

139. Advances in Chemical Eng. Vol.4, A.P., N.Y. 1963.

140. Hu, S., and Kitner, R.C., A.I.Ch.E. Journal, March, 1955, pp.42-48.

141. Recent Advances in Liquid-Liquid Extraction, Ed.C. Hanson, Univ. Bradford, U.K., Pergamon, 1971.

142. Handlos, A.E., and Baron, T., A.I.Ch.Eng.Journal, 1957, 3, pp.127-136.

143. Hadamard, M.J. (presented by M.H. Ponicare), Compte Rend. No. 152, pp.1735-1738, 1911.

144. Skelland, A.H.P., and Wellek, R.M. A.I.Ch.E. Journal, 1964, Vol.10, No. 4, pp.491-496.

145. Wellek, R.M., and Skelland, A.H.P., A.I.Ch.E. Journal, 1965, Vol.11, No. 3, pp.557-576.

146. Johnson, A.I., and Hamielec, A.E., A.I.Ch.E.. 1960. Vol.6. No. 1. pp.145-149.

147. J. Crank, the Mathematics of Diffusion, Oxford, Clarendon Press, 1964.

148. Kronig, R., and Brink, J.C., Appl.Sci.Res.1950, Vol.A2, pp.142-154.

149. Griffith, R.M., Chem.Eng.Sci., 12, p.198, 1960.

150. Aeron, S.M., Thesis, 1971, Imperial College of Sci. and Tech.

151. Steinberg, R.L., and Treybal, R., A.I.Ch.E. Journal, June, 1960, No. 2, pp.227.

152. Coulson, J.M., and Richardson, J.F., Chem.Eng. Vol. 1, 1954, Pergamon Press.

153. Taylor, J. Chemical metallurgy of Iron and Steel, BSC Corporate Labs. University of Sheffield, Symposium 1971, ISI.

154. Agarwall, D.P. and Gaskell, D.R., Met. Trans. B. Vol.6B. June, 1975, p.263-267.

155. Kozakevitch, P. Rev. de Metallurgie, 1954, Vol.51, pp.569-587.

156. Rontgen, P., Winterhager, H. and Kammel, R. BISIT 2475.

157. See reference 141, Chapter 9, Heertjes

158. Davies, J.T. Turbulence Phenomena, A.C. Press, 1972.

159. Ward, M.D. JISI, May, 1970, Vol.208, p.445-449.

160. Darken, L.S., and Gurry, R.W., Physical Chemistry of Metals, N.Y. McGraw Hill, 1953.

161. Richardson, F.D. Iron and Coal, BISRA Steelmaking Conference 1961, p.1105.

162. Higbie, R., Trans. AIChE, Vol.31, p.365, 1935.

163. Danckwerts, P.V. J. AIChE, 1, 456, 1955.

164. Szekelly, J. and Themelis, N.J. Rate Phenomena in Process Metallurgy, N.Y. Wiley, 1971.

165. Kubashewski, O., Evans, E.Ll. and Alcock, C.B., Metallurgical Thermochemistry, Pergamon Press, Oxford, 1967.

166. Scimar, R., Steel and Coal, March, 1962, p.505-509.

167. Hazeldean, G.S.F. Private communication.

APPENDIX I.

To calculate the oxygen potential in the gases used for lancing the following equations may be used:

$$2CO + O_2 = 2CO_2 \qquad A.1$$

for which ΔG^o at 1300° C is given as - 69 684 cal.
Using this equation the three gas components are related by the equilibrium constant:

$$K = \frac{P^2_{CO_2}}{P^2_{CO} \cdot P_{O_2}} \qquad A.2$$

But, it is required to determine initially the partial pressures for CO and CO_2 and these may be calculated from equilibrium considerations with the iron-carbon alloy.

For the reaction

$$\underline{C} + CO_{2\,(gas)} = 2CO_{(gas)} \qquad A.3$$

$$K = \frac{P^2_{CO}}{P_{CO_2} . a\ \underline{c}} \qquad A.4$$

and $\Delta G^o = 33\,300 - 30.4\ T \qquad A.5$

but $\Delta G^o = -RT \ln K \qquad A.6$

by substituting A.4 into A.6 and A.5

$$\Delta G^o = -RT \ln \frac{P^2_{CO}}{P_{CO_2} \cdot a\underline{c}} = 33\,300 - 30.4\ T \qquad A.7$$

from where $\log \frac{P^2_{CO}}{P_{CO} \cdot a\underline{c}} = \frac{7280}{T} - 6.64 \qquad A.8$

at 1300° C the activity of carbon is 0.72 (ref.63) and

from A.8

$$\frac{P_{CO}^2}{P_{CO_2}} = 0.007$$

For an argon-5% CO_2 gas used,

$$P_{CO} + P_{CO_2} = 0.05 \text{ atm} \qquad \text{A.9}$$

A.9 into A.8 yields:

$$\frac{P_{CO}^2}{P_{CO_2}} = \frac{(0.05 - P_{CO_2})^2}{P_{CO_2}} = 0.007 \qquad \text{A.10}$$

and $P_{CO_2} = 0.0345$ atm, $P_{CO} = 0.0155$ atm

the equilibrium constant becomes

$$K = \left(\frac{0.0345}{0.0155}\right)^2 x\left(\frac{1}{PO_2}\right) \qquad \text{A.11}$$

and $-69\,684 = -RT \ln \left(\frac{0.0345}{0.0155}\right)^2 - RT \ln \frac{1}{PO_2}$

from where PO_2 is calculated as 1.034×10^{-9} atm.

In a similar manner the oxygen potential for the different gases used for lancing were calculated and are given in the following table:

% CO_2	P_{CO_2}	Pco	PO_2
5	0.0345	0.0155	1.034×10^{-9}
50	0.444	0.056	1.313×10^{-8}
100	0.9197	0.0903	2.16×10^{-8}

The slags themselves all had oxygen potentials lower than that of inert -5% CO_2 gas. The lime bearing slags had the lowest oxygen potentials. Fayalite had the highest oxygen potential which was calculated to be 1.55×10^{-12} atm. The lime bearing slags had the lowest oxygen potentials. These are difficult to estimate. Nevertheless, attempts were made to calculate the oxygen potentials for various slags used in the present work.

One such method consisted in calculating from the appropriate thermodynamic values. The method considers a simple mixture having iron, calcium, oxygen and silica as starting materials. Calculations are made for the free energy (G^o) of the pure starting materials at 1573° K, from the following equation

(1): $$G^o_{1573} = H^o_{1573} - TS^o_{1573} \qquad (1)$$

where H^o, the enthalpy is given by:

$$\Delta H = H^\circ_{298} + \int_{T=298}^{T=T_t} C_p dT \pm L_t + \int_{T=T_f}^{T=T} C_p dT \qquad (2)$$

and the entropy by:

$$\Delta S = S^\circ_{298} + \int_{T=298}^{T=T_t} Cp\frac{dT}{T} + \frac{L_t}{T} + \int_{T_t=T_t}^{T=T} Cp\frac{dT}{T} \qquad (3)$$

L_t is the heat of transformation which takes place at temperature T_t. The value L_t is subtracted for the transformation of a reactant, and added for that of a product. C_p is the heat capacity of the substance under consideration and is usually represented as a function of temperature in equations of the form:

$$Cp = a + BT + cT^2 = dT^{-2} \qquad (4)$$

The reference state is 298° K where $H^o_{298} = 0$ for an elementary substance. Values for Cp, S^o_{298} and L_t were obtained from Kubashewski, Evans and Alcock (165). By applying equations 1 to 3, with appropriate values the following data were calculated:

$G^o_{1573^oK}$	= H^o_{1573}	- $1573 \times S^o_{1573}$ cal/mole	ELEMENT
- 43192	= - 10536.7	- 1573x20.76	IRON
- 44919	= - 11814	- 1573x21.04	CALCIUM
- 108131	= - 10321.7	- 1573x62.18	OXYGEN

The free energy of pure silica at 1573° K was taken from Elliot and Gleiser (63) given as G^o = - 143000 cal/mole.

The free energies for various slags including F_2S and C_2S at 1573°K used in the present work were then calculated for the corresponding mole fraction (N_i) of iron, oxygen, calcium and silica assuming a simple mix from:

$$G^o_{1573} = N_{Fe}\, F^o_{Fe} + N_{O_2}\, G^o_{O_2} + N_{Ca} G^o_{Ca} + N_{SiO_2} G^o_{SiO_2} \qquad (5)$$

SLAG	N_{Fe}	N_{Ca}	N_{O_2}	N_{SiO_2}	G^o_{1573} cal/mole
F-III	.389	---	.395	.215	-90258
F-IV	.387	---	.393	.218	-90384
B1	.307	.079	.395	.220	-90980
C2	.213	.183	.400	.203	-89700
C4	.217	.187	.410	.185	-88560
F_2S	.400	---	.400	.200	-89129
C_2S	----	.422	.321	.260	-90842

The oxygen partial pressures can be calculated from the above free energy values by;

$$G^o = RT \ln P_{O_2} \qquad (6)$$

at 1573 K the values calculated were:

SLAG	P_{O_2} atm($\times 10^{-13}$)
F III	2.89
F IV	2.77
B1	2.29
C2	3.45
C4	4.97
F_2S	4.15
C_2S	2.39

Known values
15.5×10^{-13} (ref.12)
7.58×10^{-36} (ref.12)

Although the calculated value of P_{O_2} for fayalite and the known value show relative agreement, the respective values for dicalcium silicate do not. The results indicate that lime bearing slags, as would be expected are far from ideal. The method described for calculating P_{O_2} (which assumes ideality of mixing) for the slags used in the present work is therefore inconvenient and prone to errors. Consequently the method, and other more sophisticated methods based upon the similar use of thermodynamic data were not pursued further. An alternative approach was explored. Two other methods exist for estimating the oxygen potentials of slags. These are either to measure the Fe^{2+}/Fe^{3+} ratio in the slag or, as in the case of blast furnace slags, to measure the activity of FeO. Using the same slags as for the above calculations the Fe^{2+}/Fe^{3+} ratio and activity of FeO are given below:

SLAG	Fe^{2+}/Fe^{3+}	^{a}FeO		
		Ref(36)	Ref(37)	Ref(162)
F-III	30.75		0.48	
F-IV	34.74		0.5	
B1	16.96	0.5		0.74
C2	17.53	0.4		0.51
C4	20.49	0.4		0.52

Although various methods have been proposed for calculating the activity of FeO it was thought more sound to use actually measured values by Botswoth (36) and Schuhmann and Ensio (37), and additionally to use Scimar's calculation method (166) as comparison. The method proposed By Scimar is briefly as follows:

From the chemical analysis of the slag calculate the mole fraction of Fe^{2+} ($N_{Fe}2+$) and the mole fraction of O^{2-} (N_O2-). From a graph of N_O2- against ($\gamma_{Fe}2-.\gamma_O2-$) read the product of the activity coefficients, and hence calculate the activity of FeO by:

$$a_{FeO} = N_{Fe}2+ \cdot N_O2 \quad \gamma_{Fe}2+ \cdot \gamma_O2$$

The activities given by reference 37 were for the $FeO-Fe_2O_3-SiO_2$ system, those by reference 36 were determined experimentally for the $CaO-FeO-SiO_2$ system. The method of Scimar takes into account other oxides present such as MgO, MnO and P_2O_5. The values calculated show reasonable agreement, but this is not the most important aspect of their inclusion in this appendix. The main point to note is the small change which takes place in FeO activities, the range of compositions of slags is transversed; this small variation is in marked contrast to the extremely wide range of values of oxygen potential. The FeO activities are included mainly as a record.

A final alternative considered for calculating the oxygen potentials of slags used in the present work is as described below. A linear relationship is assumed between the extreme oxygen potentials i.e. P_{O_2} for fayalite and P_{O_2} for dicalcium silicate. The following graph of wt% CaO vs oxygen potential was constructed. The construction assumes that within the dicalcium silicate region (see figure 12), the partial pressure of dicalcium silicate will prevail throughout i.e. 7.58×10^{-37} atm, and therefore above 35% CaO there is no change. The corresponding oxygen potential values for the slags used in the

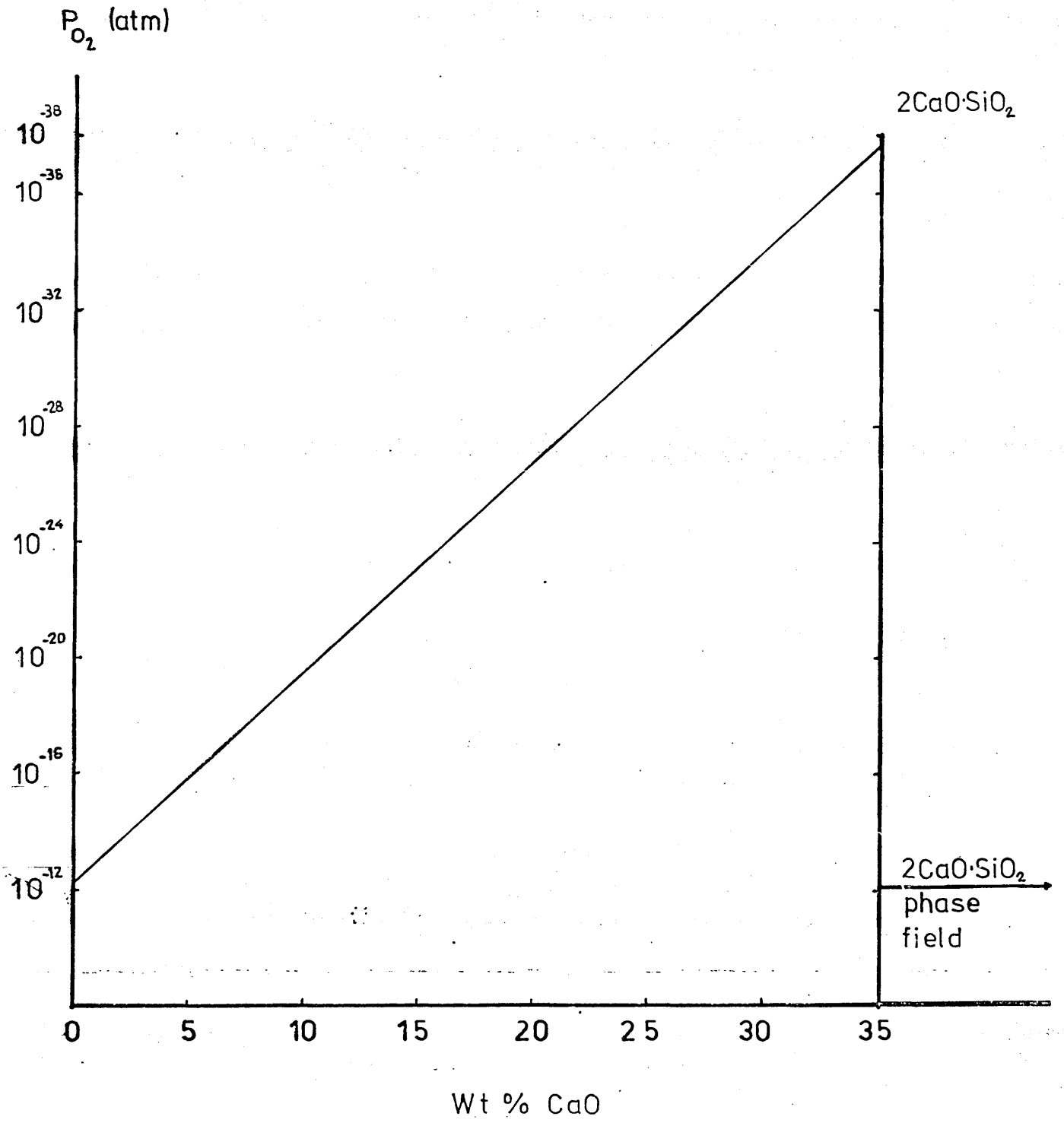
P_{O_2} (atm)
10^{-38}
10^{-36}
10^{-32}
10^{-28}
10^{-24}
10^{-20}
10^{-16}
10^{-12}
$2CaO{\cdot}SiO_2$
$2CaO{\cdot}SiO_2$ phase field
0
5
10
15
20
25
30
35
Wt % CaO

present work are therefore assumed to lie between these two limiting cases, such that, for the slags used in the calculations:

SLAG	P_{O_2}
F-III	10^{-12}
F-IV	10^{-12}
B1	2×10^{-12}
C2	8×10^{-12}
C4	10^{-33}

The present appendix outlines the difficulties in the evaluation of oxygen potentials by a reliable method, and emphasises the absence of measured values in the scientific literature for slags at these conditions. In the final analysis, adoption of a simple approximation of linearity and the lever rule has been made, even though this must introduce error.

APPENDIX II.

The rate of decarburization found from experiments varies from 0.1 to 0.3%C per minute. A mean value of 0.2%C per minute is taken for the following calculations on mass balance. The blowing rate used in lancing was 75 cc/min. For argon-5% CO_2 mixtures, this is equivalent to 3.75 cc/min of CO_2. The number of gram-moles of CO_2 per minute is thus:

$$(3.75 \times 10^{-3})/(22.4) = 1.67 \times 10^{-4}$$

Assuming reaction between the reactive gas and the metal takes place as:

$$CO_2 + \underline{C} = 2CO$$

it is seen that

$$\dot{n}_{CO_2} = \dot{n}_C$$

$1.67 \times 10^{-4} \times 12 = 20.04 \times 10^{-4}$ grams of carbon per minute which in turn corresponds to 0.2% C/min. This figure is similar to the value found from experiments without gas injection.

In a similar manner for the reaction between carbon and oxygen the calculations may be made by considering:

$$2CO + O_2 = 2CO_2$$

$$\underline{2CO_2 + 2\underline{C} = 4CO}$$

$$2\underline{C} + O_2 = 2CO$$

and $$n_C = n_{CO} = \tfrac{1}{2} n_{O_2}$$

For different gas compositions, the following maximum decarburization rates (assuming that all the reactive oxygen is consumed) are obtained:

Gas used	P_{O_2}	%C/min
Argon - 5%CO_2	1.034×10^{-9}	0.20
100% CO_2	2.16×10^{-8}	4.0
Argon - 1% O_2	10^{-2}	0.08
Argon - 10% O_2	10^{-1}	0.80

When gas lancing is carried out, account must be made of gas evolution due to reaction alone. Taking a typical decarburization rate of 0.2% C/min the volume of gas evolved from a one gram sample is calculated, for the $\underline{C} + \underline{O}$ reaction, as 3.73 cc/min. The volume of gas leaving the slag is thus: 75 cc/min (injected) + 3.73 cc/min (from reaction) - reactive gas consumed by the reaction.

APPENDIX III

Chemical composition of slags used for decarburization of iron-carbon alloys. All in wt %.

Slag	FeO	Fe_2O_3	CaO	SiO_2
F III	66.15	2.39		31.46
F IV	65.98	2.11		31.91
F V	63.74	3.40		32.86
F VI	64.31	2.69		33.00
F IX	59.50	3.47		35.02
F X	63.74	2.06		34.20
B-1	52.50	3.44	11.06	33.00
A-2	55.83	2.91	12.66	28.60
A-3	54.20	6.15	14.15	25.50
A-4	53.03	2.97	14.32	29.68
M	45.44	4.29	16.07	34.20
U-1	47.89	1.85	20.68	29.60
C-1	42.17	3.40	25.83	28.60
C-3	39.90	3.33	25.85	30.92
M-2	37.44	5.00	26.56	31.00
C-2	38.34	2.43	27.01	32.22
C-4	40.02	2.17	28.05	29.76
M-1	31.00	4.86	31.94	32.20
U-2	27.30	1.14	38.76	32.80

TABLE I

COMPOSITION RANGES OF COMMON BASIC OPEN HEARTH AND BASIC OXYGEN STEELMAKING SLAGS . (43, 72) .

COMPONENT	AMOUNT (%)
FeO	5 - 4
Fe_2O_3	1 - 10
MnO	4 - 15
MgO	3 - 12
CaO	30 - 55
Al_2O_3	0 - 4
Cr_2O_3	0 - 2
SiO_2	5 - 25
P_2O_5	1 - 4
S	0.05 - 0.30
CaF_2	0 - 2

TABLE II

WEIGHT OF REACTED DROPS BEFORE (W1) AND AFTER (W2) REACTION WITH SLAG..

W1	W2	W %
1.0035	1.1262	+ 12.2
0.9415	0.8104	- 13.9
1.0321	0.8823	- 14
0.923	1.0025	+ 8.54

TABLE III - A

TIME FOR REACTION	SLAG (FIGURE)	ANALYSED			CALCULATED	Fe analysed / Fe calculated
		Δ %FeO	Δ%Fe_2O_3	%Fe	%Fe	
5 min	M2(29)	2.64	2.10	.5	1.315	0.38
	M (31)	1.60	1.59	.5	0.688	0.73
	M1(32)	2.80	2.80	10	1.19	8.40
10 min	M2	4.00	2.70	1.2	2.166	0.55
	M2	2.44	1.80	2.0	1.267	1.58
	M	2.30	1.29	0.6	1.345	0.45
	M1	2.64	2.00	15.6	1.353	11.53
15 min	M2	4.94	2.10	2.4	3.10	0.77
	M1	3.20	2.00	14	1.79	7.82

TABLE III - B

TIME FOR REACTION	Δ % C (FIGURE)	ANALYSED			CALCULATED			Fe analysed / Fe calculated
		Δ%FeO	Δ%Fe_2O_3	%Fe	%Fe_2O_3	%FeO	%Fe	
5 min	0.81(34)	2.64(29)	2.10	.5	.36	.16	.13	3.8
	0.46(33)	2.80(32)	2.80	10	.20	.09	.07	143
10 min	1.85(34)	4.00(29)	2.70	1.2	.81	.37	.29	4.18
	1.38(33)	2.64(32)	2.00	15.6	.61	.28	.22	71
15 min	2,38(34)	4.94(29)	2.10	2.4	1.04	.48	.37	6.5
	2.00(33)	3.20(32)	2.00	14	.88	.40	.31	45

TABLE IV

CALCULATED VALUES FROM MASS TRANSPORT MODEL GIVEN BY EQUATION 5.5.3.5. THE DATA USED IN THE CALCULATIONS WERE: $D_{FeO} = 5.7 \times 10^{-6} cm^2/sec$; VISCOSITY = 0.7 poise, DENSITY = 3.2 g/cm^3, DROP DIAMETER = 0.8 cm.

TEMPERATURE ^oC	Sh number	MASS TRANSFER COEFFICIENT $\times 10^5$ cm/sec	RELATIVE VELOCITY cm/sec
1240	2.5 - 3	1.78 - 2.14	0.03 max
1300	9 - 12	6.4 - 8.5	0.18 - 0.3
1400	17 - 20	12.2 - 14.25	0.6 - 0.8
1500	14 - 25	9.97 - 17.8	0.42 - 1.2
1600	20 - 50	14.25 - 35.6	0.8 - 3.96
1300 gas lancing	11 - 13	8 - 9.5	0.26 - 0.36

SPECIAL CASES CONSIDERED:

CASE 1 AT 1240°C, $D_{FeO} = 2.2 \times 10^{-6} cm^2/sec$; CALCULATED: Sh = 10, RELATIVE VELOCITY < 0.03 cm/sec and MASS TRANSFER COEFFICIENT = 0.55×10^{-5} cm/sec.

CASE 2 At 1500°C, $D_{FeO} = 9.9 \times 10^{-6} cm^2/sec$, VISCOSITIES FROM 0.25 to 0.7 poise. CALCULATED:

Sh = 8 to 14

FOR VISCOSITY = 0.25 poise v = 0.08 to 0.25 cm/sec

FOR VISCOSITY = 0.7 pose v = 0.14 to 0.42 cm/sec

CASE 3 AT 1600°C, $D_{FeO} = 5.7 \times 10^{-6} cm^2/sec$. CALCULATED:

Sh = 20 to 50

FOR VISCOSITY = 0.25 poise, v = 0.48 to 2.35 cm/sec

TABLE V

Mean Mass Transfer coefficients, $k \times 10^{-4}$ cm·sec for the various decarburization experiments.

+ Full details of slag chemical compositions are given in Appendix III

TEMPERATURE °C					GAS INJECTION (75cc/min)			
SLAG+	1240	1300	1400	1500	ARGON	ARGON 5%CO_2	CO_2	ARGON 1% O_2
F	3.28	4.44	11.40	5.00	5.43			
F	3.58							
F	3.31							
F	3.20							
B1		5.05						
A2		6.36						
A		6.16	12.10					
C1		10.64						
C3		12.75	19.95		17.20			
M2		11.64						
C2		9.64						
C4				30.52		17.20	11.08	14.77
M1		9.46	15.62					
U1				18.45				

TABLE VI

TEMPERATURE °C	k(FROM 5.5.35) x 10^5 cm/sec	k(FROM 5.7.8) x 10^5 cm/sec	$\frac{k(5.7.8)}{k(5.5.3.5)}$
1240	2.14	52	24.3
1300	6.24 - 8.15	127 - 165	19.84 - 19.41
1400	12.20 - 14.25	234 - 269	19.18 - 18.87
1500	9.97 - 17.70	195 - 332	19.55 - 18.65
1600	14.25 - 35.60	269 - 598	18.87 - 16.78

COMPARISON OF MASS TRANSFER COEFFICIENT VALUES CALCULATED FROM THE FILM THEORY (i.e. EQUATION 5.5.3.5) AND FROM THE PENETRATION THEORY (i.e. EQUATION 5.7.8).

PLATE I. FURNACE USED FOR DECARBURIZATION EXPERIMENTS.

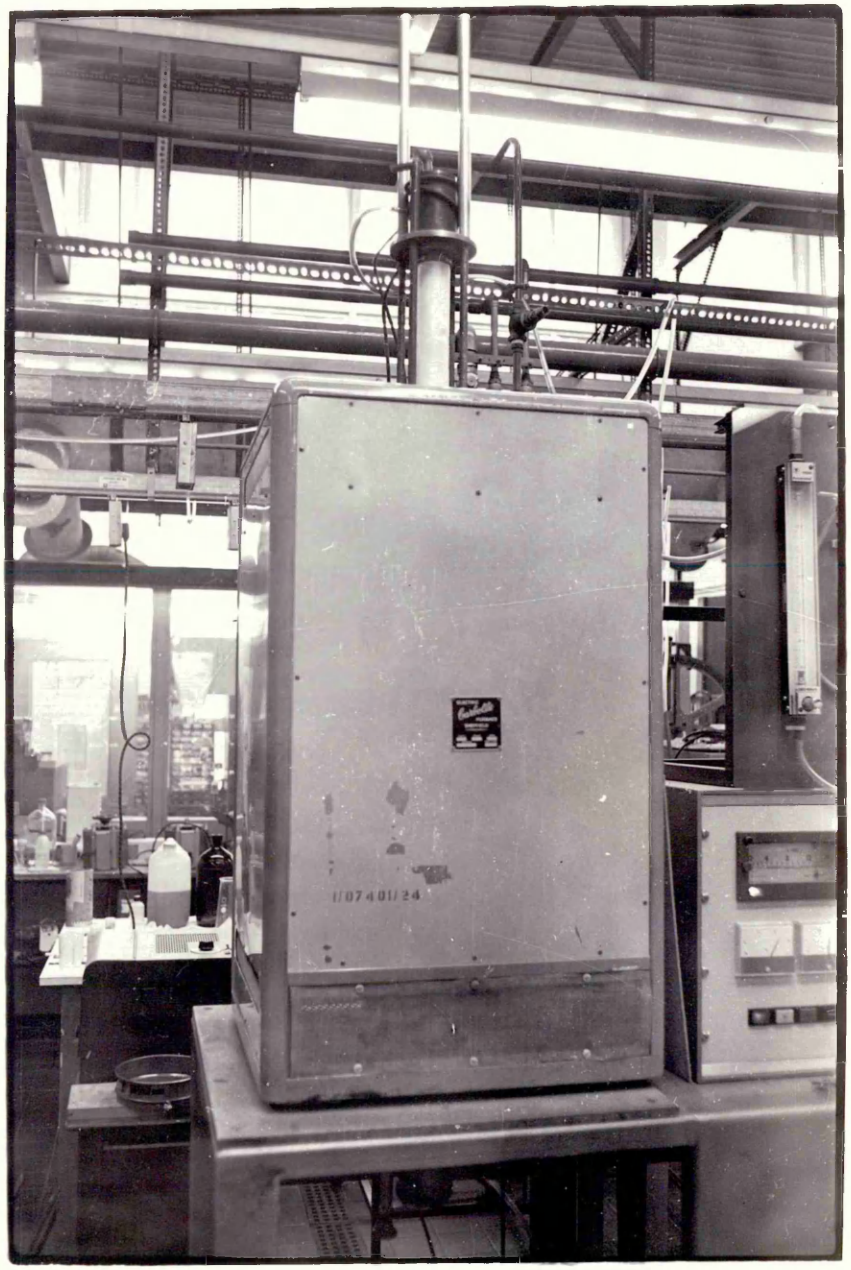
1/07401/24

PLATE II. TOP ARRANGEMENT OF FURNACE. THE PHOTOGRAPH SHOWS THE TWO PLATFORMS FOR LOWERING OF CRUCIBLES AND LANCE INTO THE HOT ZONE.

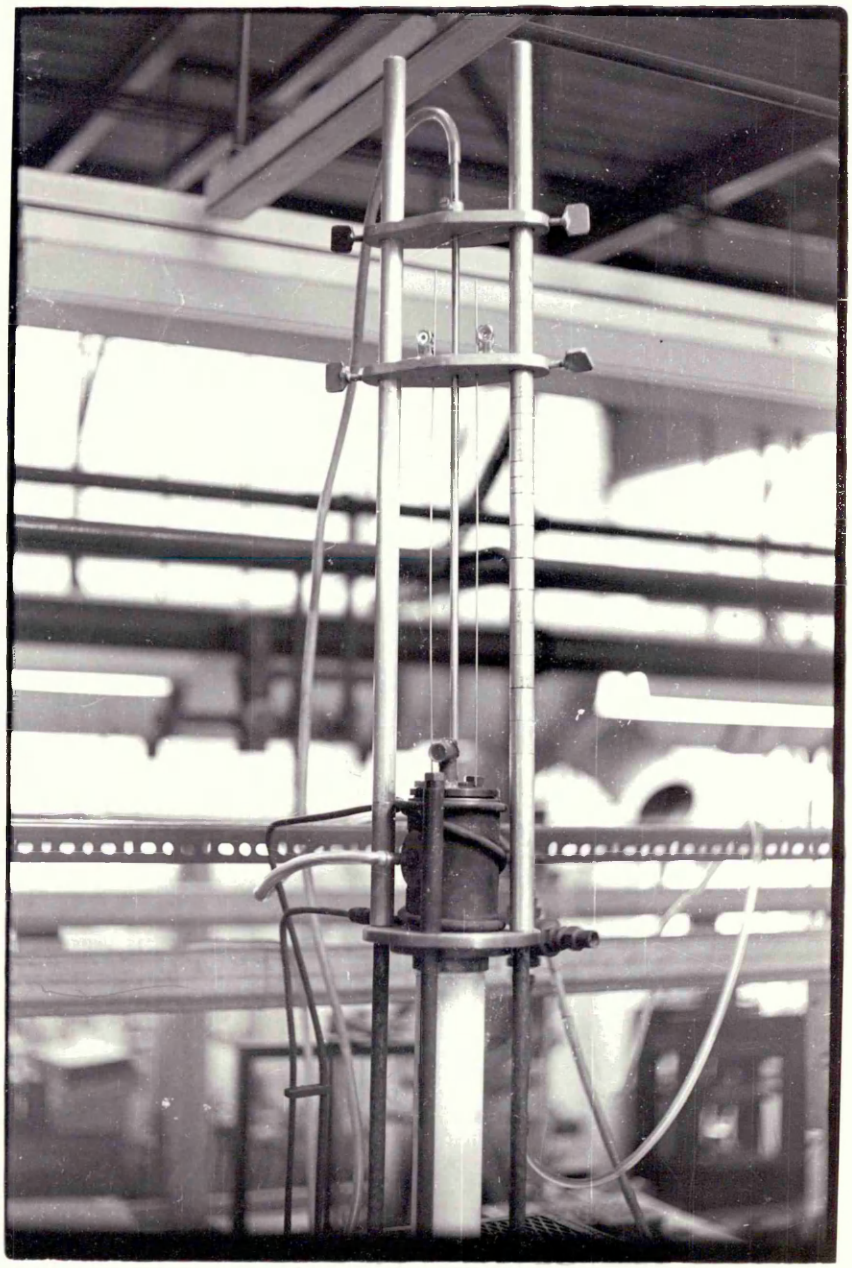

PLATE III. LOWER END OF FURNACE SHOWING QUENCHING MECHANISM.

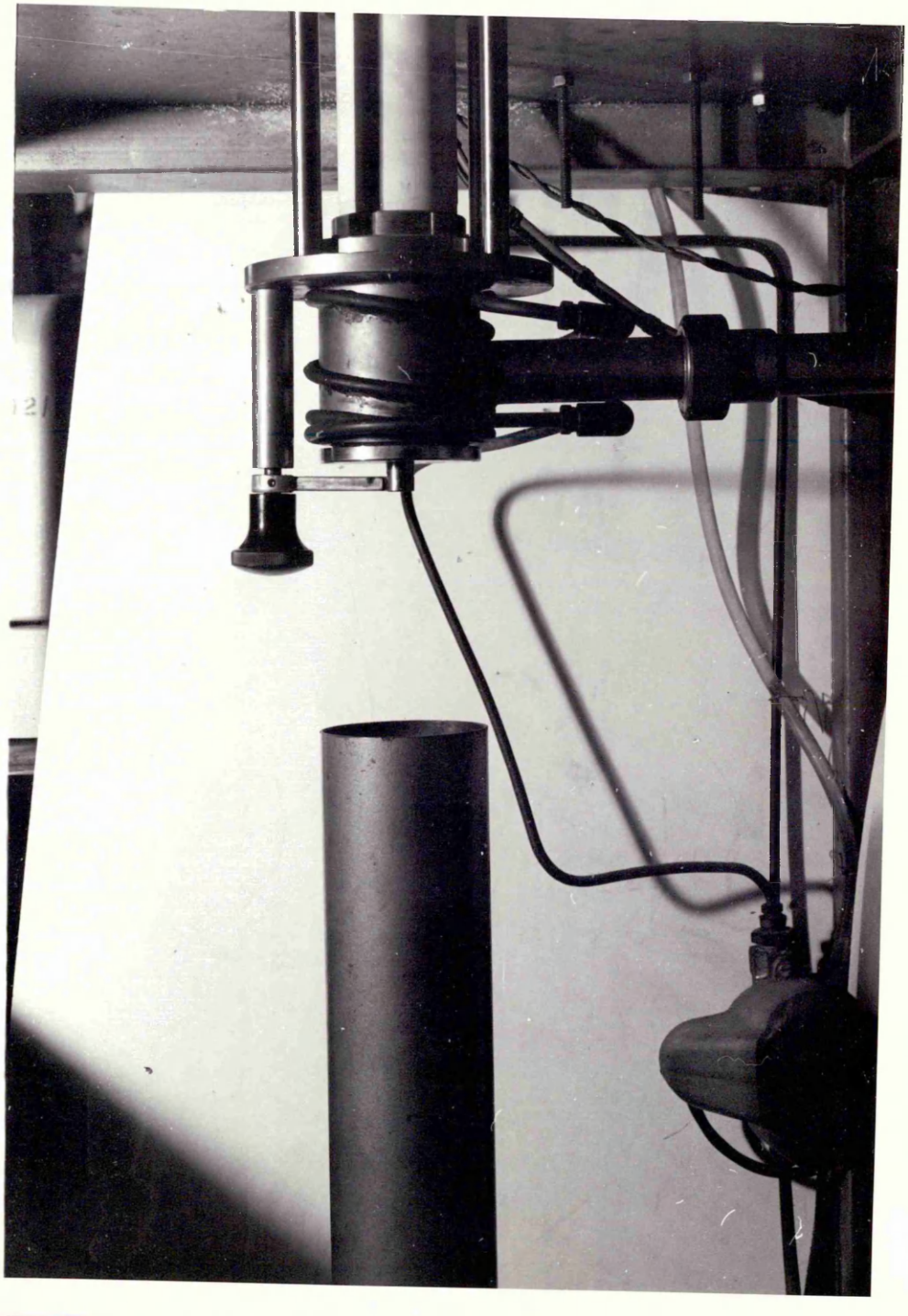

PLATE IV. ARRANGEMENT USED FOR MEASURING GAS FLOW RATES.

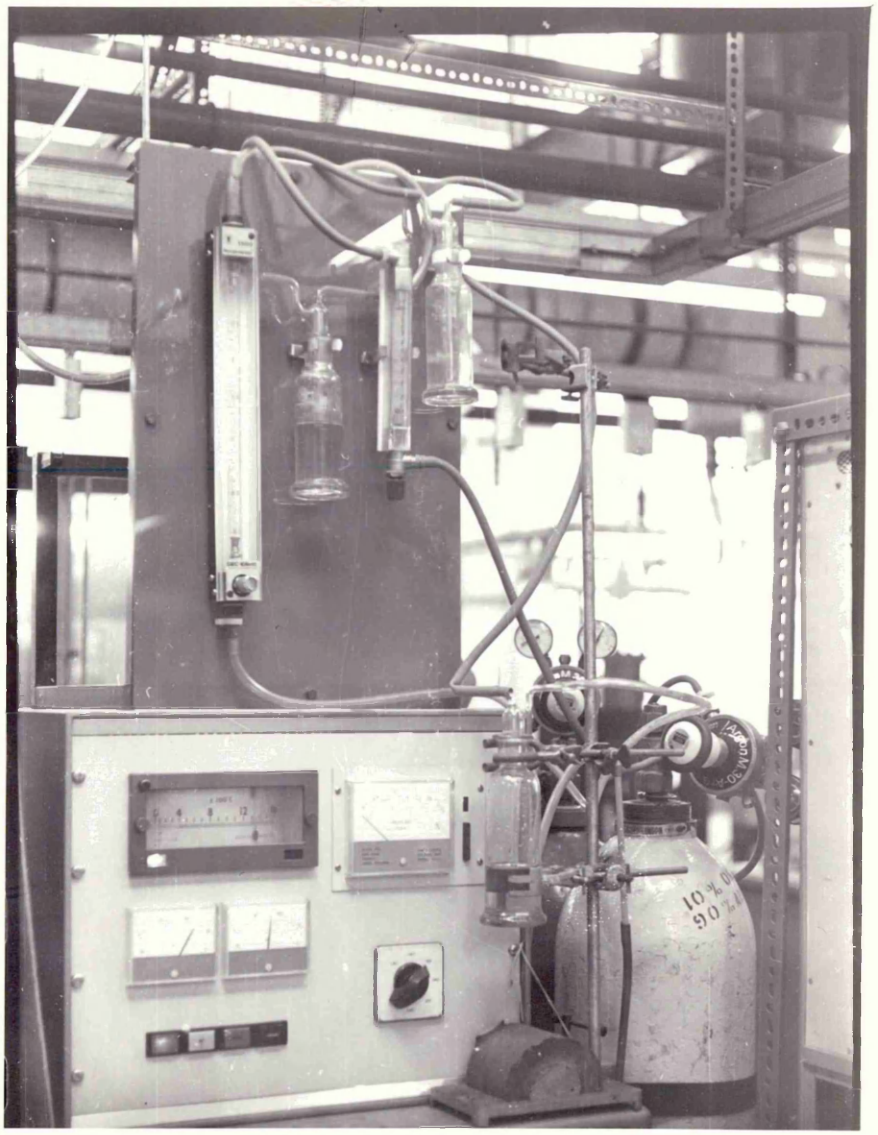

PLATE V. UHF INDUCTION FURNACE USED FOR MELTING OF IRON - CARBON ALLOYS AND SLAGS. PHOTOGRAPH SHOWS FIVE VACUUM SEALED SILICA-GLASS TUBES USED FOR OBTAINING PIN SAMPLES.

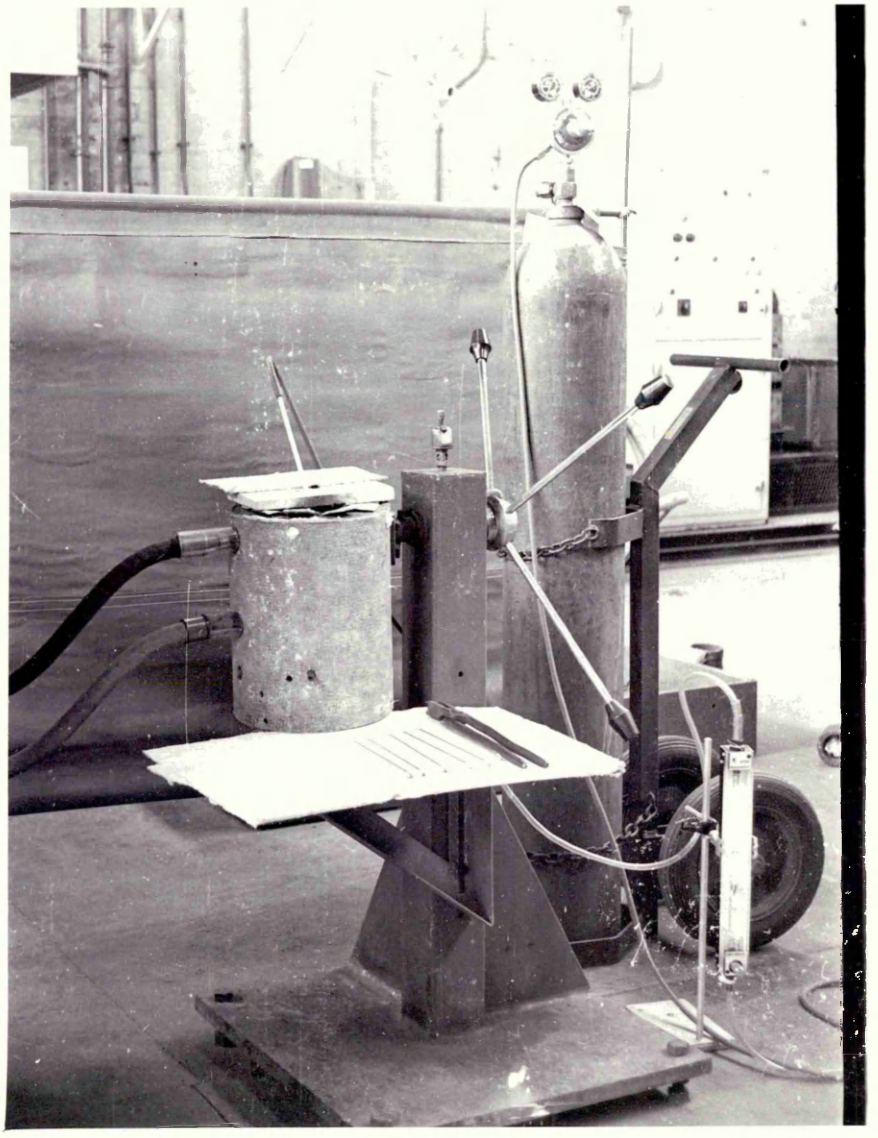

PLATE VIa. SURFACE OF SLAG AS SEEN THROUGH THE PRISM FROM THE FURNACE LID. SLAG COMMENCE TO MELT.

PLATE VIb. PHOTOGRAPH SHOWING SAMPLE FLOATING ON THE SURFACE OF THE SLAG.

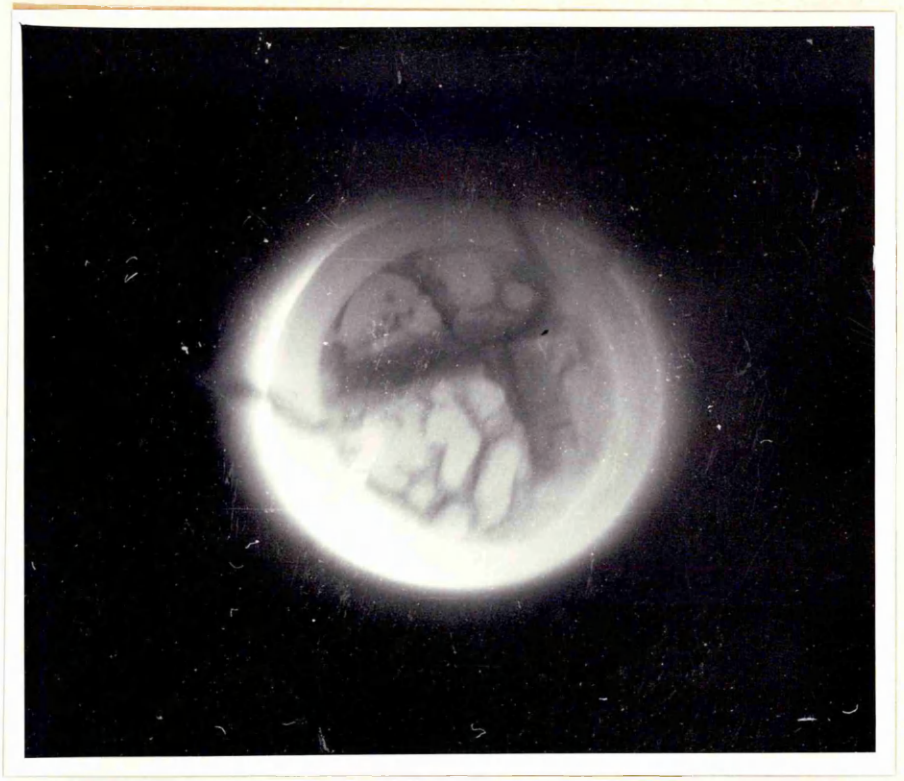

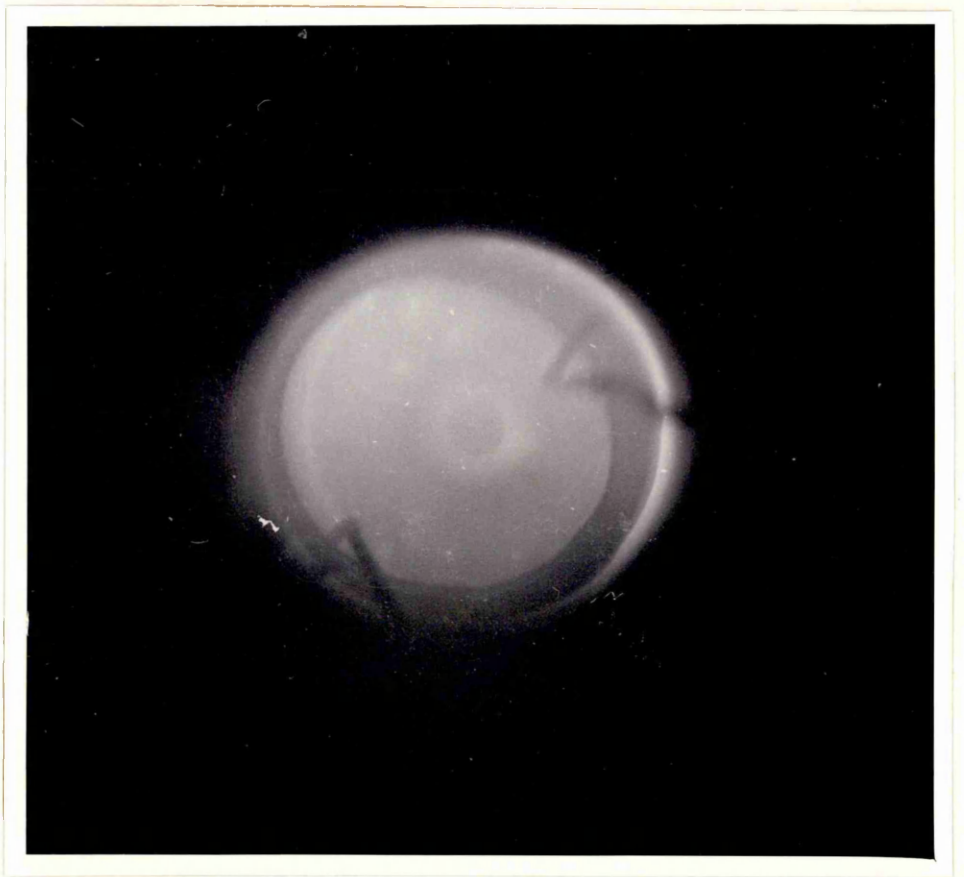

PLATE VIc. SURFACE OF SLAG WHEN TURBULENCE COMMENCES TO SUBSIDE.

PLATE VId. PHOTOGRAPH SHOWING MINUTE BUBBLES ENTRAPPED OR BURSTING THROUGH THE SLAG SURFACE.

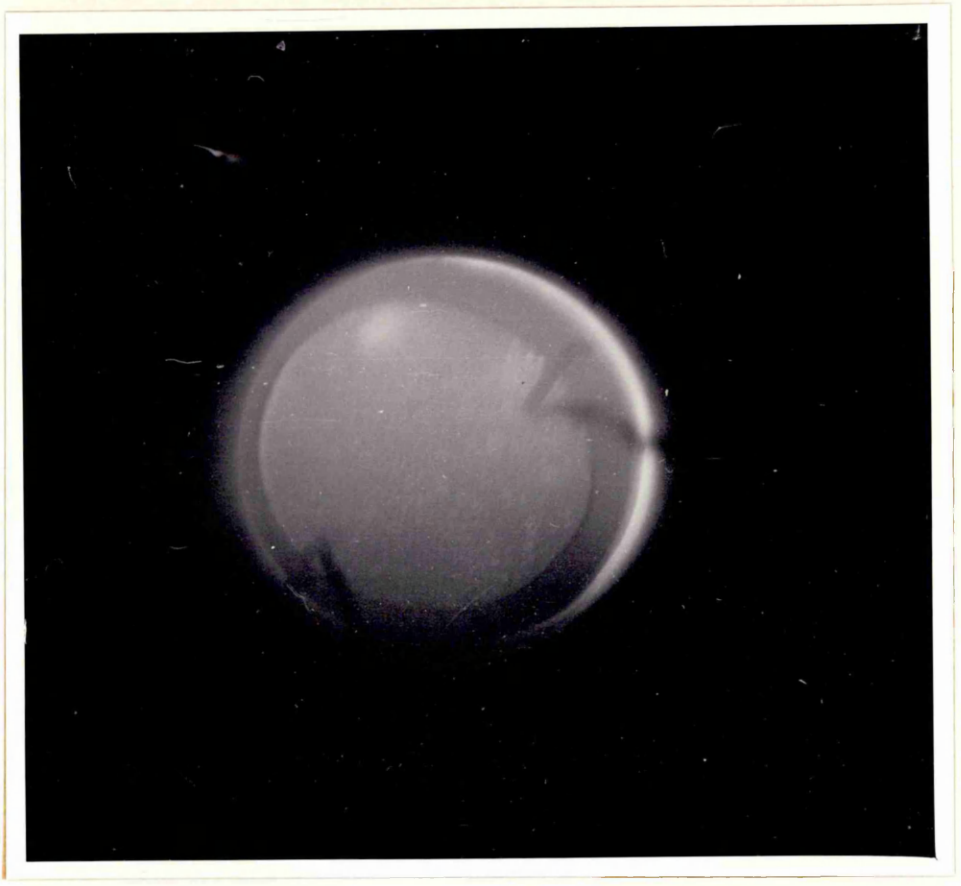

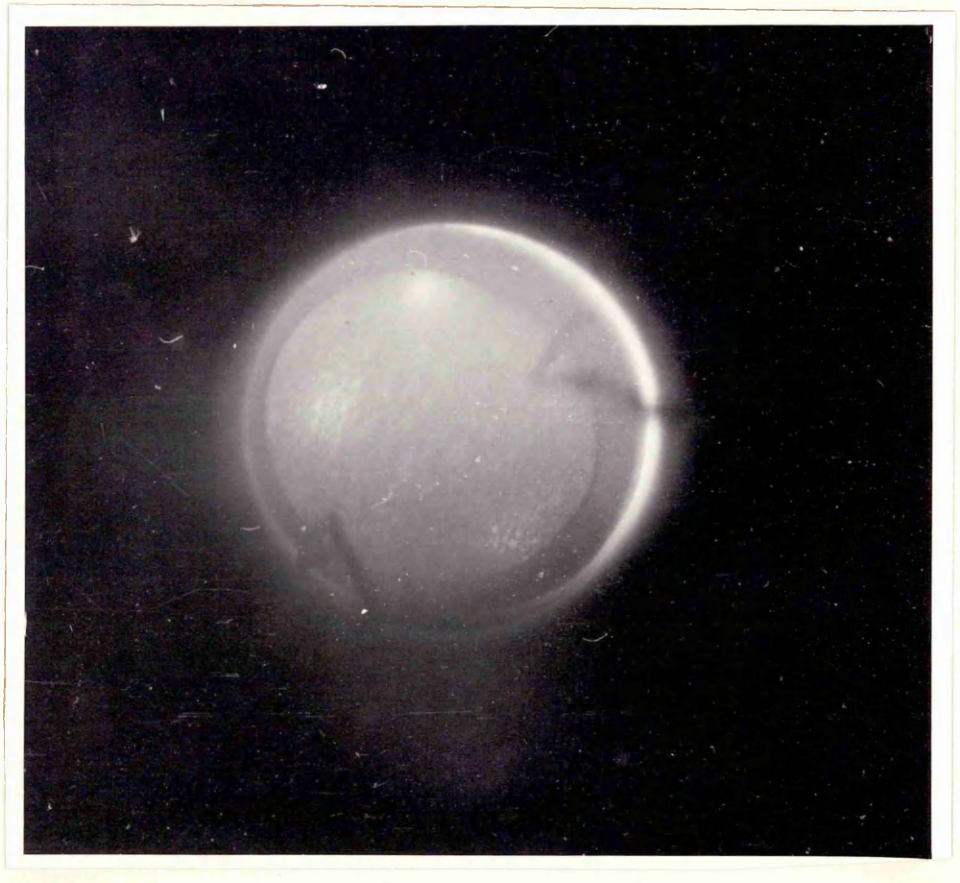

PLATE VII. LANCE AND CRUCIBLE AS ASSEMBLED PRIOR TO INTRODUCTION INTO THE FURNACE.

PLATE VIII

SURFACE APPEARANCE FROM TWO DROPLETS AFTER REACTION WITH 45.57 %FeO. 25.83 %CaO AND 28.60 %SiO_2 (WT%) AT 1300°C.

a. REACTION TIME OF 5 MIN WITH FINAL CARBON CONTENT OF 3.07 % .

b. REACTION TIME OF 10 MIN WITH FINAL CARBON CONTENT OF 2.22 % .

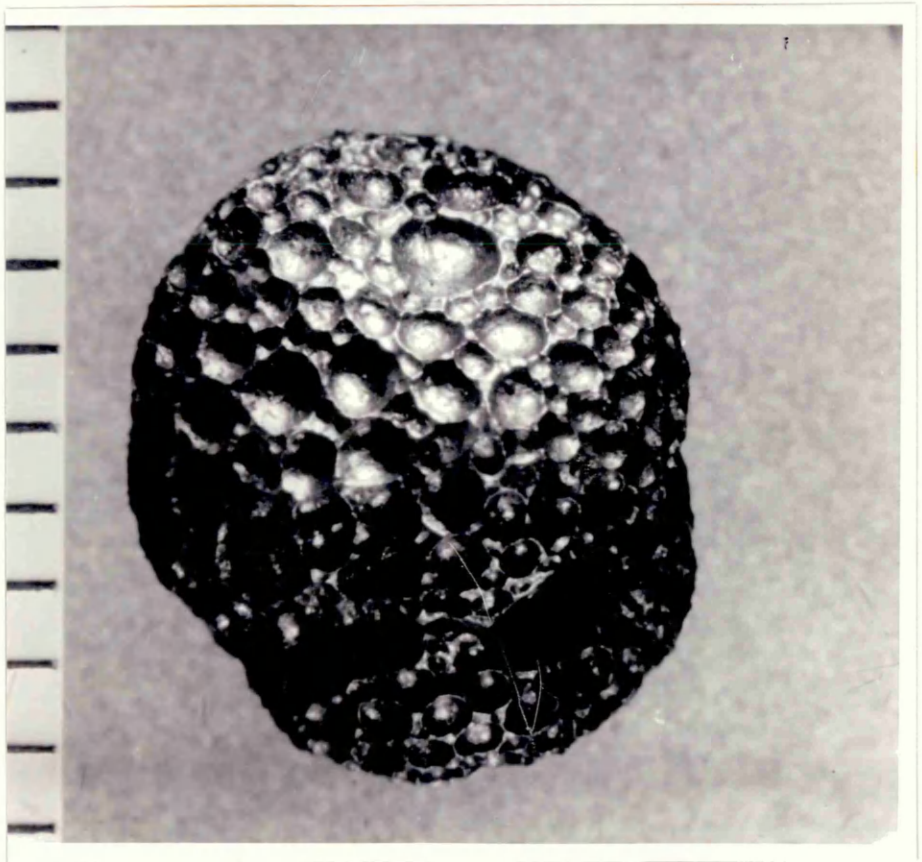

PLATE IX.

a. DROPLET REACTED FOR 15 MIN WITH 45.57 %FeO, 25.83 %CaO AND 28.60 %SiO_2. REACTION TEMPERATURE 1300°C AND FINAL CARBON CONTENT OF 1.55 %C. THE DROPLET CLEARLY SHOWS EVIDENCE OF INTERNAL AS WELL AS SURFACE NUCLEATION.

b. CONTACT PRINT FROM X-RAY NEGATIVE TAKEN FROM DROPS SHOWN IN PLATE VIII AND ABOVE.

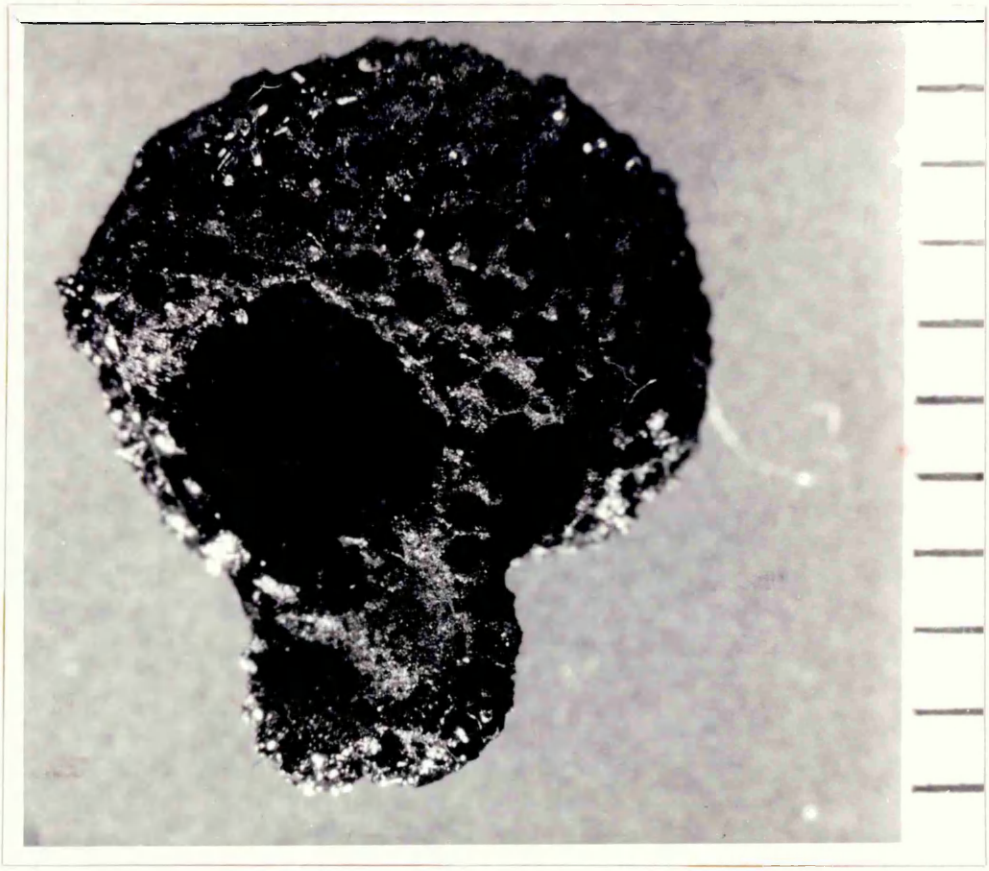

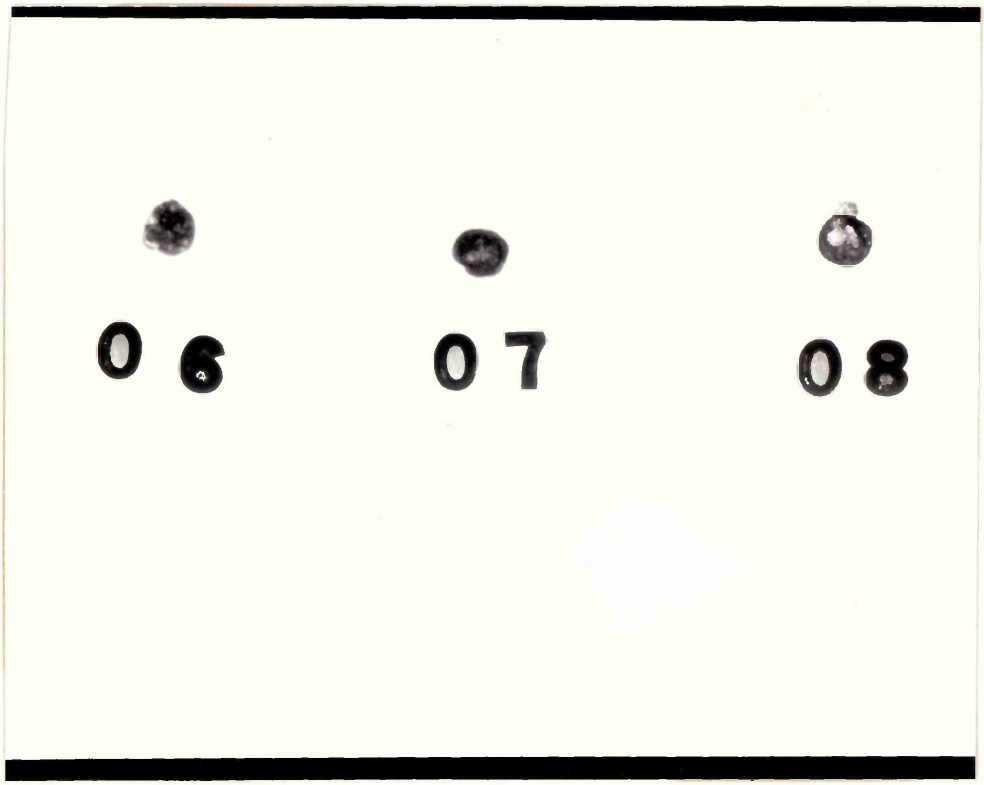
06
07
08

PLATE X.

IRON-CARBON DROPS AFTER REACTION AT 1300°C WITH 38.34 %FeO, 2.43 %Fe_2O_3, 27.01 %CaO AND 32.22 %SiO_2. INITIAL CARBON CONTENT OF 4.25 %C. OBLATE SHAPE IS CLEARLY SHOWN FOR DROPS 0 AND 1.

9. REACTION TIME OF 4 MIN WITH FINAL CARBON CONTENT OF 4.09 %C. THE SAMPLE CORRESPONDS TO NUMBER 9 OF PLATE XIII.

0. REACTION TIME OF 6 MIN WITH FINAL CARBON CONTENT OF 3.64 %C. THE SAMPIE CORRESPONDS TO NUMBER 0 OF PLATE XIII.

1. REACTION TIME OF 8 MIN WITH FINAL CARBON CONTENT OF 3.20 %C. THE SAMPIE CORRESPONDS TO NUMBER 1 OF PLATE XIII.

9

0

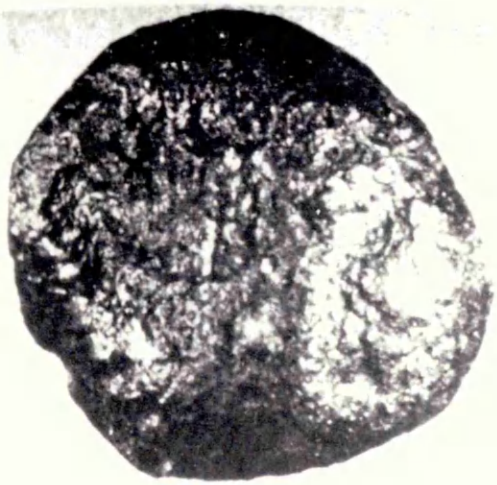

1

PLATE XI.

IRON-CARBON DROPS AFTER REACTION AT 1300°C WITH 38.34 %FeO, 2.43 %Fe_2O_3, 27.01 %CaO AND 32.22 %SiO_2. INITIAL CARBON CONTENT OF 4.25 %C. THE SURFACE CLEARLY SHOWS CHANGE FROM A KNEADING-LIKE EFFECT TO CRATER FORMATION.

2. REACTION TIME OF 10 MIN WITH FINAL CARBON CONTENT OF 2.77 %C. THE SAMPLE CORRESPONDS TO NUMBER 2 OF PLATE XIII.

3. REACTION TIME OF 12 MIN WITH FINAL CARBON CONTENT OF 2.64 %C. THE SAMPLE CORRESPONDS TO NUMBER 3 OF PLATE XIII.

4. REACTION TIME OF 14 MIN WITH FINAL CARBON CONTENT OF 2.24 %C. THE SAMPLE CORRESPONDS TO NUMBER 4 OF PLATE XIII.

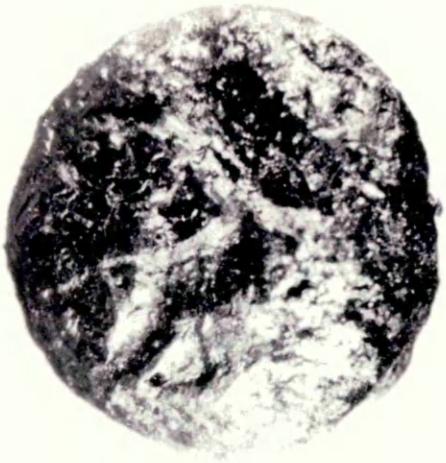

2

3

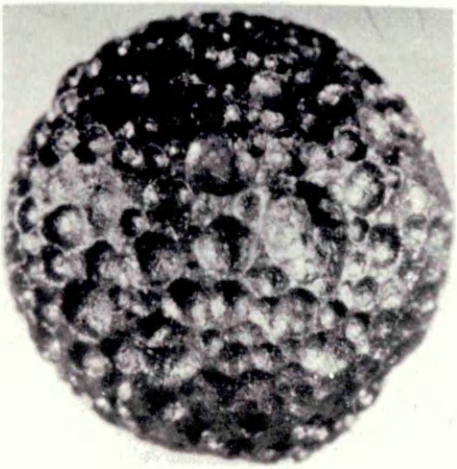

4

PLATE XII.

IRON-CARBON DROPS AFTER REACTION AT 1300°C WITH 38.34 %FeO, 2.43 %Fe_2O_3, 27.01 %CaO AND 32.22 %SiO_2. INITIAL CARBON CONTENT OF 4.25 %C. SURFACE CRATERS ARE SEEN TO DECREASE IN DIAMETER BUT INCREASE IN DEPTH.

5. REACTION TIME OF 15 MIN WITH FINAL CARBON CONTENT OF 1.96 %C. THE SAMPLE CORRESPONDS TO NUMBER 5 OF PLATE XIII.

6. REACTION TIME OF 18 MIN WITH FINAL CARBON CONTENT OF 1.93 %C. THE SAMPLE CORRESPONDS TO NUMBER 6 OF PLATE XIII.

7. REACTION TIME OF 20 MIN WITH FINAL CARBON CONTENT OF 1.66 %C. THE SAMPLE CORRESPONDS TO NUMBER 7 OF PLATE XIII.

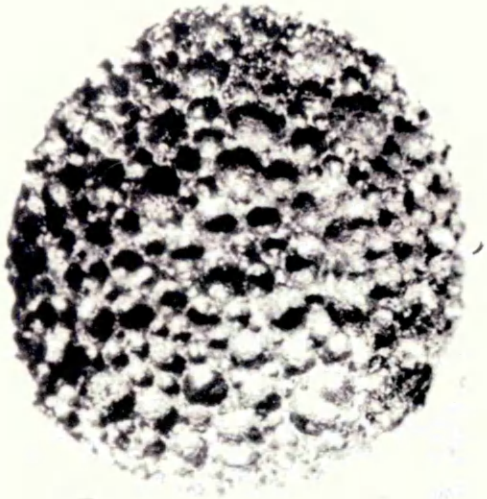

5

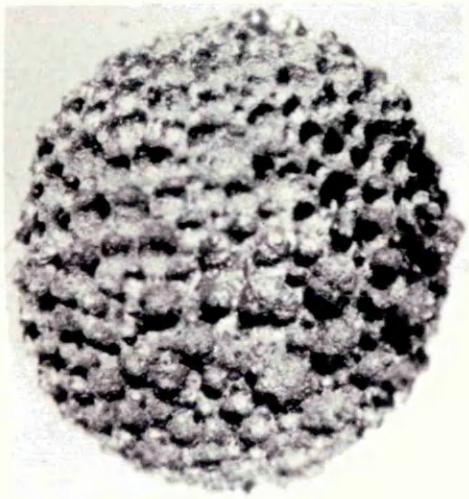

6

7

PLATE XIII.

CONTACT-PRINT OF X-RAY NEGATIVES OF 9 DIFFERENT SAMPLES. TWO DIFFERENT PROJECTIONS OF VIEW ARE SHOWN FOR EACH SAMPLE. PHOTOGRAPHS OF SAMPLES 9, 0 AND 1 ARE GIVEN IN PLATE X. PHOTOGRAPHS OF SAMPLES 2, 3 AND 4 ARE GIVEN IN PLATE XI. PHOTOGRAPHS OF SAMPLES 5, 6 AND 7 ARE GIVEN IN PLATE XII.

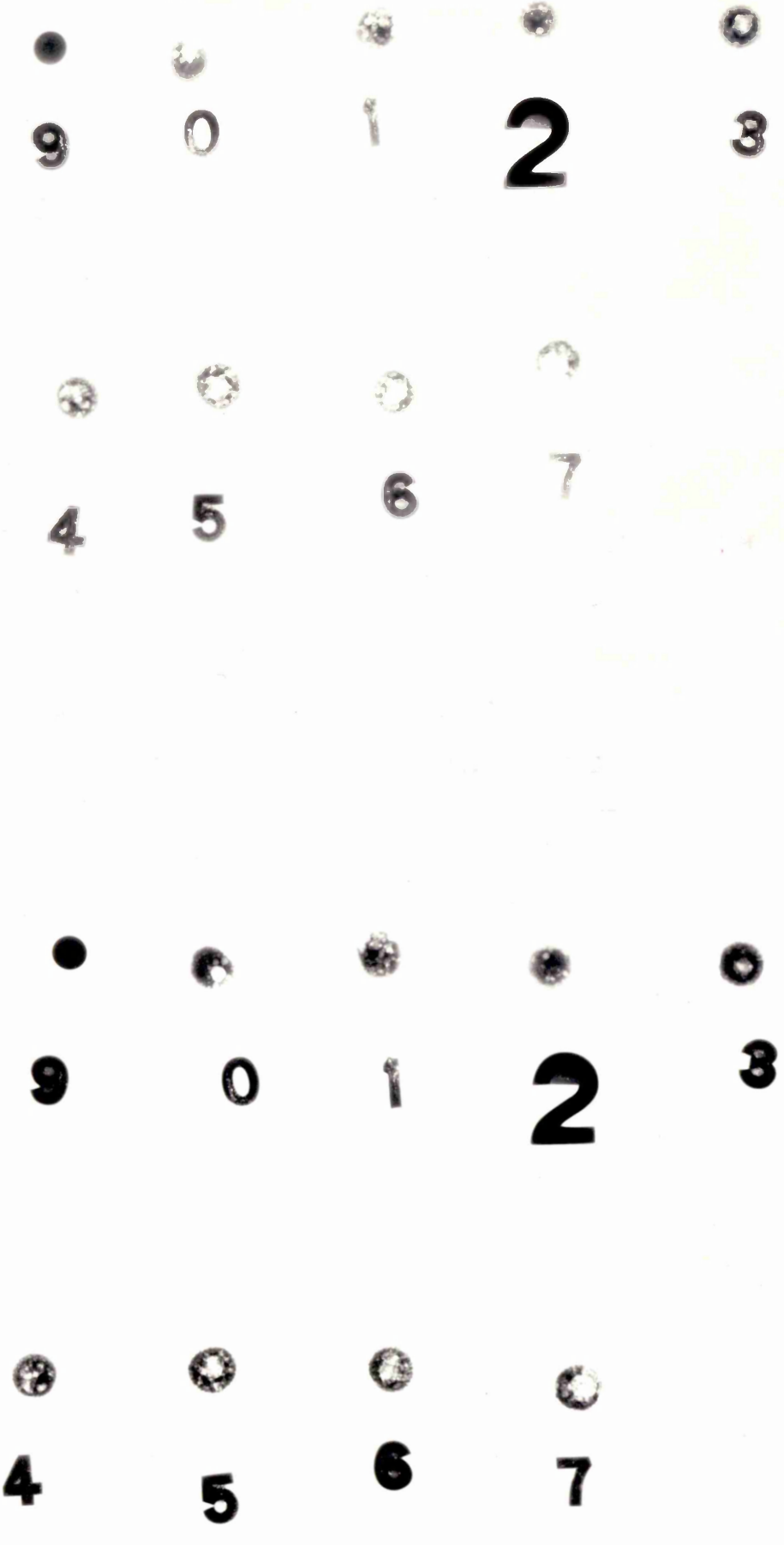
9
0
1
2
3
4
5
6
7
9
0
1
2
3
4
5
6
7

PLATE XIV. TWO VIEWS OF DROPLET REACTED IN 20.68 % CaO SLAG FOR 7 MINUTES AT 1500°C.

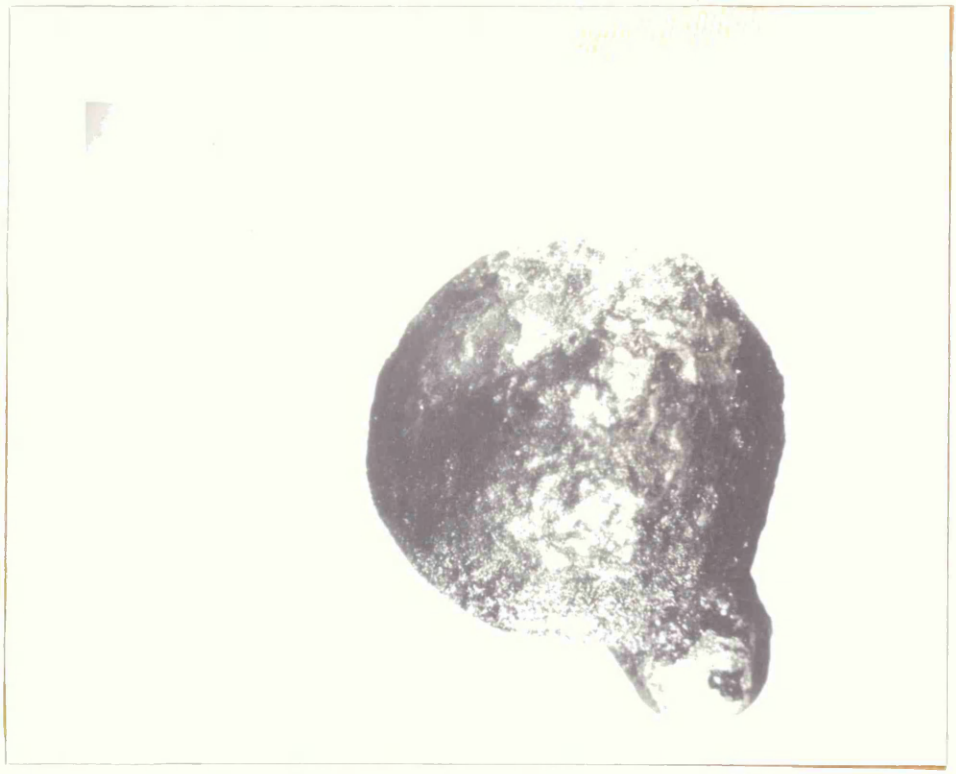

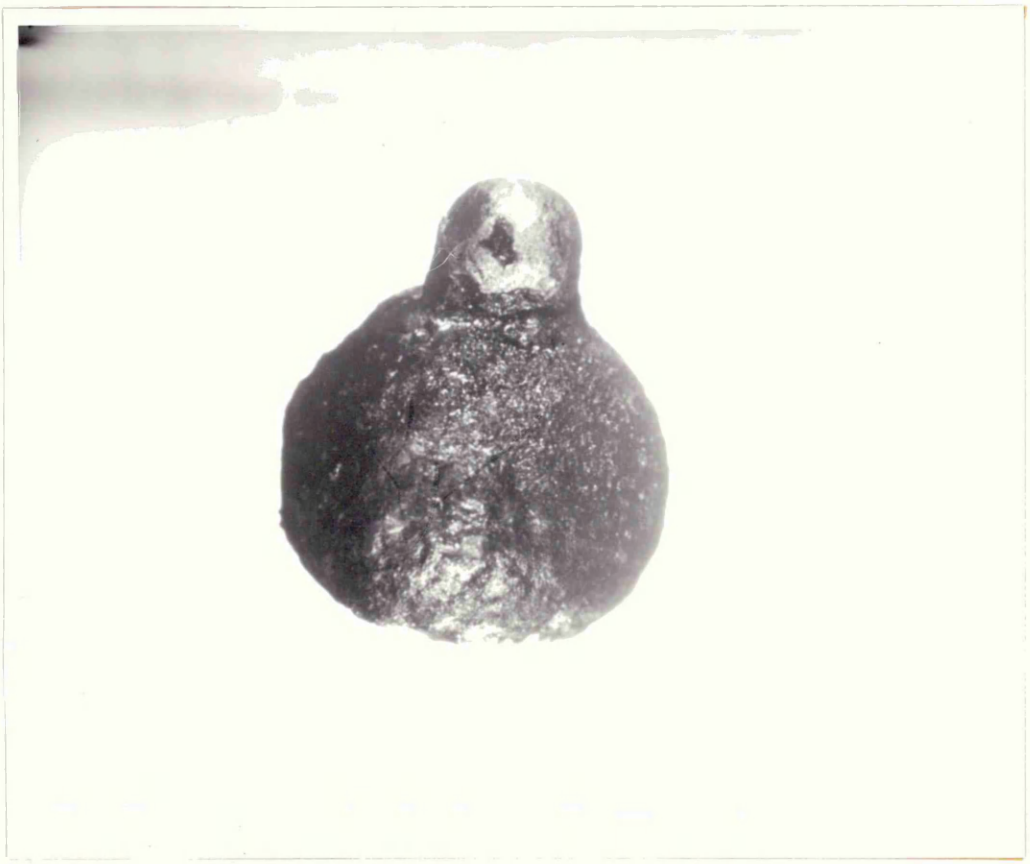

PLATE XV. DROPLETS REACTED IN 20.68 % CaO SLAG FOR 10 MINUTES (TOP) AND 15 MINUTES (BOTTOM) AT 1500°C.

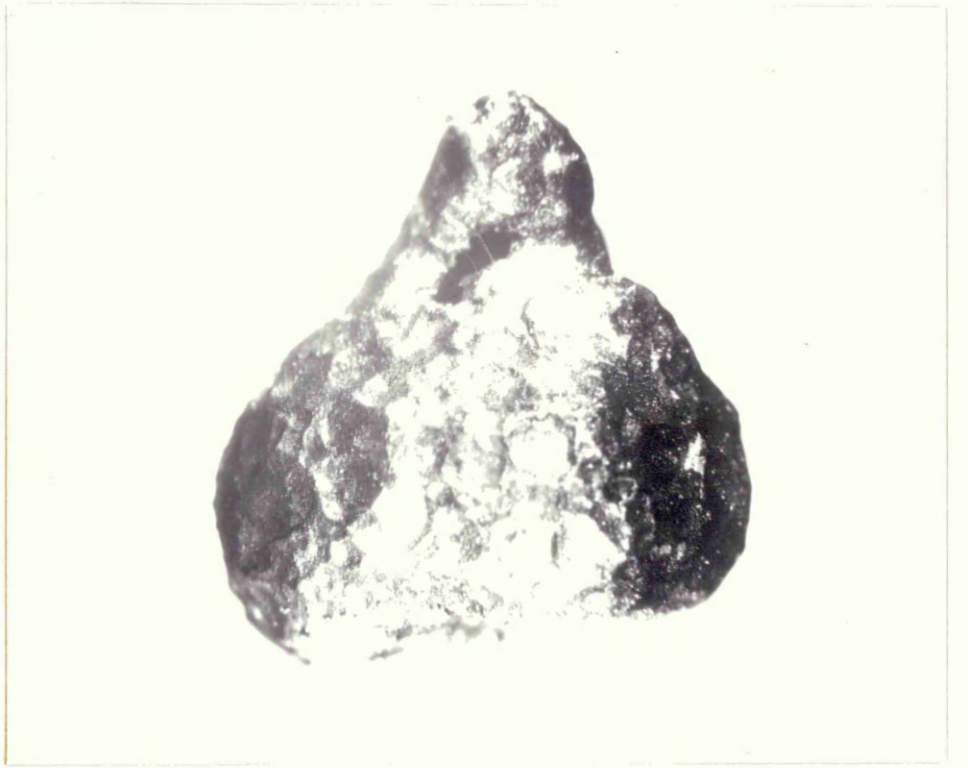

PLATE XVI. DROPLETS REACTED IN 20.68 % CaO SLAG FOR 15 MINUTE (TOP) AND 12 MINUTES (BOTTOM) AT 1500°C.

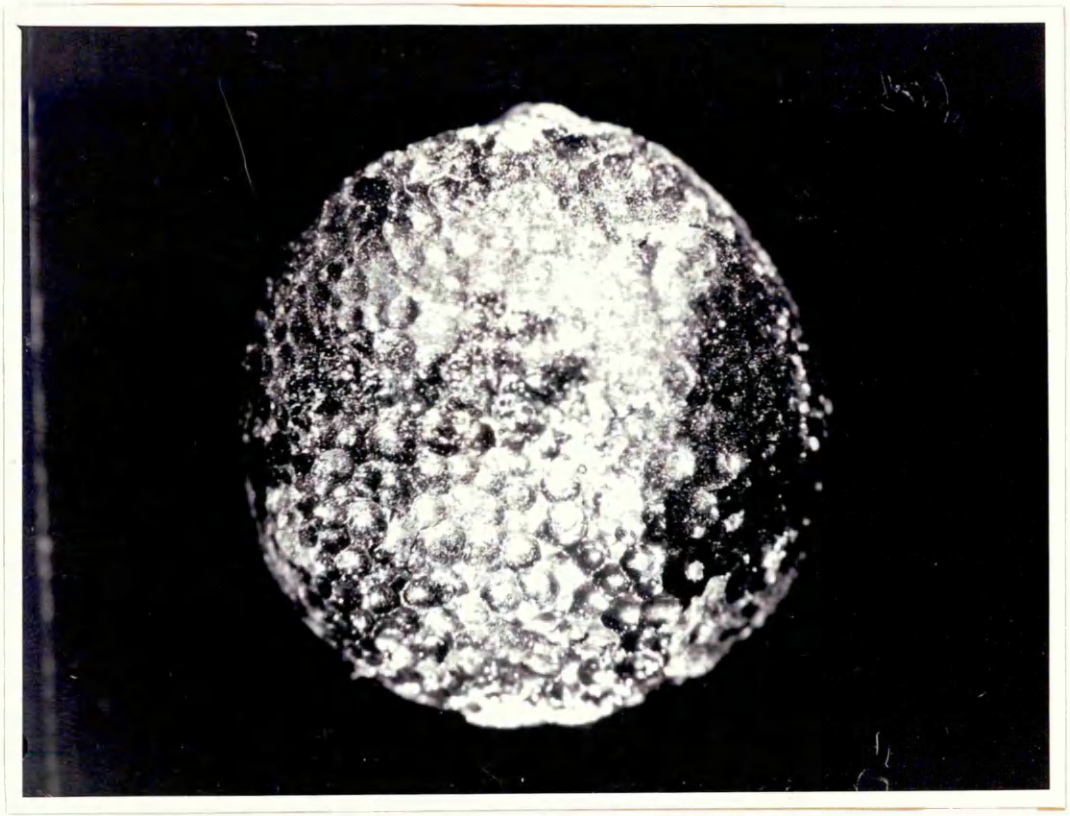

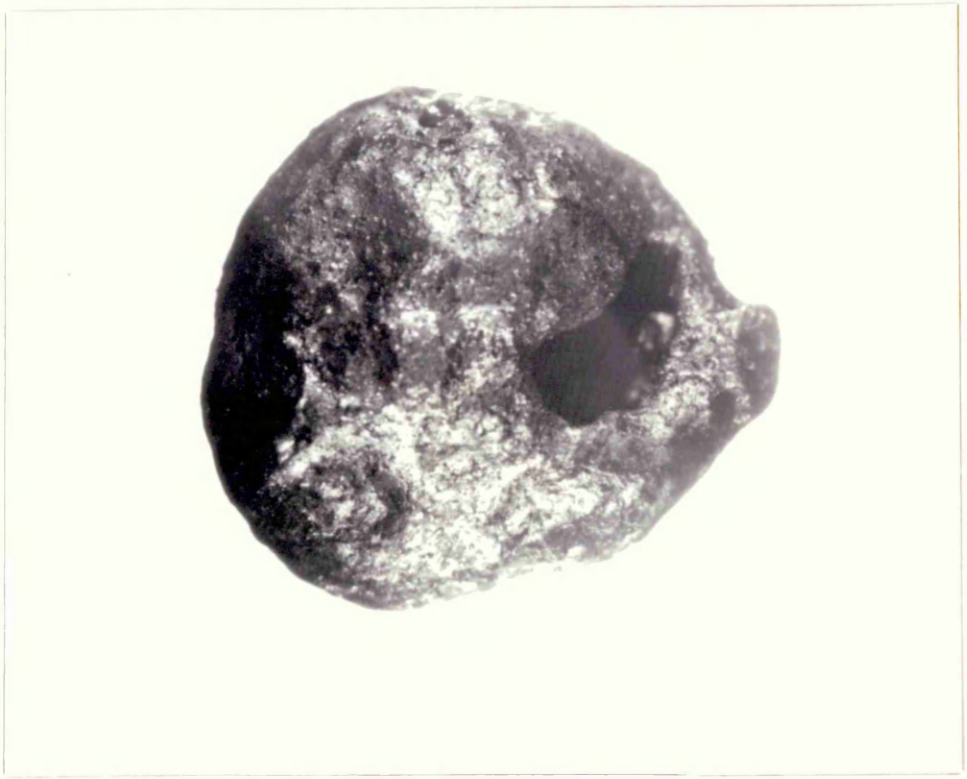

PLATE XVII. DROPLET REACTED IN 20.68 % CaO SLAG FOR 1 MINUTE 24 SECONDS AT 1600°C.

FIGURE 1. TYPICAL REFINING RATES FOR LD STEELMAKING (20,85).

FIGURE 2. RELATION BETWEEN CARBON AND OXYGEN CONTENTS OF MOLTEN IRON IN EQUILIBRIUM WITH CARBON MONOXIDE AT 1 AND 10 ATM. (14).

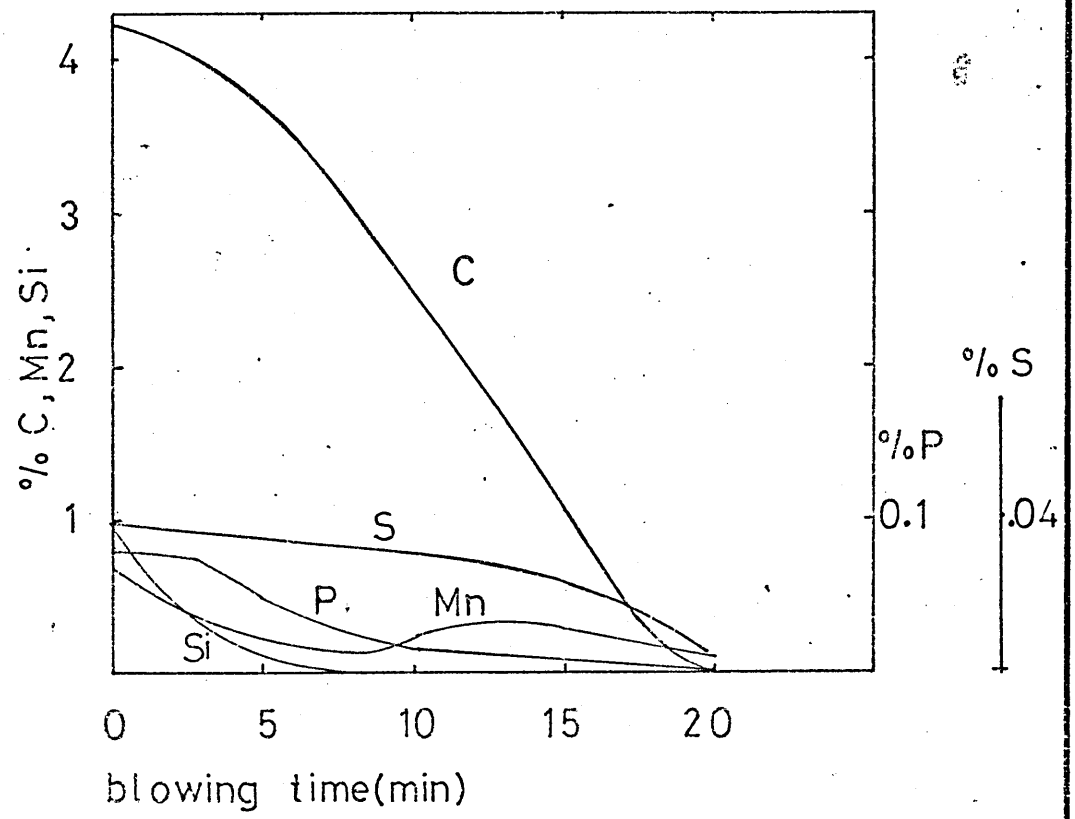
4
3
2
1
% C, Mn, Si
C
S
P
Mn
Si
%P
0.1
% S
.04
0
5
10
15
20
blowing time(min)

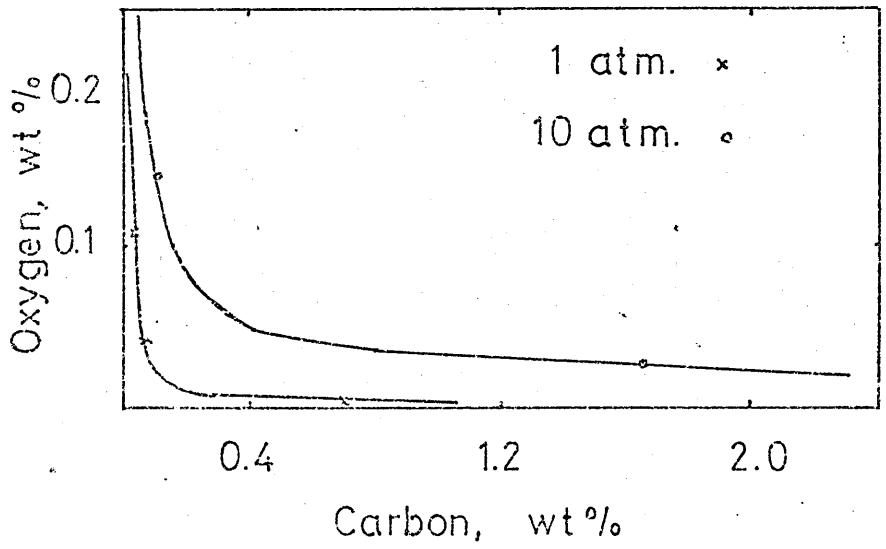
1 atm. ×
10 atm. ○
0.2
0.1
Oxygen, wt %
0.4
1.2
2.0
Carbon, wt %

FIGURE 3a. DIAGRAMMATIC REPRESENTATION OF IDEAL DECARBURIZATION PATTERN IN THE LD PROCESS.

FIGURE 3b. RATE OF DECARBURIZATION VS CARBON CONTENT FOR TWO HEATS UNDER IDENTICAL BLOWING CONDITIONS(80).

FIGURE 3c. REFINING PATHS OBTAINED FROM PLANT PRACTICE OPERATION (87).

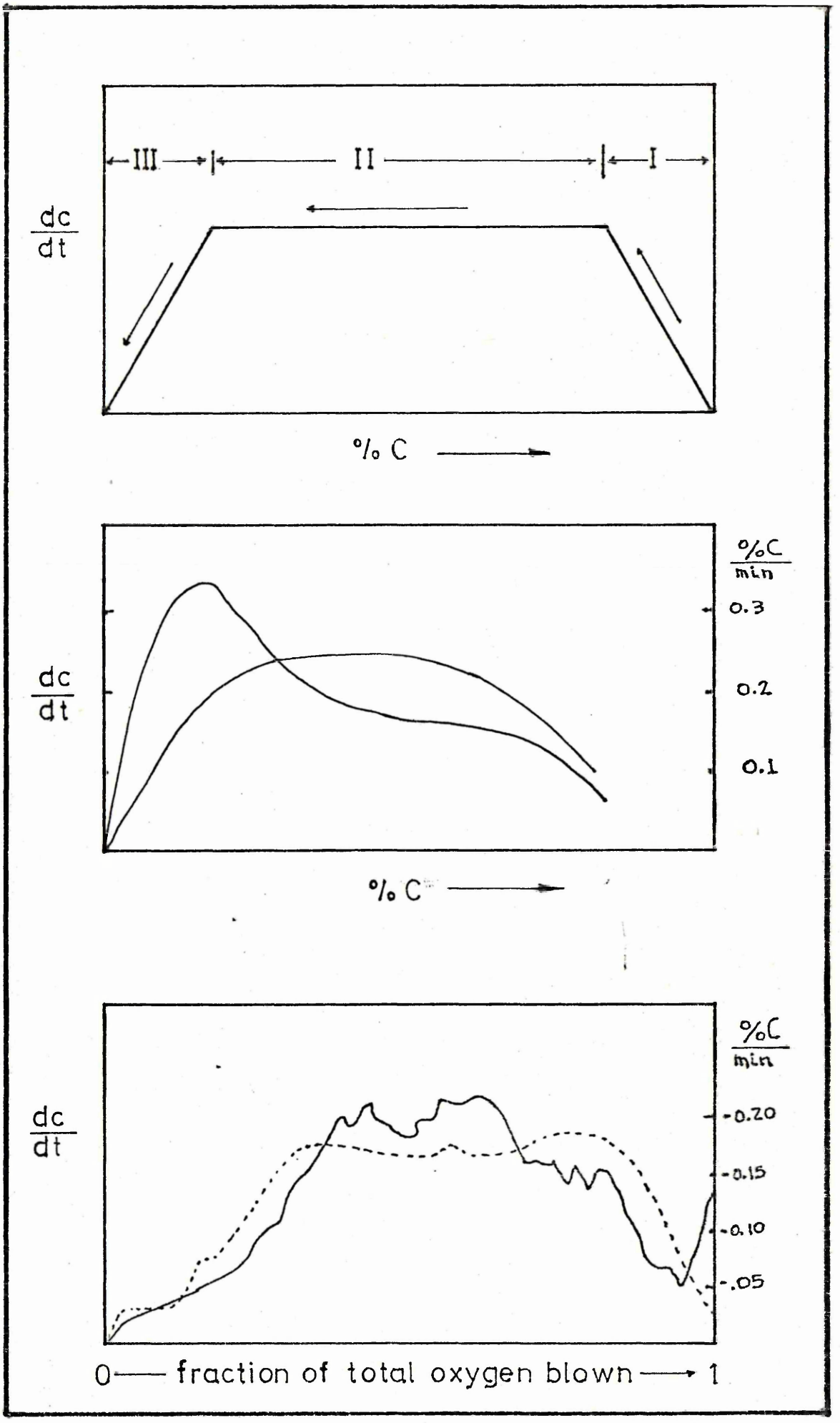
III
II
I
dc/dt
% C
dc/dt
%C/min
0.3
0.2
0.1
% C
dc/dt
%C/min
-0.20
-0.15
-0.10
-.05
0 — fraction of total oxygen blown → 1

FIGURE 4. EQUILIBRIUM PHASE DIAGRAM FOR THE SYSTEM $FeO - Fe_2O_3$. HEAVY LINES ARE BOUNDARY CURVES SEPARATING STABILITY FIELDS OF THE VARIOUS CONDENSED PHASES, AND LIGHT DASH-DOT LINES ARE OXYGEN ISOBARS. (43)

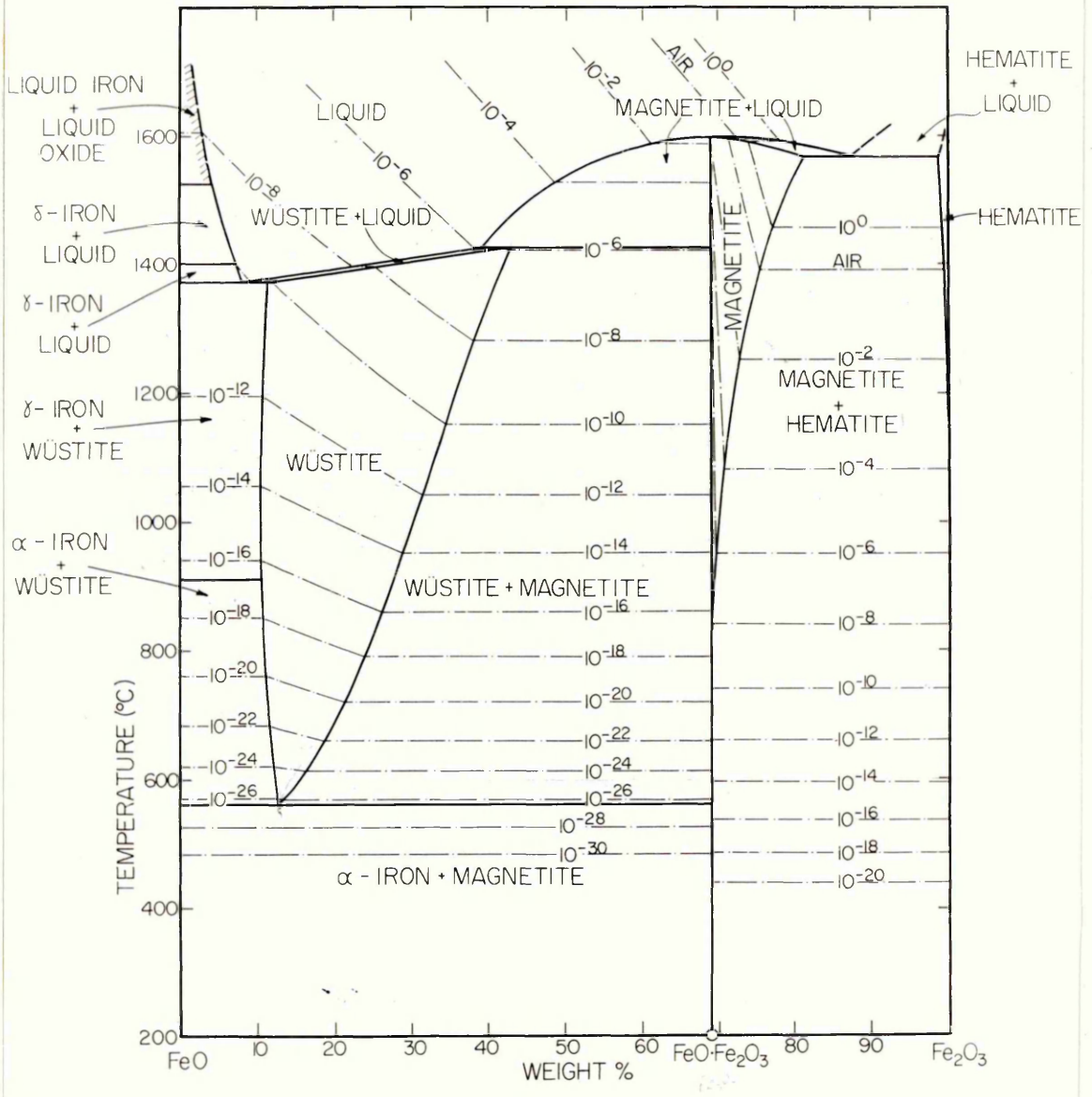
LIQUID IRON
+
LIQUID
OXIDE
δ - IRON
+
LIQUID
γ - IRON
+
LIQUID
γ - IRON
+
WÜSTITE
α - IRON
+
WÜSTITE
LIQUID
WÜSTITE + LIQUID
MAGNETITE + LIQUID
HEMATITE
+
LIQUID
HEMATITE
MAGNETITE
AIR
MAGNETITE
+
HEMATITE
WÜSTITE
WÜSTITE + MAGNETITE
α - IRON + MAGNETITE
10-2
100
10-4
10-6
10-8
10-12
10-14
10-16
10-18
10-20
10-22
10-24
10-26
10-28
10-30
10-2
100
10-4
10-6
10-8
10-10
10-12
10-14
10-16
10-18
10-20
1600
1400
1200
1000
800
600
400
200
TEMPERATURE (°C)
FeO
10
20
30
40
50
60
FeO·Fe2O3
80
90
Fe2O3
WEIGHT %

FIGURE 4a

EQUILIBRIUM PHASE DIAGRAM FOR THE SYSTEM Fe - O OUTLINING PHASE BOUNDARY POINTS FOR TEMPERATURE AND % OXYGEN (25).

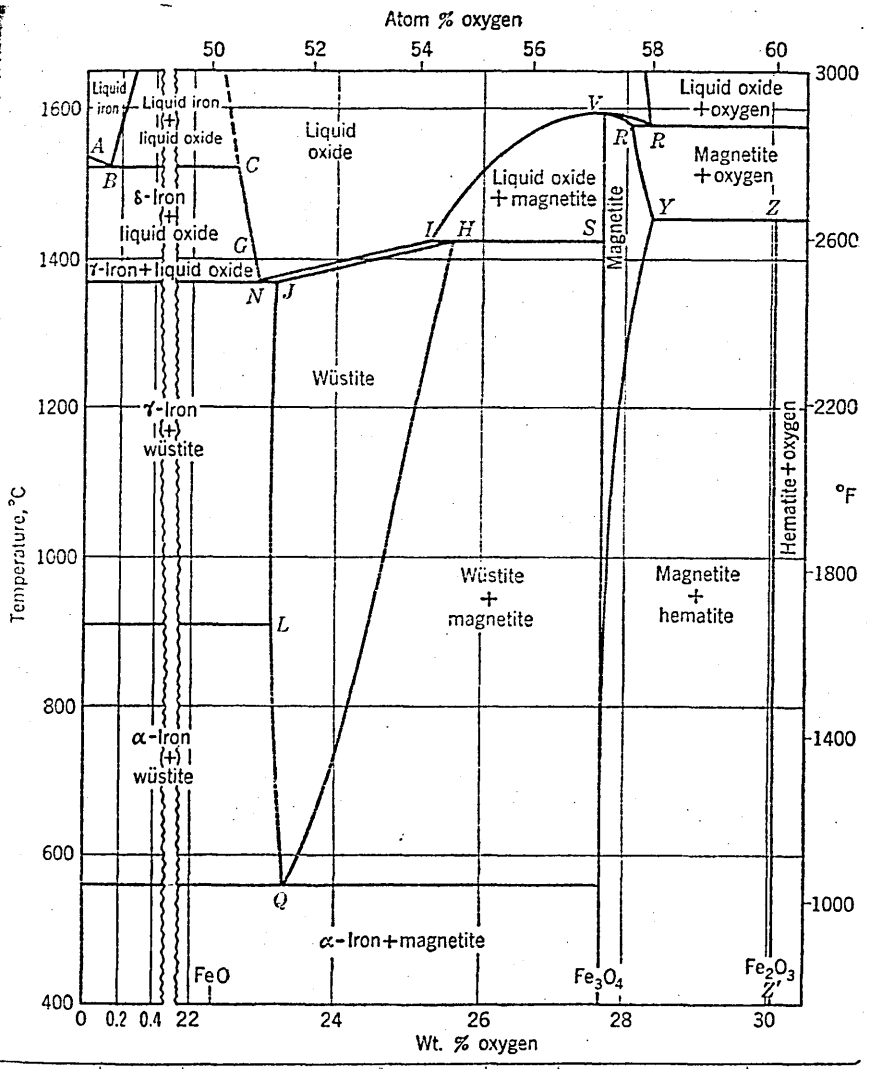

Point	°C	% O	p_{CO_2}/p_{CO}	Point	°C	% O	p_{CO_2}/p_{CO}	p_{O_2} (atm)
A.....	1539			*Q*.....	560	23.26	1.05	
B.....	1528	0.16	0.209	*R*.....	1583	28.30		1
C.....	1528	22.60	0.209	*R'*.....	1583	28.07		1
G.....	1400*	22.84	0.263	*S*.....	1424	27.64	16.2	
H.....	1424	25.60	16.2	*V*.....	1597	27.64		0.0575
I.....	1424	25.31	16.2	*Y*.....	1457	28.36		1
J.....	1371	23.16	0.282	*Z*.....	1457	30.04		1
L.....	911*	23.10	0.447	*Z'*.....		30.06		
N.....	1371	22.91	0.282					

FIGURE 5. ISOTHERMAL SECTION OF THE TERNARY Fe-Si-O AT 1545°C, 1600 AND 1650°C.(31).

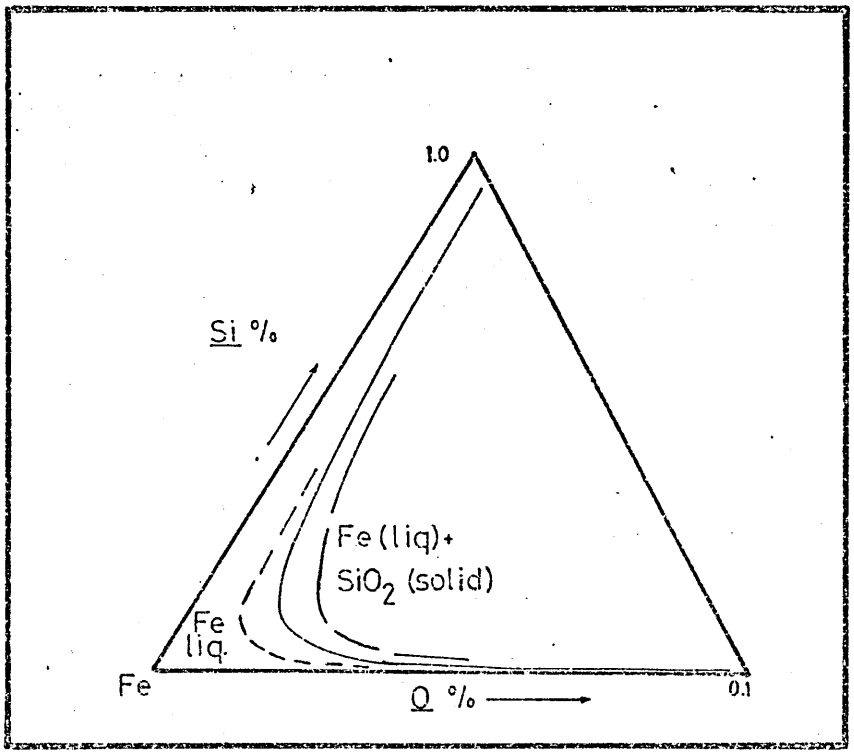
1.0
Si %
Fe (liq)+
SiO2 (solid)
Fe
liq.
Fe
O %
0.1

FIGURE 6. EQUILIBRIUM PHASE DIAGRAM FOR THE TERNARY $FeO - Fe_2O_3 - SiO_2$ SYSTEM (43).

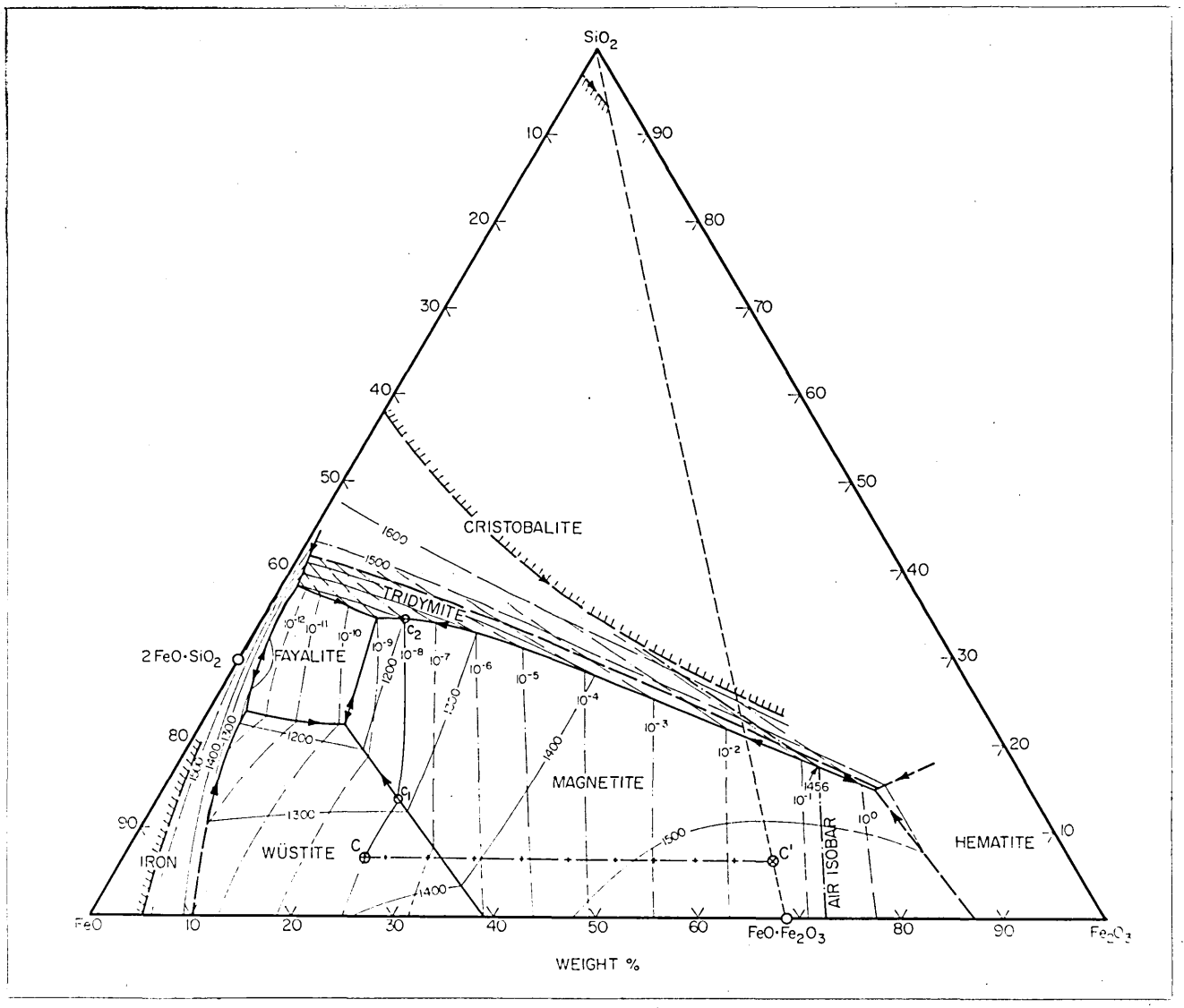
SiO2
CRISTOBALITE
TRIDYMITE
2 FeO·SiO2
FAYALITE
C2
C1
MAGNETITE
WÜSTITE
IRON
C
C'
AIR ISOBAR
HEMATITE
1456
FeO
FeO·Fe2O3
Fe2O3
WEIGHT %

FIGURE 7.

EQUILIERIUM PHASE DIAGRAM FOR THE FeO -SiO_2 SYSTEM(33).

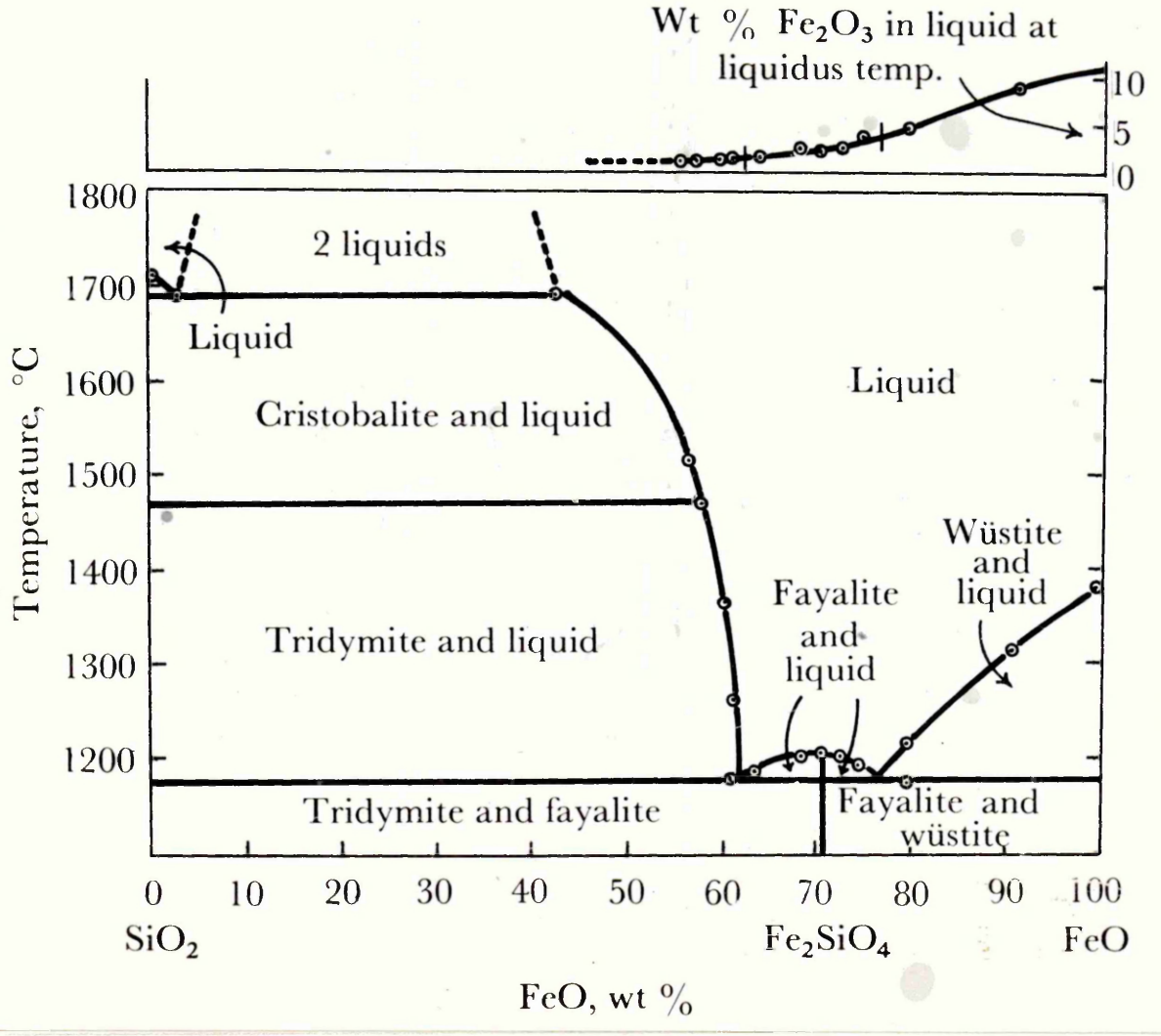
Wt % Fe_2O_3 in liquid at liquidus temp.
10
5
0
1800
1700
1600
1500
1400
1300
1200
Temperature, °C
2 liquids
Liquid
Cristobalite and liquid
Liquid
Tridymite and liquid
Fayalite and liquid
Wüstite and liquid
Tridymite and fayalite
Fayalite and wüstite
0
10
20
30
40
50
60
70
80
90
100
SiO_2
Fe_2SiO_4
FeO
FeO, wt %

FIGURE 8. ACTIVITIES OF FeO AND O_2 IN IRON SILICATE MELTS AT 1300°C (39).

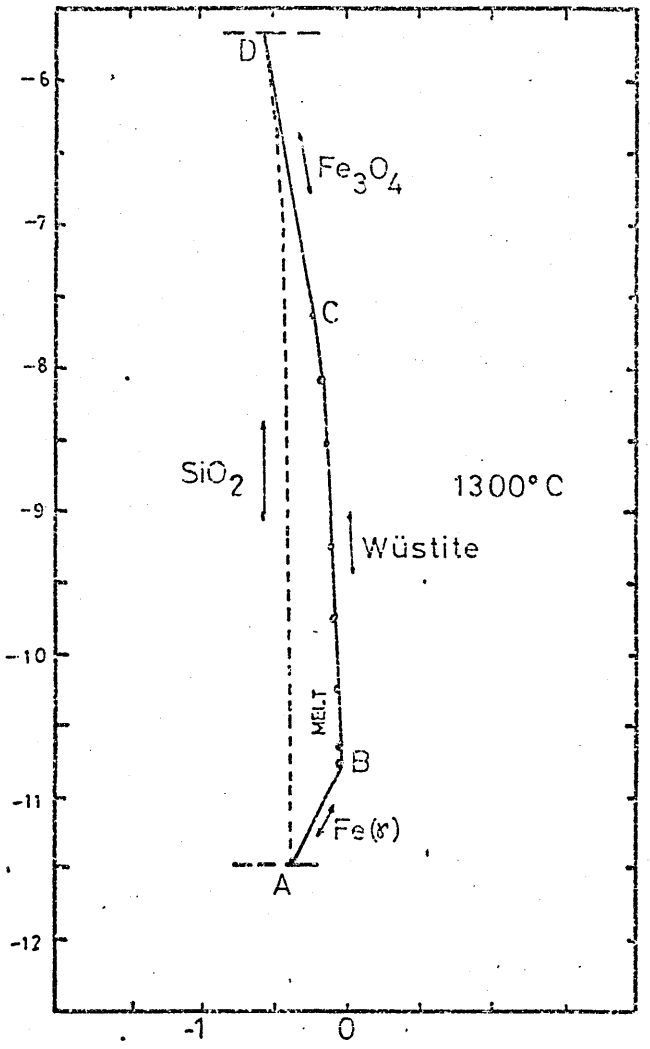
D
C
B
A
Fe_3O_4
SiO_2
Wüstite
Fe(γ)
MELT
1300°C
-6
-7
-8
-9
-10
-11
-12
-1
0
log p_{O_2}
log a_{FeO} (std state, liq oxide in equil. with Fe)

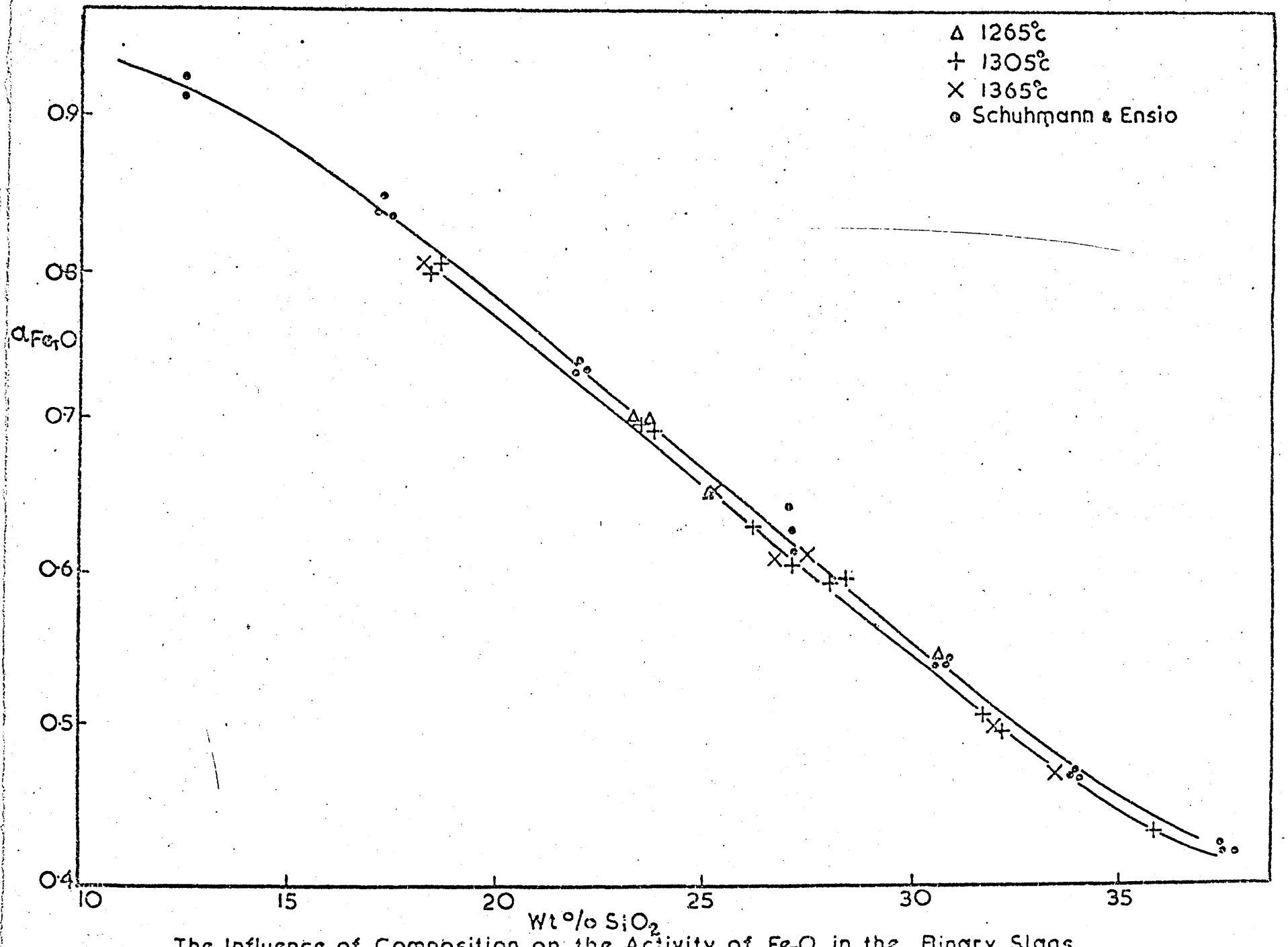

The Influence of Composition on the Activity of Fe_tO in the Binary Slags

FIGURE 10. EQUILIBRIUM PHASE DIAGRAM FOR THE SYSTEM LIME-SILICA (43).

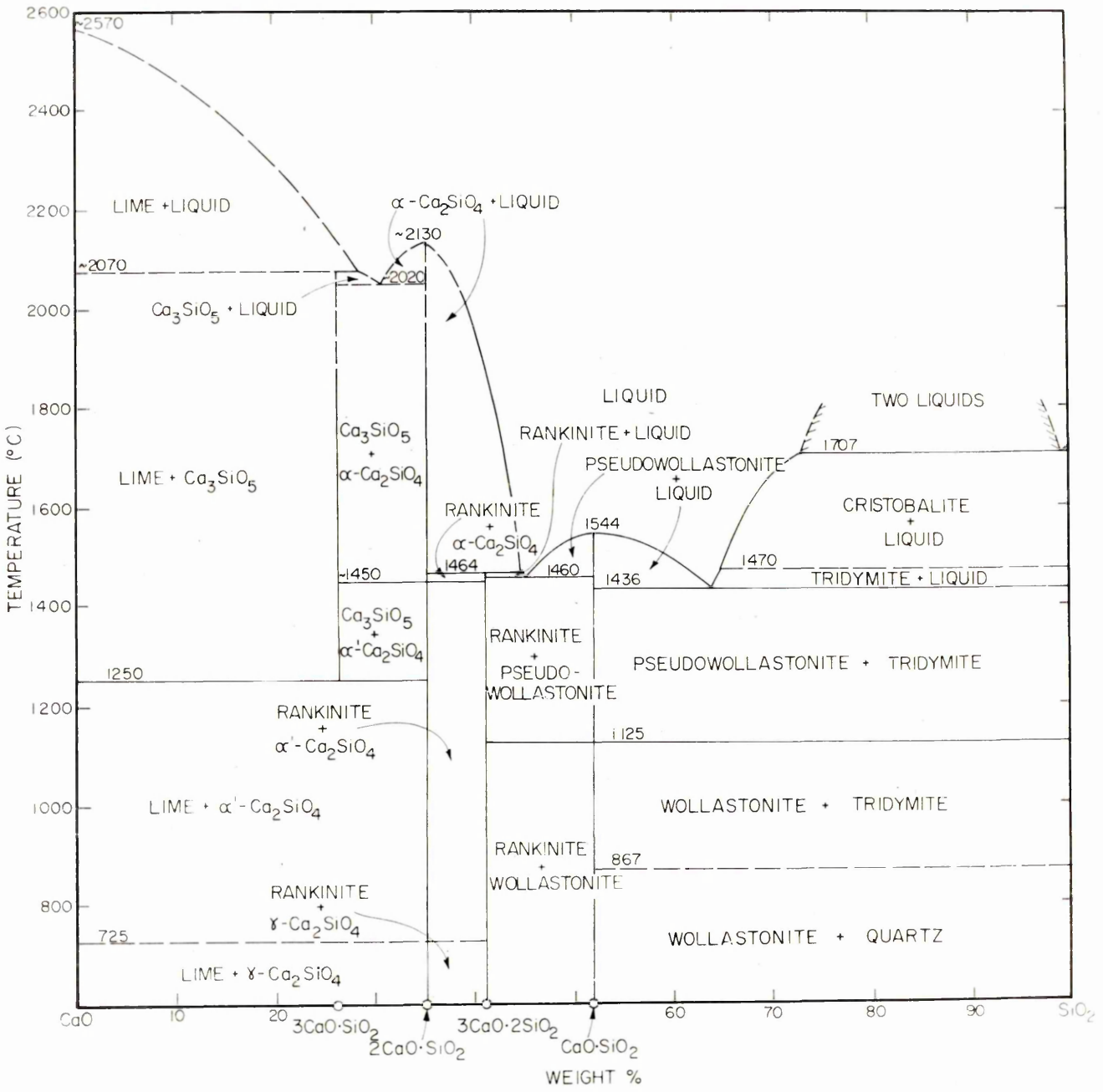
TEMPERATURE (°C)
2600
2400
2200
2000
1800
1600
1400
1200
1000
800
~2570
~2130
~2070
2020
1707
1544
1464
1460
1450
1436
1470
1250
1125
867
725
LIME + LIQUID
α - Ca2SiO4 + LIQUID
Ca3SiO5 + LIQUID
LIQUID
TWO LIQUIDS
RANKINITE + LIQUID
PSEUDOWOLLASTONITE + LIQUID
CRISTOBALITE + LIQUID
TRIDYMITE + LIQUID
LIME + Ca3SiO5
Ca3SiO5 + α-Ca2SiO4
RANKINITE + α-Ca2SiO4
Ca3SiO5 + α'-Ca2SiO4
RANKINITE + PSEUDO-WOLLASTONITE
PSEUDOWOLLASTONITE + TRIDYMITE
RANKINITE + α'-Ca2SiO4
LIME + α'-Ca2SiO4
WOLLASTONITE + TRIDYMITE
RANKINITE + WOLLASTONITE
RANKINITE + γ-Ca2SiO4
WOLLASTONITE + QUARTZ
LIME + γ-Ca2SiO4
CaO
10
20
60
70
80
90
SiO2
3CaO·SiO2
2CaO·SiO2
3CaO·2SiO2
CaO·SiO2
WEIGHT %

FIGURE 11. PHASE RELATIONS IN THE SYSTEM LIME - IRON OXIDE.

a) IN CONTACT WITH METALLIC IRON

b) IN EQUILIBRIUM WITH AIR.

C_2F = $2CaO\ Fe_2O_3$ = $Ca_2Fe_2O_5$

CF = $CaO\ Fe_2O_3$ = $CaFe_2O_4$

CF_2 = $CaO\ 2Fe_2O_3$ = $CaFe_4O_7$

H = Fe_2O_3

L = Liquid

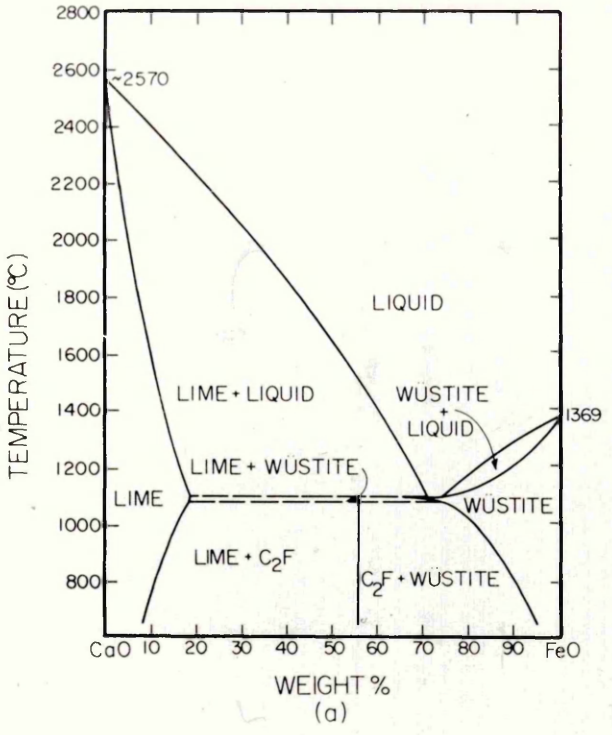
TEMPERATURE (°C)
2800
2600
2400
2200
2000
1800
1600
1400
1200
1000
800
~2570
LIQUID
LIME + LIQUID
WÜSTITE + LIQUID
1369
LIME + WÜSTITE
LIME
WÜSTITE
LIME + C2F
C2F + WÜSTITE
CaO 10 20 30 40 50 60 70 80 90 FeO
WEIGHT %
(a)

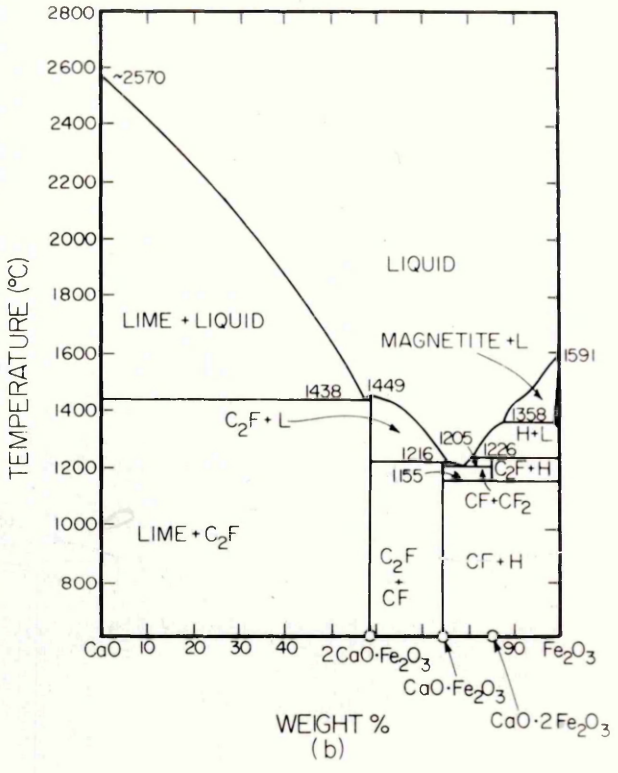
TEMPERATURE (°C)
2800
2600
2400
2200
2000
1800
1600
1400
1200
1000
800
~2570
LIQUID
LIME + LIQUID
MAGNETITE + L
1591
1438
1449
C2F + L
1358
H + L
1205
1216
1226
1155
C2F + H
CF + CF2
LIME + C2F
C2F + CF
CF + H
CaO 10 20 30 40 2CaO·Fe2O3 90 Fe2O3
CaO·Fe2O3
CaO·2Fe2O3
WEIGHT %
(b)

FIGURE 12. EQUILIBRIUM PHASE DIAGRAM FOR THE SYSTEM $CaO - FeO - SiO_2$ IN CONTACT WITH METALLIC IRON (43).

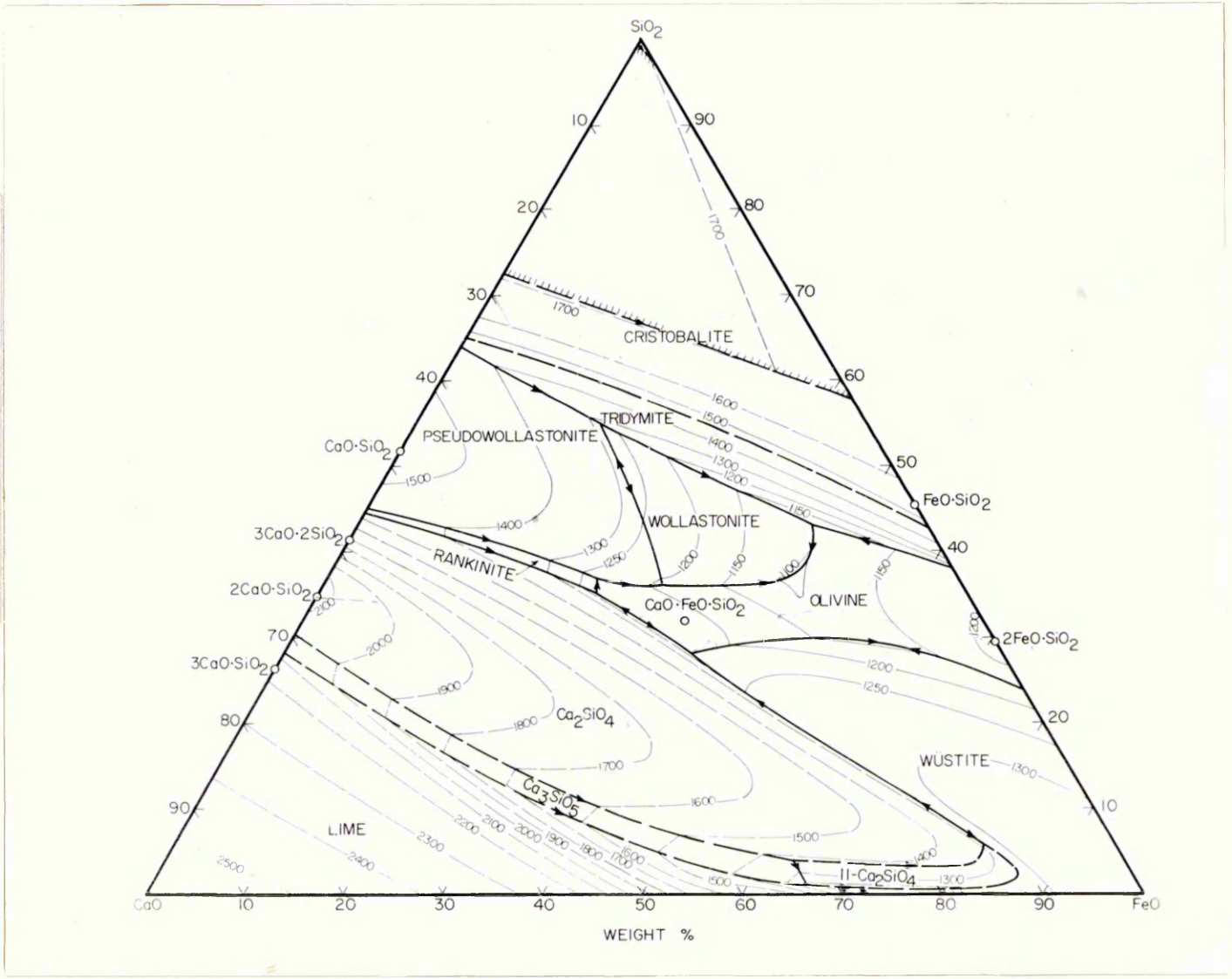
SiO2
CRISTOBALITE
TRIDYMITE
PSEUDOWOLLASTONITE
WOLLASTONITE
RANKINITE
OLIVINE
WÜSTITE
LIME
CaO·SiO2
3CaO·2SiO2
2CaO·SiO2
3CaO·SiO2
CaO·FeO·SiO2
FeO·SiO2
2FeO·SiO2
Ca2SiO4
Ca3SiO5
γ-Ca2SiO4
CaO
FeO
WEIGHT %

FIGURE 13. DIAGRAM SHOWING LINES OF AVERAGE Fe_2O_3 CONTENT OF MELTS ON THE LIQUIDUS SURFACE IN THE SYSTEM CaO - 'FeO' - SiO_2 (44).

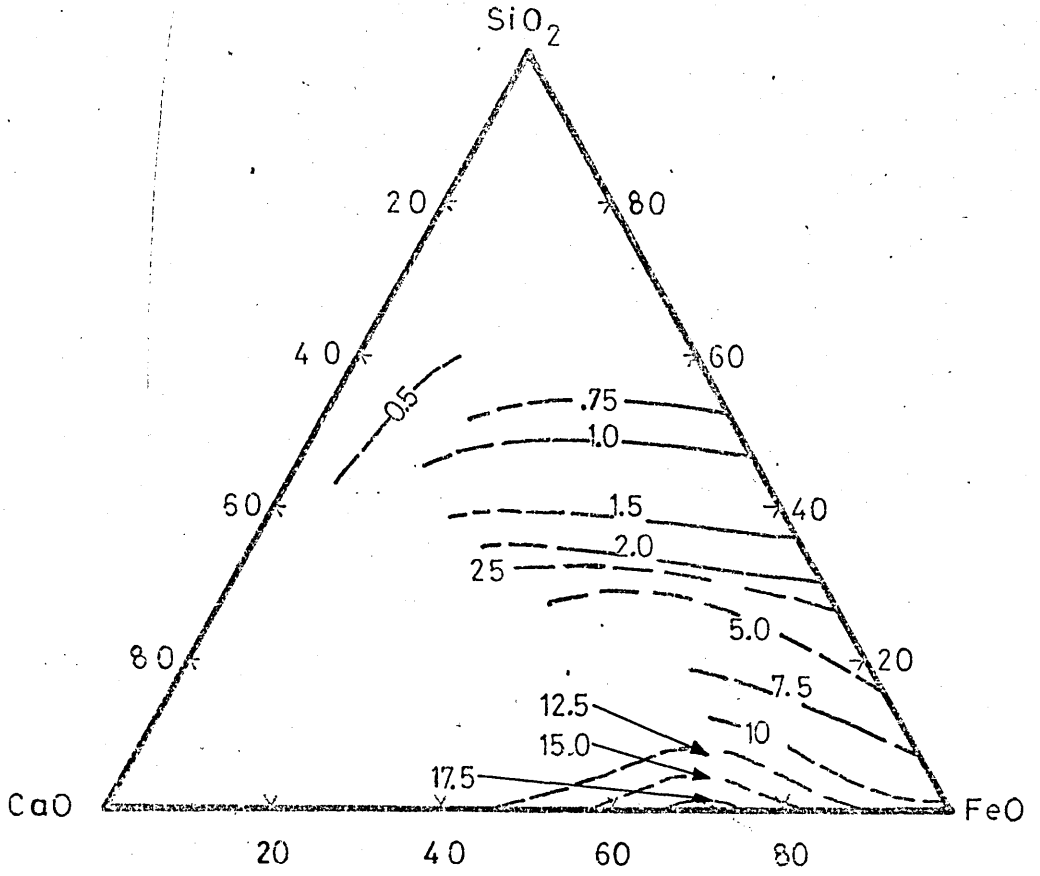
SiO2
20
80
40
60
60
40
80
20
0.5
.75
1.0
1.5
2.0
25
5.0
7.5
10
12.5
15.0
17.5
CaO
FeO
20
40
60
80

FIGURE 14. EQUILIBRIUM PHASE DIAGRAM FOR THE TERNARY $CaO - Fe_2O_3 - SiO_2$ (43).

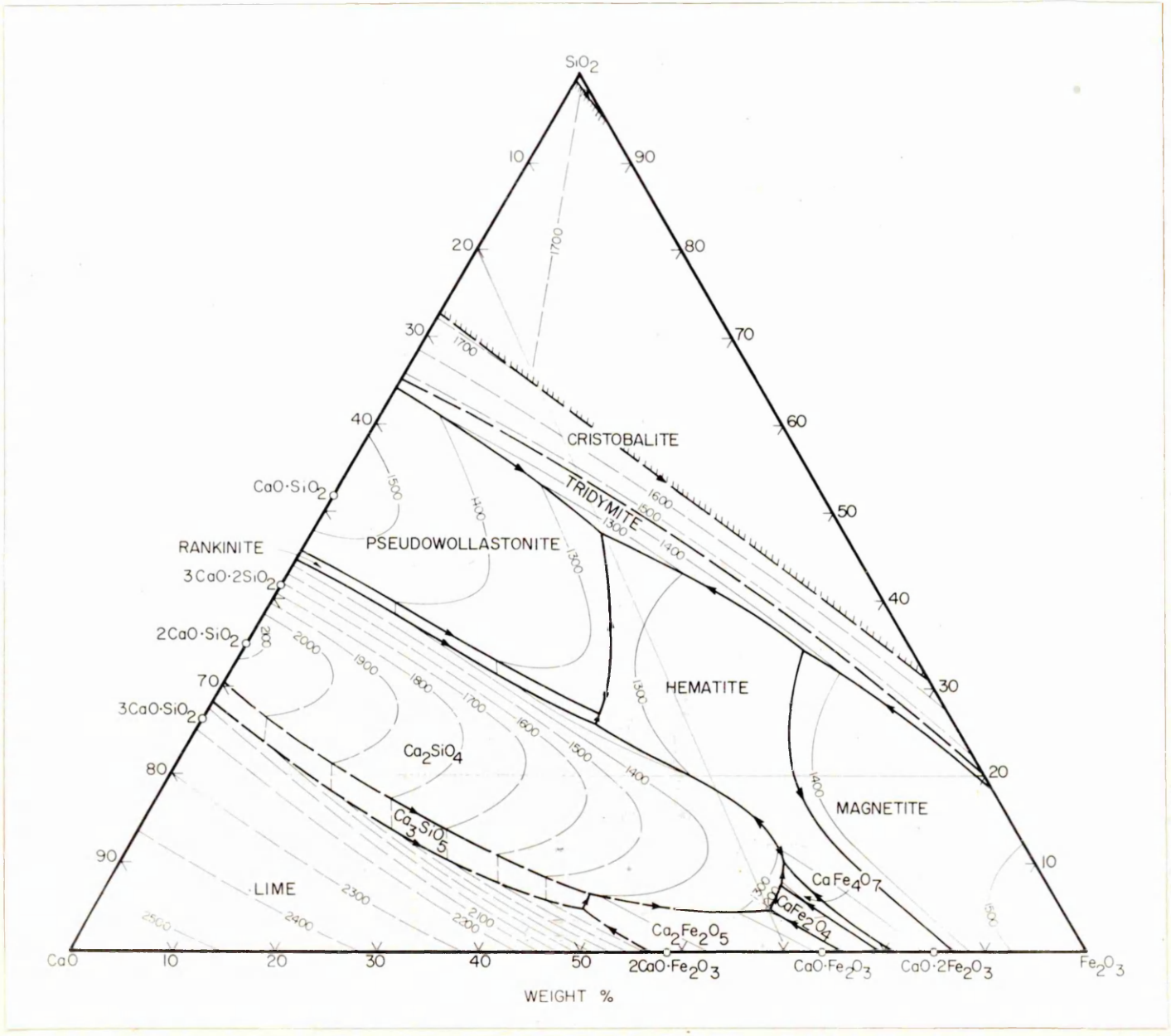
SiO2
CaO
2CaO·Fe2O3
CaO·Fe2O3
CaO·2Fe2O3
Fe2O3
WEIGHT %
CaO·SiO2
RANKINITE
3CaO·2SiO2
2CaO·SiO2
3CaO·SiO2
CRISTOBALITE
TRIDYMITE
PSEUDOWOLLASTONITE
HEMATITE
MAGNETITE
LIME
Ca2SiO4
Ca3SiO5
Ca2Fe2O5
CaFe4O7
CaFe2O4
1700
1600
1500
1400
1300
2000
1900
1800
2300
2400
2500
2200
2100

FIGURE 15.

a. TERNARY DIAGRAM SHOWING DESIRED AND POOR SLAG COMPOSITION PATHS DURING BOS REFINNING(10). AREA INCLUDED BETWEEN DASHED LINES OUTLINE CORRIDOR FOR SMOOTH REFINING PATH. SLOPPING SLAG PATH OCCURS ON ENTERING ZONE A WHILE IN ZONE B A DRY SLAG PATH IS FOLLOWED.

b. SLAG PATH FOR BOS REFINING (107). ARROWS INDICATE DIRECTION OF CHANGE IN CHEMICAL COMPOSITION.

c. CHANGES IN THE MEAN COMPOSITION OF OPEN HEARTH FURNACE SLAGS (90).

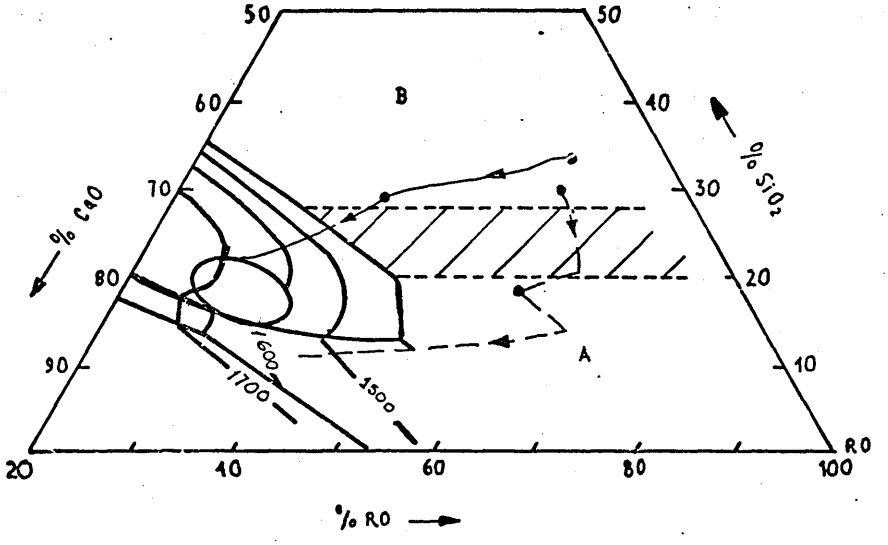
50
50
60
40
B
% SiO2
70
30
% CaO
80
20
A
1600
1700
1500
90
10
RO
20
40
60
80
100
% RO

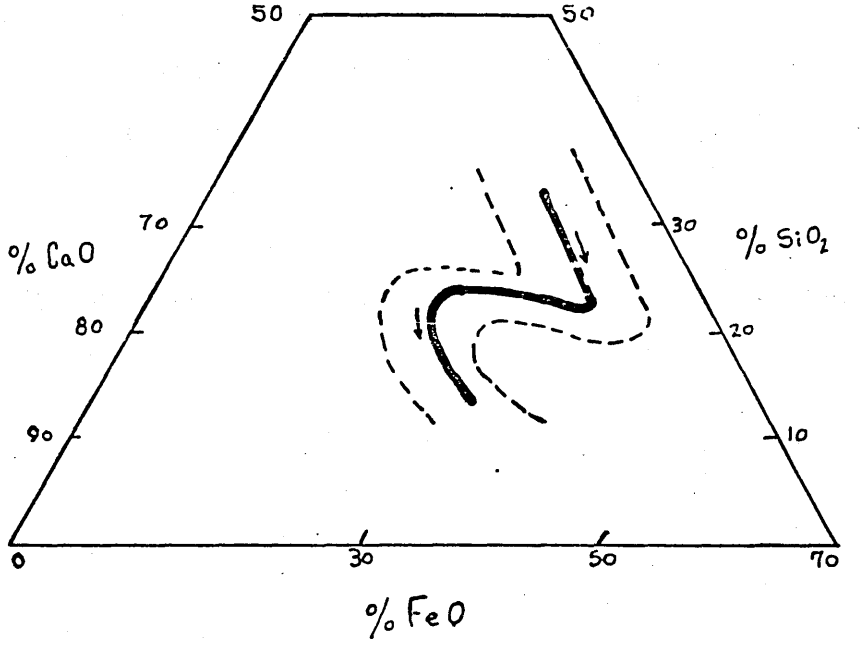
50
50
70
30
% CaO
% SiO2
80
20
90
10
0
30
50
70
% FeO

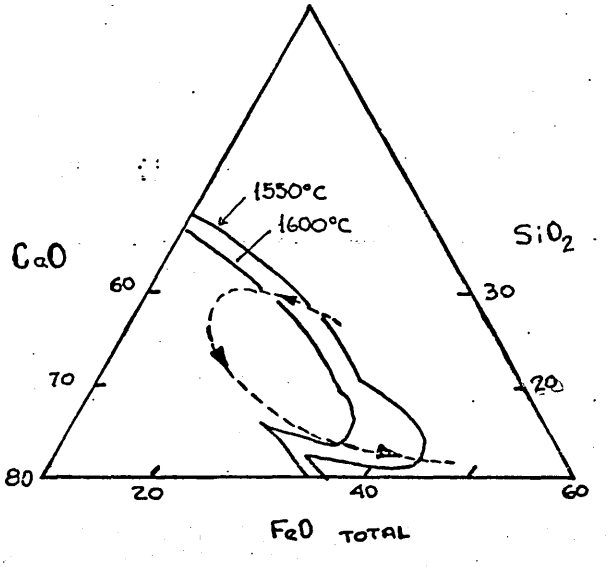
1550°C
1600°C
CaO
SiO2
60
30
70
20
80
20
40
60
FeO TOTAL

FIGURE 16. DIAGRAM OF THE UPPER PORTION OF FURNACE USED IN DECARBURIZATION EXPERIMENTS.

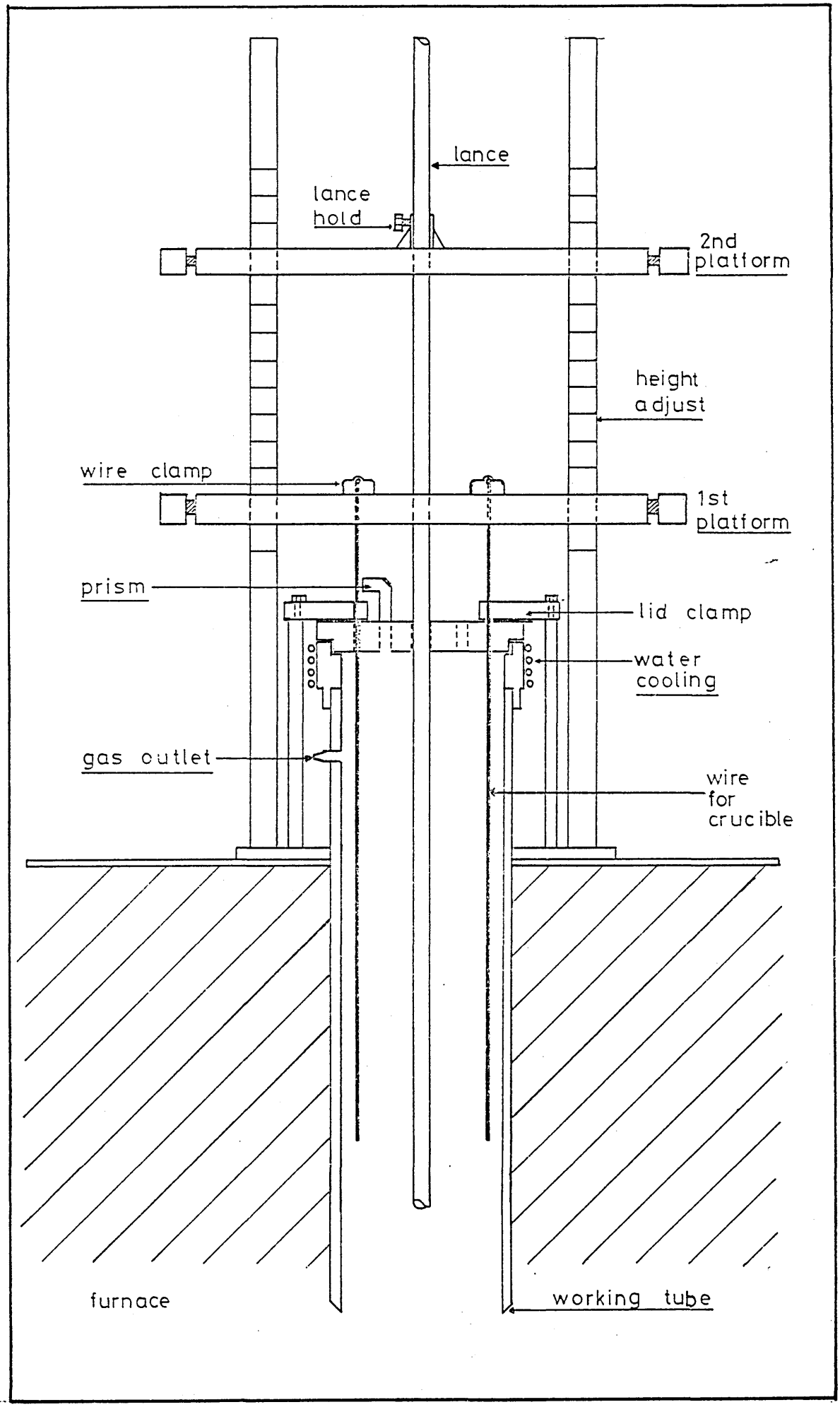
lance
lance hold
2nd platform
height adjust
wire clamp
1st platform
prism
lid clamp
water cooling
gas outlet
wire for crucible
furnace
working tube

FIGURE 17. DIAGRAM OF THE LOWER END OF THE FURNACE SHOWING ARRANGEMENT FOR QUENCHING.

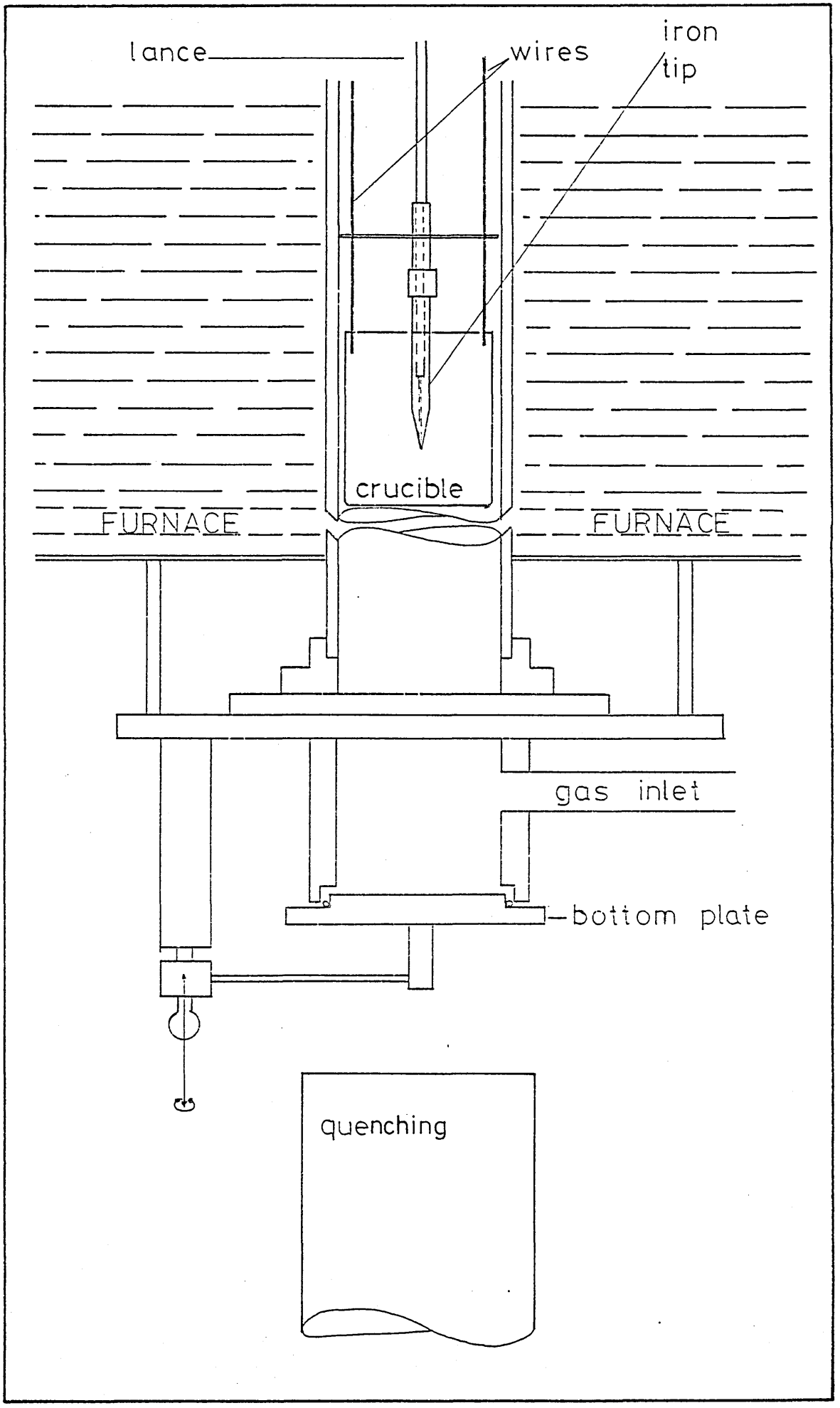
lance
wires
iron
tip
crucible
FURNACE
FURNACE
gas inlet
bottom plate
quenching

FIGURE 18.

DECARBURIZATION OF Fe - 4.17 % C and 3.6 % C ALLOYS IN FAYALITE SLAG WITH DIFFERENT PREHEATING SEQUENCES. LINE 1 AND 2 WERE TAKEN FROM ROOM TEMPERATURE UP TO 1240°C. LINE 3 WAS TAKEN FROM ROOM TEMPERATURE UP TO 875°C, HELD FOR TEN MINUTES AND THEN UP TO 1240°C.

LINE 1		LINE 2		LINE 3	
time	%C	time	%C	time	%C
0	4.17	0	3.6	0	3.60
9	4.13	12.8	2.99	5	3.49
10	3.82	15	2.83	10	2.99
10	3.86	16	2.88	17	2.51
11	3.77	20	2.65	23	2.34
12	3.87	23	2.43	35	1.82
15	3.51	30	2.01		
15	3.66				
20	3.48				
20	3.31				

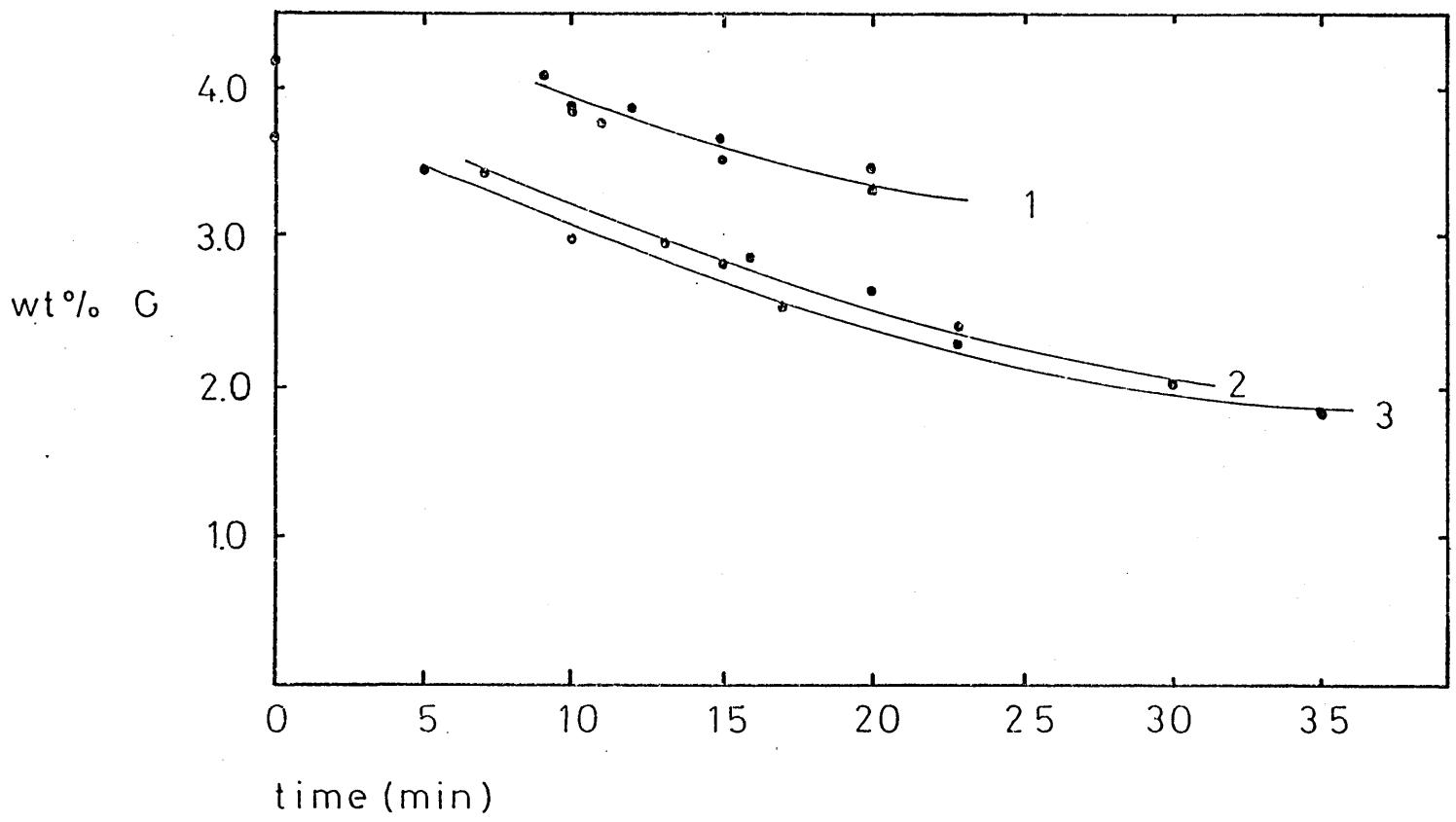
4.0
3.0
2.0
1.0
wt % C
0
5
10
15
20
25
30
35
time (min)
1
2
3

FIGURE 19. DIFFERENTIAL THERMAL ANALYSIS BETWEEN Fe - C SAMPLE AND CRUCIBLE. FIRST HOT-ZONE : 800°C HELD FOR 10 MINUTES. SECOND HOT-ZONE 1000°C HELD FOR 5 MINUTES. FINAL HOT-ZONE 1240°C. THE SLAG METAL RATIO WAS 20:1.

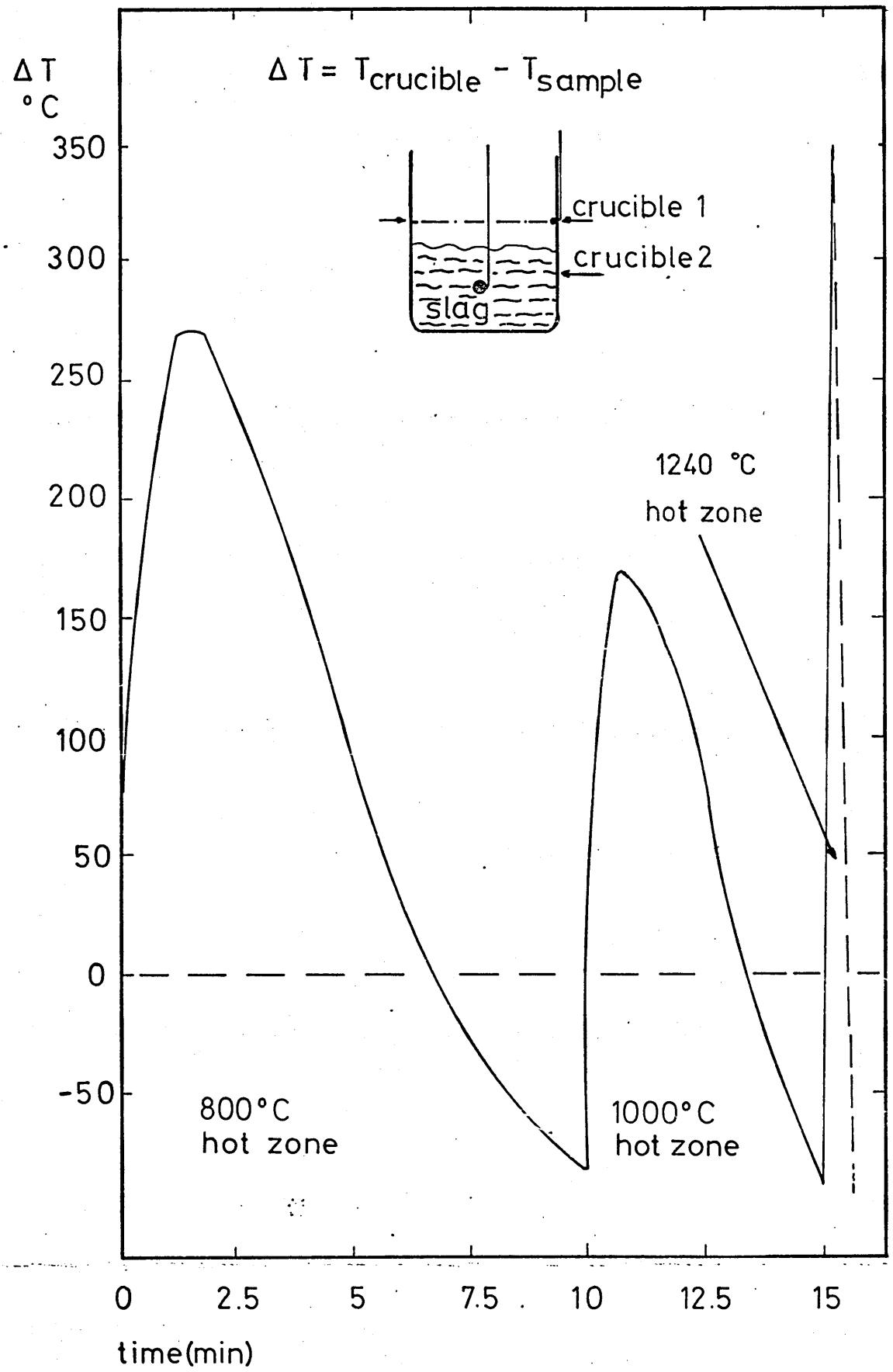
ΔT °C
ΔT = T crucible - T sample
350
300
250
200
150
100
50
0
-50
crucible 1
crucible 2
slag
1240 °C
hot zone
800°C
hot zone
1000°C
hot zone
0
2.5
5
7.5
10
12.5
15
time(min)

FIGURE 20. DIFFERENTIAL THERMAL ANALYSIS BETWEEN Fe - C SAMPLE AND CRUCIBLE. CONDITIONS ARE THE SAME AS THOSE GIVEN IN FIGURE 19.

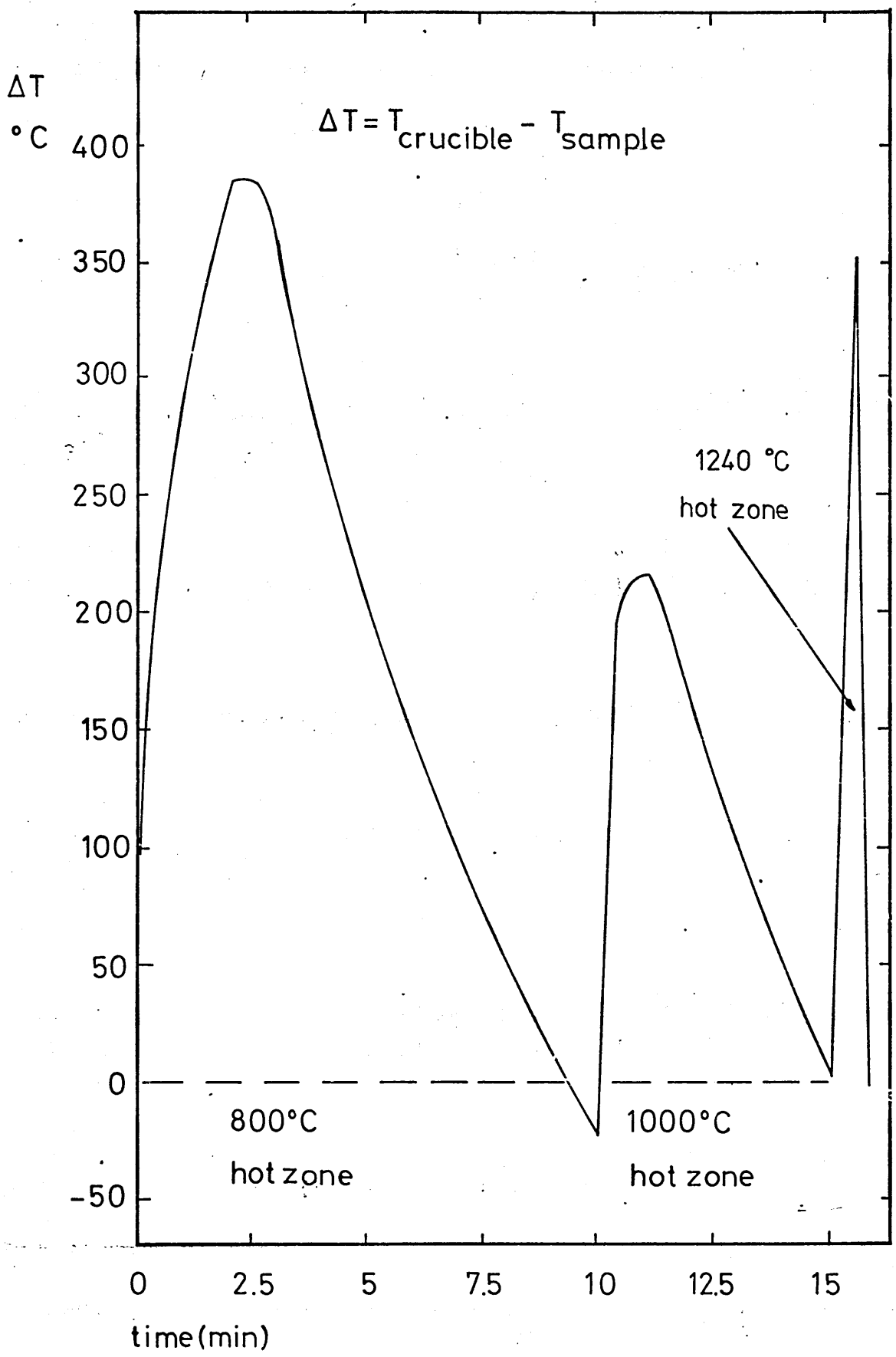
ΔT
°C
ΔT = T crucible - T sample
400
350
300
250
200
150
100
50
0
-50
1240 °C
hot zone
800°C
hot zone
1000°C
hot zone
0
2.5
5
7.5
10
12.5
15
time (min)

FIGURE 21.

DECARBURIZATION WITH FAYALITE SLAG OF AN Fe - 4.13 % C ALLOYS WITH PREHEATING ESTABLISHED FROM DTA.

time	% C	time	% C
0.0	4.13	17.5	2.74
2.5	3.91	25.0	2.31
3.0	3.75	30.0	2.50
4.0	3.78	60.0	1.66
5.0	3.69		
5.0	3.78		
5.0	3.61		
7.5	3.53		
7.5	3.54		
10.0	3.32		
12.5	3.28		
15.0	3.08		
15.5	2.95		

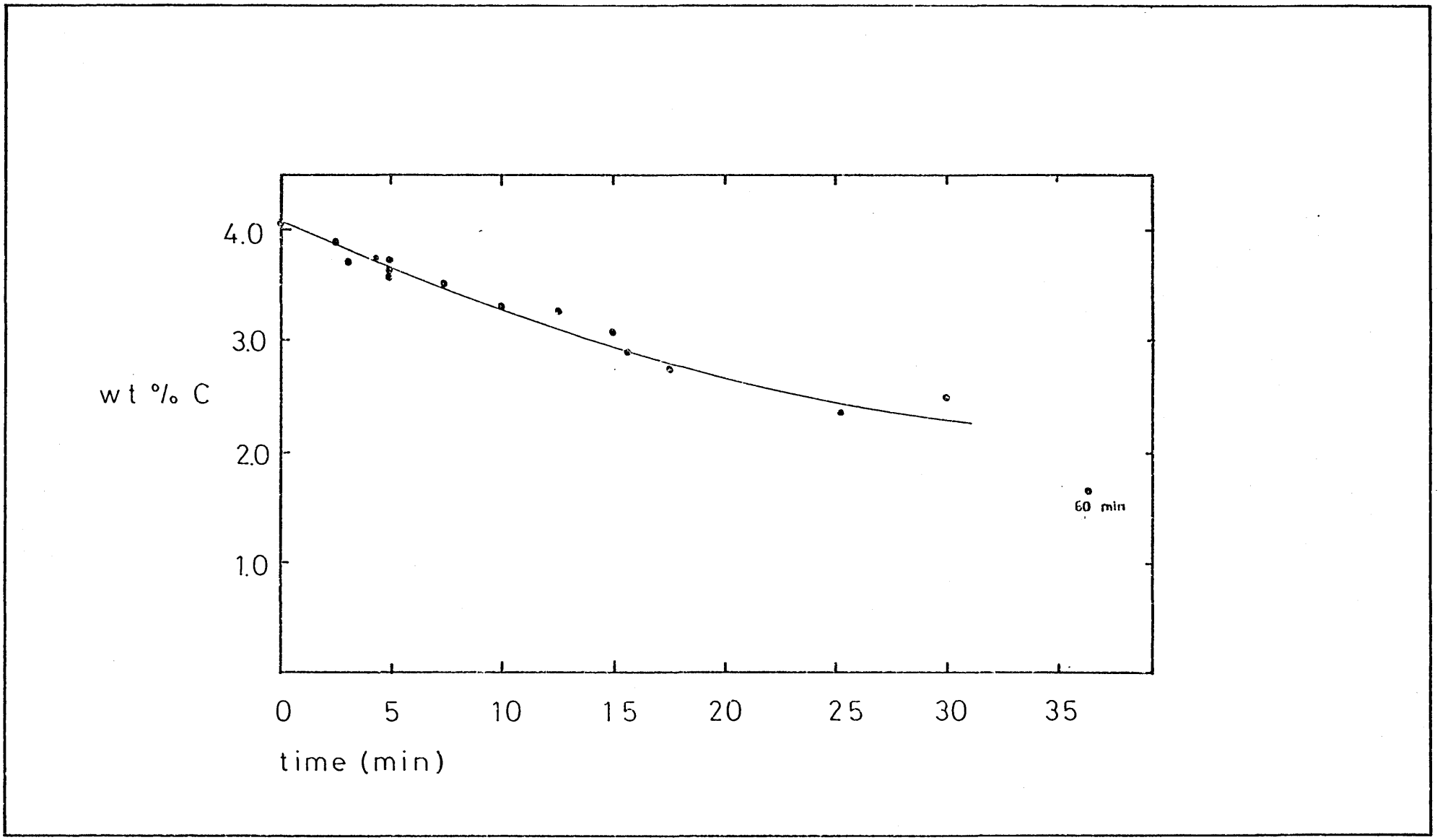
4.0
3.0
2.0
1.0
wt % C
0
5
10
15
20
25
30
35
time (min)
60 min

FIGURE 22. CONTACT-PRINT PHOTOGRAPHS FROM X-RAYED Fe - 4.13 % C SAMPLES REACTED IN FAYALITE AT 1240°C.

SAMPLE No.	time	% C
2	17.5	2.74
3	30.0	2.50
5	60.0	1.66

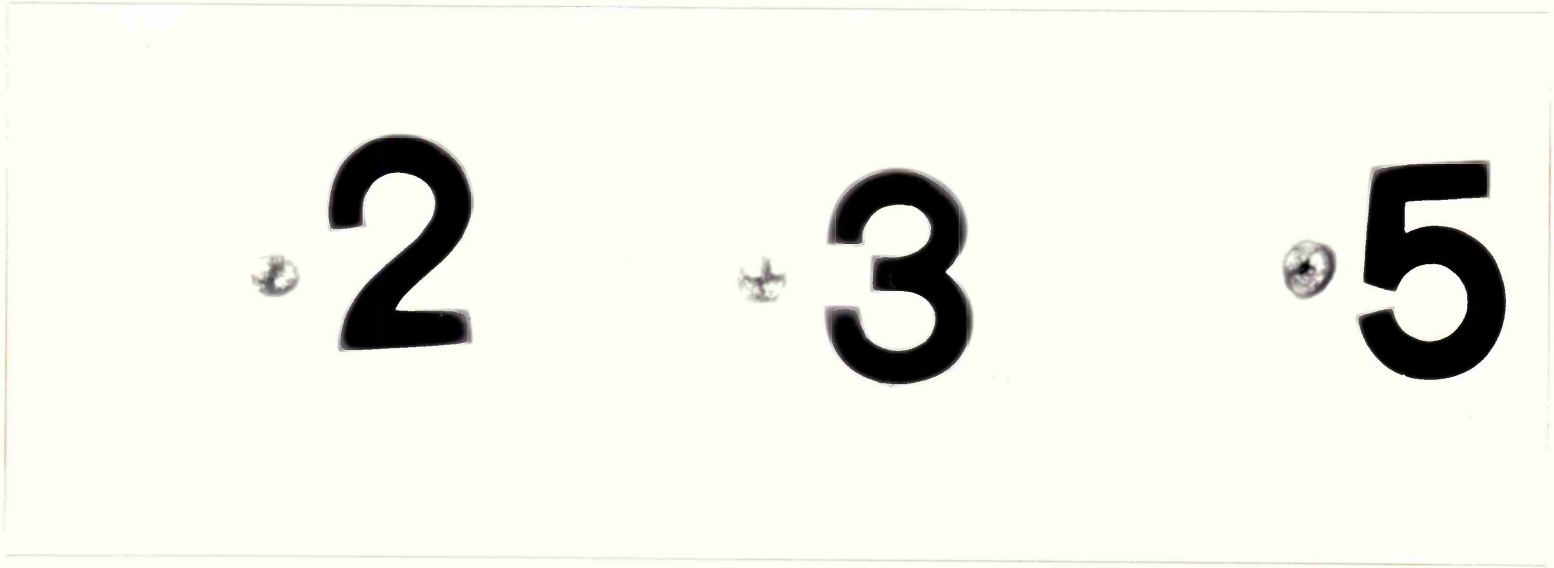
2
3
5

FIGURE 23. IRON - CARBON SAMPLE AFTER REACTING WITH FAYALITE AT 1240°C FOR 40 MINUTES.

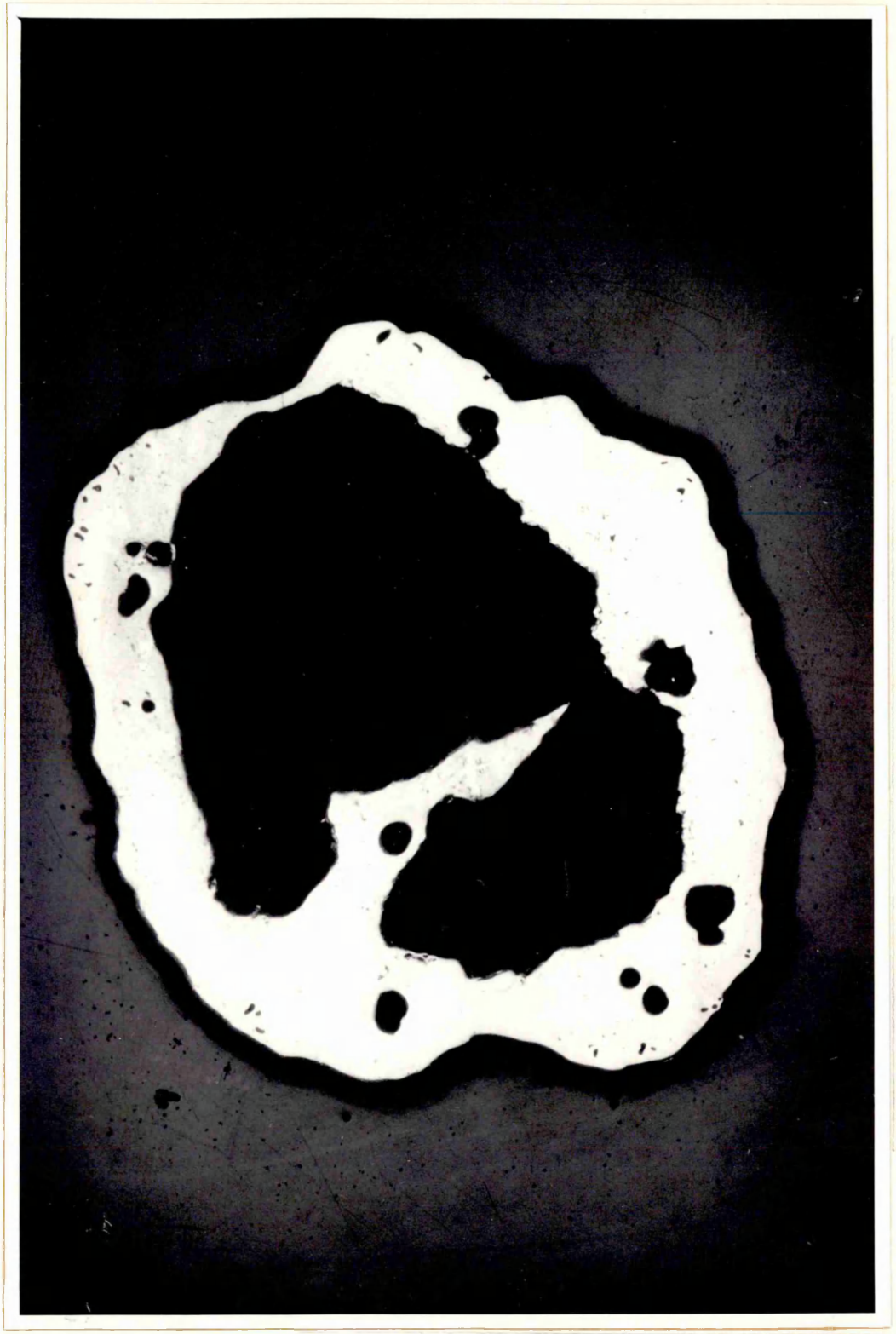

FIGURE 24. IRON - 4.2 % C ALLOYS DECARBURIZED IN FAYALITE SLAG AT 1300°C.

time (min)	% C
0.0	4.20
4.0	3.70
6.0	3.76
8.0	3.52
9.0	3.23
10.0	3.45
12.0	3.41
15.0	3.02
15.0	2.90

FIGURE 25. IRON - 3.95 % C ALLOYS DECARBURIZED WITH 52.50 % FeO, 3.44 % Fe_2O_3, 11.06 % CaO AND 33.00 % SiO_2

time (min)	% C
0	3.95
3	3.93
6	3.59
10	3.10
15	2.78

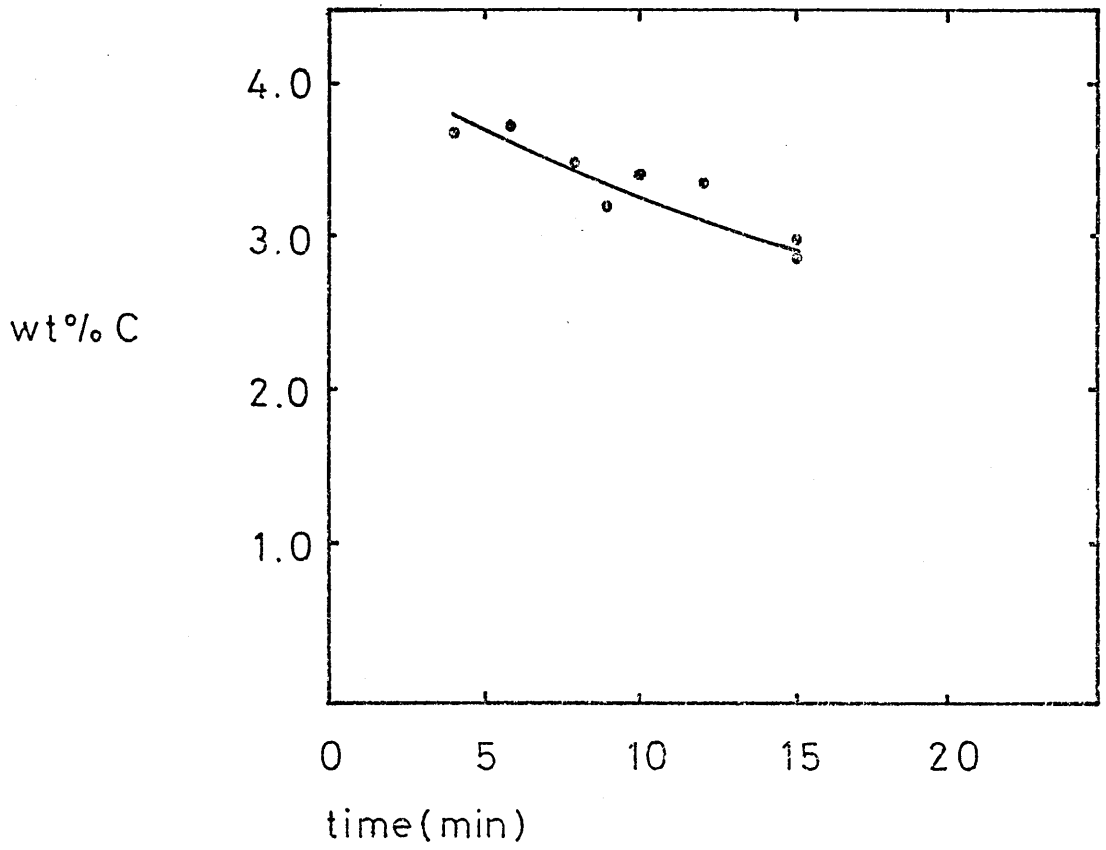
4.0
3.0
2.0
1.0
wt% C
0
5
10
15
20
time(min)

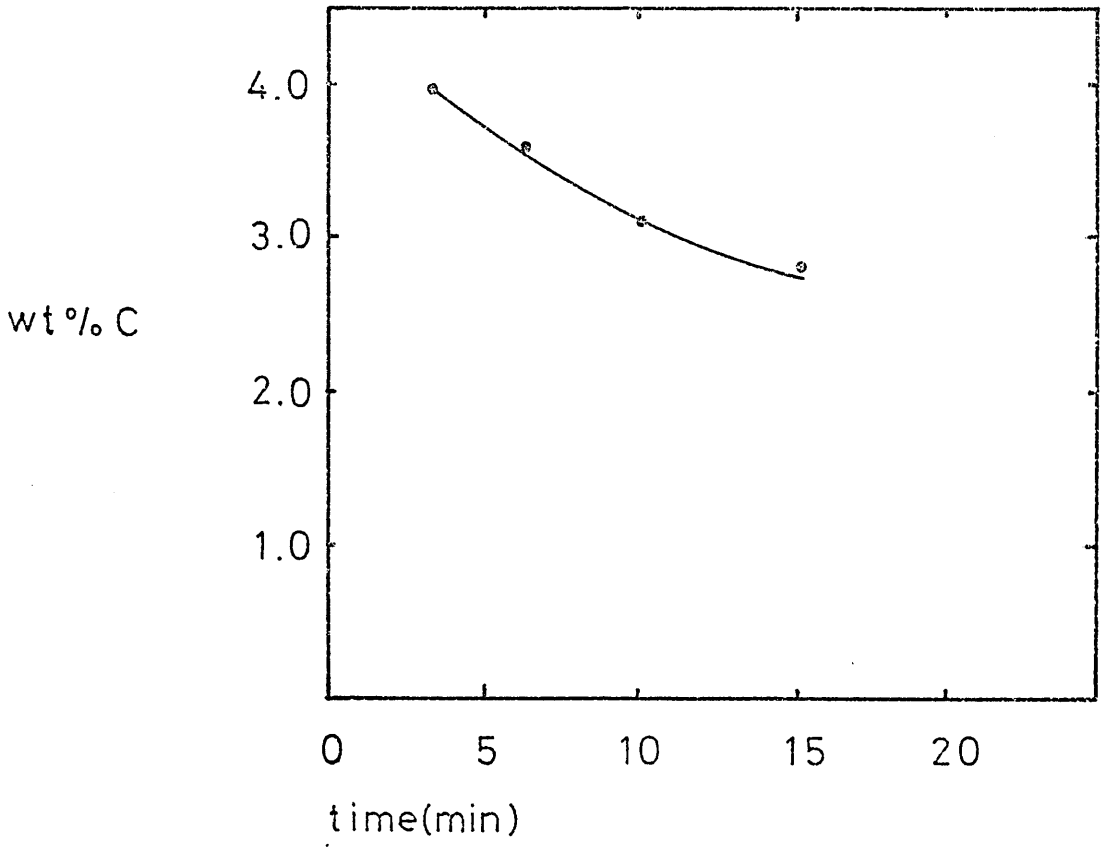
4.0
3.0
2.0
1.0
wt% C
0
5
10
15
20
time(min)

FIGURE 26. IRON-3.88 %C ALLOYS DECARBURIZED IN 55.83 %FeO 2.91 % Fe_2O_3, 12.66 % CaO AND 28.60 % SiO_2 SLAG AT 1300°C.

time (min)	% C
0	3.88
3	3.79
5	3.25
10	2.60
15	2.20
20	1.78

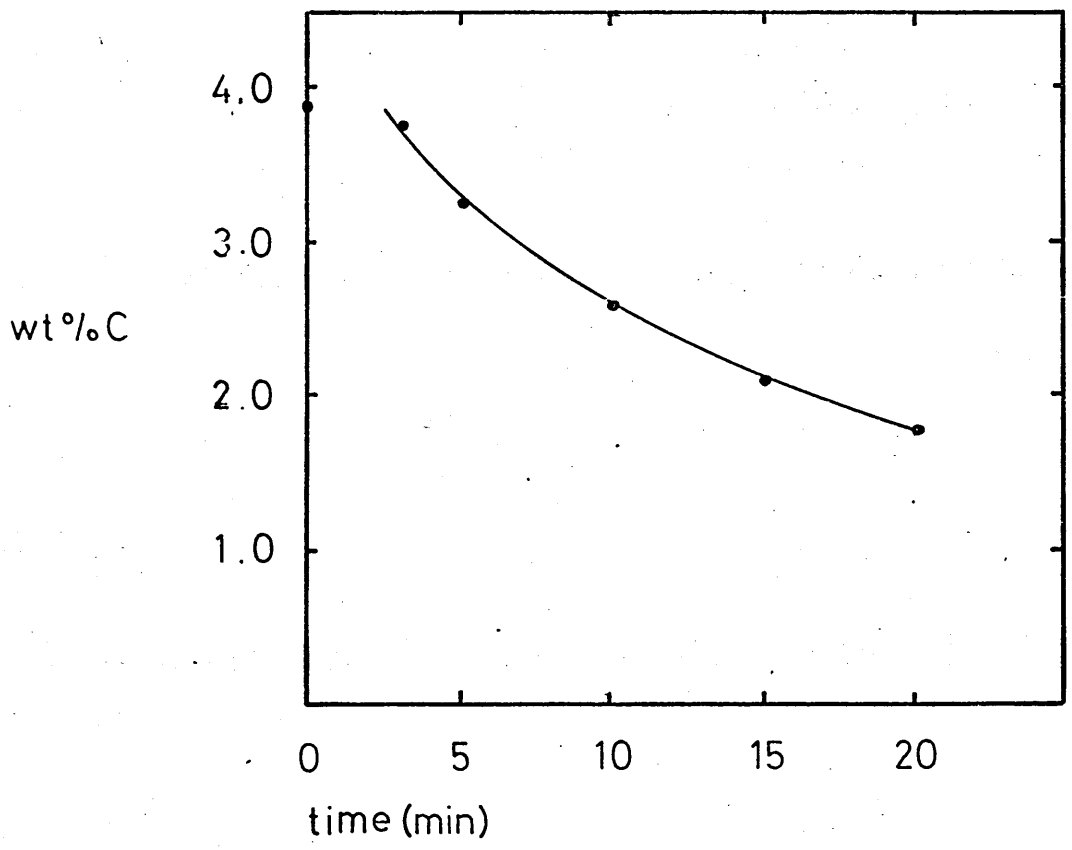
4.0
3.0
2.0
1.0
wt%C
0
5
10
15
20
time (min)

FIGURE 27. IRON - 4.25 % C ALLOYS DECARBURIZED IN 53.03 % FeO, 2.97 % Fe_2O_3, 14.32 % CaO AND 29.68 % SiO_2 SLAG AT 1300°C.

time (min)	% C
0.0	4.25
2.5	4.07
3.5	3.87
5.0	3.80
5.5	3.45
7.0	3.05
7.0	3.15
10.0	3.13
10.0	3.23
12.0	3.04
15.0	2.66
19.0	2.12

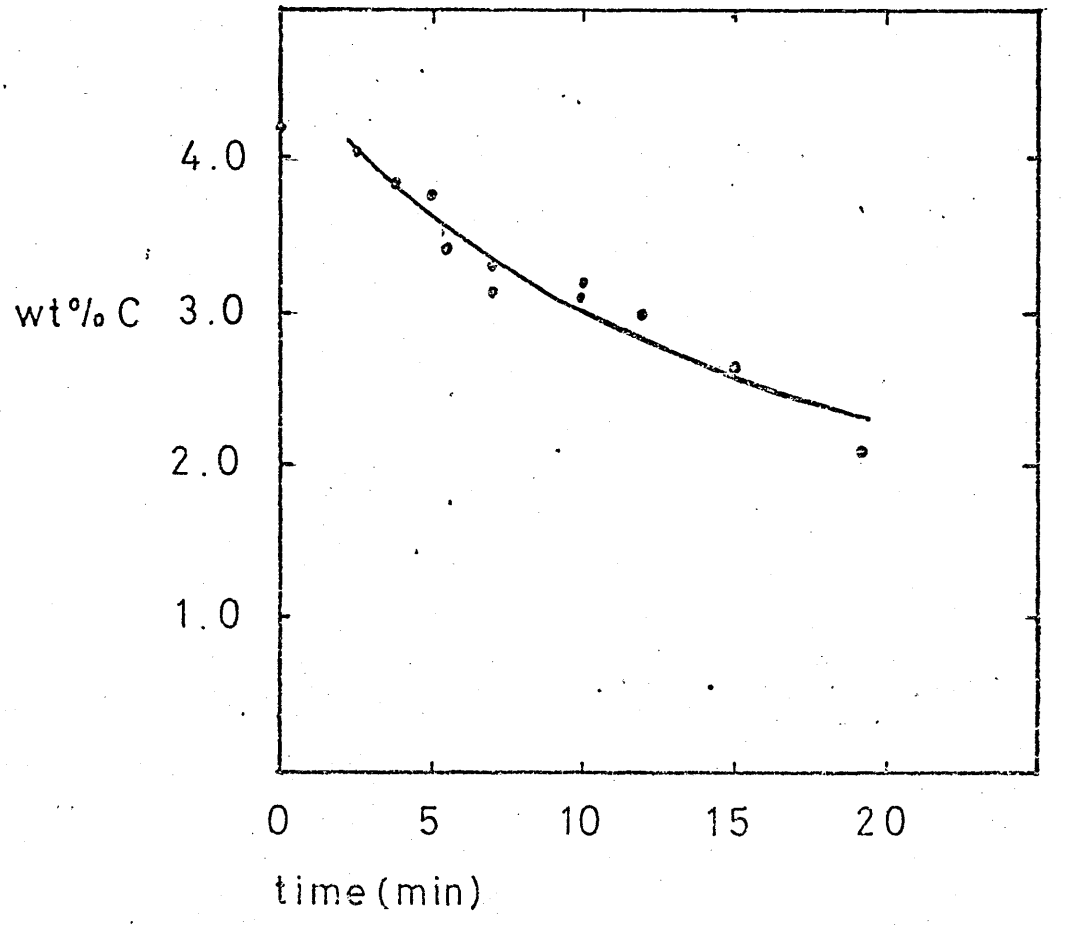
4.0
3.0
2.0
1.0
wt% C
0
5
10
15
20
time (min)

FIGURE 28. Iron 3.9% C ALLOYS DECARBURIZED IN 42.17 % FeO, 3.4 % Fe_2O_3, 25.83 % CaO AND 28.60 % SiO_2 SLAG AT 1300°C.

time (min)	% C
0	3.90
5	3.07
10	2.22
15	1.55
20	1.19

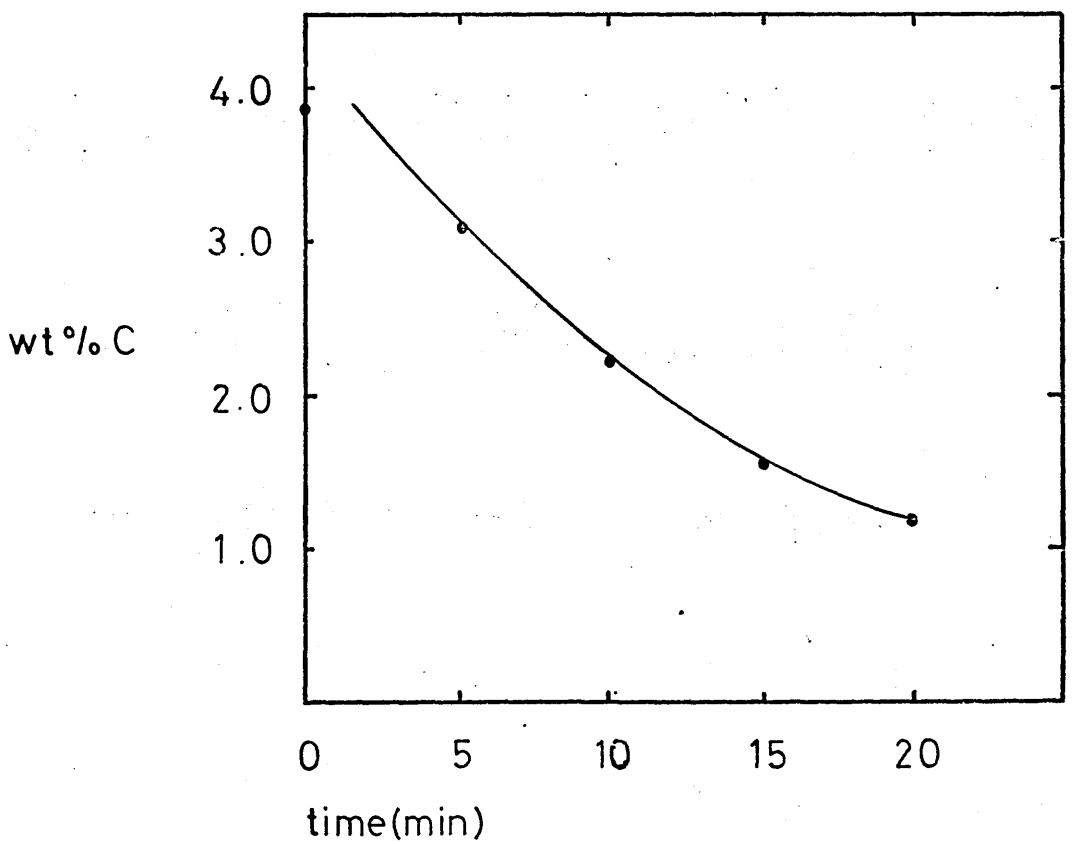
4.0
3.0
2.0
1.0
wt % C
0
5
10
15
20
time(min)

FIGURE 29. SLAG PATHS FOLLOWED BY SLAGS DURING DECARBURIZATION OF IRON - 3.95 %C ALLOYS AT 1300°C. SLAG TO METAL RATIO 30:1.

FIGURE 30. SLAG PATH FOLLOWED BY SLAG DURING DECARBURIZATION OF IRON - 3.9 % C ALLOYS AT 1300°C. SLAG TO METAL RATIO 30:1.

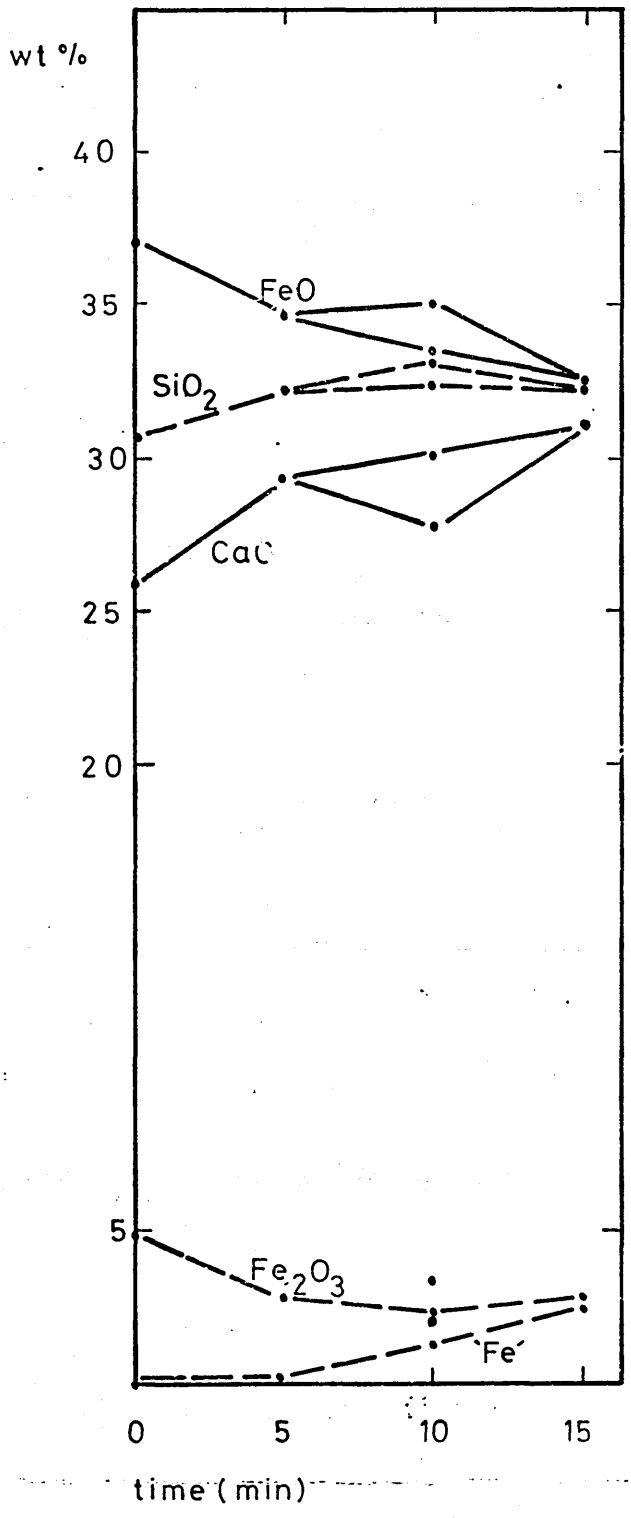
wt %
40
35
30
25
20
5
FeO
SiO2
CaO
Fe2O3
Fe
0
5
10
15
time (min)

Fig. 29

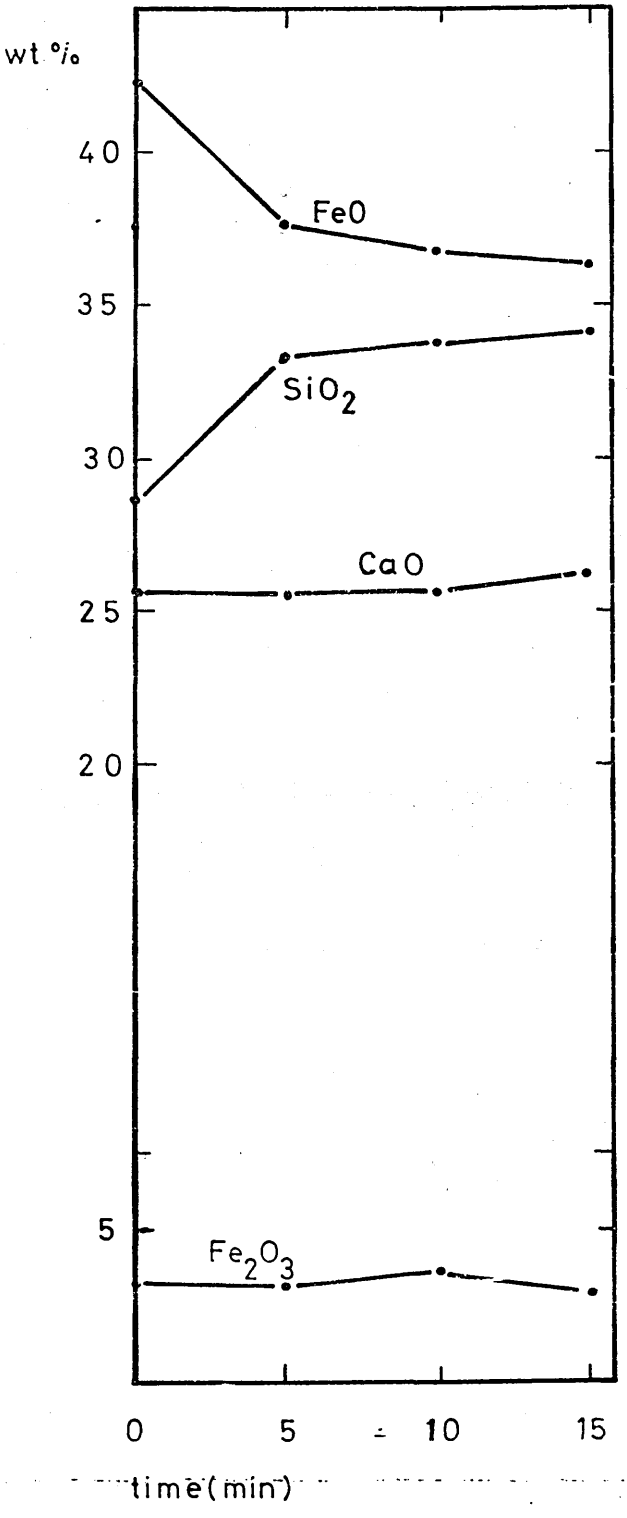
wt %
40
35
30
25
20
5
FeO
SiO2
CaO
Fe2O3
0
5
10
15
time (min)

Fig. 30

FIGURE 31. SLAG PATH FOLLOWED BY SLAG DURING DECARBURIZATION OF IRON - 3.9 % C ALLOYS AT 1300° C. SLAG TO METAL RATIO 30:1.

FIGURE 32. SLAG PATH FOLLOWE BY SLAG DURING DECARBURIZATION OF IRON - 3.95 % C ALLOYS AT 1300°C. SLAG TO METAL RATIO 30:1.

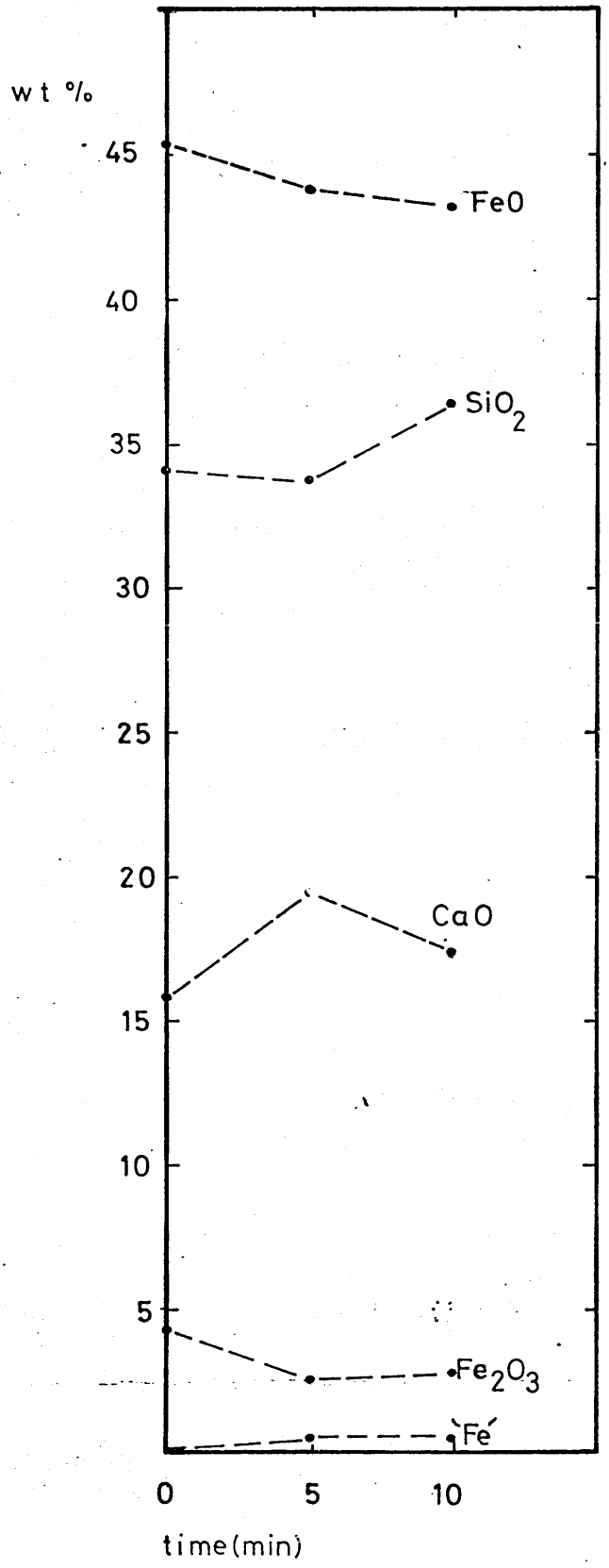
wt %
45
40
35
30
25
20
15
10
5
FeO
SiO2
CaO
Fe2O3
Fe´
0
5
10
time(min)

Fig 31

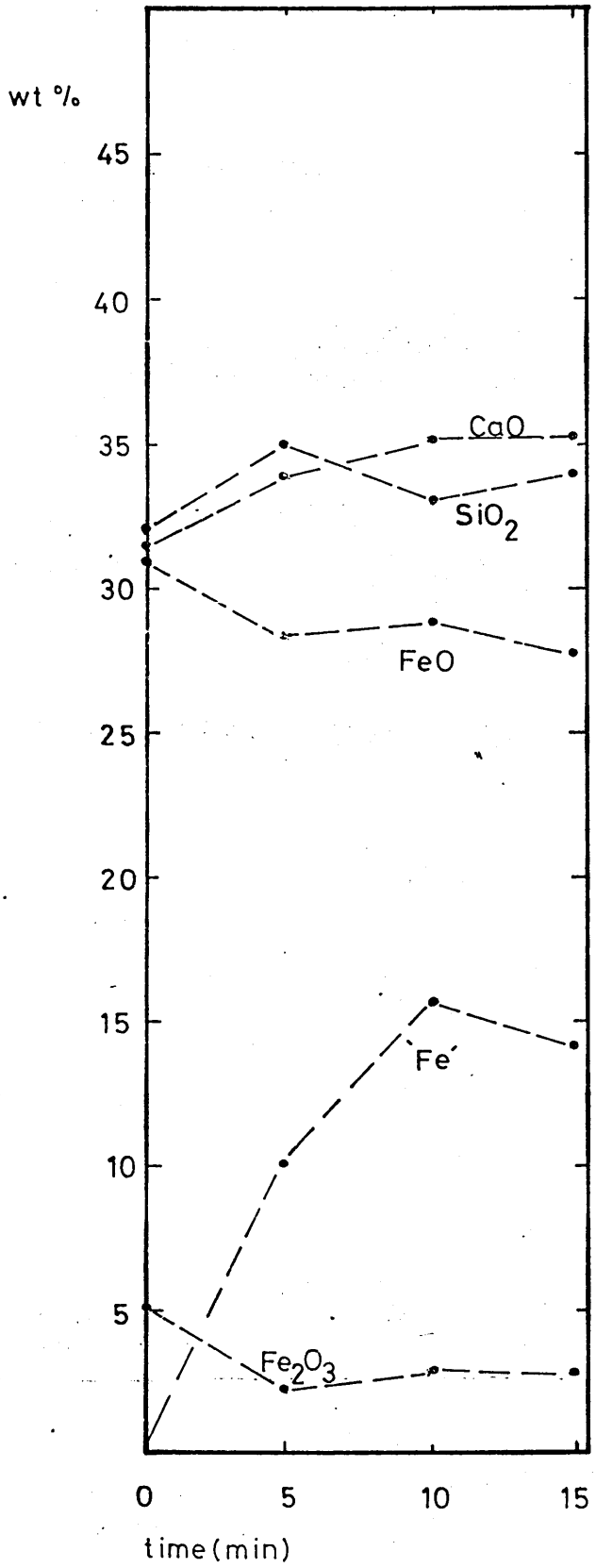
wt %
45
40
35
30
25
20
15
10
5
CaO
SiO2
FeO
Fe´
Fe2O3
0
5
10
15
time(min)

Fig. 32

FIGURE 33. IRON - 3.95 % C ALLOYS DECARBURIZED WITH 31.00 % FeO 4.86 % Fe_2O_3, 31.94 % CaO AND 32.20 % SiO_2 SLAG AT 1300°C.

time (min)	% C
0	3.95
5	3.49
10	2.57
15	1.95

FIGURE 34. IRON - 3.95 % C ALLOYS DECARBURIZED WITH 37.44 %FeO, 5.00 %Fe_2O_3, 26.56 % CaO AND 31.00 % SiO_2 SLAG AT 1300°C .

time (min)	% C
0	3.95
5	3.14
10	2.10
15	1.57
20	1.30

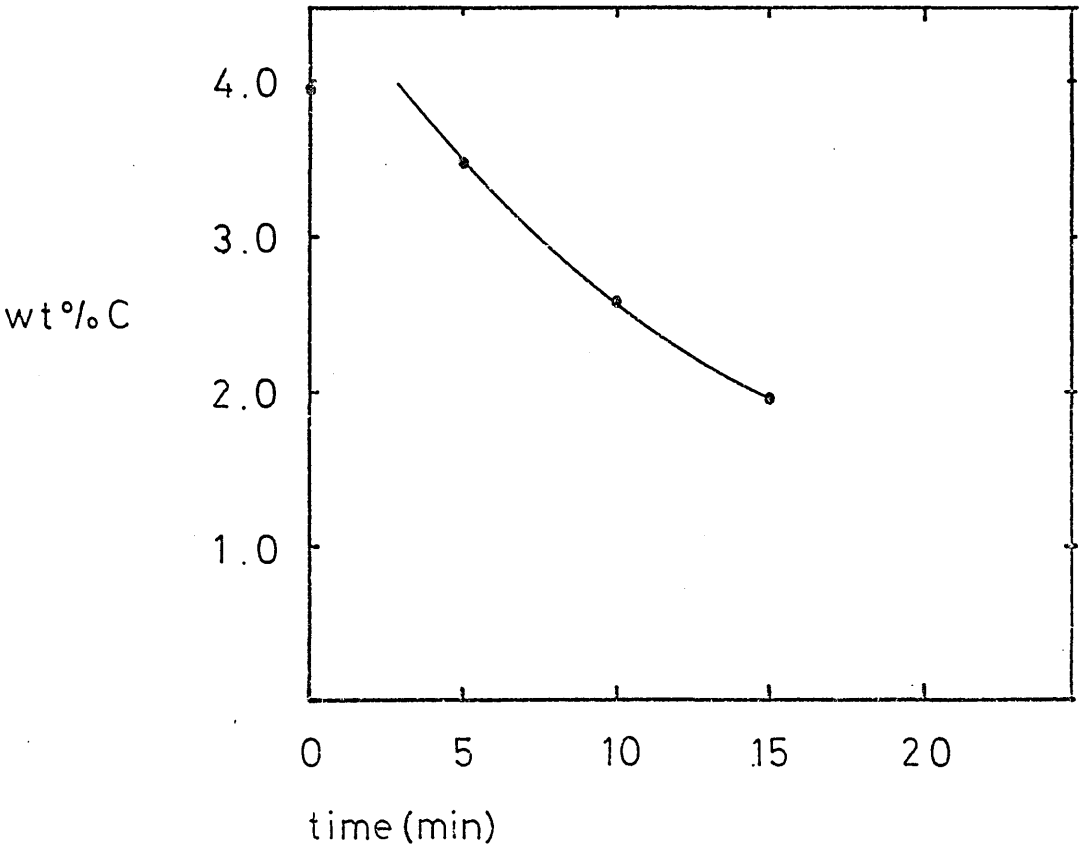
4.0
3.0
2.0
1.0
wt% C
0
5
10
15
20
time (min)

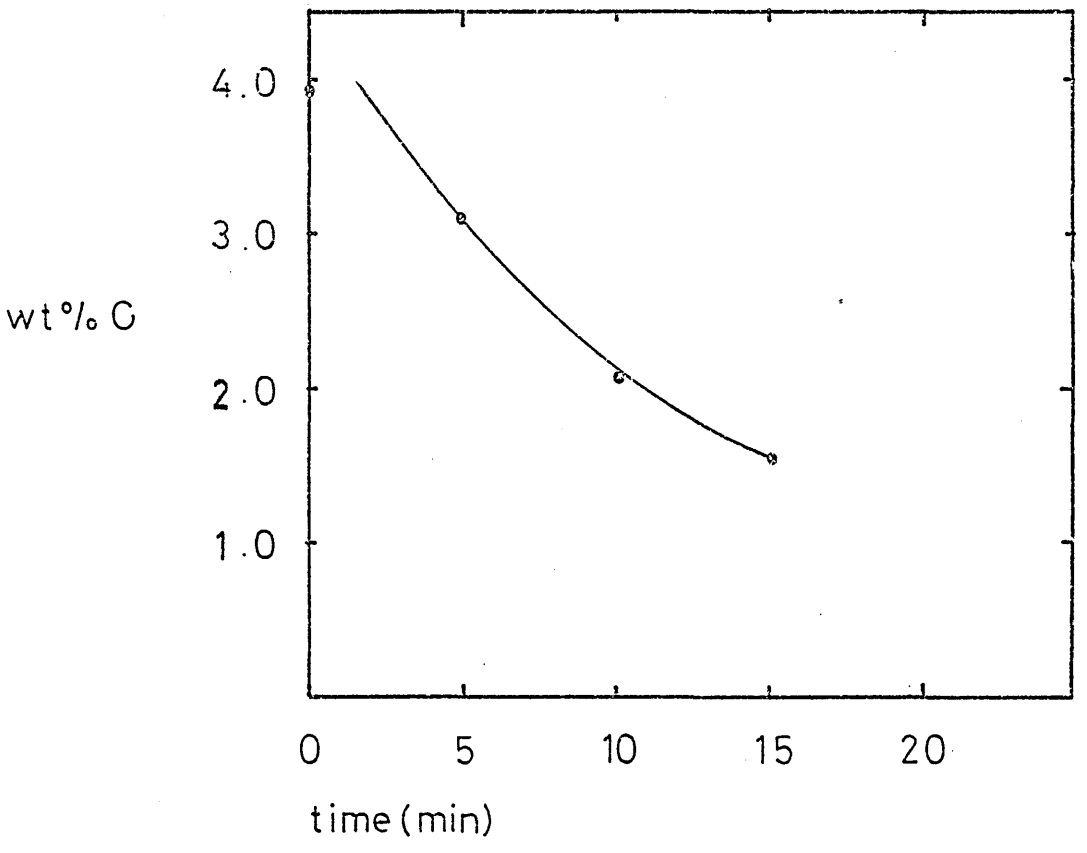
4.0
3.0
2.0
1.0
wt% C
0
5
10
15
20
time (min)

FIGURE 35. IRON - 4.25 % C ALLOYS REACTED WITH 38.34 %FeO, 2.43 %Fe_2O_3, 27.01 % CaO AND 32.22 % SiO_2 SLAG AT 1300°C.

time (min)	% C
0	4.25
4	4.09
6	3.64
8	3.20
10	2.77
12	2.64
14	2.24
16	1.90
18	1.93
20	1.66

FIGURE 36. IRON - 4.02 % C ALLOYS REACTED WITH 39.90 % FeO 3.33 % Fe_2O_3, 25.85 % CaO AND 30.92 % SiO_2 SLAG AT 1300°C.

time (min)	% C
0	4.02
4	3.83
5	3.54
7	2.76
10	2.07
14	1.75
19	1.28
20.5	1.24

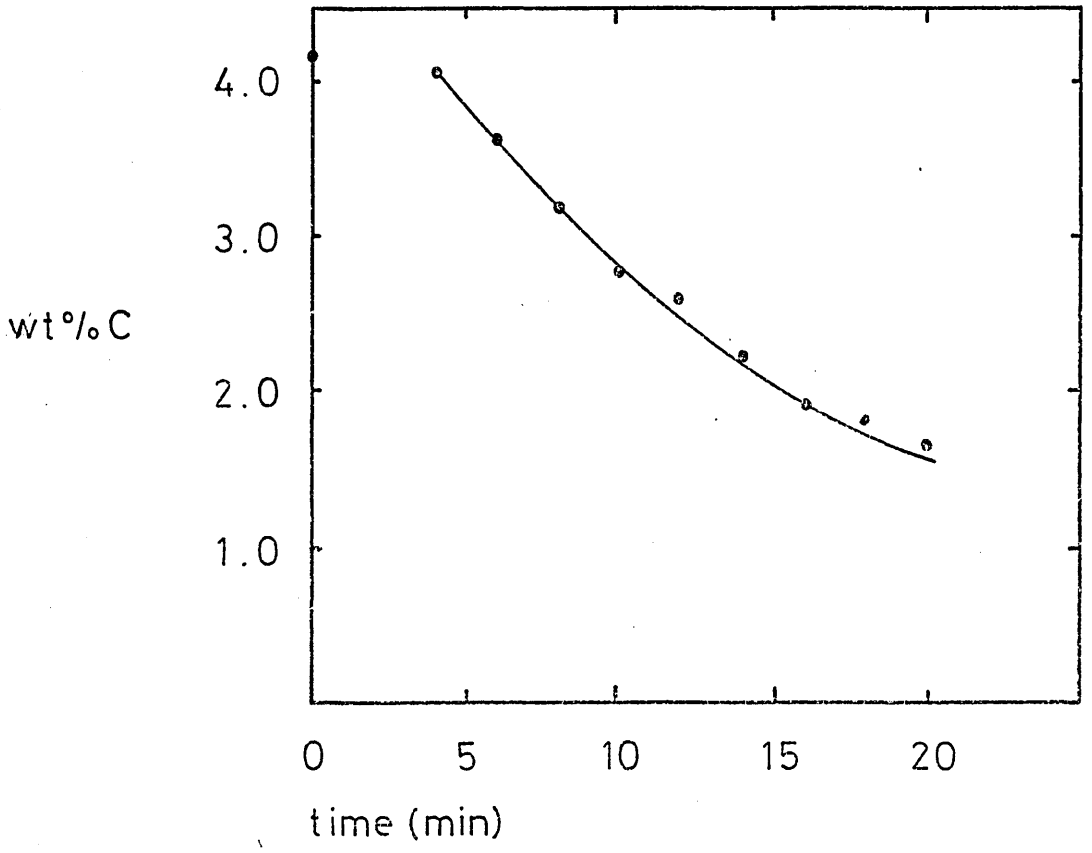
wt % C
4.0
3.0
2.0
1.0
0
5
10
15
20
time (min)

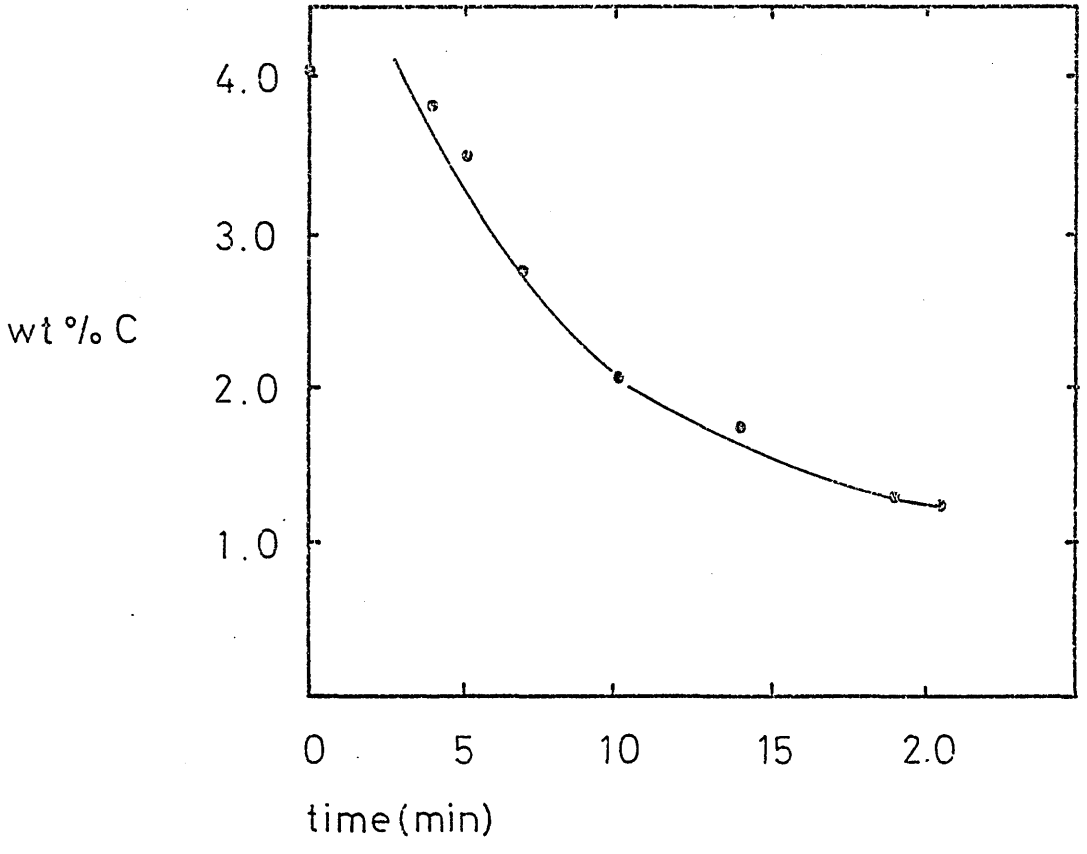
wt % C
4.0
3.0
2.0
1.0
0
5
10
15
2.0
time (min)

FIGURE 37. DIFFERENTIAL THERMAL ANALYSIS FOR AN IRON - CARBON SAMPLE AND CRUCIBLE. PREHEATING SEQUENCE OF 10 MINUTES AT 800°C, 7.5 MINUTES AT 1000°C AND FINAL REACTION TEMPERATURE OF 1300°C. SLAG TO METAL RATIO 30:1. CRUCIBLE HEIGHT 80 mm.

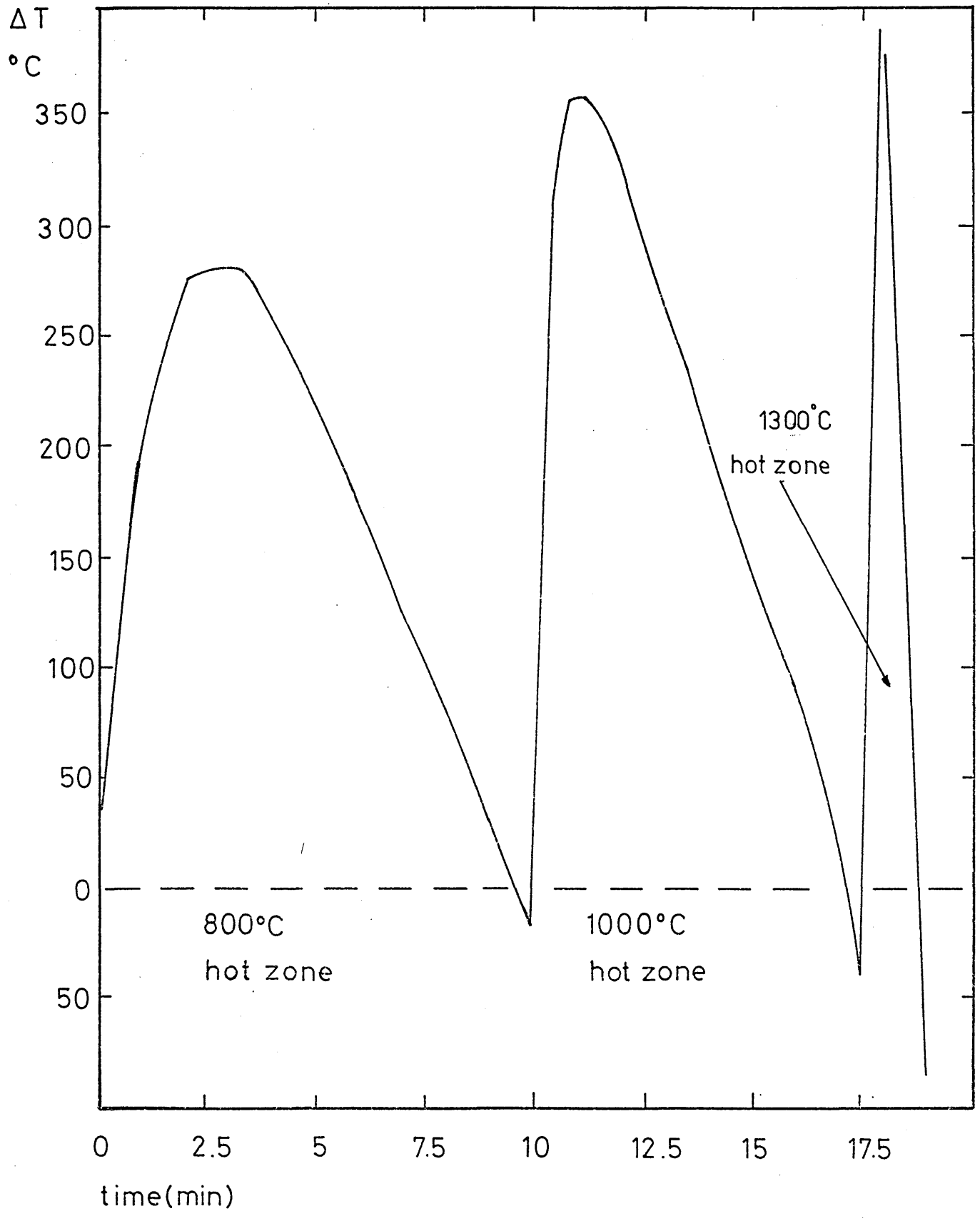
ΔT
°C
350
300
250
200
150
100
50
0
50
1300°C
hot zone
800°C
hot zone
1000°C
hot zone
0
2.5
5
7.5
10
12.5
15
17.5
time(min)

FIGURE 38. IRON - 4.26 % C ALLOYS DECARBURIZED IN FAYALITE SLAG AT 1400°C.

time (min)	% C
0	4.26
2	4.21
3	4.20
4	4.06
5	3.85
5	3.40
7	3.09
8	2.12
8	2.88
10	1.34
12	1.71
15	1.68

FIGURE 39. IRON - 4.3 % C ALLOYS DECARBURIZED WITH 53.03 %FeO, 2.97 % Fe_2O_3, 14.32 % CaO AND 29.68 % SiO_2 SLAG AT 1400°C.

time (min)	% C	time (min)	% C
0.0	4.30	5.0	3.30
2.0	3.95	7.0	3.35
2.5	4.00	7.5	3.15
3.5	3.5	8.0	1.56
4.0	3.37		
5.0	3.42		

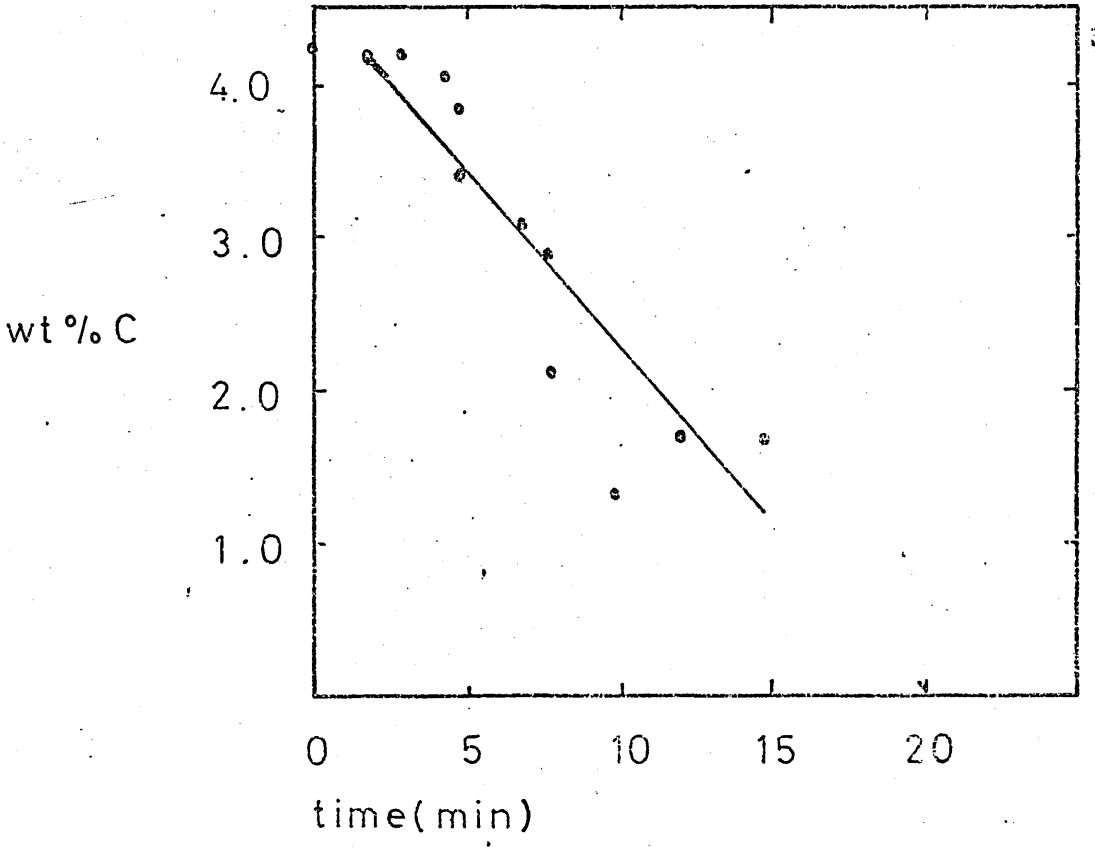
4.0
3.0
2.0
1.0
wt % C
0
5
10
15
20
time(min)

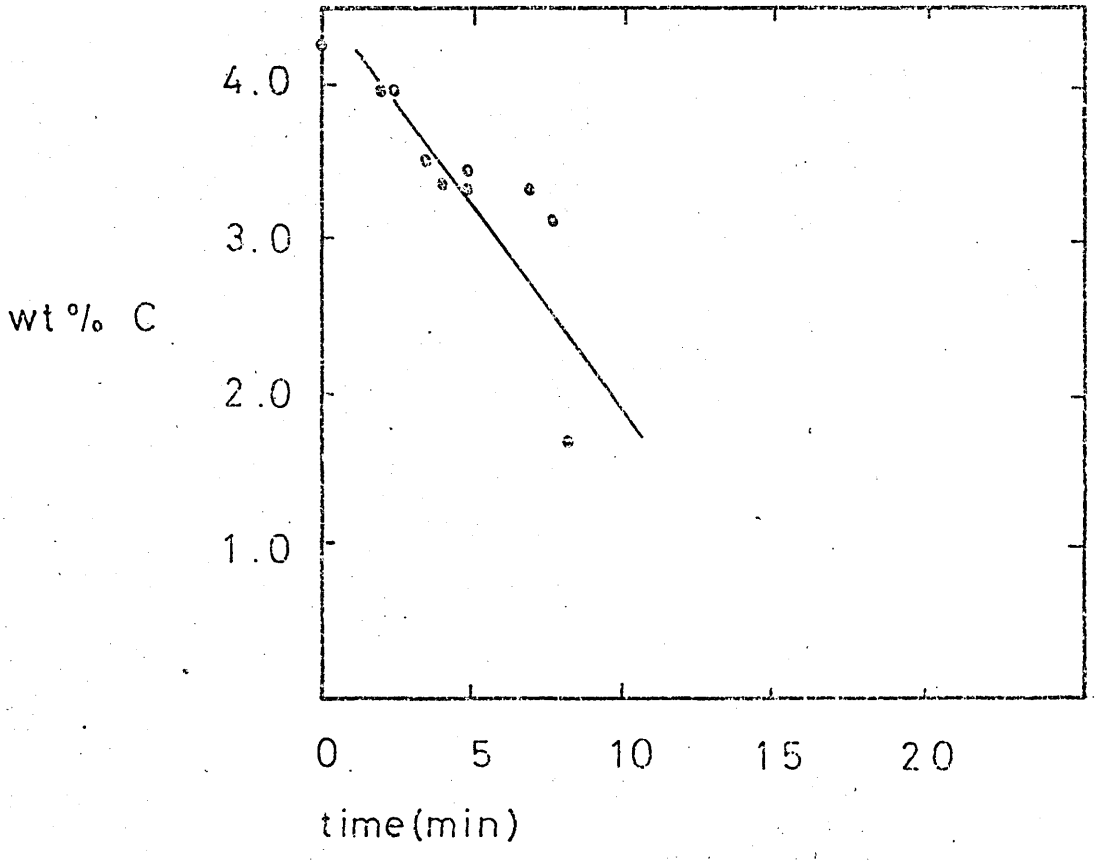
4.0
3.0
2.0
1.0
wt % C
0
5
10
15
20
time(min)

FIGURE 40. IRON - 4.02 % C ALLOYS DECARBURIZED IN 31.00 % FeOm 4.86 % Fe_2O_3, 31.94 % CaO AND 32.20 % SiO_2 SLAG AT 1400°C.

time (min)	%C
0	4.02
2	3.85
4	3.30
6	2.70
8	1.82
9	1.60
10	1.10

FIGURE 41. IRON - 4.35 % C ALLOYS DECARBURIZED IN 39.90 % FeO, 3.33 % Fe_2O_3, 25.85% CaO AND 30.92 % SiO_2 SLAG AT 1400°C.

time (min)	%C
0	4.35
2	4.20
3	3.92
3	3.80
4	3.77
5	3.12
6	2.80
7	2.63
10	1.26
12	1.10

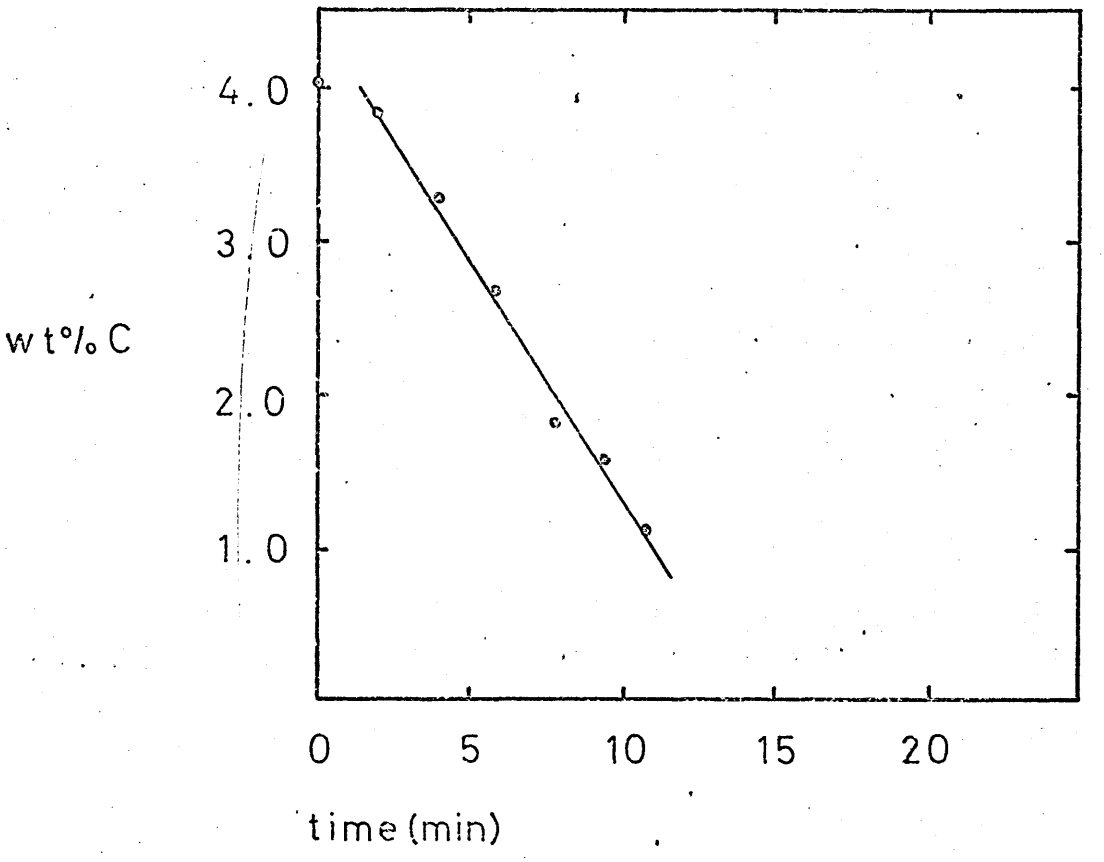
4.0
3.0
2.0
1.0
wt% C
0
5
10
15
20
time (min)

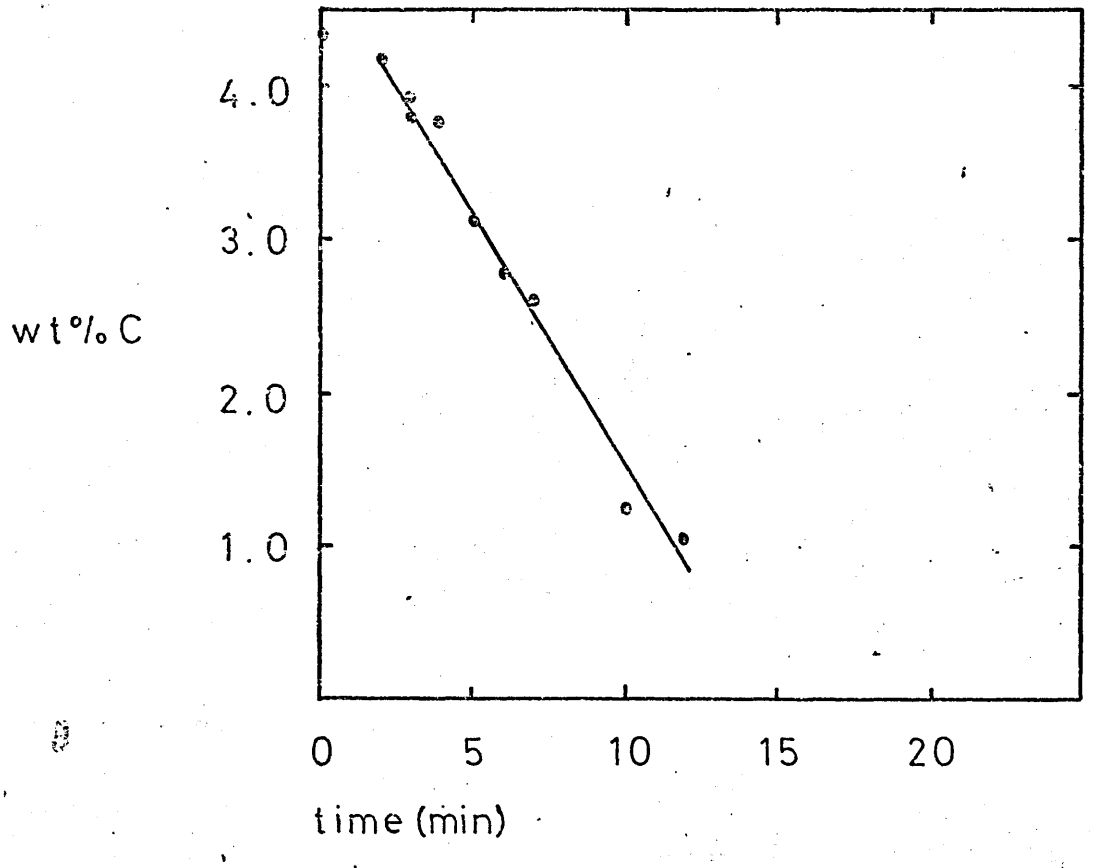
4.0
3.0
2.0
1.0
wt% C
0
5
10
15
20
time (min)

FIGURE 42. IRON - 4.26 % C ALLOYS DECARBURIZED WITH FAYALITE AT 1500°C.

time (min)	% C
0.0	4.26
1.0	4.08
1.5	4.16
2.5	4.08
4.0	3.54
7.0	3.49
9.0	3.26

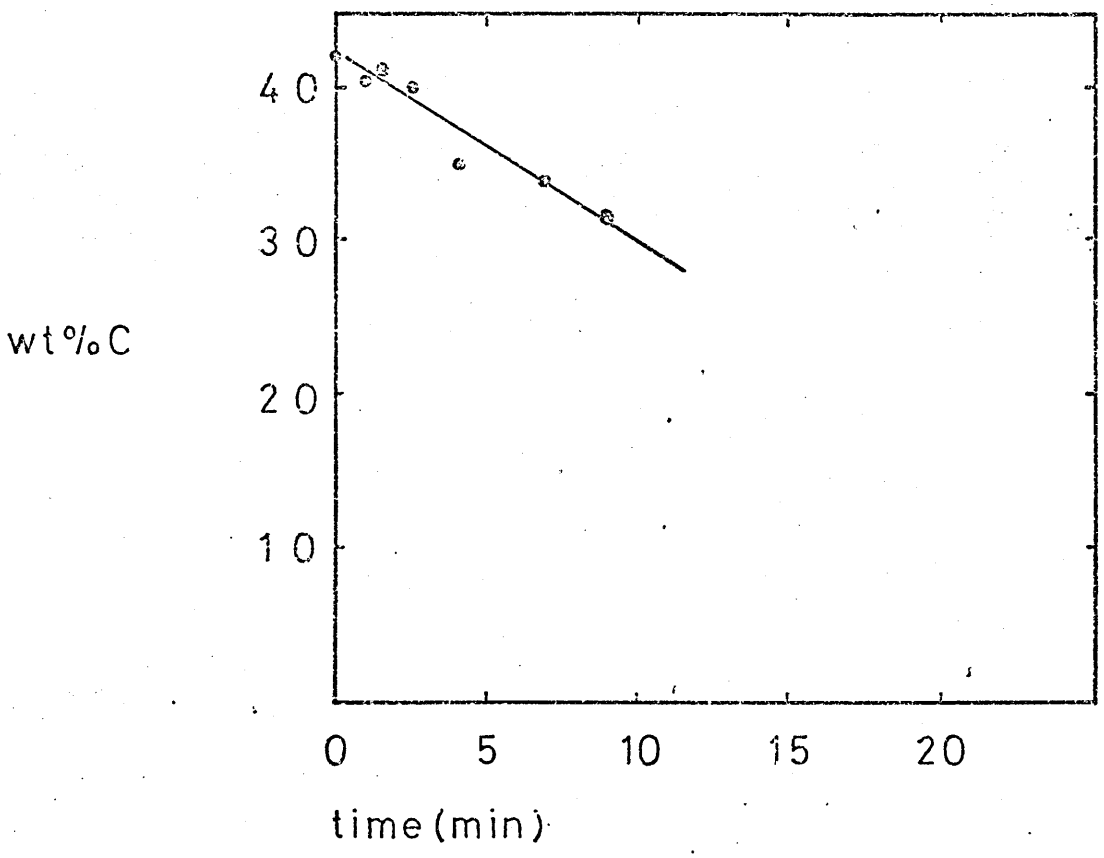
wt%C
40
30
20
10
0
5
10
15
20
time (min)

FIGURE 43. IRON - 4.26% C ALLOYS DECARBURIZED IN 40.02 % FeO, 2.17 % Fe_2O_3, 28.05 % CaO AND 29.76 % SiO_2 SLAG at 1500°C.

time (min)	% C
0	4.26
5	2.15
7	0.98
9	0.98
12	0.87

FIGURE 44. IRON - 4.12 % C ALLOYS DECARBURIZED IN 47.89 % FeO, 1.85 % Fe_2O_3, 20.68 % CaO AND 29.60 % SiO_2 SLAG AT 1500°C.

time (min)	% C	time (min)	% C
0	4.12	12	1.70
5	1.69	13	1.15
7	2.22	15	1.52
10	1.50		
11	1.68		

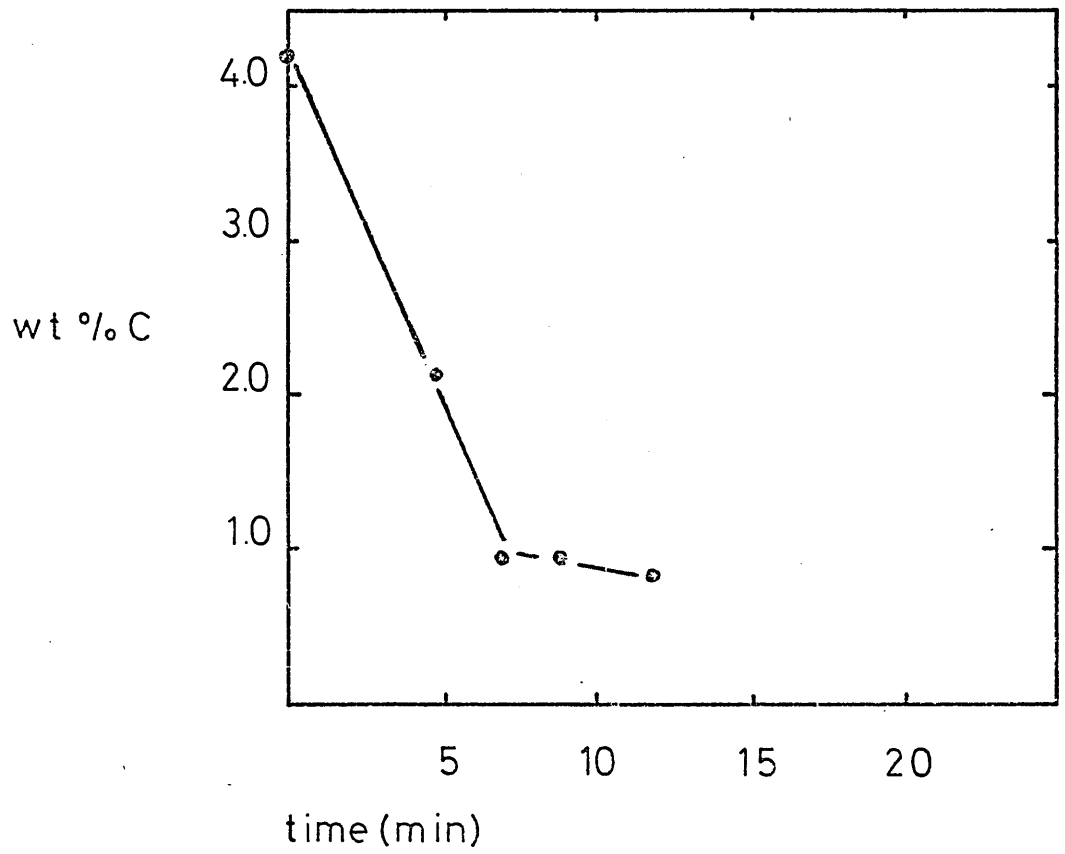
4.0
3.0
2.0
1.0
wt % C
5
10
15
20
time (min)

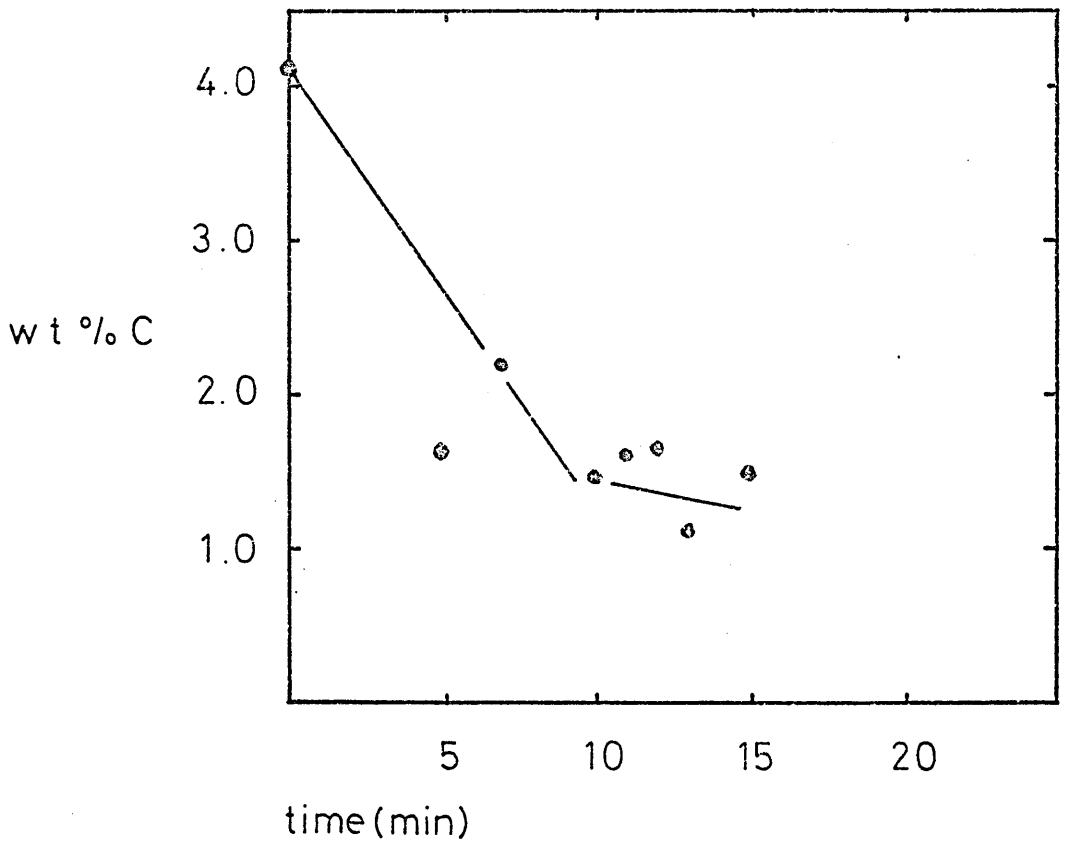
4.0
3.0
2.0
1.0
wt % C
5
10
15
20
time (min)

FIGURE 45. CRUCIBLE ASSEMBLY FOR 1500°C AND 1600°C EXPERIMENTS INSIDE MF INDUCTION FURNACE.

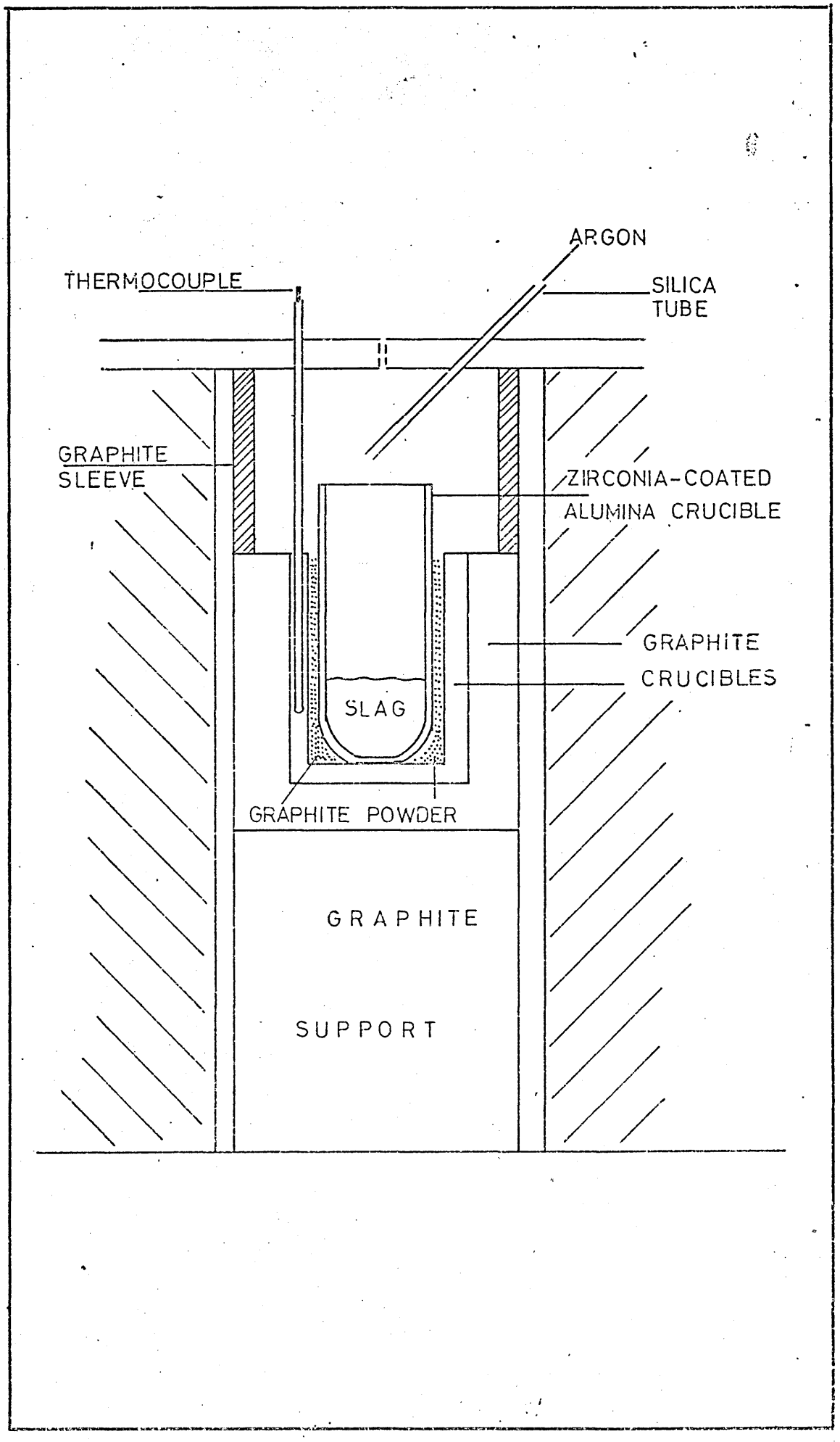
ARGON
THERMOCOUPLE
SILICA TUBE
GRAPHITE SLEEVE
ZIRCONIA-COATED ALUMINA CRUCIBLE
GRAPHITE CRUCIBLES
SLAG
GRAPHITE POWDER
GRAPHITE SUPPORT

FIGURE 46. IRON - 4.08 % C ALLOYS DECARBURIZED AT 1600°C IN 47.89 % FeO, 1.85 % Fe_2O_3, 20.68 % CaO AND 29.60 % SiO_2 SLAG.

time (min)	% C
0.0	4.08
1min 24 sec	2.45
2 min 14 sec	3.08
3 min	2.28

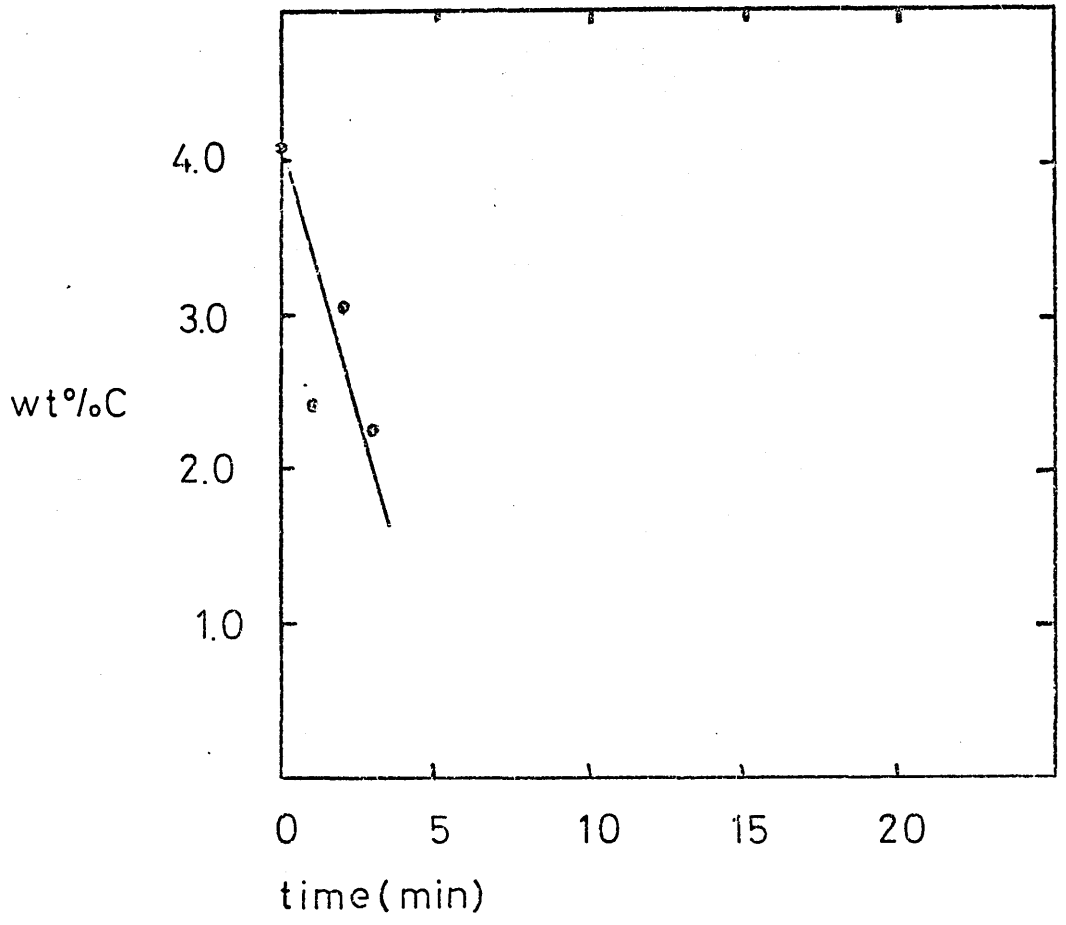
4.0
3.0
2.0
1.0
wt%C
0
5
10
15
20
time(min)

FIGURE 47. IRON - 4.16 % C ALLOYS DECARBURIZED IN FAYALITE SLAG AT 1300°C WITH ARGON BUBBLING AT 75 cc/min.

time (min)	% C
0	4.16
4	3.78
7	3.66
9	3.25
12	2.89
15	2.88
15	2.66

FIGURE 48. IRON - 4.16 % C ALLOYS DECARBURIZED IN 39.90 % FeO, 3.33 % Fe_2O_3, 25.85 % CaO AND 30.92 % SiO_2 SLAG AT 1300°C WITH ARGON BUBBLING AT 75 cc / min.

time (min)	% C
0	4.16
3	3.90
5	3.19
7	2.52
8	2.14
10	1.70
12	1.52
14	1.26

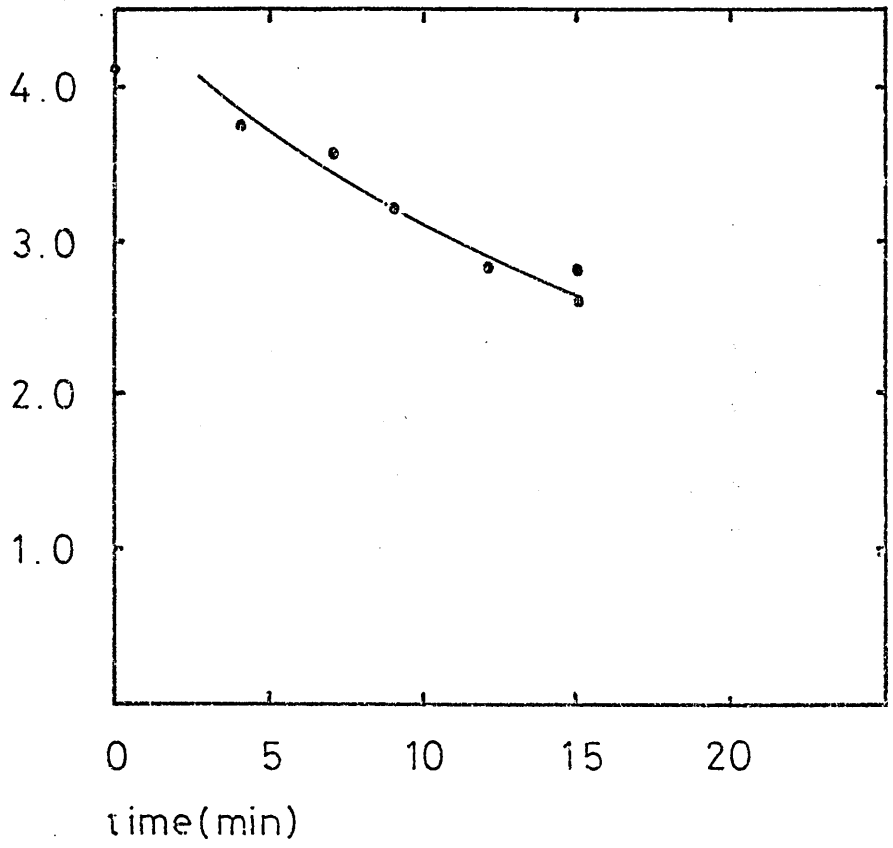
4.0
3.0
2.0
1.0
wt % C
0
5
10
15
20
time (min)

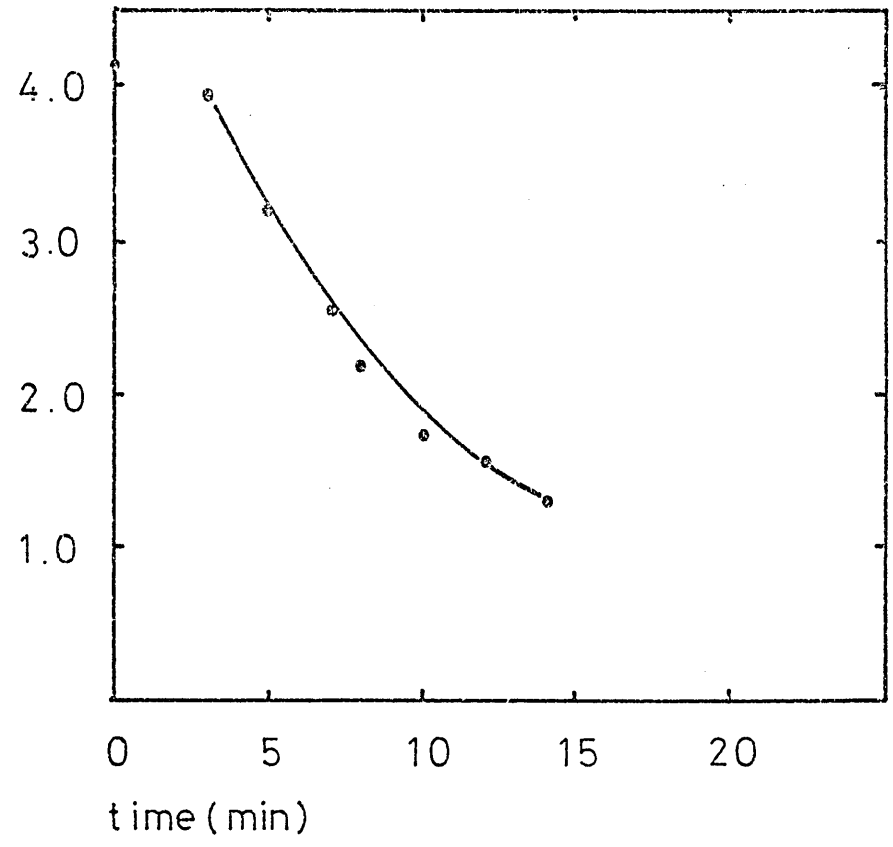
4.0
3.0
2.0
1.0
wt % C
0
5
10
15
20
time (min)

FIGURE 49. IRON - 4.16 % C ALLOYS DECARBURIZED IN 40.02 % FeO, 2.17 % Fe_2O_3, 28.05 % CaO AND 29.76 % SiO_2 SLAG AT 1300°C WITH ARGON - 5 % CO_2 GAS LANCING.

time (min)	% C
0	4.16
3	3.88
5	3.21
7	2.65
7	2.82
9	1.80
9	2.32
12.5	1.80
15.75	1.27

FIGURE 50. IRON - 4.0 % C ALLOYS DECARBURIZED IN SLAG OF EQUIVALENT CHEMICAL COMPOSITION AS ABOVE. REACTION TEMPERATURE OF 1300°C AND PURE CO_2 GAS INJECTED.

time (min)	% C	time (min)	% C
0	4.0	15	1.55
5	2.92	19	1.43
6	3.25		
7.5	2.43		
9	2.15		
9	2.10		
10	2.22		
11	1.95		
12.5	1.79		

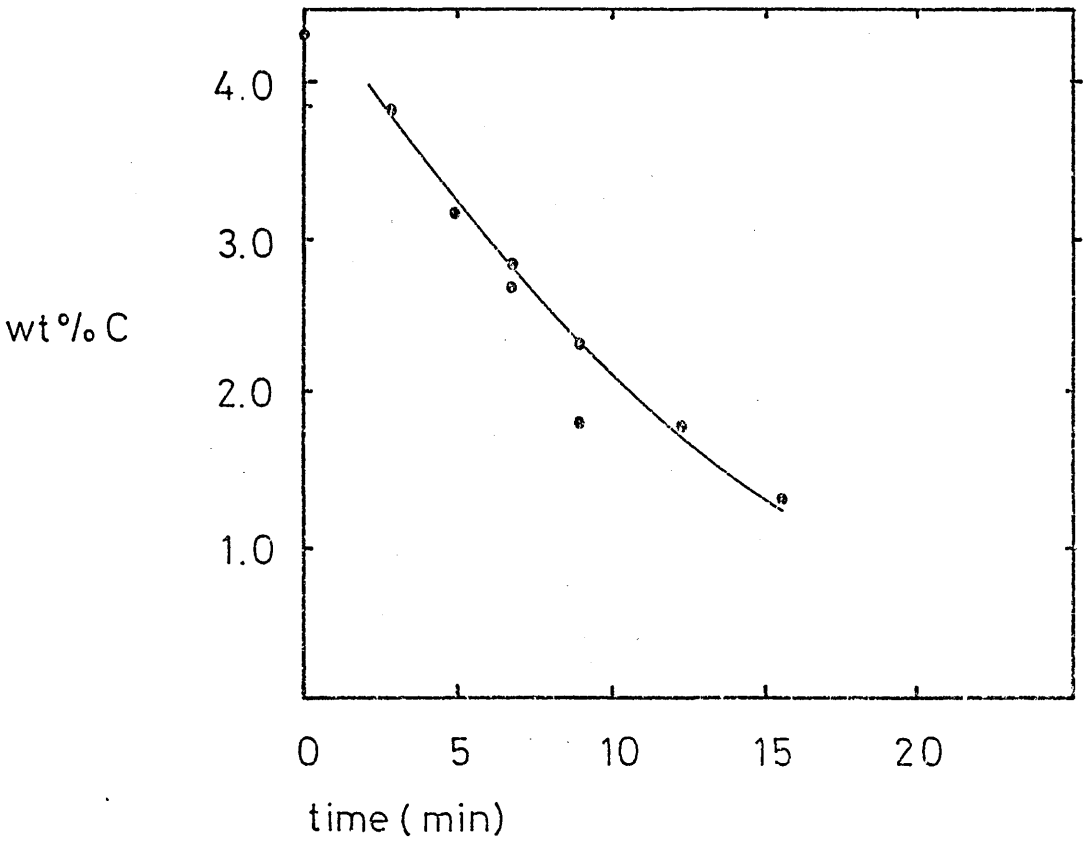
wt % C
4.0
3.0
2.0
1.0
0
5
10
15
20
time (min)

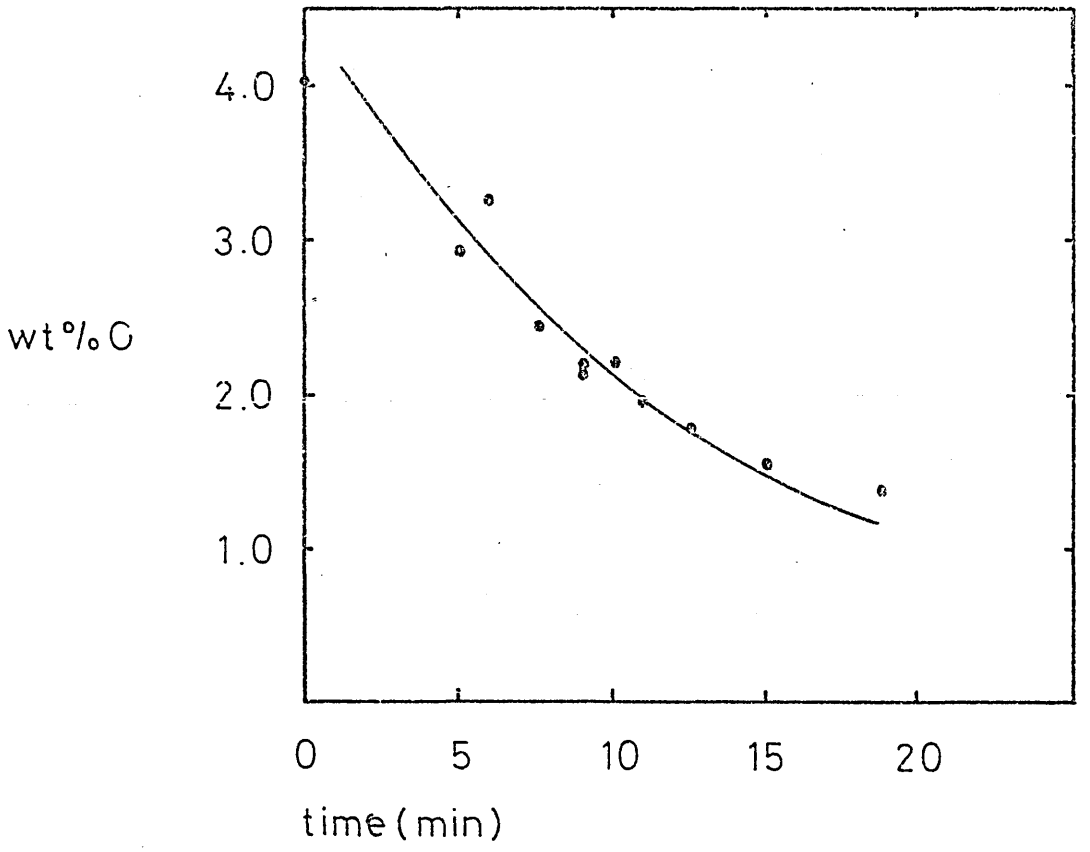
wt % C
4.0
3.0
2.0
1.0
0
5
10
15
20
time (min)

FIGURE 51. IRON - 4.0 % C ALLOYS DECARBURIZED IN 40.02 % FeO, 2.17 % Fe_2O_3, 28.05 % CaO AND 29.76 % SiO_2 SLAG AT 1300°C WITH ARGON - 1 % O_2 GAS LANCING.

time (min)	% C
0	4.0
4	3.56
6	3.16
8	2.68
8	2.95
10	2.22
13	1.66
16	1.34
20	0.91

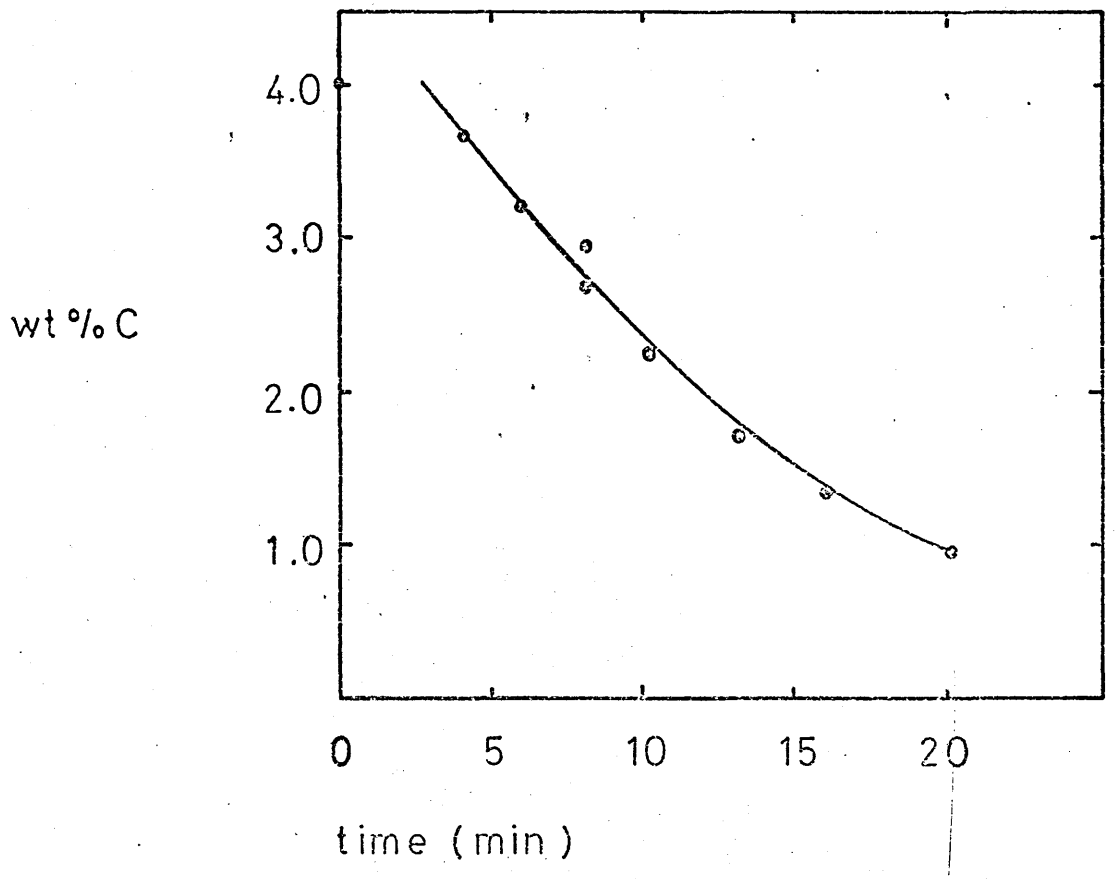
4.0
3.0
2.0
1.0
wt % C
0
5
10
15
20
time (min)

FIGURE 52. QUALITATIVE ENERGY DISPERSE ANALYSIS FOR AN UNREACTED IRON - CARBON SAMPLE.

FIGURE 53. QUALITATIVE ENERGY DISPERSE ANALYSIS FOR Si, Ca AND Fe FOR SLAG U-2 GIVEN IN APPENDIX III.

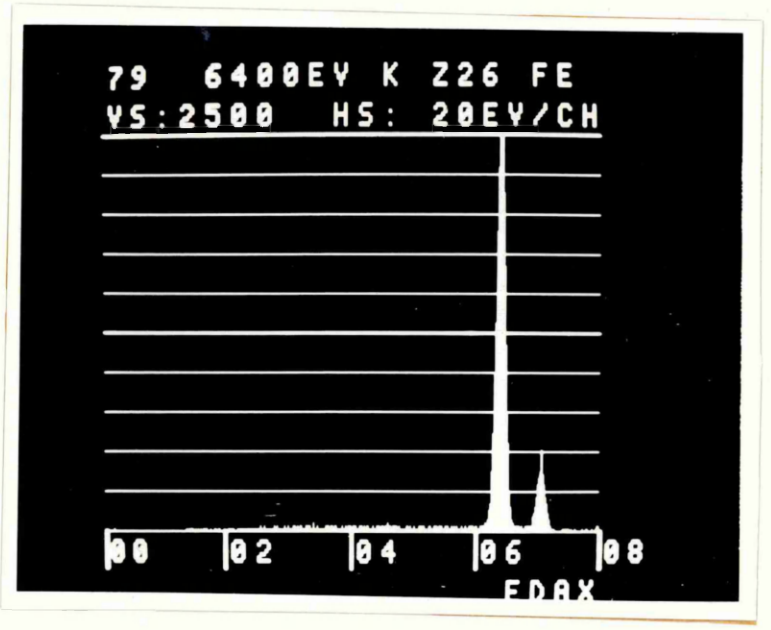
79 6400EV K Z26 FE
VS:2500 HS: 20EV/CH
00
02
04
06
08
EDAX

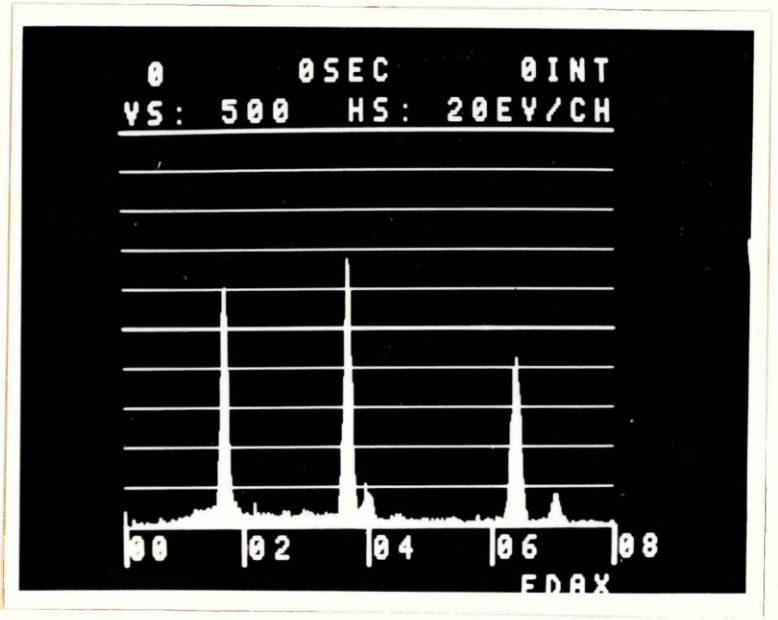
0 0SEC 0INT
VS: 500 HS: 20EV/CH
00
02
04
06
08
EDAX

FIGURE 54. FRACTURED INTERFACE FROM REACTED DROPLET PHOTOGRAPH FROM SCANNING ELECTRON MICROSCOPE.

FIGURE 55. X-RAY MAPPING FOR CALCIUM FROM SCANNING ELECTRON MICROSCOPE. THE AREA CORRESPONDS TO THAT OF FIGURE 54.

FIGURE 56. X - RAY MAPPING FOR SILICON FROM SCANNING ELECTRON MICROSCOPE. THE AREA CORRESPONDS TO THAT OF FIGURE 54.

FIGURE 57. STREAMLINES FOR HANDLOS AND BARON MODEL FOR INTERNALLY CIRCULATING DISPERSED PHASE. TURBULENT FLOW REGIME (142).

FIGURE 58. FIRST CASE OF MASS TRANSPORT AT THE INTERFACE. MASS TRANSPORT CONTROL IN DISPERSED (METAL) PHASE.

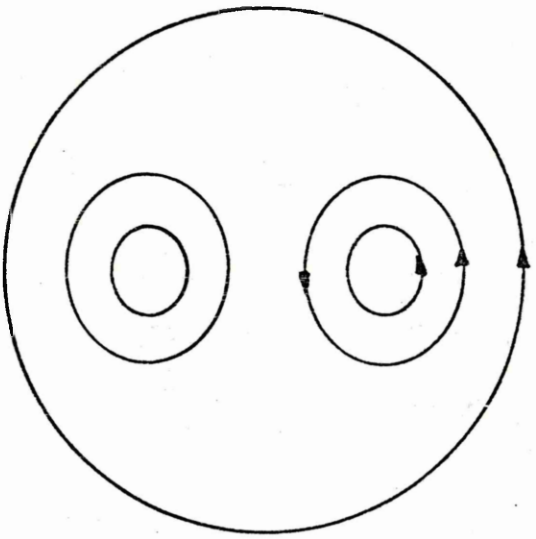

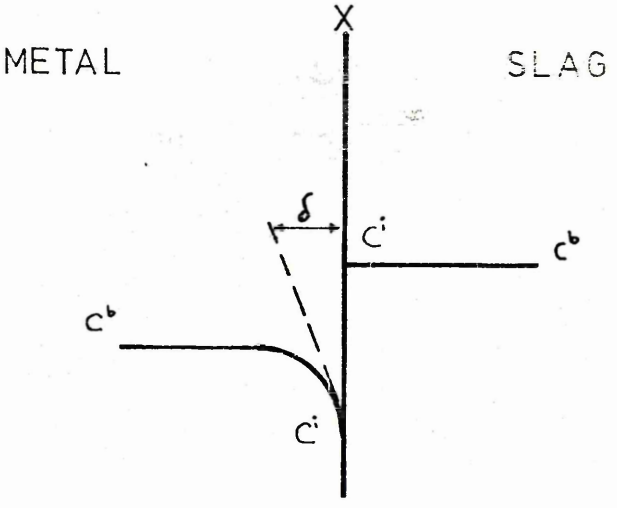
METAL
SLAG
X
δ
C^i
C^b
C^b
C^i

FIGURE 59a. GRAPHICAL SOLUTION OF FICKS SECOND LAW (EQUATION 5.5.1.2) FOR: Dc = 4.5 x 10^{-5} cm^2/sec, a = 0.4 cm, Co = 4.25% C, Cs = 0, r/a = 0.2, 0.4 and 0.8,

FOR n = 1

time (sec)	r/a = 0.2	r/a = 0.4	r/a = 0.8
0	7.95	6.41	1.99
100	6.04	4.88	1.49
200	4.59	3.69	1.15
300	3.45	2.80	0.85
400	2.64	2.12	0.64
600	1.53	1.23	0.38
900	0.64	0.53	0.17
1200	0.30	0.23	0.09

FOR n = 2

time (sec)	r/a = 0.2	r/a = 0.4	r/a = 0.8
0	1.53	4.46	3.61
100	3.92	4.20	2.04
200	3.87	3.48	1.32
300	3.23.	2.72	0.94
400	2.55	2.08	0.68
600	1.49	1.23	0.38
900	0.64	0.53	0.17
1200	0.30	0.23	0.09

FOR n = 3

time (sec)	r/a = 0.2	r/a = 0.4	r/a = 0.8
0	5.82	3.10	4.67
100	4.25	4.11	2.12
200	3.91	3.47	1.32
300	3.23	2.72	0.94
400	2.55	2.08	0.68
600	1.49	1.23	0.38
900	0.64	0.53	0.17
1200	0.30	0.23	0.09

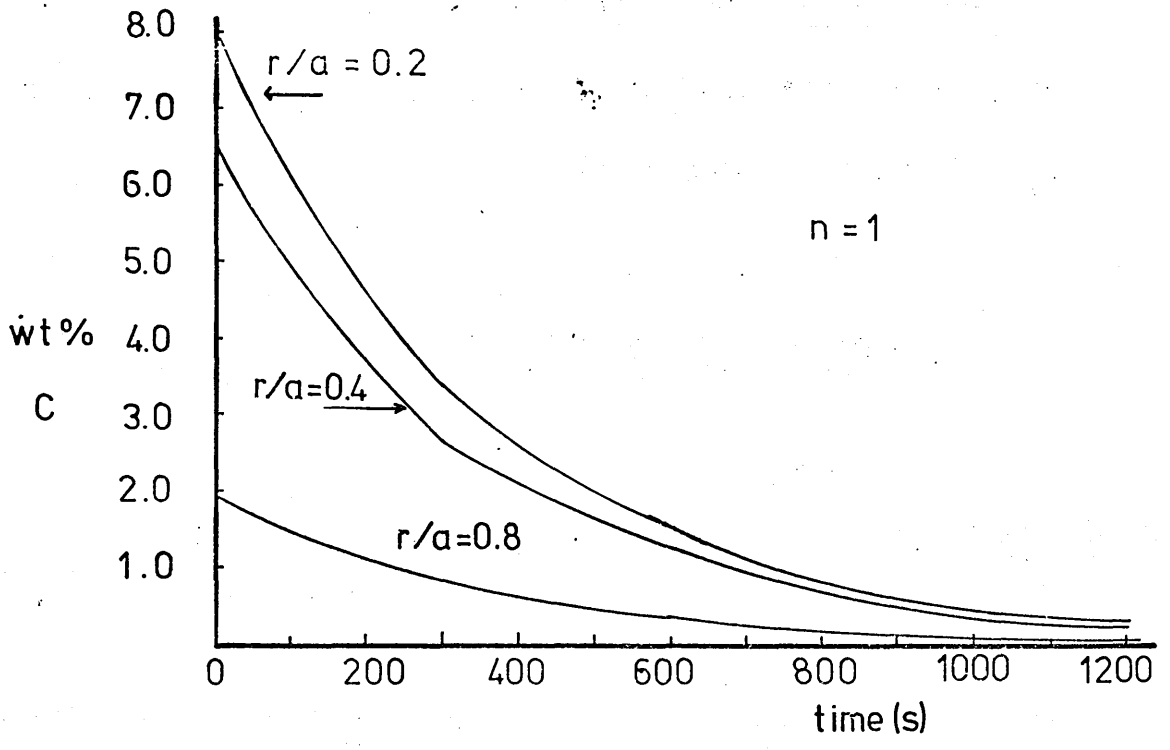
8.0
7.0
6.0
5.0
4.0
3.0
2.0
1.0
wt%
C
r/a = 0.2
r/a=0.4
r/a=0.8
n = 1
0
200
400
600
800
1000
1200
time (s)

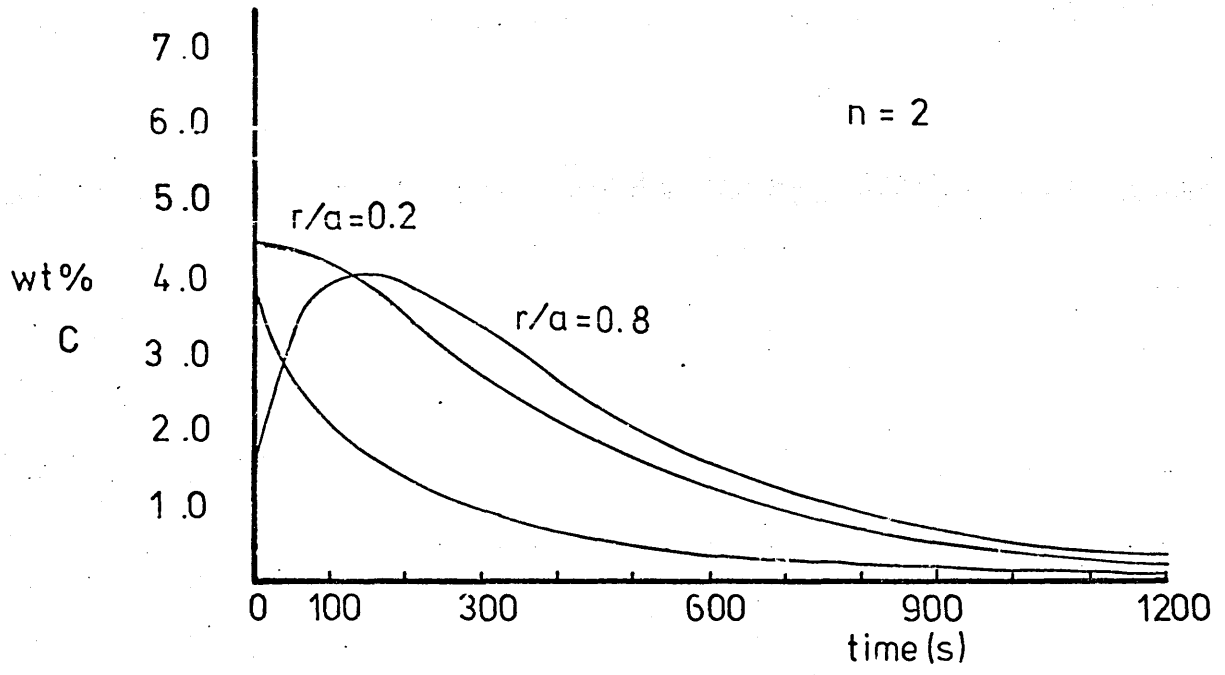
7.0
6.0
5.0
4.0
3.0
2.0
1.0
wt%
C
n = 2
r/a=0.2
r/a=0.8
0
100
300
600
900
1200
time (s)

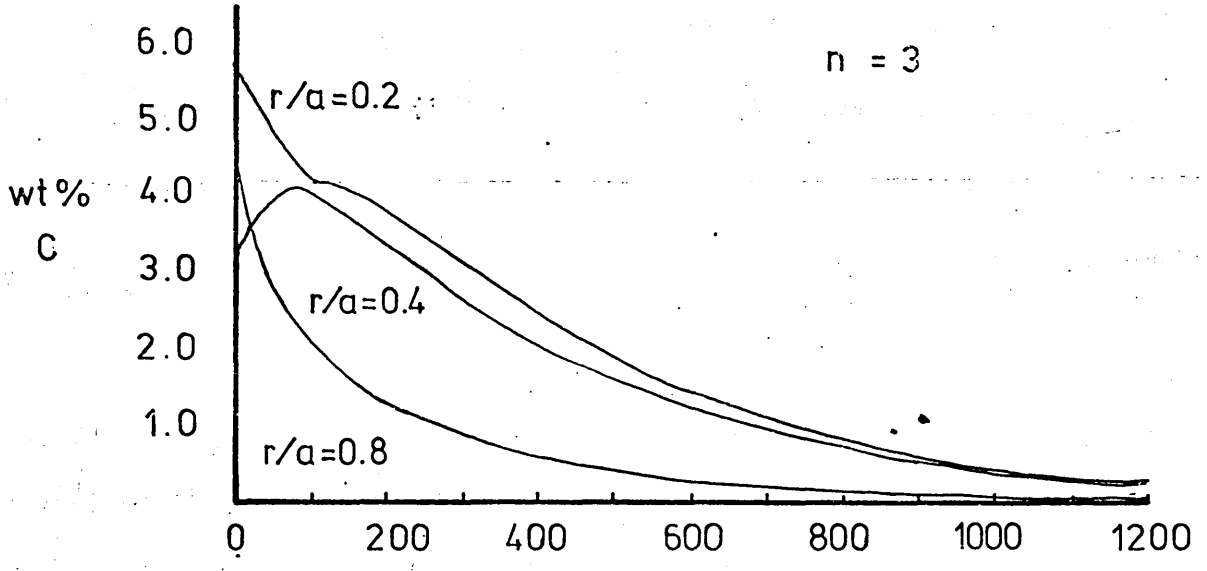
6.0
5.0
4.0
3.0
2.0
1.0
wt%
C
n = 3
r/a=0.2
r/a=0.4
r/a=0.8
0
200
400
600
800
1000
1200

FIGURE 59b.

GRAPHICAL SOLUTION OF FICKS SECOND LAW (EQUATION 5.5.1.2) CALCULATED FROM RESULTS GIVEN IN FIGURE 59a.

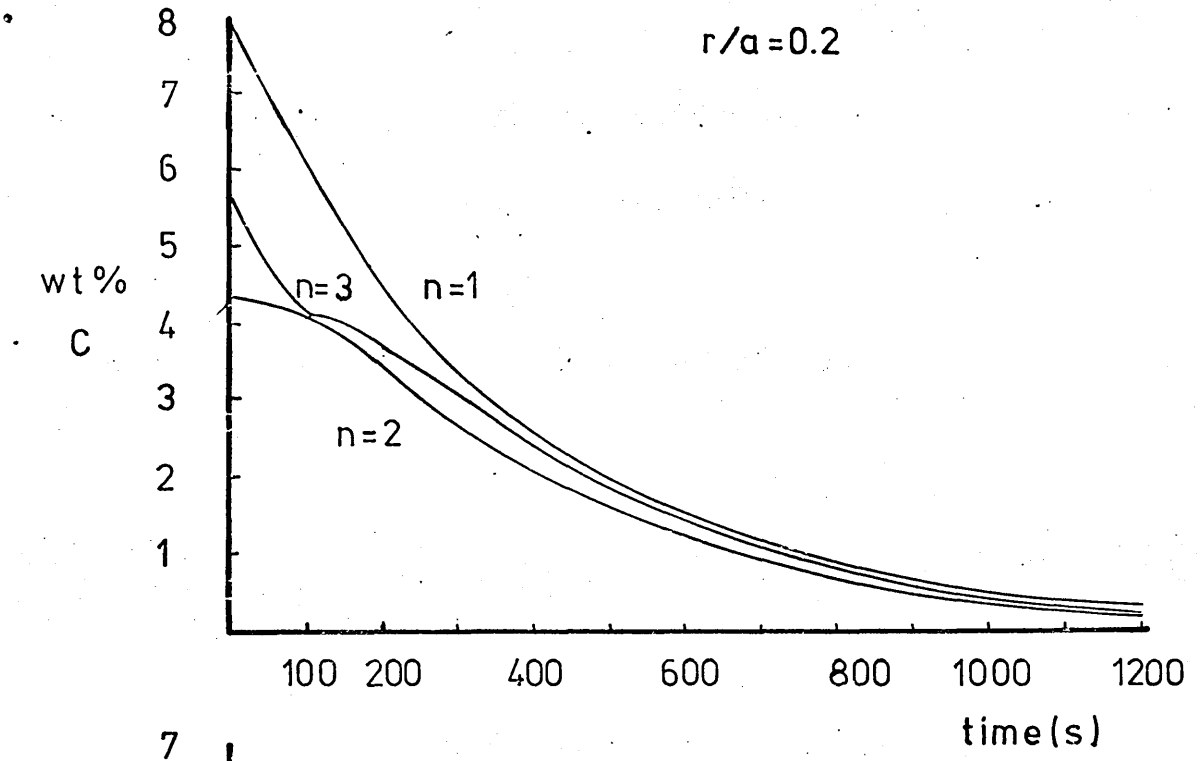
r/a = 0.2
wt %
C
8
7
6
5
4
3
2
1
n=3
n=1
n=2
100
200
400
600
800
1000
1200
time(s)

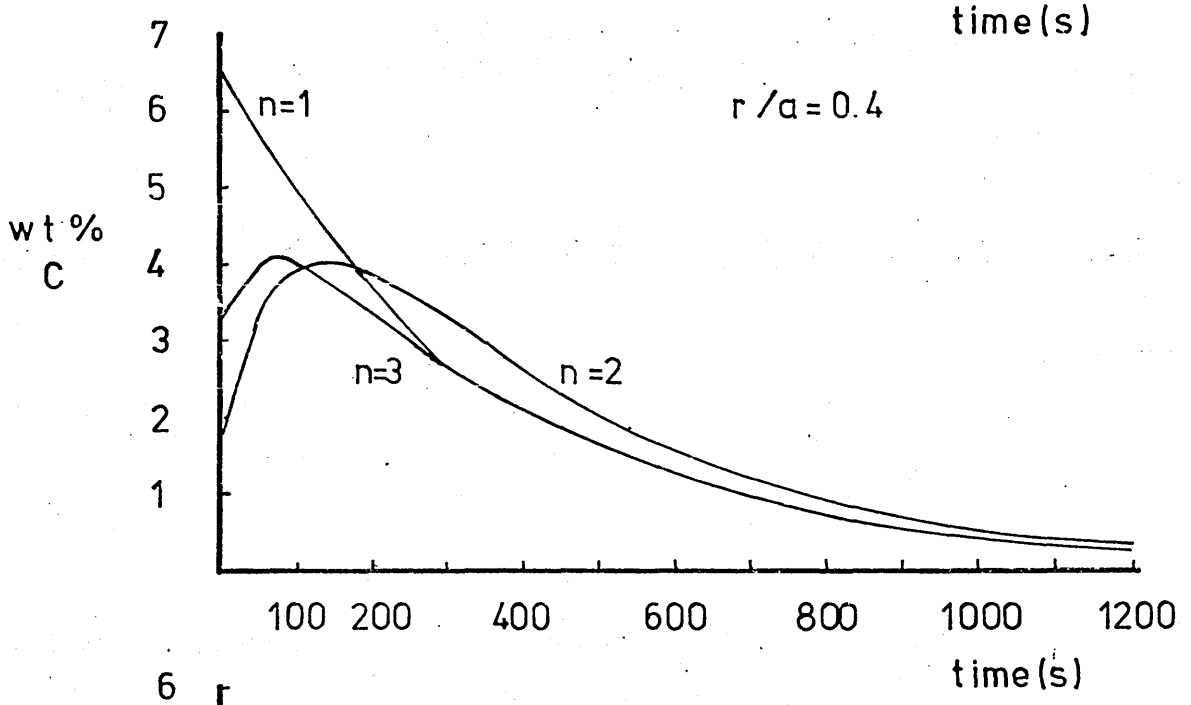
r/a = 0.4
wt %
C
7
6
5
4
3
2
1
n=1
n=3
n=2
100
200
400
600
800
1000
1200
time(s)

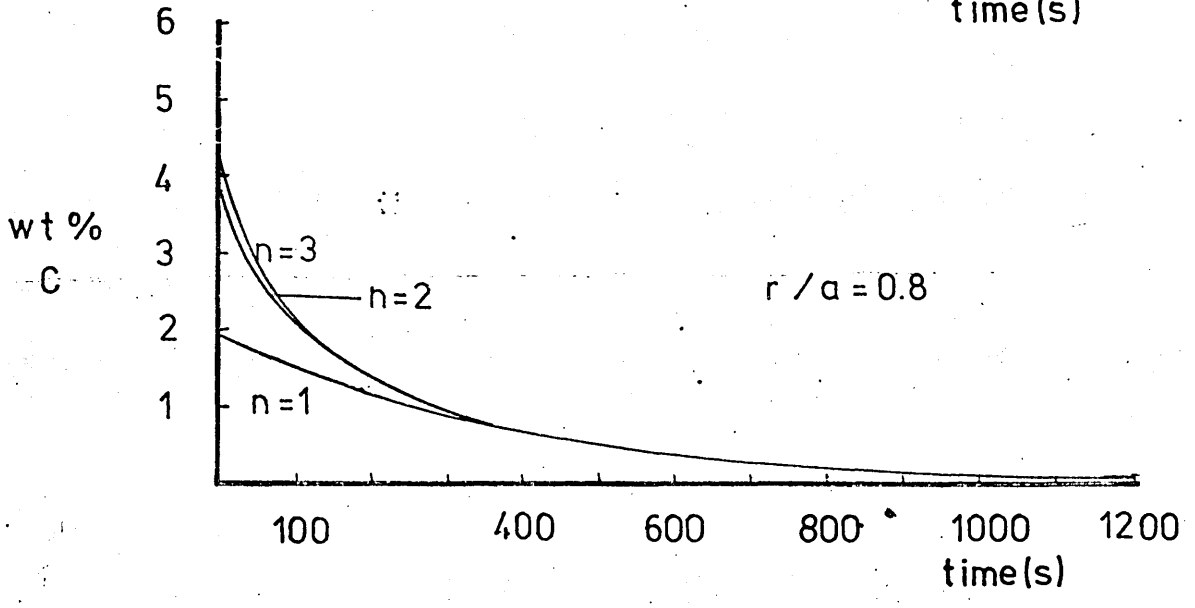
r/a = 0.8
wt %
C
6
5
4
3
2
1
n=3
n=2
n=1
100
400
600
800
1000
1200
time(s)

FIGURE 60. SPECIFIC SOLUTION FOR FICKS SECOND LAW FOR THE CASE WHEN $r \rightarrow 0$ (i.e. CONCENTRATION AT THE CENTRE OF THE SPHERE). DATA USED: $Dc = 4.5 \times 10^{-5} cm^2/sec$, $a = 0.4$ cm, $Co = 4.25$ %C, $Cs = 0$ AND $t = 0$ TO 1200 sec.

FIGURE 61. COMBINATION OF DATA FROM FIGURE 59a AND 60 TO OBTAIN CARBON GRADIENTS WITHIN THE SPHERE FOR $n = 1$, $n = 2$ AND $n = 3$.

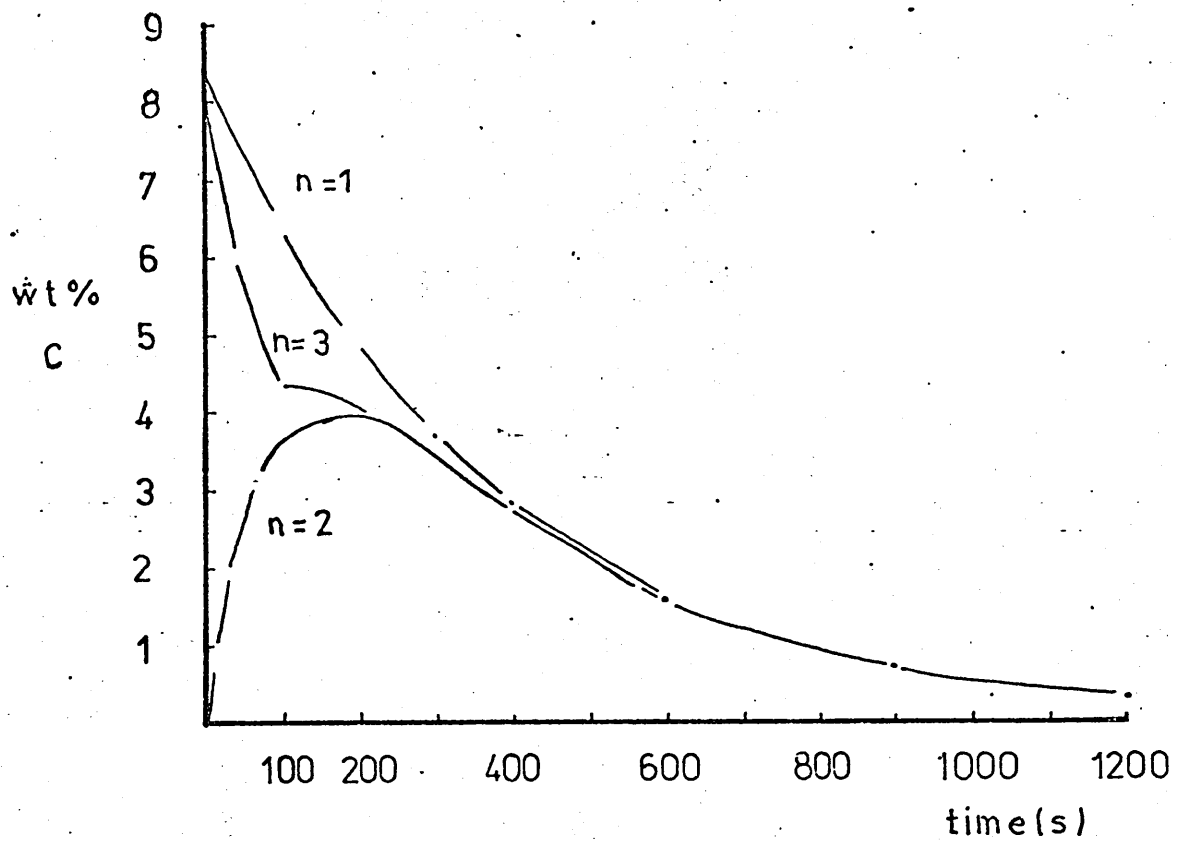
9
8
7
6
5
4
3
2
1
wt%
C
n=1
n=3
n=2
100
200
400
600
800
1000
1200
time(s)

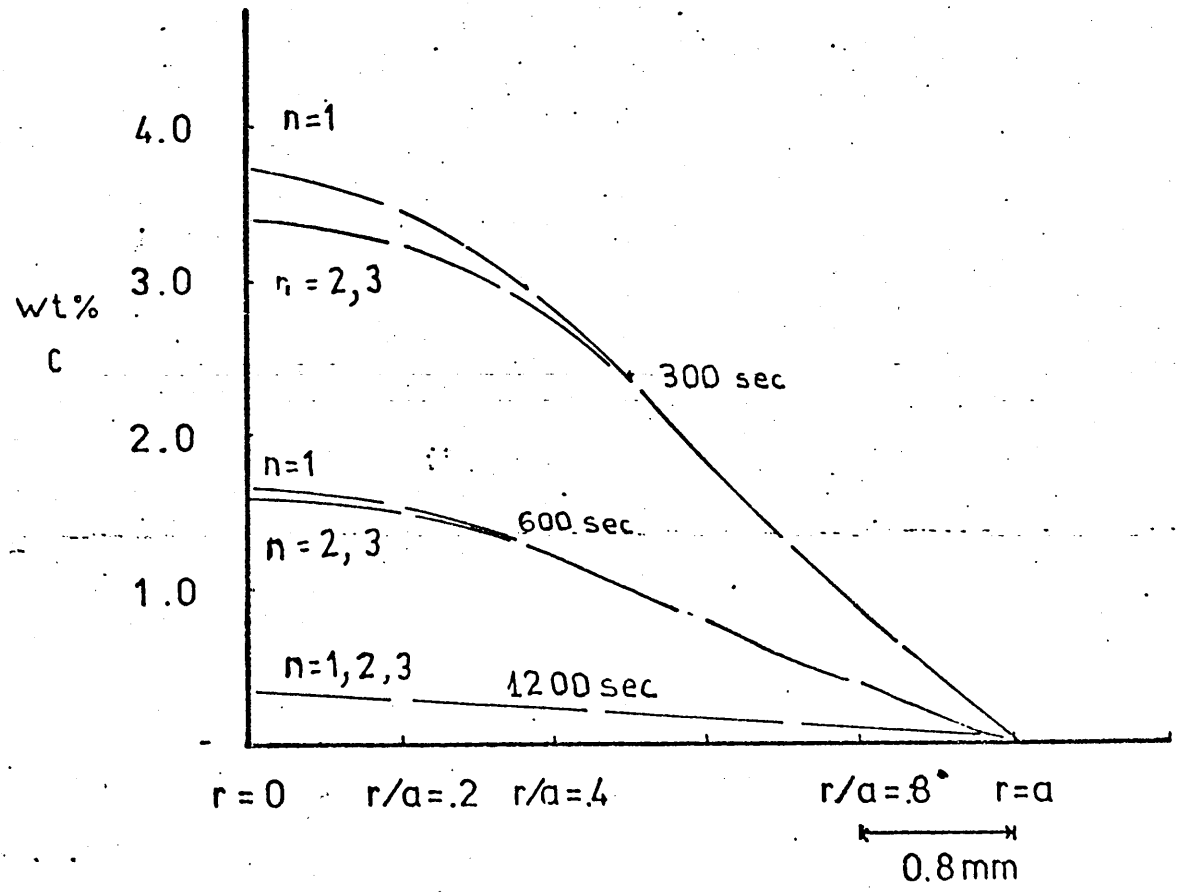
4.0
3.0
2.0
1.0
wt%
C
n=1
n=2,3
300 sec
n=1
600 sec
n=2,3
n=1,2,3
1200 sec
r=0
r/a=.2
r/a=.4
r/a=.8
r=a
0.8mm

FIGURE 62. GRAPHICAL SOLUTION OF EQUATION 5.5.1.4
DATA: $D_c = 5.7 \times 10^{-5}$ cm^2/sec, a = 0.4 cm and n = 3.

FIGURE 63. COMPARISON OF WT % C AGAINST TIME AS CALCULATED FROM EQUATION 5.5.1.4 AND AS OBTAINED FROM EXPERIMENT. THE EXPERIMENTAL DATA WERE TAKEN FROM FIGURE 35.

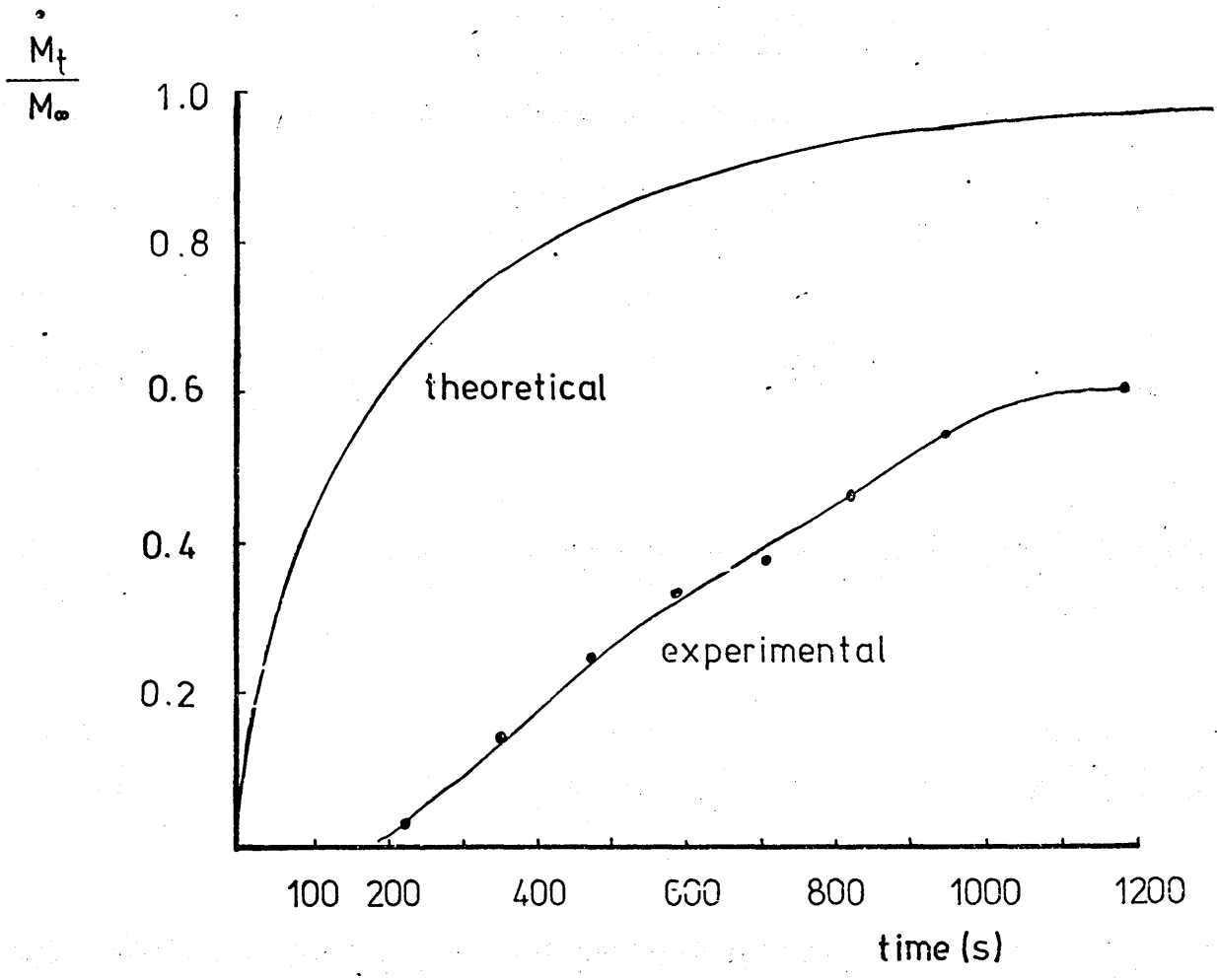
$\frac{M_t}{M_\infty}$
1.0
0.8
0.6
0.4
0.2
theoretical
experimental
100
200
400
600
800
1000
1200
time (s)

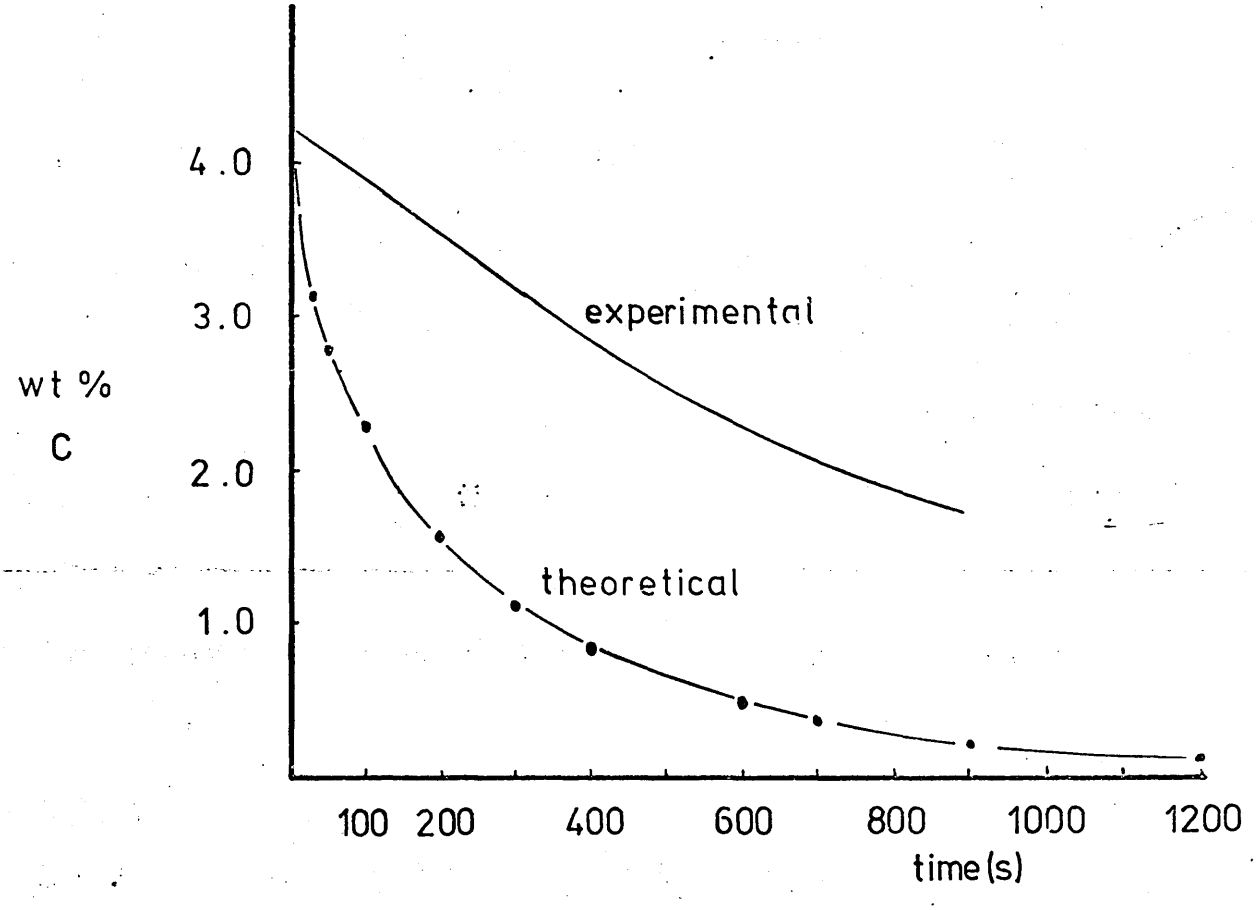
wt %
C
4.0
3.0
2.0
1.0
experimental
theoretical
100
200
400
600
800
1000
1200
time (s)

FIGURE 64. SECOND CASE FOR MASS TRANSPORT AT THE INTERFACE. RESISTANCE IN AN INTERNALLY CIRCULATING DISPERSED PHASE.

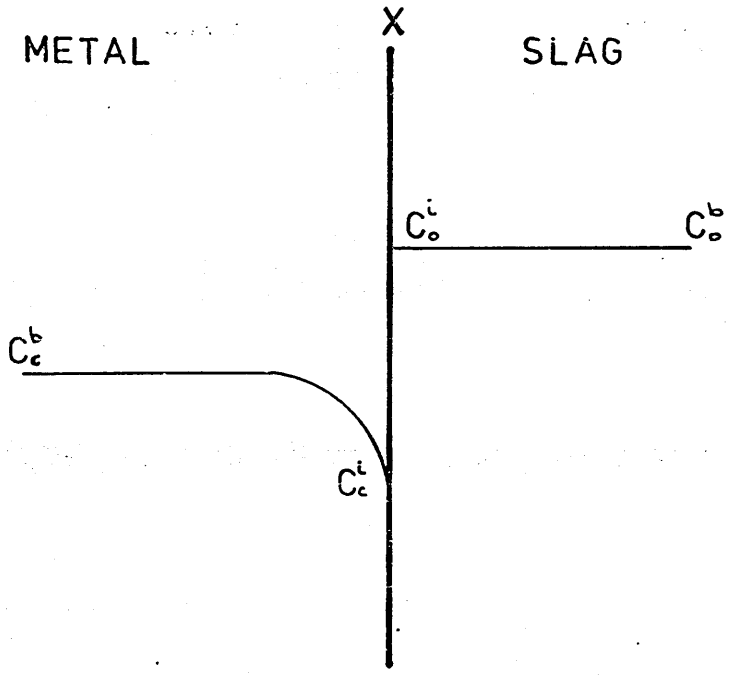
METAL
X
SLAG
C_o^i
C_o^b
C_c^b
C_c^i

FIGURE 65. LAMINAR CIRCULATION PATTERN FOR DISPERSED PHASE AS PROPOSED BY KRONIG AND BRINK (148).

FIGURE 66. CASE THREE FOR MASS TRANSPORT AT THE INTERFACE. RESISTANCE IN THE CONTINUOUS PHASE.

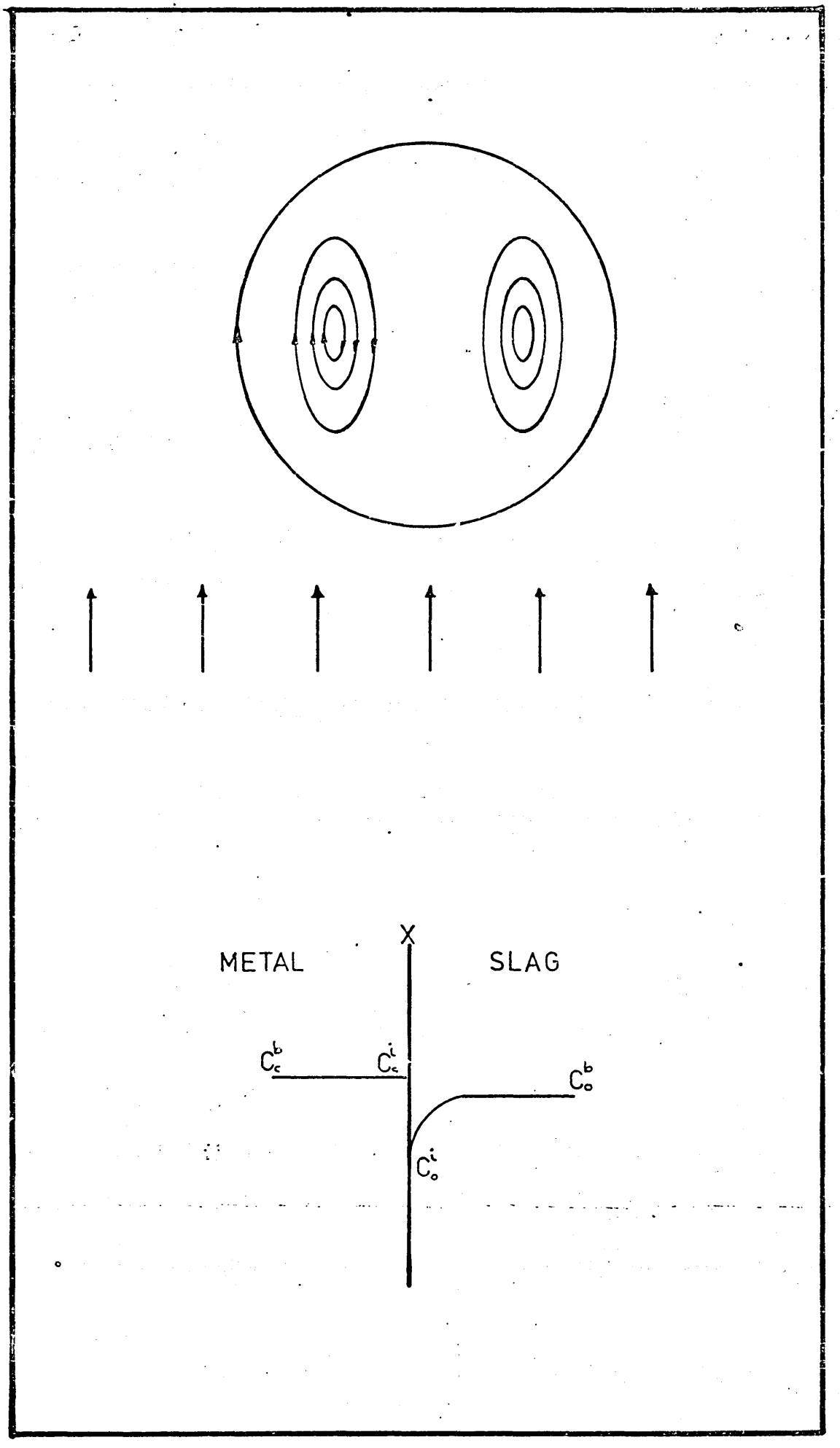
X
METAL
SLAG
C_c^b
C_c^i
C_o^b
C_o^i

FIGURE 67. CALCULATED VALUES FOR RATES OF DECARBURIZATION OBTAINED FROM SECTION 5.5.3 DATA: $D_{FeO} = 5.7 \times 10^{-6} cm^2/sec$, DIAMETER OF DROP (d) = 0.8 cm, MASS TRANSFER COEFFICIENT FOR SLAG (k_{slag}) = 1.43×10^{-5} cm/sec FOR Sh = 2. CALCULATED VALUES FOR MASS TRANSFER COEFFICIENT FOR Sh NUMBERS OTHER THAN TWO ARE GIVEN IN THE TEXT AND IN TABLE IV.

FIGURE 68. VARIATION OF MASS TRANSFER COEFFICIENT WITH Sh NUMBER FOR $D_{FeO} = 5.7 \times 10^{-6}$ cm^2/sec.

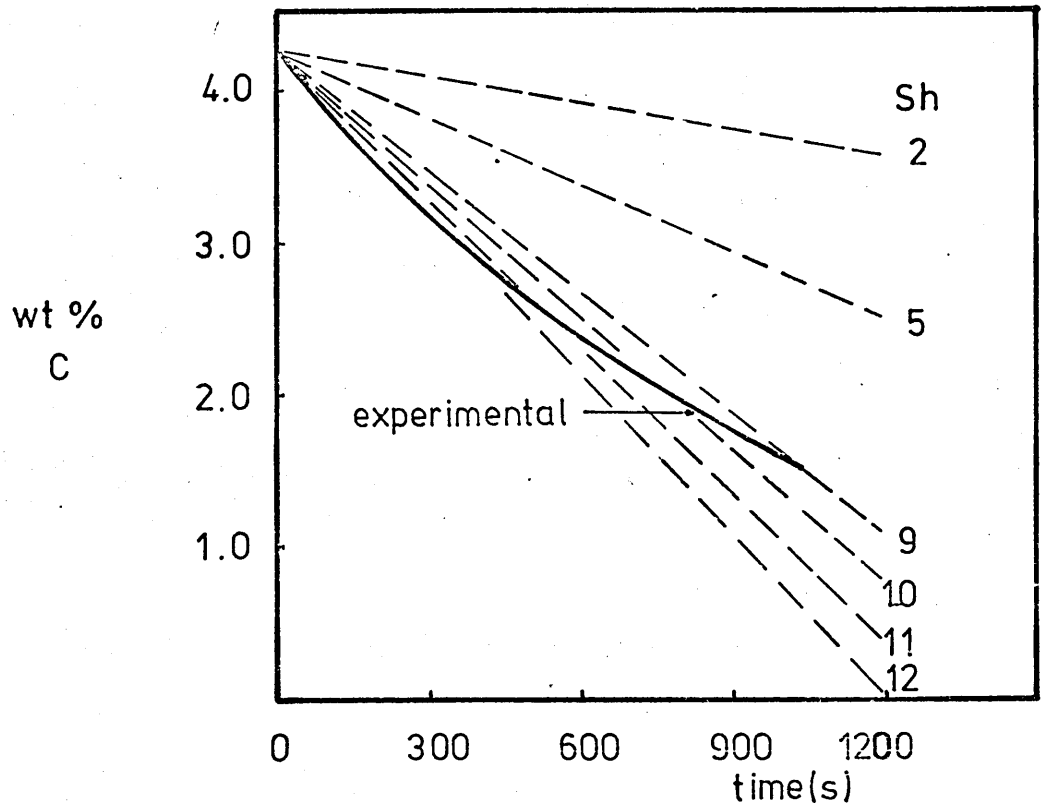
wt %
C
4.0
3.0
2.0
1.0
Sh
2
5
experimental
9
10
11
12
0
300
600
900
1200
time(s)

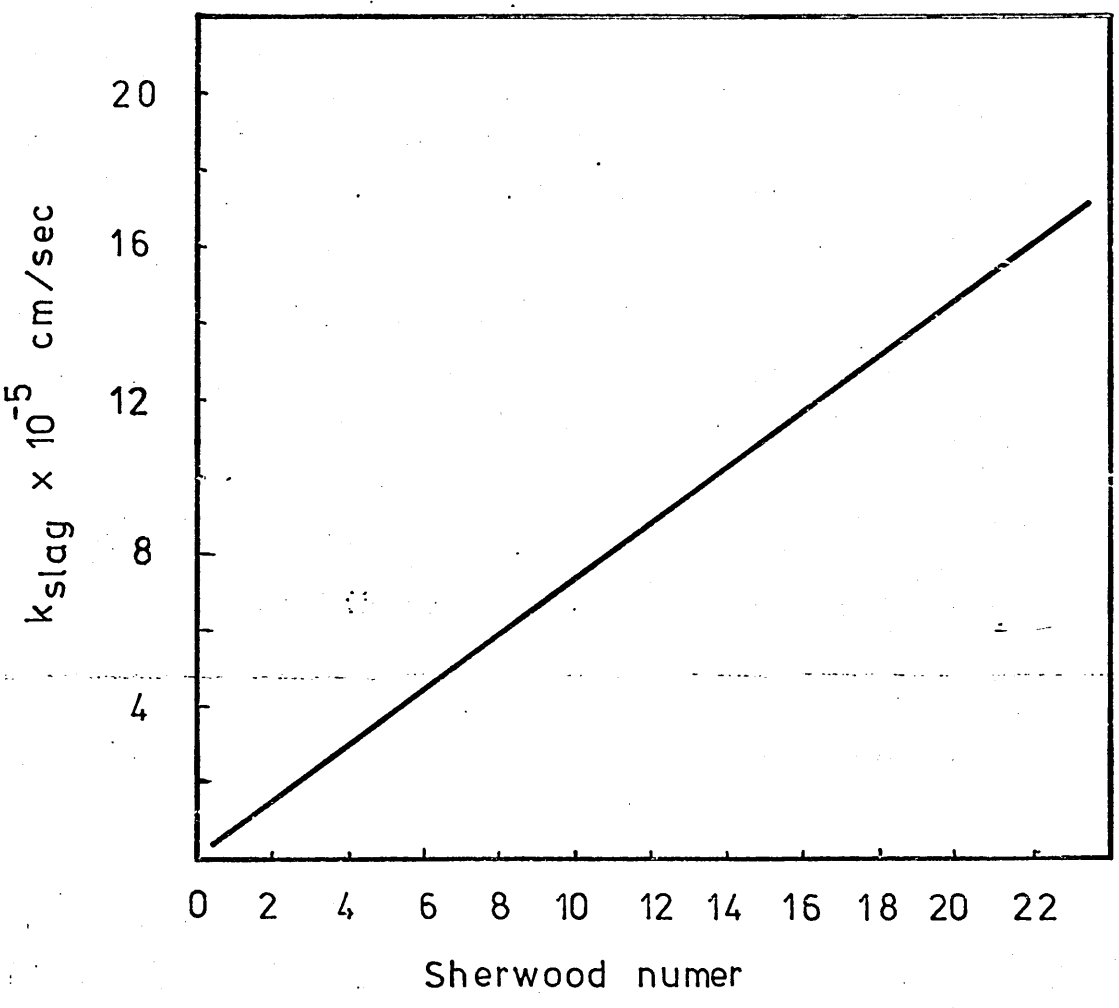
$k_{slag} \times 10^{-5}$ cm/sec
20
16
12
8
4
0
2
4
6
8
10
12
14
16
18
20
22
Sherwood numer

FIGURE 69. VARIATION OF THE Sc NUMBER WITH SLAG VISCOSITIES (POISE).

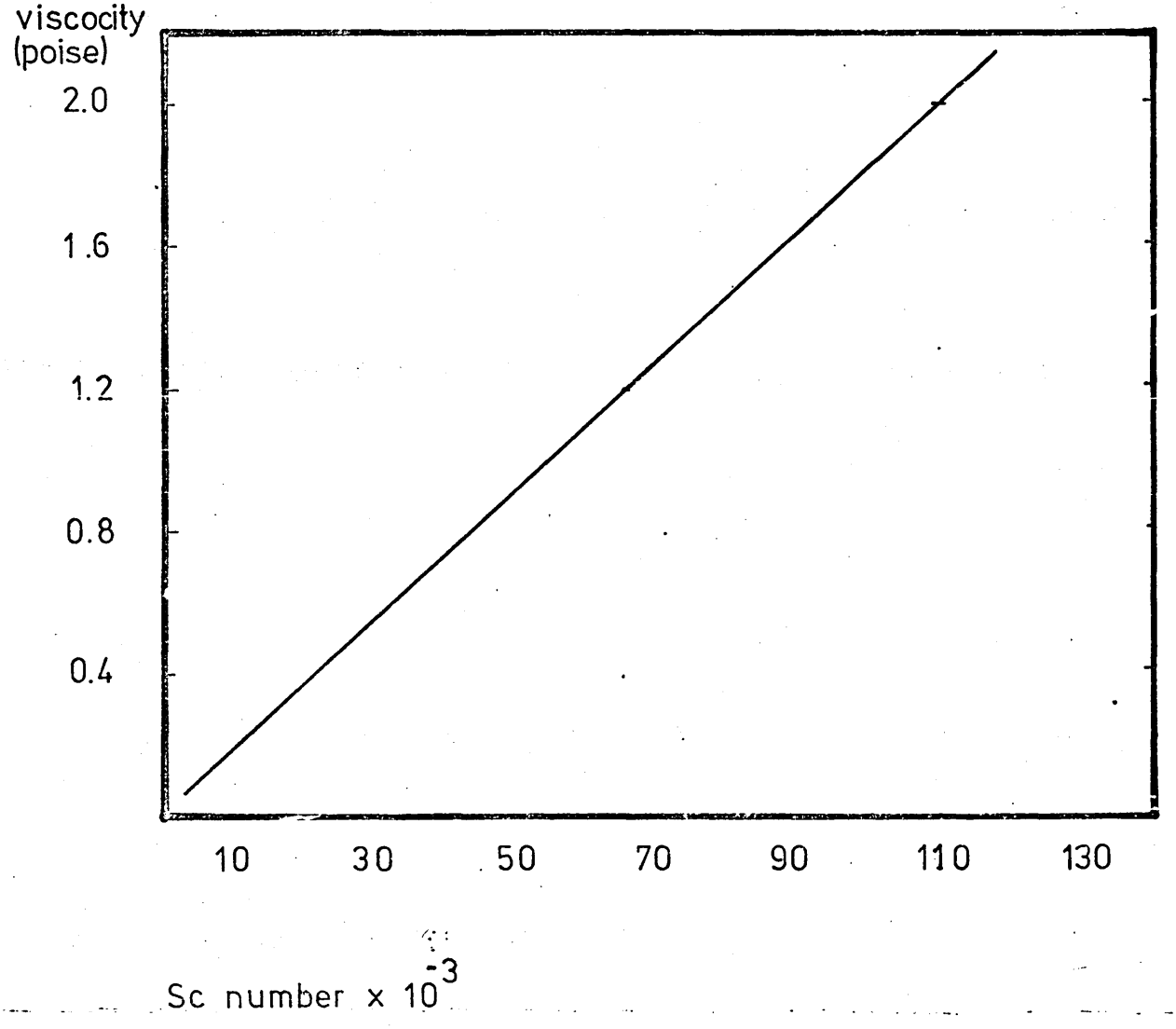
viscocity
(poise)
2.0
1.6
1.2
0.8
0.4
10
30
50
70
90
110
130
Sc number x 10^-3

FIGURE 70. VARIATION OF Sh NUMBER WITH Gr NUMBER (FOR MASS TRANSPORT) FOR VARIOUS SLAG VISCOSITIES.

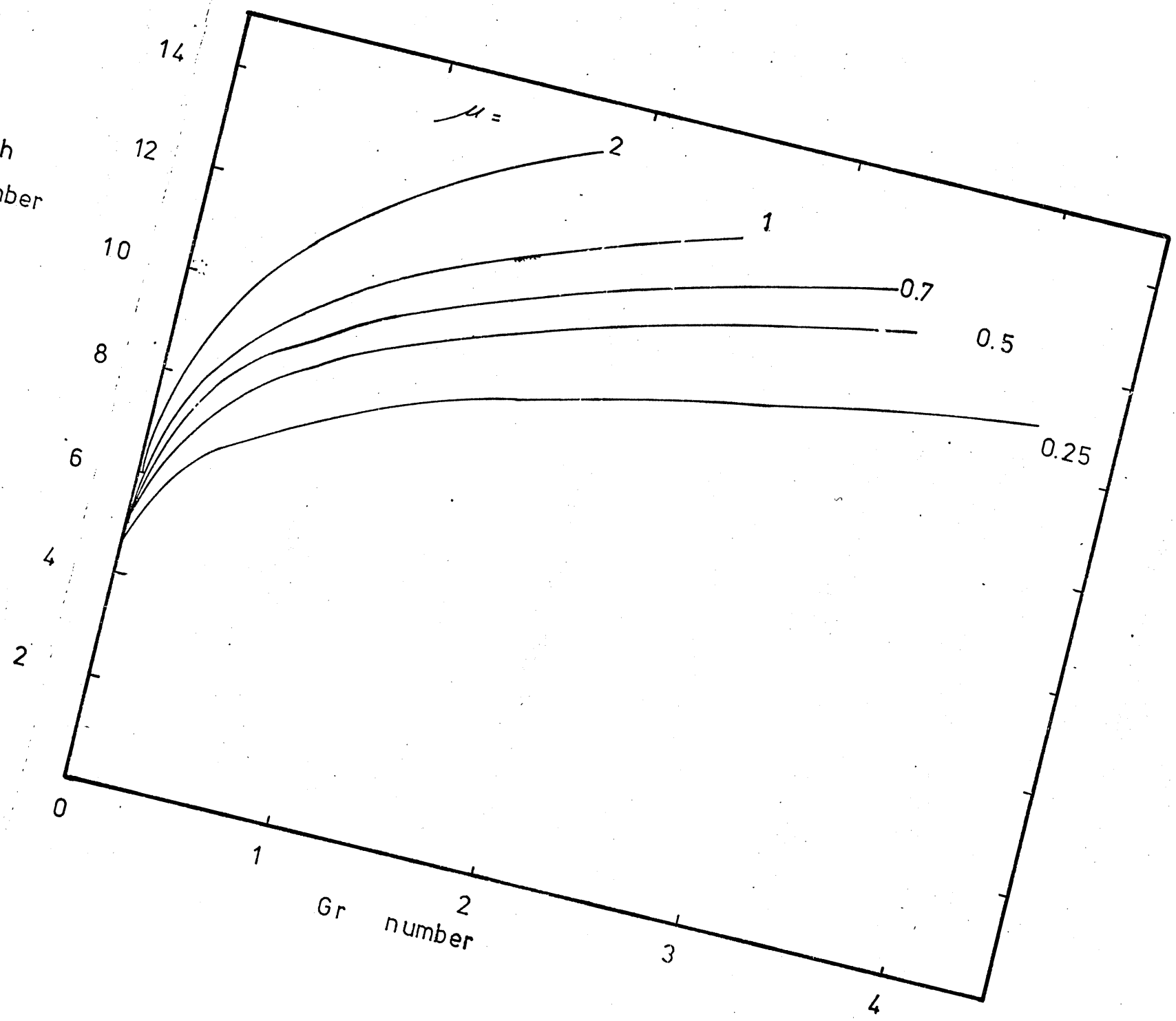
Sh
number
14
12
10
8
6
4
2
0
μ =
2
1
0.7
0.5
0.25
1
2
3
4
Gr number

FIGURE 71. VARIATION OF Sh NUMBER WITH Re NUMBER FOR VARIOUS SLAG VISCOSITIES.

FIGURE 72. VARIATION OF Sh NUMBER WITH RELATIVE VELOCITY BETWEEN SLAG AND METAL PHASES WITH VARYING SLAG VISCOSITY,

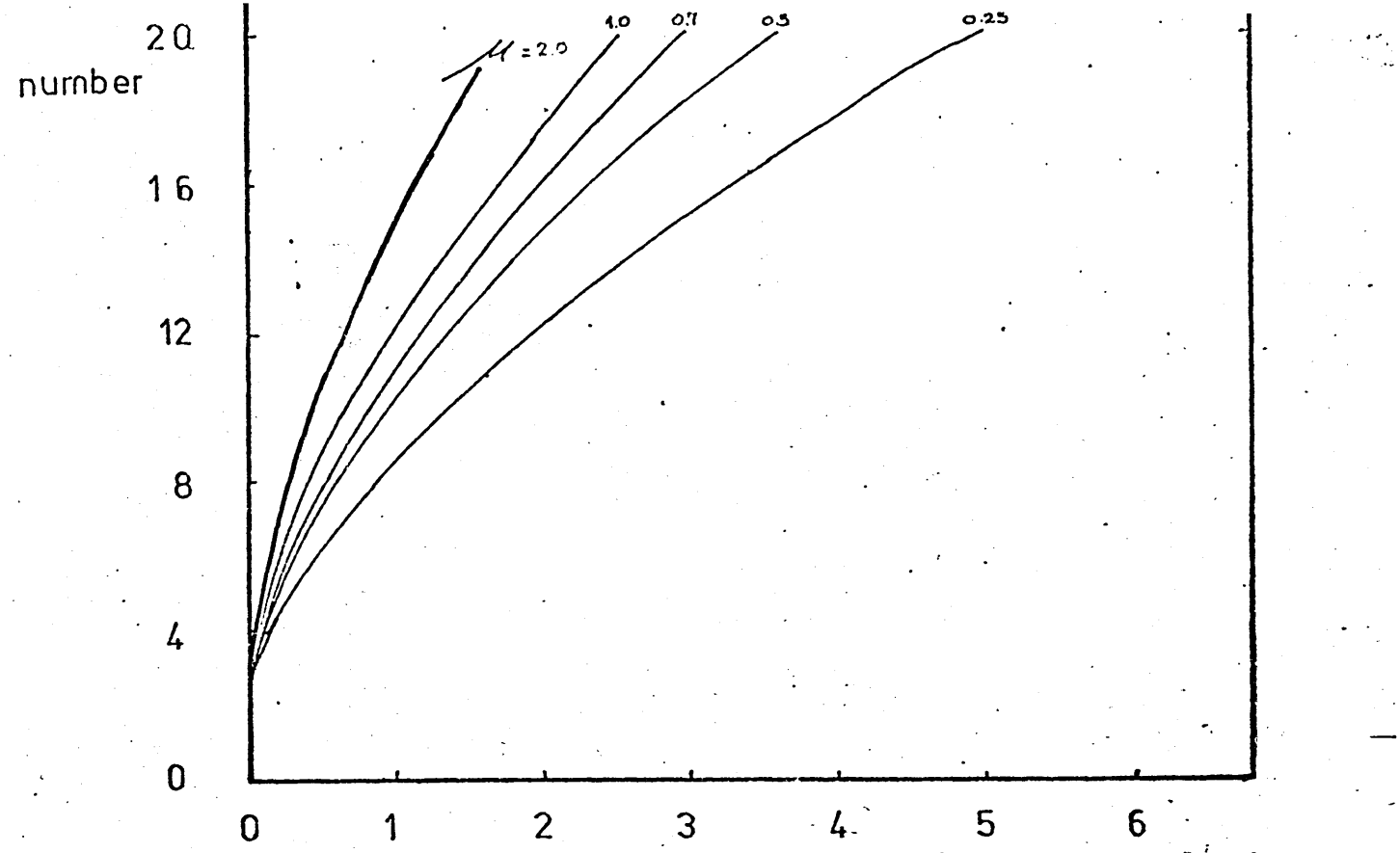
20
number
16
12
8
4
0
μ = 2.0
1.0
0.7
0.5
0.25
0
1
2
3
4
5
6
Re number

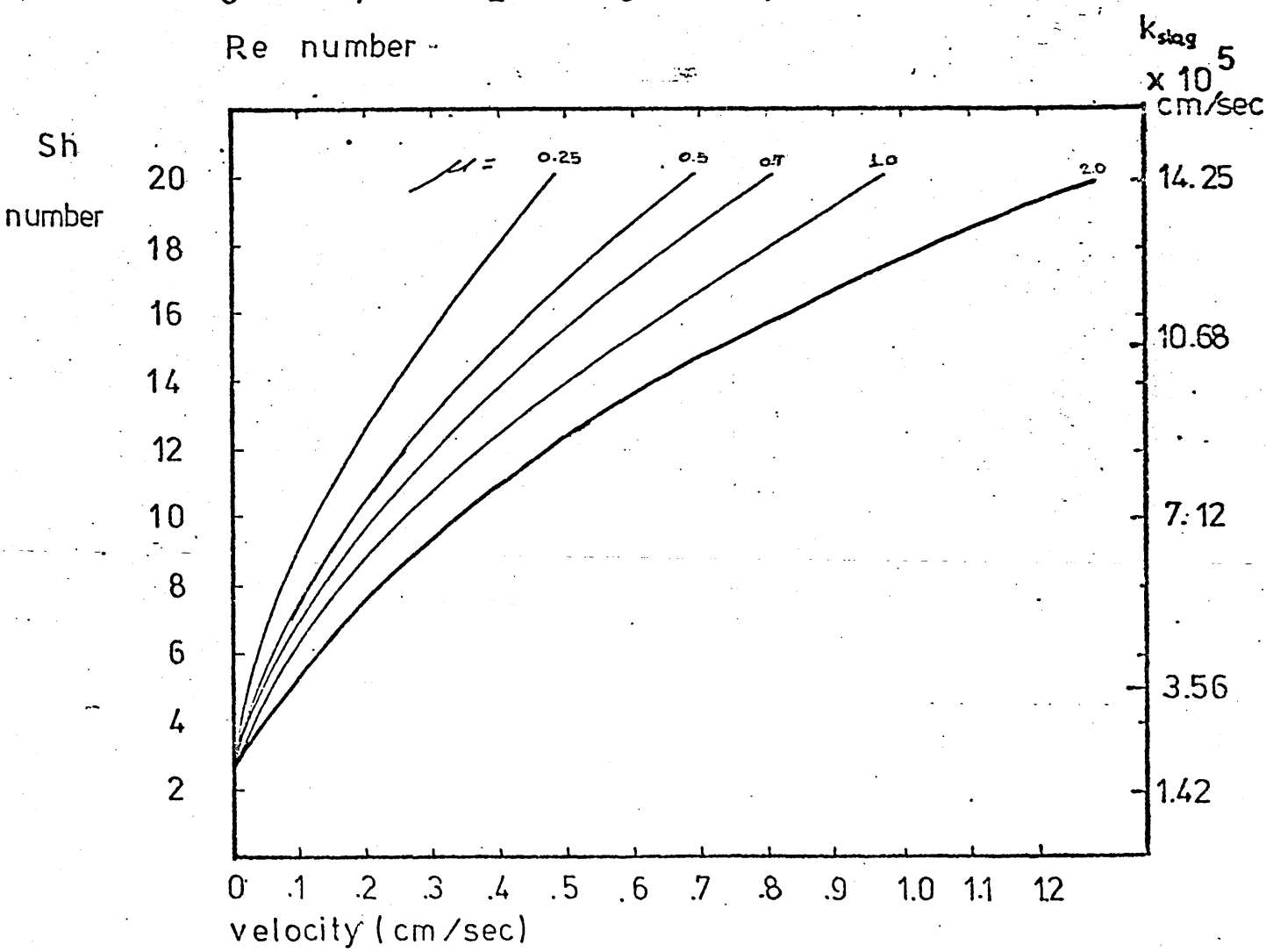
Sh
number
20
18
16
14
12
10
8
6
4
2
μ =
0.25
0.5
0.7
1.0
2.0
k_{slag}
x 10^5
cm/sec
14.25
10.68
7.12
3.56
1.42
0
.1
.2
.3
.4
.5
.6
.7
.8
.9
1.0
1.1
1.2
velocity (cm/sec)

FIGURE 73. SCHEMATIC REPRESENTATION OF CHEMICAL REACTION CONTROL AT THE INTERFACE.

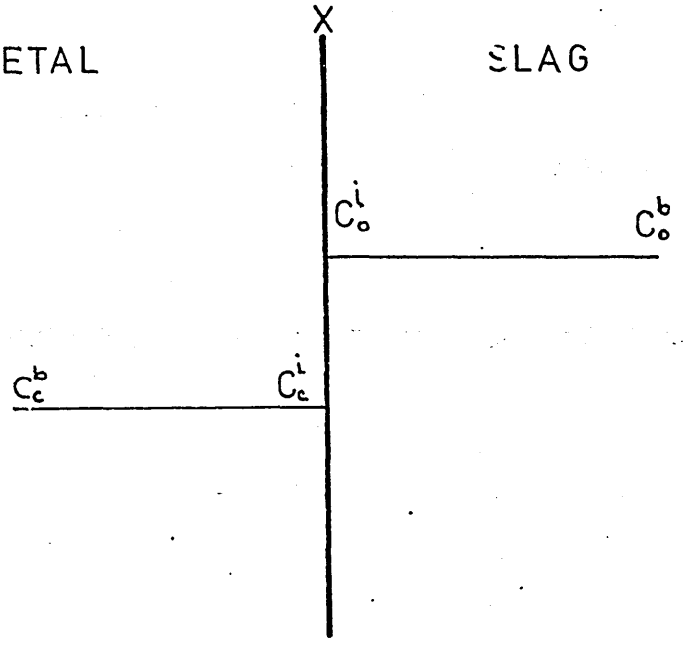
X
METAL
SLAG
C_o^i
C_o^b
C_c^b
C_c^i

FIGURE 74. METHOD FOR CALCULATING THE OVERALL MASS TRANSFER COEFFICIENT.

PIVOT (minute)	C_f / C_o	$(k) \times 10^4$ $\frac{1}{360} \ln (C_f/C_o)$
6	3.00/4.12	8.81
8	2.66/3.82	10.05
10	2.37/3.38	9.86
12	2.10/3.00	9.91
14	1.87/2.66	9.79
16	1.69/2.37	9.40

$k = 9.64 \times 10^{-4}$

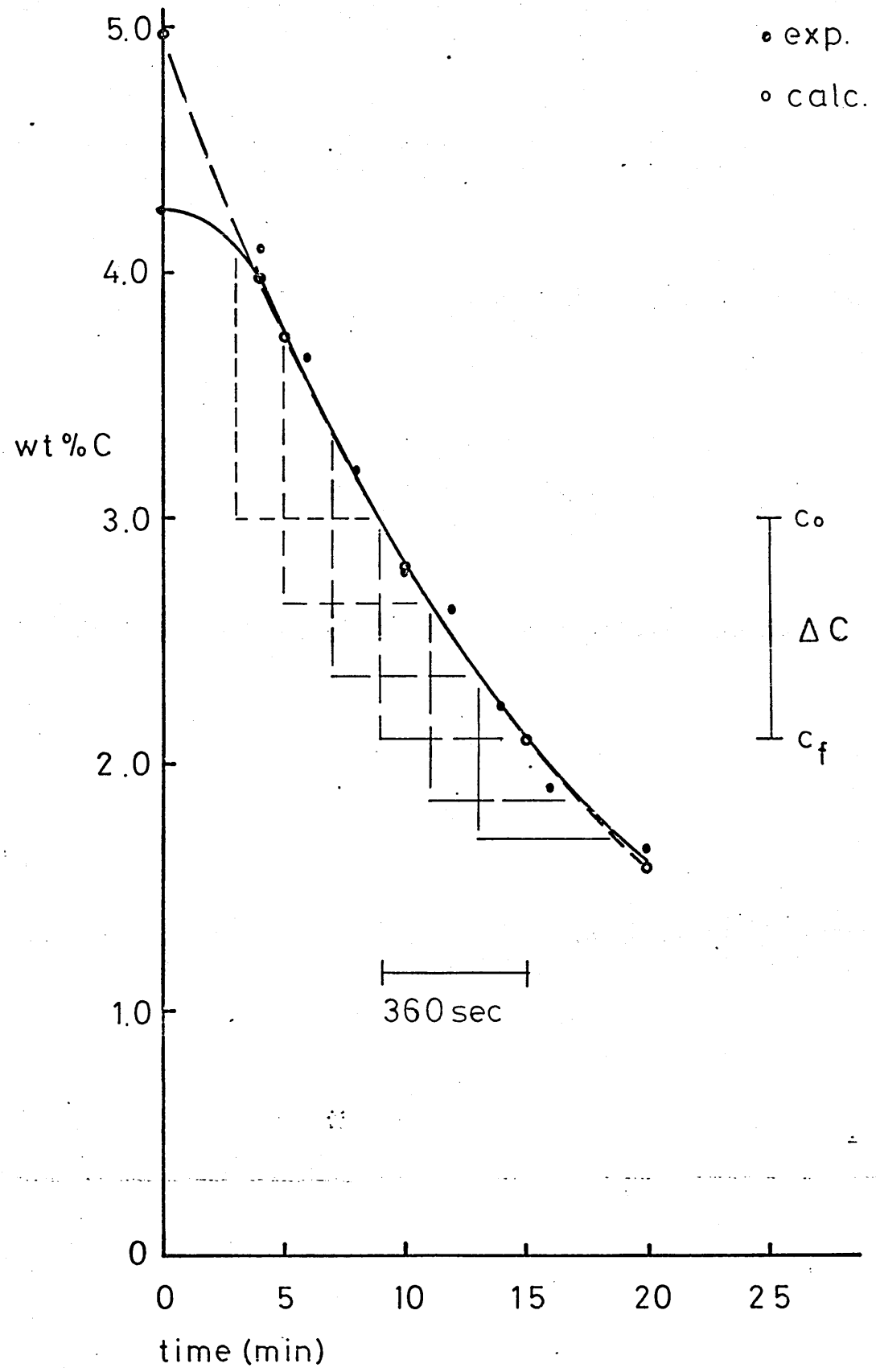
5.0
4.0
3.0
2.0
1.0
0
wt %C
• exp.
∘ calc.
C_o
ΔC
C_f
360 sec
0
5
10
15
20
25
time (min)

FIGURE 75. ACTIVATION ENERGIES CALCULATED FROM:

$$-\log k \quad \text{vs} \quad 1/T \times 10^4$$

SLAG 1	FAYALITE	$E_1 = 29,436$ cal
SLAG 2	M-1	$E_2 = 18,116$ cal
SLAG 3	C-1	$E_3 = 13,800$ cal
SLAG 4	C-3	$E_4 = 16,137$ cal

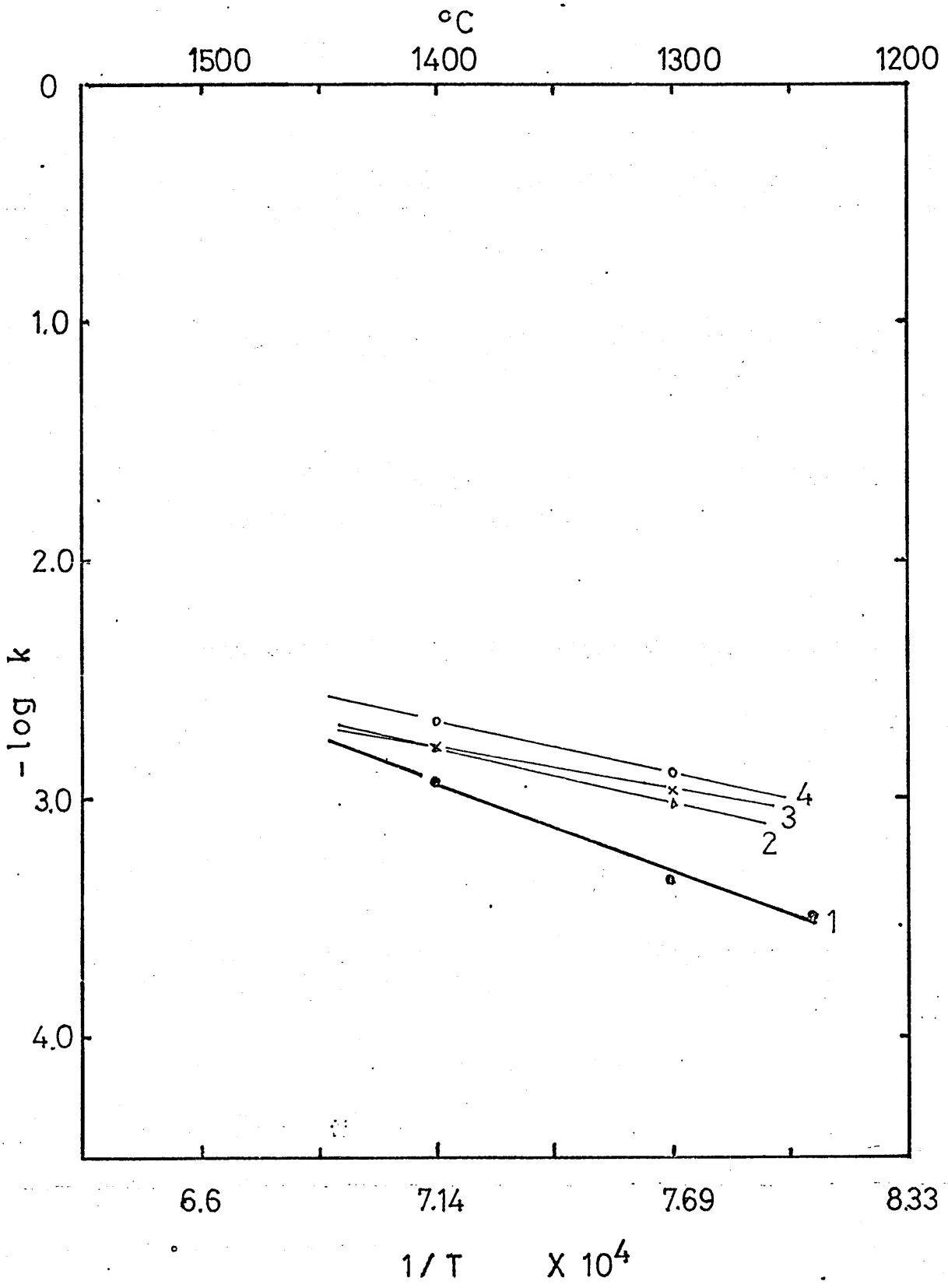
°C
1500
1400
1300
1200
0
1.0
2.0
3.0
4.0
- log k
4
3
2
1
6.6
7.14
7.69
8.33
1 / T X 10⁴

FIGURE 76. CALCULATED Sh NUMBERS WHICH GIVE SIMILAR DECARBURIZATION RATES AS THOSE FOUND FROM EXPERIMENTS AT 1240°C. THE EXPERIMENTAL RESULTS WERE TAKEN FROM FIGURE 21. LINE A HAS BEEN CALCULATED USING A VALUE OF $D_{FeO} = 2.2 \times 10^{-6} cm^2/sec$. ALL OTHER RESULTS WERE CALCULATED USING THE VALUE OF $D_{FeO} = 5.7 \times 10^{-6} cm^2/sec$.

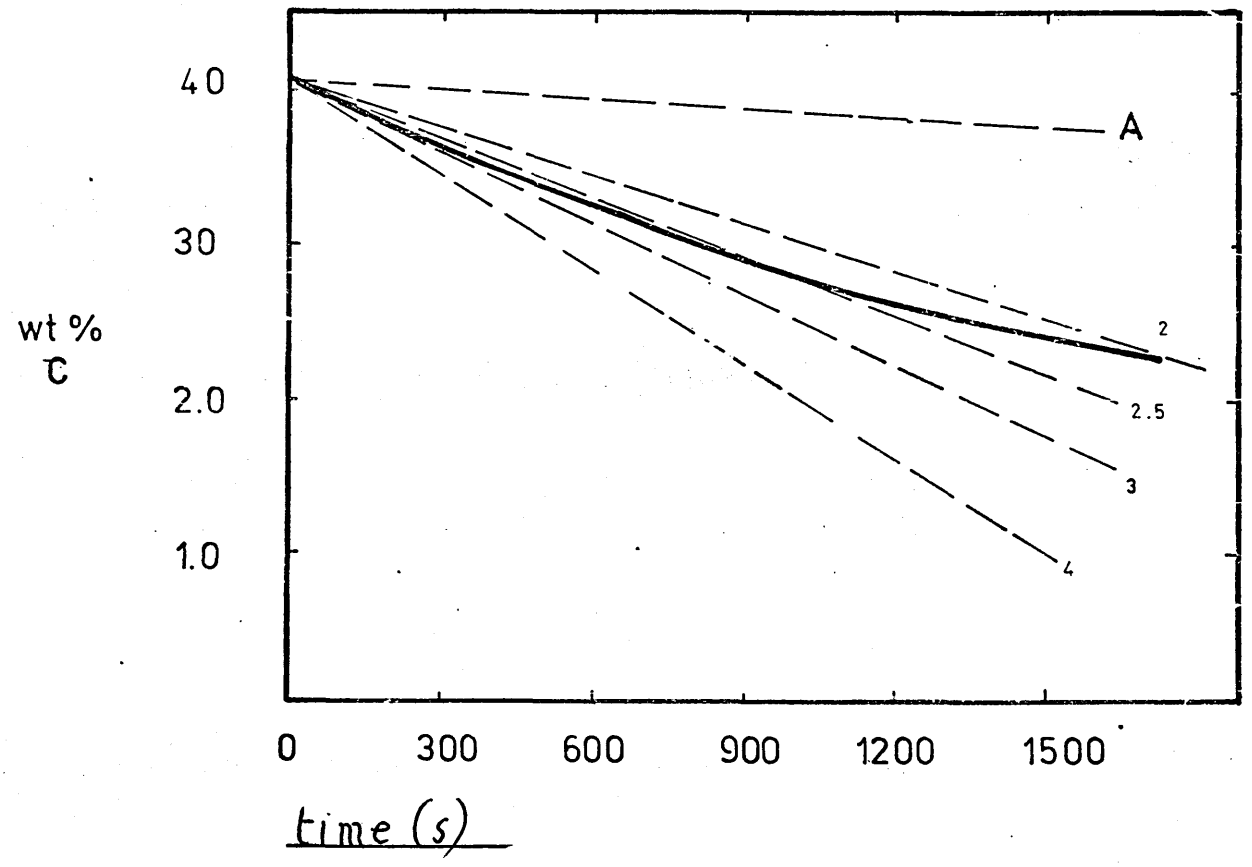
40
30
2.0
1.0
wt %
C
A
2
2.5
3
4
0
300
600
900
1200
1500
time (s)

FIGURE 77. CALCULATED Sh NUMBERS TO GIVE SIMILAR DECARBURIZATION RATES AS FOUND FROM EXPERIMENTS WITH AND WITHOUT GAS LANCING. THE EXPERIMENTAL RESULTS HAVE BEEN TAKEN FROM FIGURE 35 (WITHOUT GAS LANCING) AND FROM FIGURE 49. LINE REPRESENTED BY .-.- CORRESPONDS TO FIGURE 35. FULL LINE REPRESENTS FIGURE 49 . ALL OTHER LINES REPRESENT CALCULATED VALUES FOR Sh NUMBERS.

FIGURE 78. CALCULATED Sh NUMBERS TO GIVE SIMILAR DECARBURIZATION RATES AS FOUND FROM EXPERIMENTS AT 1400°C. FULL LINE REPRESENT EXPERIMENTAL DATA TAKEN FROM FIGURE 40.

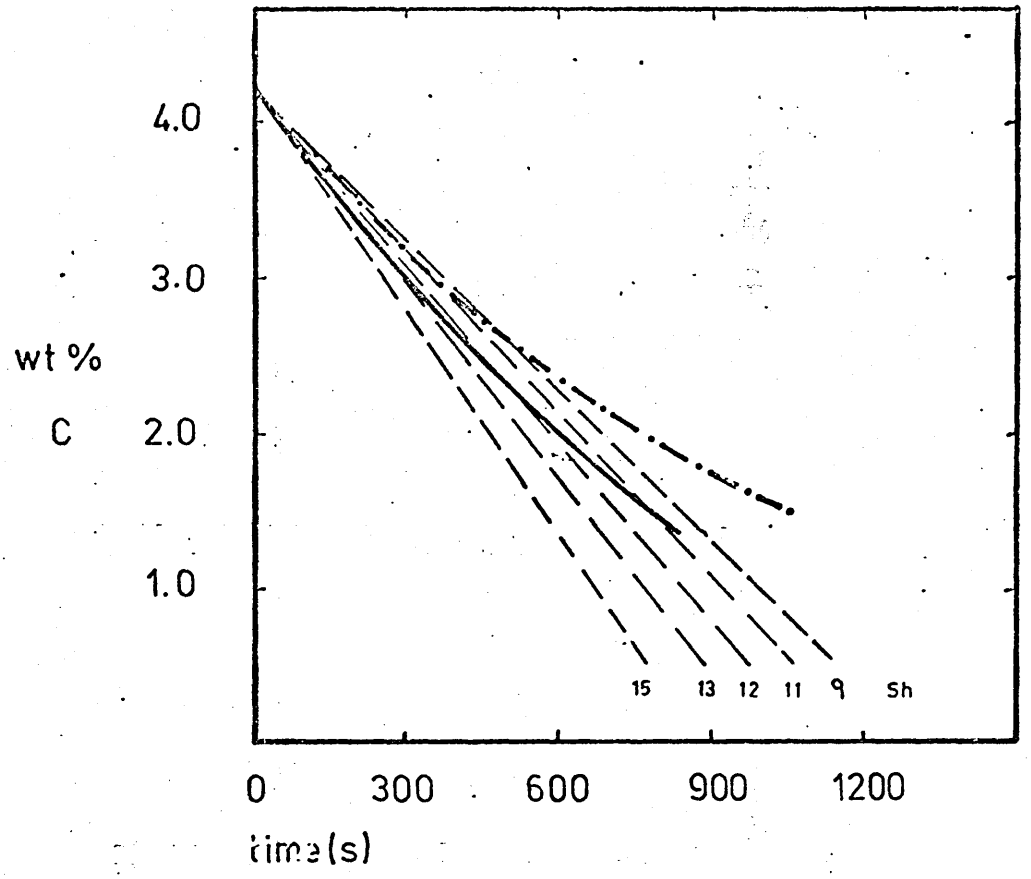
4.0
3.0
wt %
C
2.0
1.0
15
13
12
11
9
Sh
0
300
600
900
1200
time(s)

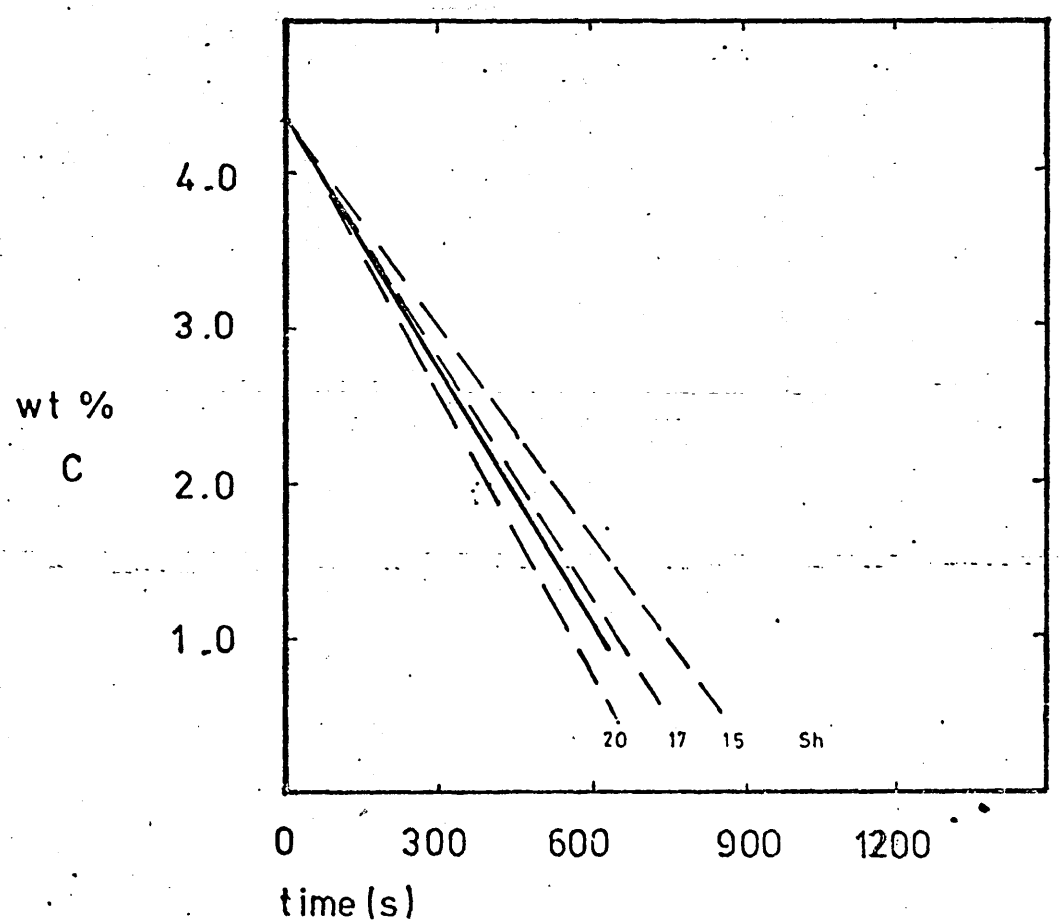
4.0
3.0
wt %
C
2.0
1.0
20
17
15
Sh
0
300
600
900
1200
time (s)

FIGURE 79. CALCULATED Sh NUMBERS TO GIVE SIMILAR DECARBURIZATION RATES AS FOUND FROM EXPERIMENTS AT 1500°C. THE EXPERIMENTAL DATA WERE TAKEN FROM FIGURE 43.

FIGURE 80. CALCULATED Sh NUMBERS TO GIVE SIMILAR DECARBURIZATION RATES AS THOSE FOUND FROM EXPERIMENTS AT 1600°C. DATA FOR EXPERIMENTS AT 1600°C WERE TAKEN FROM FIGURE 46.

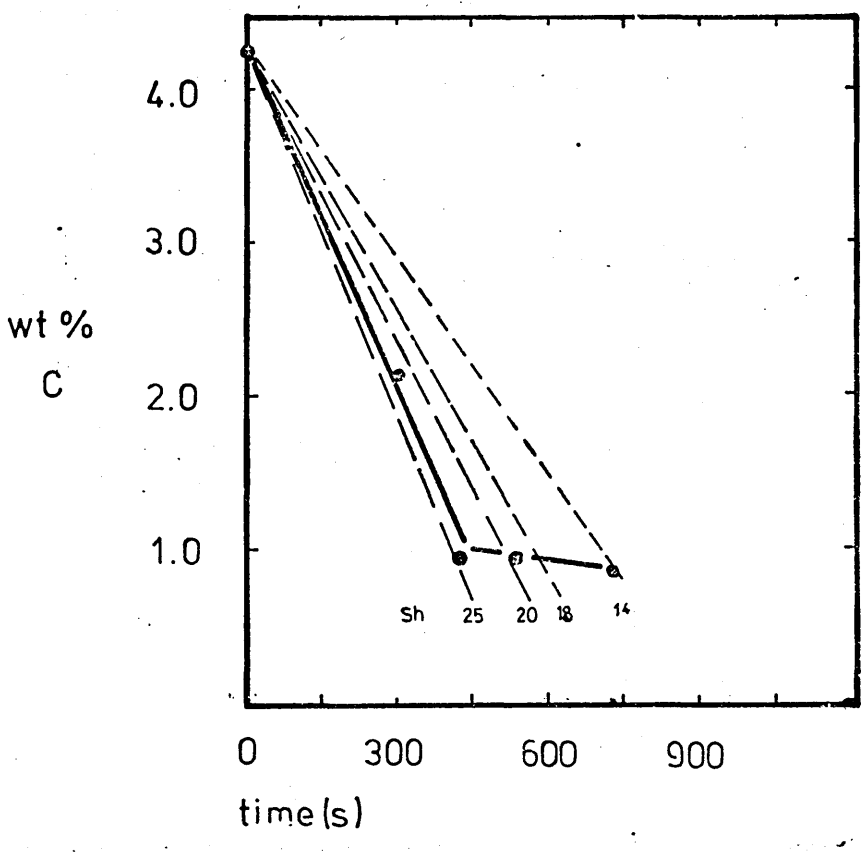
4.0
3.0
wt %
C
2.0
1.0
Sh
25
20
18
14
0
300
600
900
time (s)

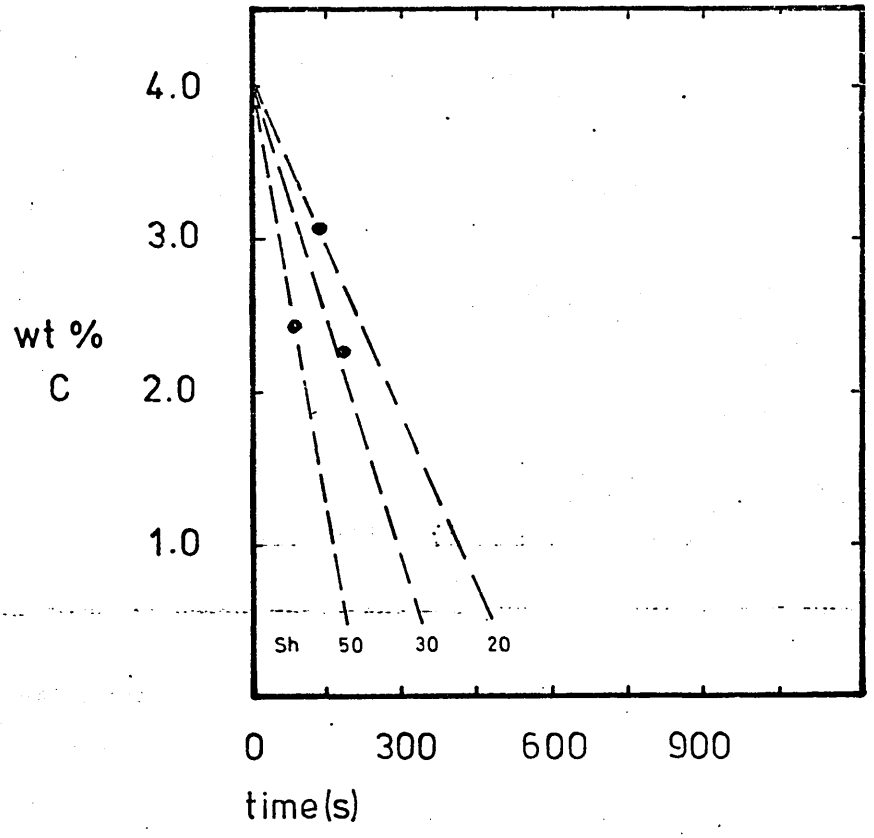
4.0
3.0
wt %
C
2.0
1.0
Sh
50
30
20
0
300
600
900
time (s)

FIGURE 81. VARIATION OF MASS TRANSFER COEFFICIENTS TAKEN FROM TABLE V WITH LIME CONTENT IN SLAGS.

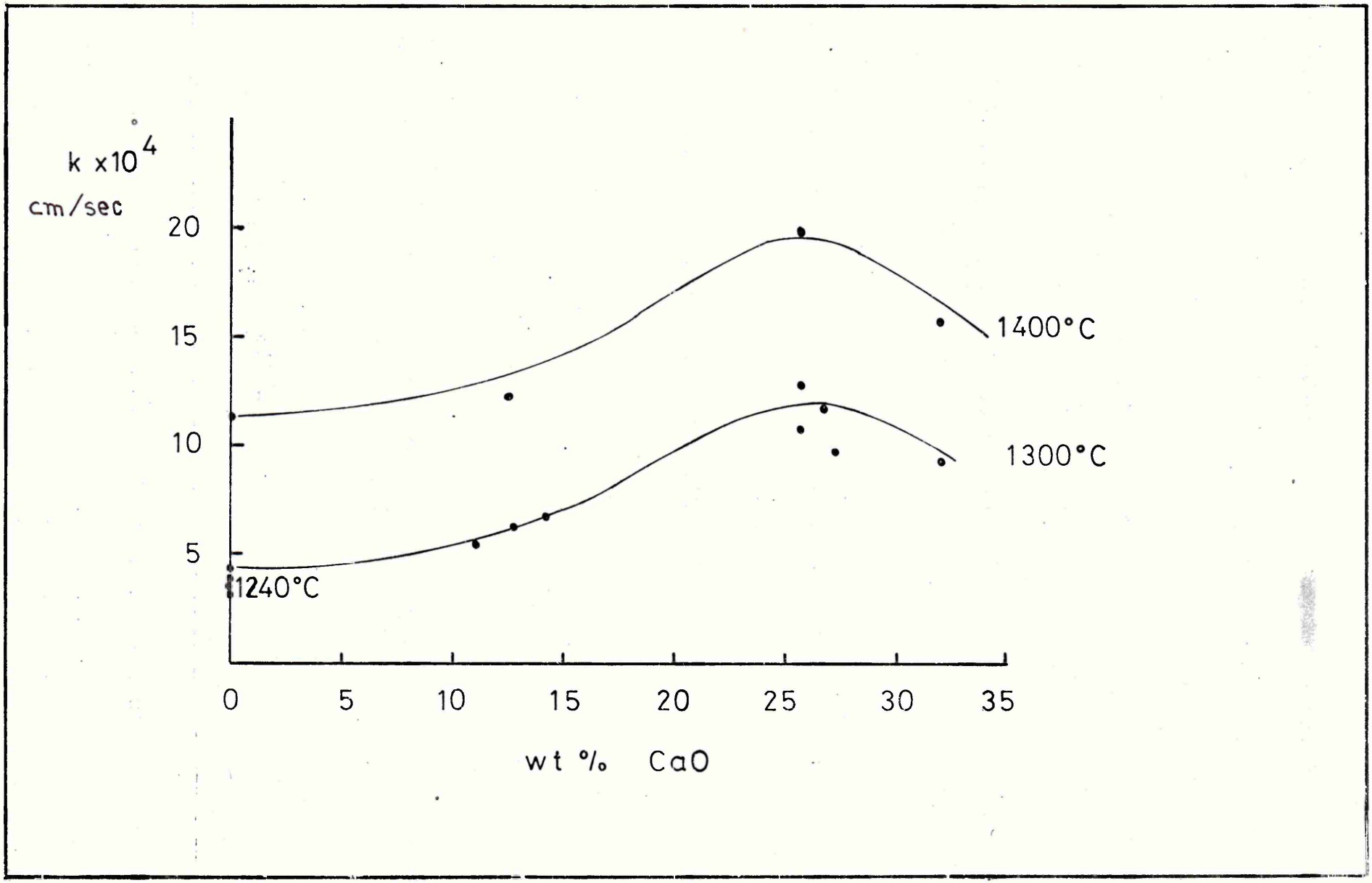
k x10^4
cm/sec
20
15
10
5
1400°C
1300°C
1240°C
0
5
10
15
20
25
30
35
wt % CaO